UNIVERSITAT POLITÈCNICA DE VALÈNCIA

ESCOLA TÈCNICA SUPERIOR D'ENGINYERIA DEL DISSENY

Design, Synthesis and Evaluation of Chromo-fluorogenic Probes for Contaminating Species.

PhD. THESIS

Submitted by

Andrea Barba Bon

PhD. Supervisors:

Dr. Félix Sancenón Galarza
Prof. Salvador Gil Grau

Valencia, December 2014

FÉLIX SANCENÓN GALARZA, PhD in Chemistry and Lecturer at the *Universitat Politècnica de València*, and SALVADOR GIL GRAU, PhD in Chemistry and Professor at the *Universitat de València*.

CERTIFY:

That the work *"Design, Synthesis and Evaluation of chromo-fluorogenic probes for contaminating species detection"* has been developed by **Andrea Barba Bon** under their supervision in the Centro de Reconocimiento Molecular y Desarrollo Tecnológico (IDM) of the *Universitat Politècnica de València*, as a thesis Project in order to obtain the degree of PhD in Chemistry at the *Universitat Politècnica de València.*

Valencia, November 17th 2014.

Dr. Félix Sancenón Galarza Prof. Salvador Gil Grau

A mis abuelos.

"No amount of experimentation can ever prove me right;
a single experiment can prove me wrong"
Albert Einstein

"Cuando hay tormenta, los pajaritos se esconden;
pero las águilas vuelan más alto"
Mahatma Gandhi

Acknowledgements

Agradecimientos

Aún recuerdo como si fuese ayer, el día que hable por primera vez con Boro y me convenció para que empezara esta aventura que es la tesis doctoral. Cinco años después aquí estoy al final de este largo camino, en el cual he conocido a personas maravillosas con las que he compartido muchos momentos y experiencias.

En primer lugar quiero agradecer profundamente a mis directores de tesis Salvador Gil y Félix Sancenón, por su guía, enseñanza, consejos, dedicación y paciencia que han tenido a lo largo de este trabajo.
A Ana. M. Costero, por toda su ayuda, entrega, paciencia, por su confianza en mí y por no permitir que me rindiera bajo ningún concepto.
A Margarita Parra y a Pablo Gaviña por sus consejos, sus palabras de ánimo y por acudir (siempre con una sonrisa) en mi auxilio cuando me veían histérica por el pasillo.

I would like to thank to Prof. A. Harriman in Newcastle University, for giving me the opportunity to visit his lab and all the help he has provided me; and all the members from Molecular Photonics Laboratory for the kind hospitality they showed during the whole time I was there.

A todos mis compañeros de laboratorio (sin duda, ellos son los que mejor entienden el esfuerzo que supone la realización de una tesis) porque sin su presencia las horas que pasamos en el lab. serían mucho más largas, pesadas y aburridas. En los últimos años hemos convivido muchísimas horas de prisas, estreses, enfados, agobios, gritos… sin embargo también nos hemos ofrecido apoyo, ayuda y motivación para seguir adelante y mucho es lo que hemos compartido: risas, congresos, cumpleaños, concursos de muffins y cupcakes, cenas… e incluso picnics en medio del campus! Por todo ello y por la amistad que hemos forjado muchísimas gracias!
A los compañeros del lab. 2.6 que a pesar de no trabajar en el mismo laboratorio, hemos compartido confidencias, comidas, cenas, "Bocho a las Ocho"… haciendo que el trabajo fuera más llevadero al saber que al final del día nos reuniríamos para contarnos nuestras desventuras.

A mis padres y mi hermano, por su cariño, su apoyo y por la paciencia que han tenido conmigo a lo largo de este camino y sobre todo por soportarme cuando volvía a casa un "pelín" irascible.

A todos los que habéis contribuido de una forma u otra… MUCHAS GRACIAS!

Resumen

La presente tesis doctoral titulada "*Design, Synthesis and Evaluation of Chromo-fluorogenic Probes for Contaminating Species"* (Diseño, Síntesis y Evaluación de Sensores Cromo-Fluorogénicos para la Detección de Especies Contaminantes) está centrada en el desarrollo de nuevos sensores cromo-fluorogénicos, basados en los principios básicos del reconocimiento molecular.

La primera parte de la tesis se centra en el diseño y la preparación de nuevos compuestos orgánicos que puedan ser empleados cómo sensores para cationes metálicos. El paradigma seleccionado para la detección está basado en la aproximación *unidad coordinante-unidad indicadora*. Los receptores sintetizados emplean un cromóforo (fluoresceína o BODIPY) como unidad indicadora funcionalizada con grupos aminoetoxi como unidad coordinante; la coordinación con el metal reduce la capacidad electrón-dadora del átomo de nitrógeno conjugado con el cromóforo, produciendo unos claros cambios ópticos visibles al ojo humano. El receptor preparado presenta una selectividad elevada para cationes trivalentes (Fe^{3+}, Al^{3+} y Cr^{3+}) con notables límites de detección. Los receptores derivados de BODIPY permiten la detección selectiva de los cationes trivalentes en medios acuosos.

El resto de la tesis está centrada en la detección y eliminación de simulantes de agentes nerviosos. Para la detección se han diseñado, sintetizado, caracterizado y estudiado nuevos *sensores químicos* basados en el esqueleto de BODIPY. Dichos quimiosensores presentan diferentes puntos de reacción con el fin de evitar las interferencias que podrían producirse por ácidos o por los productos de hidrolisis; además de permitir una respuesta diferente para cada uno de los simulantes de los agentes nerviosos de tipo G (DCNP y DFP). Dichos sensores químicos permiten la detección a simple vista (mediante cambios de color) de los simulantes de los agentes nerviosos con excelentes límites de detección. Los quimiodosímetros se soportaron en soportes sólidos para ampliar su aplicación práctica en tiempo y ambientes reales.

Para el desarrollo de sensores para la detección de agentes nerviosos de tipo V se ha empleado la aproximación de *ensayos de desplazamiento.* Para ello, basándonos en lo desarrollado en el 2do capitulo, se han diseñado y preparado complejos de Eu^{3+} y Au^{3+} coordinados con un ligado basado en el cuerpo BODIPY. En este caso, el simulante de agente nervioso de tipo V es capaz de coordinarse con el metal, liberando el ligando. Esta liberación produce cambios en las propiedades ópticas del BODIPY fácilmente detectables a simple vista.

Finalmente, se ha estudiado el posible uso de catalizadores supramoleculares para la eliminación de los agentes nerviosos organofosforados. Los estudios de hidrolisis se llevaron a cabo en presencia de 1,3-diindolilureas y tioureas, aminas, aminoalcoles y glicoles. La adición del catalizador incrementa el carácter electrófilo del átomo de fosforo, con lo que la velocidad de hidrólisis es mucho mayor. Tras el consiguiente ataque nucleofílico del agua, se liberan los correspondientes derivados organofosforados de menor toxicidad.

Resum

La present tesi doctoral titulada "*Design, Synthesis and Evaluation of Chromo-fluorogenic Probes for Contaminating Species"* (Disseny, Síntesi y Avaluació de Sensors Cromo-fluorogenics per a la detecció de especies contaminants) està centrada en el desenvolupament de nous sensors cromo-fluorogenics basats en els principis bàsics del reconeixement molecular.

La primera part de la tesi es centra en el disseny i la preparació de nous compostos orgànics que poden ser emprats com sensors per a cations metàl·lics. El paradigma seleccionat per als processos de reconeixement va a ser l'aproximació *unitat coordinant-unitat indicadora*. El receptor sintetitzat empra un cromòfor (Fluoresceïna o BODIPY) com a unitat indicadora funcionalitzada amb grups aminoetoxi com unitat complexant ; la coordinació amb el metall redueix la capacitat electro-donadora del àtom de nitrogen conjugat amb el cromòfor, produint-se uns canvis òptics apreciables a simple vista. El receptor preparat presenta una detecció selectiva al cations trivalents (Fe^{3+}, Al^{3+} y Cr^{3+}) amb notables límits de detecció. Els receptors derivats del BODIPY permeten la detecció selectiva del cations trivalents en medis aquosos.

La resta de la tesi es centra en la detecció i eliminació del simulants de agents nerviosos. Per a la detecció s´han dissenyat i preparat nous *sensors químics* basats en el cos de BODIPY. Aquests *sensors químics* s´han dissenyat de manera que continguin diferents grups de reacció, per tal d'evitar les interferències produïdes pels àcids o pels subproductes de hidròlisis, a més s'observa una resposta diferent per a cadascun dels simulants dels agents nerviosos de tipus G(DCNP amb DFP). Aquests sensors químics permeten la detecció a simple vista (mitjançant canvi de color) dels simulants dels agents nerviosos amb excel·lents límits de detecció. Els quimiosensors es van sostenir en suports sòlids per ampliar la seva aplicació pràctica en temps i ambients reals.

Per al desenvolupament de sensors per a la detecció d'agents nerviosos de tipus V s'ha emprat l'aproximació *d'assajos de desplaçament*. En base de lo descobert al segon capítol es varen dissenyar i preparar complexos de Eu^{3+} i Au^{3+} coordinats amb un lligand basat en el cos BODIPY. En aquest cas, el simulant d'agent nerviós de tipus V és capaç de coordinar-se amb el metall, alliberant el lligant. Aquest alliberament produeix canvis en les propietats òptiques del BODIPY observant canvis fàcilment detectables a simple vista.

Finalment, s'ha estudiat la possibilitat d´emprar catalitzadors supramoleculars per a l'eliminació dels agents nerviosos organofosforats. Els estudis d´hidròlisi es van dur a terme en presència de 1,3-diindolilureas i tiourees, amines, aminoalcols i glicols. L'addició del catalitzador incrementa el caràcter electrofílic del àtom de fòsfor, de manera que la velocitat de hidròlisi és molt més gran. Després del consegüent atac nucleofílic de l'aigua, s'alliberen els corresponents derivats organofosforats de menor toxicitat.

Abstract

The present PhD thesis entitled "*Design, Synthesis and Evaluation of Chromo-fluorogenic Probes for Contaminating Species"* is focused on the development of new chromo-fluorogenic sensors based on the principles of molecular recognition.

The first part of this thesis is focused on the design and synthesis of suitable organic compounds as sensors for metal cations. The selected sensing paradigm was the *binding site-signalling subunit* approach. The synthetized receptors employs a chromophore (fluorescein or BODIPY) skeleton as signalling subunit and it is functionalized with aminoethoxy moieties as binging site; the metal coordination reduces the electron-donating ability of the nitrogen atom conjugated to the chromophore resulting in optical changes noticeable to the naked-eye. The sensing behavior is highly selective to trivalent cations (Fe^{3+}, Al^{3+} and Cr^{3+}) with remarkable limits of detection. The receptors based on BODIPY-dyes retain the sensing abilities in mixed aqueous solutions.

The remaining chapters of the thesis are centered in the detection and removal of nerve agents surrogates. The design, synthesis, characterization and application of new BODIPY *chemosensors* were studied. These chemosensors were designed containing different reactive sites in order to avoid interferences produced by acids or hydrolysis products, and also be able to distinguish between the different G-nerve agent mimics (DCNP and DFP). The BODIPY-probes allows screening of nerve agent surrogates with remarkable limits of detection and optical changes noticeable to the naked-eye. The sensing abilities are retained in solid support, allowing practical application in real-time monitoring by simple colorimetric tests.

The *displacement assay* approach has been used to develop a selective sensor for V-nerve agent surrogates versus G-type. For this purpose, two Eu^{3+} and Au^{3+} BODIPY-complexes were prepared. In this case, V-surrogate is capable of coordinate the metallic center, releasing the BODIPY ligand. This causes a change in the optical properties visible to the naked-eye.

Finally, the use of supramolecular-based organocatalyst for destruction of OP nerve agent surrogates was studied. Hydrolysis studies were performed in presence of 1,3-diindolylureas and thioureas, amines, aminoalcohol and glycols. Addition of catalyst enhances the electrophilic character of the P atom, and the final nucleophilic attack of water that results in the formation of the corresponding less toxic organophosphate derivatives, thus higher hydrolysis rates are obtained.

Publications

The results of this PhD thesis have been included in the following scientific publications:

- **Andrea Barba-Bon**, Ana M. Costero, Salvador Gil, Margarita Parra, Juan Soto, Ramón Martínez-Máñez, and Felix Sancenón; "A new selective fluorogenic probe for trivalent cations", *Chem.Commun*., **2012**, *48*, 300-3002.

- **Andrea Barba-Bon**, Ana M.Costero, Margarita Parra, Salvador Gil, Ramón Martínez-Máñez, Félix Sancenón, Philip A. Gale and Jennifer R. Hiscock; "Neutral 1,3-Diindolylureas for Nerve Agent Remediation", *Chem. Eur.J.*, **2013**, *19*, 1586-1590.

- **Andrea Barba-Bon**, Laura Calabuig, Ana M. Costero, Salvador Gil, Ramón Martínez-Máñez, and Felix Sancenón; "Off-on BODIPY-based chemosensors for selective detection of Al^{3+} and Cr^{3+} versus Fe^{3+} in aqueous media", *RSC Adv*., **2014**, *4*, 8962-8965.

- **Andrea Barba-Bon**, Ana M. Costero, Salvador Gil, Anthony Harriman, and Felix Sancenón; "Highly Selective Detection of Nerve-Agent Simulants with BODIPY Dyes", *Chem.Eur.J.,* **2014**, *20*, 6339-6347.

- **Andrea Barba-Bon**, Ana M. Costero, Salvador Gil, Ramón Martinez-Mañez, and Felix Sancenón; "Chromo-fluorogenic BODIPY-complexes for selective detection of V-type nerve agent surrogate", *Chem. Commun*., **2014**, *50*, 13289-13291.

- **Andrea Barba-Bon**, Ana M. Costero, Salvador Gil, Ramón Martinez-Mañez, and Felix Sancenón; "Selective chromo-fluorogenic detection of DFP (a Sarin and Soman mimic) and DCNP (a Tabun mimic) with a unique probe based on a boron dipyrromethene (BODIPY) dye", *Org. Biomol. Chem.,* **2014**, *12*, 8745-8751.

- **Andrea Barba-Bon**, Ramón Martínez-Máñez, Felix Sancenón, Ana M.Costero, Salvador Gil, Francisco Pérez-Pla, and Elisa Llopis; "Towards the design of organocatalysts for nerve agents remediation: the case of the active hydrolysis of DCNP (a Tabun mimic) catalyzed by simple amine-containing derivatives", ***Submitted***

Abbreviations and Acronyms

BODIPY	4,4-difluoro-4-bora-3a,4a-diaza-s-indacene
$(EtO)_2OP\text{-}O\text{-}OP(EtO)_2$	Tetraethyl pyrophosphate
^{13}C-NMR	Carbon Nuclear Magnetic Resonance
^{1}H-NMR	Proton Nuclear Magnetic Resonance
^{31}P-NMR	Posphorous Nuclear Magnetic Resonance
abs	Absorbance
AChE	Acethyl-cholinesterase Enzime
Ar	Argon
$BF_3{\cdot}Et_2O$	Boron trifluoride diethyl etherate
BOC_2O	Di-tert-butyl dicarbonate
CaH_2	Calcium Hydride
CD_3CN	Acetonitrile-d3
$CDCl_3$	Chloroform-d
CF_3	Trifluoromethyl
CH_2Cl_2	Dichloromethane
CH_3Cl	Chloromethane
CH_3CN	Acetonitrile
Cl^-	Chloride
CN^-	Cyanide
CT	Charge transfer
CWA	Chemical Warfare Agent
d	Doublet
δ	Chemical Shift
D_2O	Deuterium Oxide
DCNP	Diethylcyanophosphonate
DCP	Diethylchlorophosphate
dd	Doublet of doublets
DDQ	2,3-Dichloro-5,6-dicyano-1,4-benzoquinone
DFP	Diisopropylfluorophosphate
DIPEA	*N,N*-Diisopropylethylamine
DMF	Dimethylformamide
DMSO	Dimethylsulfoxide
dt	Doublet of triplets
EDC·HCl	*N*-(3-Dimethylaminopropyl)-*N'*-ethylcarbodiimide hydrochloride
em	Emission

Et_3N	Triethylamine
EtOH	Ethanol
$Eu(NO_3)_3{\cdot}5H_2O$	Europium(III) nitrate pentahydrate
FRET	Fluorescence Resonance Energy Transfer
GC/MS	Gas Chromatography–Mass Spectrometry
GC-FID	Gas Chromatography – Flame Ionization Detector
h	Hours
H_2	Hydrogen
H_2SO_4	Sulfuric Acid
$HAuCl_4$	Chloroauric Acid
HCl	Hydrochloric acid
He	Helium
HOBt	1-Hydroxybenzotriazole hydrate
HOMO	Highest Ocupied Molecular Orbital
HRMS	Hight Resolution Mass Spectrometry
Hz	Hertz
ICT	Internal Change Transfer
J	J-coupling
K_2CO_3	Potassium Carbonate
KOH	Potassium Hydroxide
KPF_6	Potassium hexafluorophosphate
$LiAlH_4$	Lithium aluminium hydride
LUMO	Lowerst Unnocupied Molecular Orbital
m	Multiplet
MeOH	Methanol
MES	2-(*N*-Morpholino)ethanesulfonic acid hydrate,
$MgSO_4$	Magnesuim Sulfate
min	Minutes
mL	Mililitres
MOFs	Metal Organic Frameworks
MTHF	2-Methyltetrahydrofuran
Na	Sodium
$NaAuCl_4$	Sodium tetrachloroaurate(III) hydrate
$NaHCO_3$	Sodium bicarbonate
NaOH	Sodium hydroxide
NBS	*N*-Bromosuccinimide
***n*-BuLi**	*n*-Buthyllithium

NH_4OAc	Ammonium acetate
OH^-	Hydroxil
OPC	Organophosphorus compounds
P	Phosphorous
ϕ	Quantum yield
P_2O_5	Diphosphorus pentoxide
Pd	Palladium
Pd/C	Palladium on Carbon
PET	Photoinduced Electron Transfer
$PO(OH)(EtO)_2$	Diethylphosphoric acid
$PO_2(OEt)_2$	Diethylpyrophosphate
POPs	Porous Organic Polymers
ppm	Parts per million
PTC	Photoinduced Charge Transfer
q	Quartet
S	Single exited state
s	Singulet
S_E	Electrophilic substitution
S_EAr	Electrophilic aromatic substitution
S_NAr	Nucleophilic aromatic substitution
t	Triplet
T	Trple excited state
TBAOH	Tetrabutylammonium hydroxide solution
TEA	Triethylamine
TFA	Trifluoroacetic acid
THF	Tetrahydrofuran
TLC	Thin Layer Chromathography
UV	Ultraviolet
λ	Wavelength
ρ-chloranil	tetrachloro-1,4-benzoquinone,
ε	Molar absorption coefficient

Table of contents

Chapter 1:

General introduction

1.1 Molecular recognition

At the end of 19th century, H. E. Fisher defined the main principle in which molecular recognition is based when he suggested that the enzyme-substrate interactions take the form of "*lock and key".* According to this principle, molecular recognition can be defined as the selective interaction between a host molecule *(receptor)* and a guest molecule *(substrate)* through *non-covalent interactions*. To produce this recognition event, specific conditions of spatial and electronic compatibility must be satisfied; in which the guest has a geometric size or shape complementary to the host, thus enabling the discrimination by a host between a number of different guests. (see figure 1.1)

Bearing in mind this concept, in order to design a suitable receptor for a specific guest, some factors of the guest should be considered, as for example, the size, charge, geometry, hydrophobicity or lipophilicity or the possible formation of hydrogen bonds.

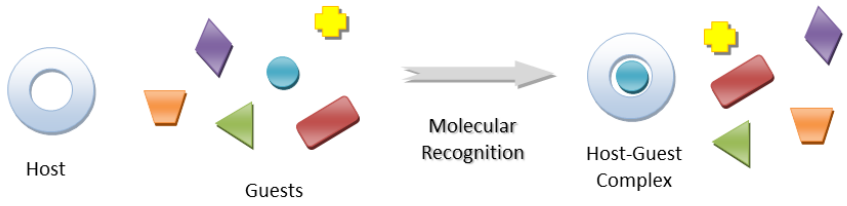

Figure 1.1. Scheme of a molecular recognition event: specific host-guest interaction.

The first receptors based on this principle were synthesized by Pedersen[1] ; they were crown ethers capable of coordinate alkali and alkaline cations. In the last decades, many advances have been achieved in this area and a myriad of receptors that mimic the behavior of biological systems have been described. These synthesized abiotic receptors are able to recognize cations, anions and neutral molecules.[2]

One of the major applications of these receptors is their use in the preparation of **molecular sensors**.

1.2 Chemosensors

A *molecular sensor* or *chemosensor* is a molecule that specifically interacts with an analyte producing a detectable and easy-to measure signal. In this sensing

[1] C. J. Pedersen, *J. Am. Chem. Soc.,* **1967**, *89*, 7017-7036.

[2] a) M. D. Best, S. L. Tobey, E. V. Anslyn, *Coord. Chem. Rev*., **2003**, *240*, 3-15. b) K. Severin, *Coord. Chem. Rev*., **2003**, *245*, 3-10. c) J. M. Llinares, D. Powell, K. Bowman-James, *Coord. Chem. Rev*., **2003**, *240*, 57-75. d) K. A. Schug, W. Lindner, *Chem. Rev*., **2005**, *105*, 67-113. e) P. Blondeau, M. Segura, R. Pérez-Fernández, J. de Mendoza, *Chem. Soc. Rev*., **2007**, *36*, 189-197. f) J. W. Steed, *Chem. Soc .Rev.*, **2009**, *38*, 506-519. g) Z. Xu, S. K. Kim J. Yoon, *Chem. Soc. Rev*., **2010**, *39*, 1457-1466.

process, information at the molecular level, such as the presence or not of a certain guest, is amplified to a macroscopic level; therefore sensing might open the door to the determination (qualitative or quantitative) of certain guests. A good sensor must fulfill a number of requirements such as: selective recognition, the interaction should be reversible and not slow to allow real-time readings.

Whereas *chemical sensors* (or *chemosensors*) usually refer to systems that typically employ coordinative forces for guest binding, the term *chemodosimeter* (or *reagents)* is related with the use of specific irreversible reactions involving guests.[3] A chemosensor or chemodosimeter is usually composed by two units:

- A *receptor subunit*, which is the unit responsible of the recognition event and grants the specificity of the interaction with a particular analyte, allowing the discrimination between a number of different substrates. The receptor subunit must be designed in order to achieve a selective coordination with the target guest; a high degree of complementarity between the receptor and the guest (in terms of size, shape, charge, etc.) is mandatory.

- A *signaling subunit*, which acts as a signal transducer, and informs that the recognition process, that occurs at molecular level, through changes in a measurable macroscopic signal. Traditionally, changes in the optical properties (colour or fluorescence) or a modification in the electrochemical properties (redox potential) have been used as signal outputs.

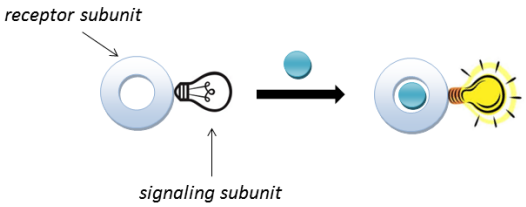

Figure 1.2. Schematic representation of a chemosensor.

[3] M. E. Moragues, R. Martínez-Máñez, F. Sancenón, *Chem. Soc. Rev.*, **2011**, *40*, 2593-2643.

Among the changes to be observed, the simple instrumentation required (using colorimetric signalling) and the low detection limit usually obtained (especially using fluorescence signalling) make the optical approach largely appealing when compared for instance with electrochemical approximation.

There are three main approaches to the design of optical chemical sensors. The choice of one or another format depends on selectivity to be achieved and the synthetic effort required to obtain the sensor/chemosensor. (see also Figure 1.2)

- *Binding site–signalling subunit approach:* Chemosensors based on this approach are formed by two subunits namely a "binding site" and a "signaling subunit" that are covalently linked. The interaction of guest with the binding site changes the electronic properties of the signaling subunit resulting in a sensing event via color or emission modulation.[4] This is still the most widely used approach in the development of chemosensors.

- *The displacement approach*: In this approach the selected receptor (binding site/receptor unit) forms an inclusion complex with a dye (signaling subunit). The sensing paradigm relies on a displacement reaction because the coordination of the target molecule with the receptor induced the release of the dye. An optical response is obtained because the color or emission of the signaling subunit in the sensing ensemble is different than those presented when it is free in solution.[5] Based on this principle, the main requirement is that the stability constant of the "receptor-dye" complex should be lower than the stability constant of the "receptor-target molecule" complex.

[4] a) T. S. Snowden and E.V. Anslyn, *Chem. Biology*, **1999**, *3, 740*-746. b) T. Gunnlaugsson, M. Glynn, G. M. Tocci, P. E. Kruger, F. M. Pfeffer, *Coord. Chem. Rev*., **2006**, *250*, 3094-3117.

[5] a) S. L. Wiskur, H. Ait-Haddou, J. J. Lavigne, E. V. Anslyn, *Acc. Chem. Res*., **2001**, *34*, 963-972. b) B. T. Nguyen, E. V. Anslyn, *Coord. Chem. Rev*., **2006**, *250*, 3118-3127.

- The *''chemodosimeter'' approach*: In this approach the target molecule induced specific chemical reactions (generally irreversible) and commonly involves the rupture and/or formation of covalent bonds. In general, there is a remarkable chemical modification of the molecular probe after reaction with the target molecule and therefore this approach is usually associated with remarkable spectroscopic modulations.[6]

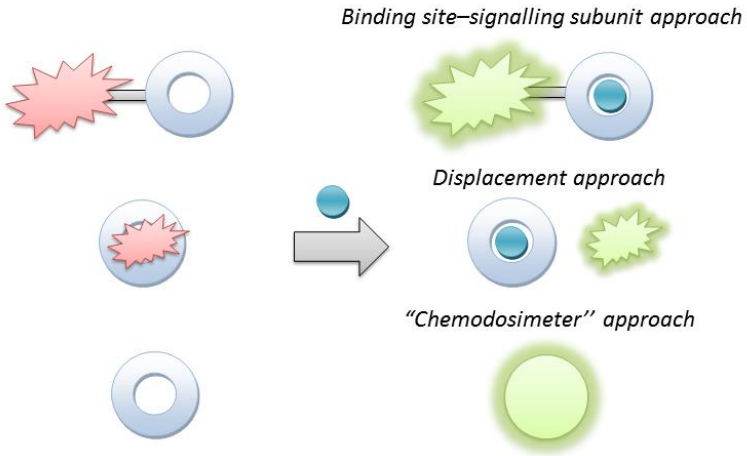

Figure 1.3. Schematic representation of the three main paradigms used in the development of chemosensors.

Whereas in the chemodosimeter approach the objective is to find specific reactivity, the goal in both, the binding site-signaling subunit and displacement approaches, is to find systems displaying a selective coordination.

Due to the advantages presented by optical sensors over electrochemical sensing (non-destructive detection method, uses simple and extended instrumentation, needs small amounts of samples and usually allows in situ detection and in real-time measurements) this doctoral thesis will be concentrate on the use of optical sensors for the detection of contaminating species such as trivalent cations and

[6] a) M-Y. Chae and A.W.Czarnik, *J. Am. Chem. Soc.*, **1992**, *114*, 9704-9705.b) S. Solé and F. P. Gabbaï, *Chem. Commun*., **2004**, 1284–1285.

neutral molecules (nerve agents). Therefore, a more extensive introduction will follow on the concept of optical sensors as well the response mechanisms after coordination with the species of interest.

1.3 Optical Sensors

Optical sensors represent a group of chemical sensors in which electromagnetic radiation is used as signal after analytical recognition. Optical sensors can be based on various optical principles (absorbance, reflectance, luminescence, fluorescence), covering different regions of the spectra (UV, visible, IR, NIR) allowing measurement not only of the intensity of light but also other related properties as lifetime, refractive index, diffraction, etc…
However, for sensor applications, the most commonly applied methods in optical sensing are those based on light absorption or light emission.

1.3.1 Optical detection principles

Color is a visual perception generated in the brain to interpret nerve signals perceived by the photoreceptors of the ocular retina, which in turn is able to interpret and distinguish the different wavelengths of the electromagnetic spectrum. Color derives from the spectrum of light interacting in the eye with the spectral sensitivities of the light receptors.
Every illuminated surface absorbs some of the electromagnetic waves and reflects the others. The reflected waves are captured by the retina and interpreted by the brain as colors. There are two kinds of visible objects: those that emit light by themselves and those who reflect the light. For the latter, the color depends on the spectrum of the incident light and the absorption of the object, which determines which waves are reflected. The human vision is adapted to sense different colors in a small range of the whole electromagnetic radiation: visible

spectrum. The observed colors are determined by the spectral distribution of the transmitted radiation.[7]

Electromagnetic radiation such as visible light is commonly treated as a wave phenomenon, characterized by a wavelength or frequency. Visible wavelengths cover a range from approximately 400 to 800 nm (figure 1.4).

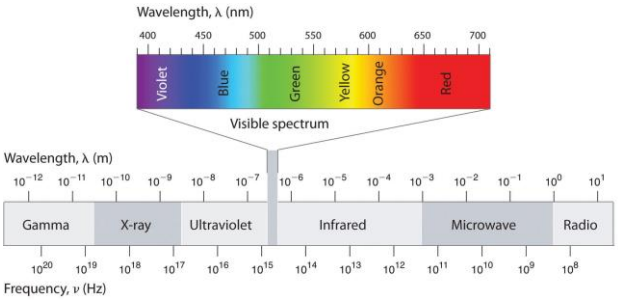

Figure 1.4. Electromagnetic spectra.

The absorption of visible or ultraviolet radiation may result in the electron transitions between the ground state and the excited states of atoms and/or molecules.[8]

The electrons in a molecule can be of one of three types: namely σ (single bond), π (multiple-bond), or n- (non-bonding; caused by lone pairs). These electrons when imparted with energy in the form of light radiation get excited from the highest occupied molecular orbital (HOMO) to the lowest unoccupied molecular orbital (LUMO) and the resulting species is known as the excited state or anti-bonding state (figure 1.5).

- *σ-bond electrons* have the lowest energy level and are the most stable electrons. These would require a lot of energy to be displaced to higher energy levels. As a result these electrons generally absorb light in the lower wavelengths of the ultraviolet light and these transitions are rare.
- *π-bond electrons* have much higher energy levels for the ground state. These electrons are therefore relatively unstable and can be more easily

[7] R. C. Denney, R. Sinclair, *Visible and Ultraviolet Spectroscopy*, John Wiley & Sons. Ed., **1987**.
[8] T. Engel and P. Reid, *Physical Chemistry*, Pearson new International edition, **2012**.

excited and would require lesser energy for excitation. These electrons would therefore absorb energy in the ultraviolet and visible light radiations.

* *n-electrons* or *anti-bonding electrons* are generally electrons belonging to lone pairs of atoms. These are of higher energy levels than π-electrons and can be excited by ultraviolet and visible light.

Most of the absorption in the ultraviolet-visible spectroscopy occurs due to π-electron transitions or n-electron transitions.

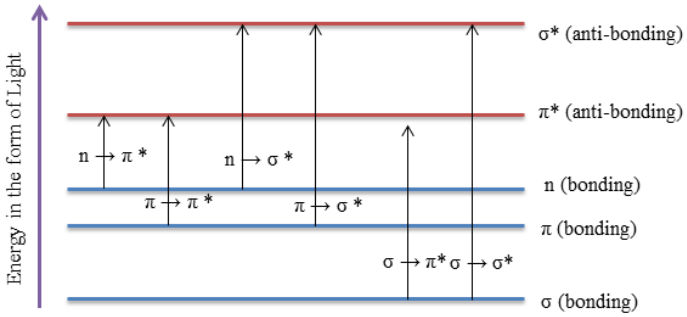

Figure 1.5. Electron transitions in ultraviolet/visible spectroscopy.

Light absorbed by molecules can be emitted by luminescent processes. In general, luminescence is the emission of light from an electronically excited state of any substrate and consists of two mains categories: *fluorescence* (is the emission arising from a single excited state; S) and *phosphorescence* (which describes the emission occurring from a triplet excited state; T).[9] The terminologies *singlet* and *triplet excited state* describe the nature of the excited state orbital with respect to that of the ground state orbital. While a singlet excited state describes the promotion of the electron to an orbital where the spin is conserved by light excitation, in a triplet excited state the excited electron has "twisted" its spin state which in most cases is a process energetically unfavorable.

In 1935, Jablonski interpreted the various fates of an excited species at the electronic level by representing a diagram (See figure 1.6).[10]

[9] B. Wang and E. V. Anslyn, *Chemosensors: Principles, Strategies and Applications*, John Wiley & Sons, Inc. **2011**.

[10] H. Xu, R. Chen, Q. Sun, W. Lai, Q. Su, W. Huang and X. Liu , *Chem. Soc. Rev*., **2014**, *43*, 3259-3302.

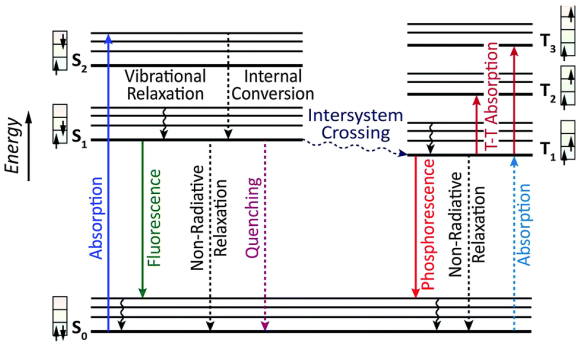

Figure 1.6. Jablonski energy level diagram.

The absorption process occurs primarily between the ground state S_0 and the singlet states S_1, S_2, etc. This process is fast, usually taking place within 10^{-15} s. The principal fluorescence emission is generally induced by the transition from the lowest excited singlet state S_1 to the ground state irrespective of the initial state excited. This can be ascribed to the rapid non-radiative process of internal conversion between higher excited states S_2, S_3, etc... and the lowest excited state S_1. Non-radiative processes can also be observed in intersystem crossing from the singlet manifold to the triplet manifold and *vice versa*. The radiative decay from the excited triplet state back to a singlet state is known as phosphorescence ($T_1 \rightarrow S_0$). The excited state can also be deactivated by other ways than luminescence. This is referred to as *quenching* of the excited state, which can occur through thermal deactivation, by collision with solvent molecules, or by other external influences such as energy transfer from other molecules.

The energy needed to produce an excited state depends directly on the gap between the ground and excited state which differs among molecules. Depending on the size of this energy gap, the fluorescence can occur at high energy and short wavelengths (referred as *short* or *blue emission*, occurring underneath 430 nm), within the visible region (430-800 nm referred as *long emission*) and within the near-infrared regions (800-1600 nm, *NIR emitters*).

Alternatively, the formation of the excited state can also occur by indirect excitation, by a sensitizing antenna[11] or a chromophore than can pass on its excited state energy to the receiving substrate.[12]

1.3.2 Chromogenic sensors

Color changes as signaling events have been widely used because it requires the use of inexpensive equipment or no equipment at all as color changes can be detected by the naked eye. The colorimetric sensors have been widely used for cations, anions and neutral molecules.[13] Organic compounds become colored by absorbing electromagnetic radiation in the visible range and investigations related with the correlation between chemical structure and color in organic dyes have been carried out extensively. Many dyes contain systems of conjugated bonds, and the energy gap between the HOMO and the LUMO is critical in determining the color of a certain organic dye. Is well-established that the larger the conjugated system is, the shorter the difference between fundamental and excited states, resulting in a more bathochromic shift of the absorption band of lesser energy.[14] Along with the incremental conjugation, the absorption wavelength can be modified by anchoring electron donor (NR_2, NHR, NH_2, OH, OMe, etc.) or electron acceptor (NO_2, SO_3H, SO_3^-, COOH, CN, etc.) groups to the conjugated system. When both an electron donor and an electron acceptor group are connected through a conjugated system in a certain molecule, a Charge Transfer (CT) band can be observed. This corresponds to a CT transition where, upon excitation with light, there is an important fraction of electronic charge that is transferred from the donor to the acceptor. What is important, related to the design of chromogenic reagents, is that the interaction of analyte with the donor

[11] R. Ziessel and A. Harriman, *Chem. Commun*, **2011**, *47*, 611-631.
[12] A.P. de Silva, H. Q. N. Gunaratne, T. Gunnlaugsson, A. J. M. Huxley, C. P. McCoy, J. T. Rademacher and T.E. Rice, *Chem. Rev*. **1997**, *97*, 1515−1566.
[13] a) F. P. Schmitdchem, M. Berguer, *Chem. Rev.* **1997**, *97*, 1609- 1646.b) P. Anzenbacher, Jr., A. C. Try, H. Miyaji, K. Jursíkova ,V. M. Lynch, M. Marquez and J. L. Sessler*, J. Am. Chem. Soc*., **2000,** *122*, 10268–10272.c) G. J. Mohr , *Anal. Chim. Acta*, **2004**, *508*, 233–237. d) G. Y. Qing, T. L. Sun, F. Wang, Y. B. He and X. Yang, *Eur. J. Org. Chem*., **2009**, 841–849
[14] H. Zollinguer, *Color Chemistry*, VCH, Weinheim, **1991**.

or acceptor groups in those systems affect the position of the charge transfer band resulting in a color modulation. Thus, for instance, the interaction of a cation with a donor group will make it less donor, pumping fewer electrons to the conjugated system, inducing a hypsochromic shift (blueshift). Conversely if the cation interacts with the acceptor group, the excited state is more stabilized than the fundamental, causing a bathochromic shift (redshift) in the absorption band of the chromophore (see figure 1.7).

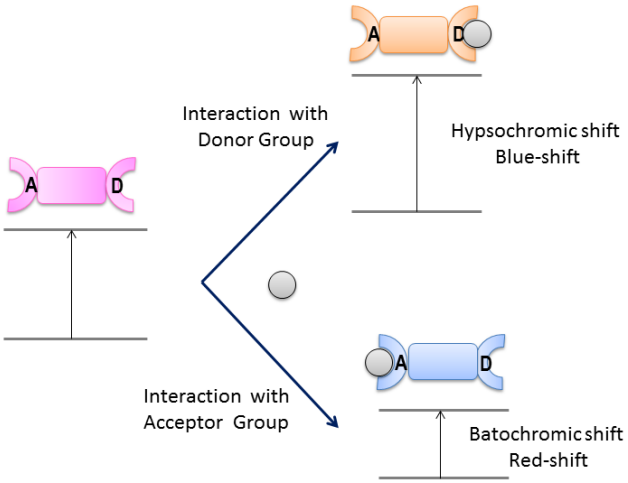

Figure 1.7. CT in chromogenic electron donor-aceptor sensors.

1.3.3 Fluorescent sensors

Fluorescence spectroscopy, fluorescence imaging and fluorescence indicators are nowadays indispensable tools in various fields in modern science and medicine, including clinical diagnostics, biotechnology, molecular biology and biochemistry, materials science and analytical and environmental chemistry[15] due to the fine instrument manipulability, commercial availability, lower detection limits and *in situ* and *in vivo* detection ability.[16]

[15] a) E. V. Anslyn, *Curr. Opin. Chem. Biol*., **1999,** *3*, 740-746.b) M. E. Jun, B. Roy and K.H. Ahn, *Chem.Commun*., **2011**, *47*, 7583-7601.c) N. Boens, V. Leen and W. Dehaen, *Chem. Soc. Rev*., **2012,** *41*, 1130-1172.

[16] H. Kobayashi, M. Ogawa, R. Alford, P. L. Choyke and Y. Urano, *Chem. Rev*. **2010**, *110*, 2620–2640.

There are different photoluminescent mechanisms involved in the detection of analytes; the most widely used are:

- ***Photoinduced Electron Transfer (PET):*** As described above, fluorescence in a molecule is observed when an excited electron, for instance in the LUMO, goes to the HOMO, releasing the excess of energy as light. Thus, when a lone electron pair is located in an orbital of the fluorophore itself or an adjacent molecule and the energy of this orbital lies between those of the HOMO and LUMO, efficient electron transfer of one electron of the pair to the hole in the HOMO created by light absorption may occur, followed by transfer of the initially excited electron to the lone pair orbital providing a mechanism for non-radiative deactivation of the excited state (see figure 1.8), leading to a "*quenching*" of the fluorescence.[17] Fluorescence quench as a result of PET may be recovered if it is possible to involve the lone pair in a bonding interaction. Thus, protonation or binding effectively places the electron pair in an orbital of lower energy and inhibits the electron-transfer process.[18]

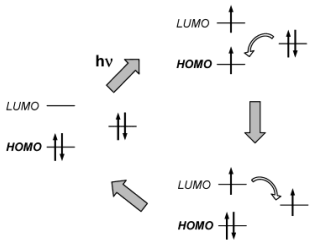

Figure 1.8. Mechanism for PET system.

- ***Photoinduced Charge Transfer (PCT):*** Electronic excitation involves some degree of charge transfer, but in fluorophores containing electron donor and acceptor substituents, this charge transfer may occur over long distances and be associated with major dipole moment changes, making the process particularly sensitive to the microenvironment of the fluorophore.[17] Thus,

[17] a) H.F. Ji, G. M. Brown and R. Dabestani, *Chem. Commun*. **1999**, *7*, 609-610. b) J. S. Kim and D.T. Quang, *Chem. Rev*., **2007**, *107*, 3780-3799.
[18] H.F. Ji, G. M. Brown and R. Dabestani ,*J. Am. Chem. Soc*. **2000**, *122*,9306-9307.

interaction of the target molecule with the donor or acceptor moiety will change the photophysical properties of the fluorophore; shifts on the emission spectra, changes in quantum yields and lifetimes can be observed. [19]

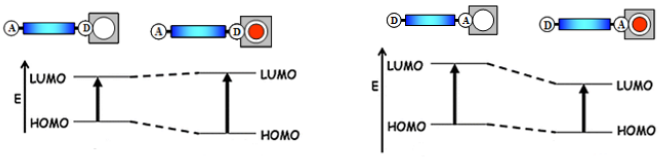

Figure 1.9. Mechanism for PCT system.

× ***Excimer Formation:*** An excimer can be defined as a complex formed by interaction of a fluorophore in the excited state with another fluorophore of the same structure in its ground state.[20] Compared with the monomer the excimer typically provides a redshifted and broad emission band, and in several cases both emission bands of the monomer and the excimer are observed simultaneously.[21] A requirement for excimer formation is that two monomers need to be in close proximity in order to give stacking interactions and the molecular excimer state.

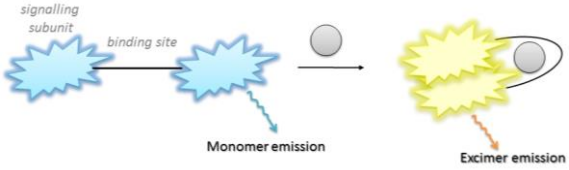

Figure 1.10. Excimer formation fluorescent system.

× ***Fluorescence Resonance Energy Transfer (FRET):*** also known as Förster Resonance Energy Transfer; is a non-radiative process between a pair of

[19] a) M. Narita, Y. Higuchi, F. Hamada and H. Kumagai, *Tetrahedron Lett*. **1998**, *39*, 8687-8690. b) R. Metivier, I. Leray and B. Valeu, *Chem.Commun*. **2003**, *8*, 996-997.
[20] a) R. Martnez-Mañez and F. Sancenon, *Chem. Rev.* **2003**,*103*, 4419-4476. b) A. M .Costero, M. Colera, P. Gaviña and S. Gil, *Chem. Commun*., **2006**,761-763.
[21] M. A. McKewey, E. M. Seward, G. Ferguson, B. Ruhl and S. J. Harrisc, *Chem. Commun*. **1985**, 388-390.

dissimilar fluorophores in with one act as a donor of excited-state energy to the other (acceptor). The donor returns to its electronic ground state, and the observed emission is from the acceptor fluorophore (see Figure 1.11). FRET is influenced by three factors: the distance between the donor and the acceptor, the extent of spectral overlap between the donor emission and acceptor absorption spectrum and the relative orientation of the donor emission dipole moment and acceptor absorption moment.[22]

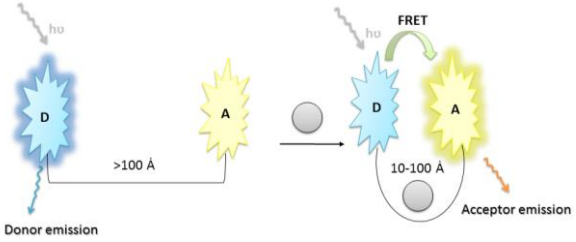

Figure 1.11. Schematic diagram of the FRET sensing.

1.3.4 Design principles

Summarizing, an optical sensor consists in a compound incorporating a binding site (a chromophore or a fluorophore) and a mechanism for communication.[23] In presence of the target molecule, the receptor modifies their electronic properties displaying changes in either color or in fluorescence or in both. Optical sensing (colorimetric and/or fluorescent) is particularly appealing because:

- ✓ Requires easily, low-cost and widely used instrumentation.
- ✓ Offers the possibility of detecting the target molecule "to the naked eye".
- ✓ They are non-destructive detection methods.
- ✓ Requires small amounts of sample.
- ✓ Performs a rapid detection of the guest.
- ✓ Allows real time monitoring.

[22] a) Z. Zhou, M. Yu, H. Yang, K. Huang, F. Li, T. Yi and C. Huang, *Chem. Commun*., **2008**, *29*, 3387–3389. b) K. Sreenath, J. R. Allen, W. M. Davidson and L. Zhu, *Chem .Commun*., **2011**, *47,* 11730-11732. c) N. Kumar, V. Bhalla and M. Kumar, *Analyst*, **2014,** *139*, 543-558.

[23] A. W. Czarnik, *Acc. Chem. Res*., **1994**, *27*, 302-308.

In view of these benefits we decided to design new chromo-fluorogenic sensors for the detection of contaminating species. Among the numerous classes of colorimetric and fluorescent dyes,[24] the set based on 4,4-difluoro-4-bora-3*a*,4*a*-diaza-*s*-indacene[25] (hereafter known as BODIPY; difluoro*bo*ron *dipy*rromethene) is perhaps the most promising. Therefore it has been the base of *signaling subunit* in most of the sensors designed and evaluated in this thesis.

1.4 BODIPY dyes

Although the first BODIPY was reported by Treibs and Kreuzer in 1968, [26] their possible uses for biological labeling, for electroluminescent devices, as tunable laser dyes, as potential candidates for solid-state solar concentrators, as fluorescent switches and as fluorophores in sensors and labels were fully recognized only since the mid-1990s.[27] Since then, the number of research papers and patents has increased. This growing success can be explained because of its outstanding photophysical properties such as excitation/emission wavelengths in the visible spectral region (≈500 nm), the relatively high molar absorption coefficients (ε) and fluorescence quantum yields (ϕ), fluorescence lifetimes (τ) in the nanosecond range and negligible triplet-state formation. They are relatively insensitive to the pH and they present good solubility, resistance towards self-aggregation in solution and robustness against light and chemicals.[28] Moreover, the spectroscopic and photophysical profiles can be switched by introducing different electron releasing/withdrawing groups at the appropriate positions of the BODIPY-core.

[24] R. P. Haugland, *The Handbook. A Guide to Fluorescent Probes and Labeling Technologies, Molecular Probes,* Invitrogen, Carlsbad, CA, 10th ed. **2005**.
[25] A. Loudet and K. Burgess, *Chem. Rev*., **2007**, *107*, 4891-4932.
[26] A. Treibs and F.H. Kreuzer, *Liebigs. Ann. Chem*., **1968**,*718*, 208-223.
[27] N. Boens, V. Leen and W. Dehaen, *Chem. Soc. Rev*., **2012**, *41*, 1130-1172.
[28] a) R. Ziessel, G. Ulrich and A. Harriman; *New. J. Chem.,* **2007**,*31*, 496-501. b) G. Ulrich, R. Ziessel and A. Harriman, *Angew. Chem. Int. Ed.*, **2008**, *47*, 1184-1201.

1.4.1. The BODIPY core

The IUPAC numbering system for BODIPY dyes is different to that used for dipyrromethenes,[29] however, the terms α-, β-positions, and *meso*- are used in the same way for both systems. The numbering of any substituents follows rules set up for the carbon polycycle *s*-indacene; Figure 1.12 shows the representation of the BODIPY framework with the numbering. The 8-position is often specified by *meso*-. The 3,5- positions are sometimes referred to by α, while β is used to denote the 2,6-positions. All the positions of the BODIPY core are possible sites for functionalization.

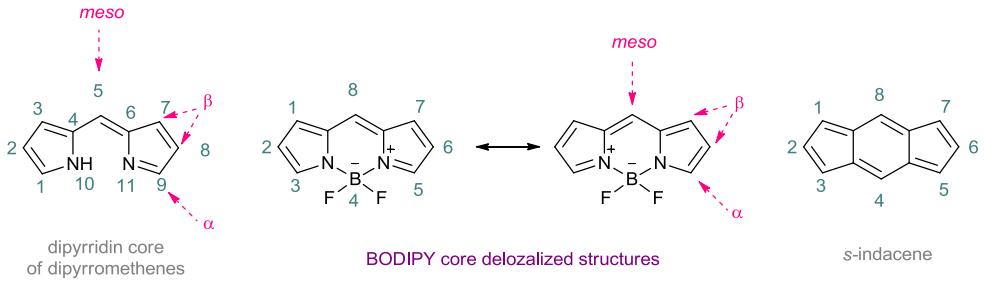

Figure 1.12. The "BODIPY-core".

1.4.2. Synthesis of BODIPY core

BODIPY dyes tend to be relatively easy to prepare from commercially available pyrrole-based materials, often in high yield and multi-gram quantity. Different approaches have been described to the synthesis of the BODIPY dyes:

- ***Synthesis from pyrroles and aldehydes:*** The acid-catalyzed condensation of aldehydes with pyrrole affords dipyrromethanes (**III**), which are used immediately after preparation (because they are sensitive to light, air and acid, they are unstable compounds). Oxidation of dipyrromethane yields a dipyrromethene (or dipyrrin) (**IV**). This oxidation can be carried out with 2,3-dichloro-5,6-dicyano-*p*-benzoquinone (DDQ) or 2,3,5,6-tetrachloro-*p*-

[29] H. B. F.Dixon, A. Cornish-Bowden, C. Liebecq, K. L. Loening, G. P. Moss, J. Reedijk, S. F. Velick, P. Venetianer and J. F. G. Vliegenthart, *Pure Appl. Chem.* **1987**, *59*, 779-832.

benzoquinone (*p*-chloranil).The boron difluoride bridging unit is introduced by treatment with boron trifluoride diethyl etherate ($BF_3.Et_2O$) in the presence of a base[30] (scheme 1.1).

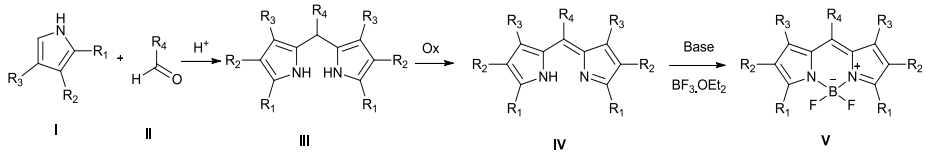

Scheme 1.1. General outline of a typical synthesis by condensation of a pyrrole with an aldehyde.

× ***Synthesis from pyrroles and acid chlorides or anhydrides:*** Other route is based on the condensation of a pyrrole with an acylium equivalent (**VI**). The intermediate acylpyrrole (**VII**) reacts under acidic conditions with an excess of pyrrole(**VIII**) to form a dipyrrinium salt (**IX**). Again, application of an excess of base and $BF_3.Et_2O$ yields the BODIPY dye (**X**).[31] The particular advantage of this approach lies in the possibility of the synthesis of asymmetric BODOPY dyes, because the isolated acylpyrrole can be combined with a second (different) pyrrole moiety in an acidic condensation. The acylium equivalent can be an acid chloride[32] an acid anhydride[33] or an orthoester[34] (scheme 1.2)

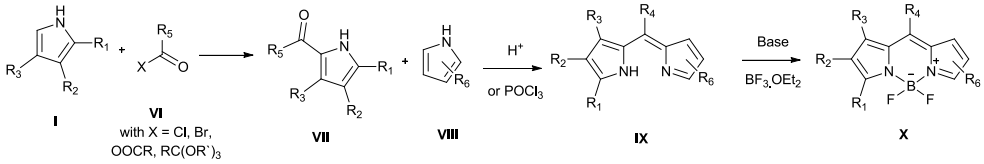

Scheme 1.2. Outline for the synthesis of asymmetric BODIPY dyes.

[30] a) R. W. Wagner and J. S. Lindsey, *Pure Appl. Chem.,* **1996,** *68*, 1373-1380. b) S. Y. Moon, N. R. Cha, Y. H. Kim and S. K. Chang, *J. Org. Chem.,* **2004**, *69*, 181-183. c) M. Baruah, W. Qin, N. Basaric, M. De Borggraeve, M. Wim and N. Boens, *J. Org. Chem.* **2005**, *70*, 4152-4157.

[31] M. Shah, K. Thangaraj, M. L. Soong, L. T. Wolford, J. H. Boyer, I. R. Politzer and T. G. Pavlopoulos, *Heteroat. Chem*., **1990**, *1*, 389–399.

[32] J. H. Boyer, A. M. Haag, G. Sathyamoorthi, M. L. Soong, K. Thangaraj and T. G. Pavlopoulos, *Heteroat. Chem*., **1993**, *4*, 39–49.

[33] Z. Li, E. Mintzer and R. Bittman, *J. Org. Chem.,* **2006**, *71*, 1718–1721.

[34] V. P. Yakubovskyi, M. P. Shandura and Y. P. Kovtun, *Eur. J. Org. Chem*., **2009**, *19*, 3237–3243.

× ***Synthesis from an acylated pyrrole:*** A third route, is an alternative described by Wu and Burgess; [35] is the condensation of an acylated pyrrole (**XI**). A second pyrrole equivalent is not always required, and phosphorus oxychloride is able to promote the condensation of pyrrole-2-carbaldehyde with itself. In the proposed mechanism, phosphorus oxychloride substitutes the aldehyde oxygen, resulting in a chlorinated azafulvene (**XII**), which is attacked by a second pyrrole aldehyde. Subsequent nucleophilic attack by chloride, followed by decomposition of the unstable intermediate, yields dipyrrinium (**XV**). The dipyrromethene can undergo complexation with excess of base and $BF_3.Et_2O$ to yield the symmetric BODIPY (**XVI**). The products, arising from a one-pot procedure and requiring minor purification, are generally obtained in high yields (scheme 1.3).

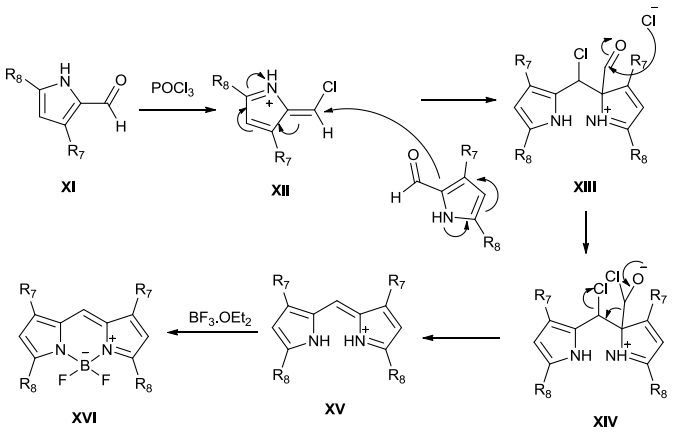

Scheme 1.3. Condensation-decarbonylation of pyrrole-2-carbaldehydes.

1.4.3. Derivatization of the BODIPY core

The versatility of the BODIPY scaffold is because of its synthetic adaptability. Progresses in BODIPY chemistry make possible to build dyes by postfunctionalization of the BODIPY core instead by starting from appropriately substituted pyrroles. By connecting suitable electron releasing/withdrawing groups to the BODIPY core, its spectroscopic and photophysical profiles can be tuned. The 3,5-positions can undergo nucleophilic aromatic substitution (S_NAr)

[35] L. Wu and K. Burgess, *Chem. Commun*., **2008,** 4933–4935.

(including thiol-halogen S_NAr), direct hydrogen substitutions, direct styrylation, and Pd-catalyzed cross-coupling or electrophilic substitution with NBS and Knoevenagel-type reaction on methyl groups.[36] It is possible to operate electrophilic aromatic substitution (S_EAr), direct hydrogen substitutions and Pd-catalyzed cross-coupling in the 2,6- positions.[37] The 1,7-positions can be halogenated and further substituted by S_NAr or Pd-catalyzed cross-coupling reactions.[38] S_NAr, Liebeskind cross-coupling and installation of a meso-CF_3 group at the 8-position are possible.[39] In addition nucleophilic substitutions (S_N) of fluorine by oxygen or carbon nucleophiles on the boron center have been reported[40] (figure 1.13).

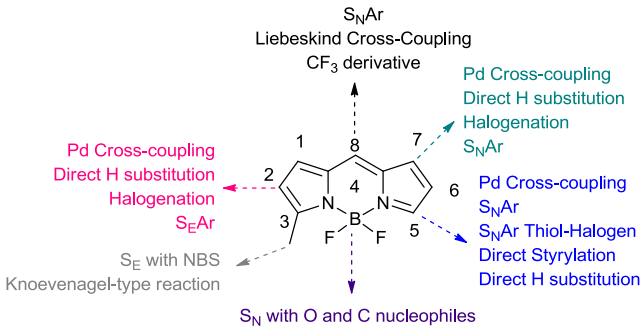

Figure 1.13. Derivatization of BODIPY-core.

[36] a) B. Verbelen, V. Leen, L. Wang, N. Boens and W. Dehaen, *Chem. Commun.*, **2012**, *48*, 9129–9131. b) L. Y. Niu, Y. S. Guan, Y. Z. Chen, L. Z. Wu, C. H. Tung and Q. Z. Yang, *J. Am. Chem. Soc.*, **2012**, *134*, 18928–18931. c) G. Ulrich, R. Ziessel and A. Haefele, *J. Org. Chem*., **2012**, *77*, 4298–4311. d) L. Wang, B. Verbelen, C. Tonnele, D. Beljonne, R. Lazzaroni, V. Leen, W. Dehaen and N. Boens, *Photochem. Photobiol. Sci.*, **2013**, *12*, 835–847. e) V. Leen, M. Van der Auweraer, N. Boens and W. Dehaen, *Org. Lett.*, **2011**, *13*, 1470–1473.

[37] a) H. He and D. K. P. Ng, *Org. Biomol. Chem*., **2011**, *9*, 2610-2613. b) W. Wu, H. Guo, W. Wu, S. Ji and J. Zhao, *J. Org. Chem*., **2011**, *76*, 7056-7064.c) W. J. Shi, P. C. Lo, A. Singh, I. Ledoux-Rak and D. K. P. Ng, *Tetrahedron*, **2012**, *68*, 8712-8718. d) A. Bessette and G. S. Hanan, *Chem. Soc. Rev.*, **2014**, *43*, 3342-3405.

[38] V. Leen, D. Miscoria, S. Yin, A. Filarowski, J. Molisho-Ngongo, M. Van der Auweraer, N. Boens and W. Dehaen, *J. Org. Chem*., **2011**, *76*, 8168–8176.

[39] a) T. V. Goud, A. Tutar and J. F. Biellmann, *Tetrahedron*, **2006**, *62*, 5084–5091. b) E. Peña-Cabrera, A. Aguilar-Aguilar, M. Gonzalez-Dominguez, E. Lager, R. Zamudio-Vazquez, J. Godoy-Vargas and F. Villanueva-Garcia, *Org. Lett*., **2007**, *9*, 3985–3988. c) L. N. Sobenina, A. M. Vasiltsov, O. V. Petrova, K. B. Petrushenko, I. A. Ushakov, G. Clavier, R. Meallet-Renault, A. I. Mikhaleva and B. A. Trofimov, *Org. Lett*., **2011**, *13*, 2524–2527.

[40] a) C. Goze, G. Ulrich, L. J. Mallon, B. D. Allen, A. Harriman and R. Ziessel, *J. Am. Chem. Soc*., **2006**, *128*, 10231–10239. b) C. Tahtaoui, C. Thomas, F. Rohmer, P. Klotz, G. Duportail, Y. Mely, D. Bonnet and M. Hibert, *J. Org. Chem*., **2007**, *72*, 269–272. c) P. Didier, G. Ulrich, Y. Mely and R. Ziessel, *Org. Biomol. Chem.*, **2009**, *7*, 3639–3642.

Replacement of C-8 in the BODIPY by nitrogen gives the called "AzaBODIPYs"[41] (figure 1.14). These are an extremely interesting set of dyes because the *meso*-nitrogen induces a large redshift in both the absorption and fluorescence emission. Nearly all the substituted compounds feature aryl groups in the 3,5-positions. To date, some NIR fluorescent probes based on the aza-BODIPY scaffold for various targets (metal ions, H^+, anions and small biomolecules) have been reported.[41]

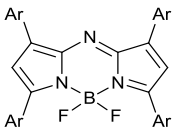

Figure 1.14. AzaBODIPYs.

1.4.4. Applications

In addition to the numerous synthetic advantages offered by BODIPY dyes, they are tolerant to a wide range of photochemical, thermal, pH, polarity and solubility conditions. Their stability in physiological environments makes them a prime choice for image techniques and protein labeling.[42] In 2007, Peng´s group reported the first intracellular emission fluorescent Cd^{2+} sensor **1** based on the ICT mechanism.[43] In sensor **1**, BODIPY was chosen as fluorophore and *N,N*-bis(pyridin-2-ylmethyl)benzenamine as Cd^{2+} receptor (and ICT donor). The λ_{abs} in the absorption spectra of free **1** in the ICT band is near 600 nm when Cd^{2+} was added gradually, the λ_{abs} showed a 29 nm blue shift and the color of the solution turned from light blue to bright pink. The fluorescence of **1** with physiologically important

[41] a) J. Killoran, L. Allen, J. Gallagher, W. Gallagher and D. O'Shea, *Chem. Commun*., **2002**, 1862-1863. b) A. Gorman, J. Killoran, C. O'Shea, T. Kenna, W. Gallagher, D. O'Shea, *J. Am. Chem. Soc.,* **2004**, *126*, 10619-10631. c) S. O. McDonnel and D. O'Shea, *Org. Lett.,* **2006**, *8*, 3493-3496.

[42] a) Do. Wang, J. Fan, X. Gao, B. Wang, S. Sun, and X. Peng, *J. Org. Chem*. **2009**, *74*, 7675–7683.b) J. J. Lee, S.C. Lee, D. Zhai, Y.H. Ahn, H. Y. Yeo, Y. L, Tana and Y. T. Chang, *Chem. Commun.,* **2011**, *47*, 4508–4510.c) R. Weinstain, J. Kanter, B. Friedman, L.G. Ellies, M.E. Baker, and R. Y. Tsien *Bioconjugate Chem.,* **2013**, *24*, 766−771. d) R. D. Moriarty, A. Martin, K. Adamson, E. O´Reilly, P. Mollard, R.J. Forster and T.E. Keyes, *J. of Microscopy,* **2014**, *235*, 204-218.

[43] X. Peng, J. Du, J. Fan, J. Wang, Y. Wu, J. Zhao, S. Sun and T. Xu *J. Am. Chem. Soc.,* **2007**, *129*, 1500-1501.

metal ions that exist in living cells (Ca^{2+}, Mg^{2+}, Na^{+}, K^{+} ,Fe^{3+}) do not give any responses at a 30-fold excess concentration. The increases in the fluorescence intensity in living cells were observed upon addition of Cd^{2+} (5 μM) into the medium and incubation for 0.5 h at 37 °C (see figure 1.15[43]).

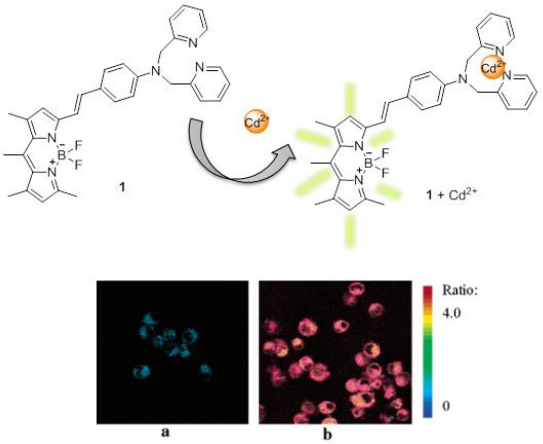

Figure 1.15. Up**:** Intracellular emission fluorescent Cd^{2+} sensor **1.** Down: Fluorescence ratio (F597/F697) images of Cd^{2+} in DC cells (Leica TCS-SP2 confocal fluorescence microscope, 20× objective lens). (a) DC cells incubated with 1 (5 μM). (b) DC cells incubated with **1** and then further incubated with 5 μM $CdCl_2$.

The radiometric BODIPY-linked azacrown ether sensor **2** with high selectivity for potassium over other alkali ions in acetonitrile is the first example of a probe synthesized using S_NAr of 3,5-dichloroBODIPY (figure 1.16).[44] The sensor absorbs and emits light in the visible wavelength range. Quantum chemical calculations suggest that the experimental hypsochromic shifts in absorption and fluorescence upon potassium binding are due to complexation, which induces a large conformational change of the sensor.

[44] M. Baruah, W. Qin, R. A. L. Vallee, D Beljonne, T. Rohand, W. Dehaen and N. Boens, *Org. Lett.,* **2005**, *7*, 4377-4380.

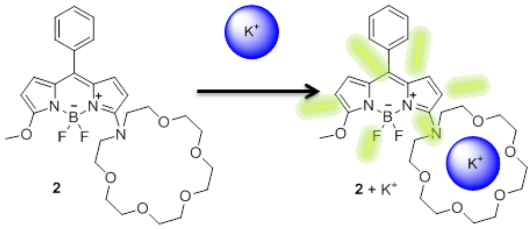

Figure 1.16. BODIPY-linked azacrown sensor **2** selective for K^+.

Recently a fluorescent heteroditopic receptor based on BODIPY core for the simultaneous recognition of anions and cations has been reported.[45] In the presence of cations with non-active counterions a hypsochromic shift of both the absorption and emission band was observed. By contrast, in the presence of anions with non-active counterions a bathochromic shift of both the absorption and emission band along with a fluorescence quenching were observed. This compound also gives rise to different responses in the presence of zwitterionic amino acids (figure 1.17).

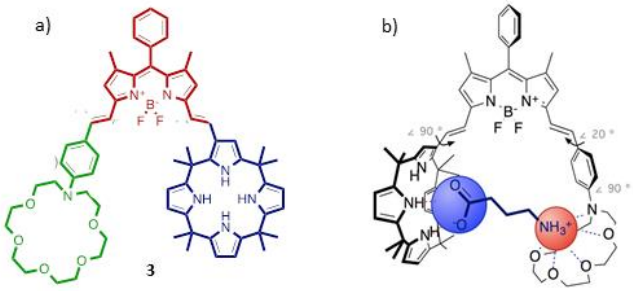

Figure 1.17. a) Hetetoditopic receptor based on BODIPY core for recognition of anions and cations. b) Illustration of receptor coordinated with glycine amino acid.

Photochromic dithienylethene moieties covalently attached to fluorescent BODIPYs via a phenylacetylene linker allows formation of new photoswitches.[46] UV light induced isomerization of the photochrome resulting in a significant decrease in fluorescence intensity (figure 1.18). This fluorescence can be

[45] R. Gotor, A. M. Costero, S. Gil, P. Gaviña and K. Rurack, *Eur. J. Org. Chem*., **2014**, *19*, 4005–4013.
[46] T. A. Golovkova, D. V. Kozlov and D.C. Neckers, *J. Org. Chem.,* **2005**, *70*, 5545-5549.

recovered with visible light. Steady-state fluorescence measurements demonstrate that the emission of the dye can be modulated by external light. An intramolecular energy transfer mechanism accounts for the fluorescence quenching in the UV light produced isomers.

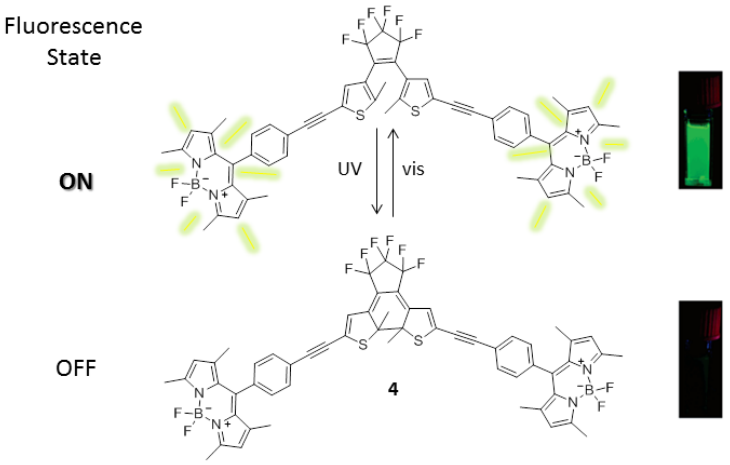

Figure 1.18. BODIPY fluorescent switches.

The number and range of applications of BODIPYs have blossomed and include uses as diverse as chromogenic probes and cation sensors[27], drug delivery agents,[47] or their use in other advanced applications such as laser dyes, and as components of light-harvesting (LH) systems is noteworthy. Ziessel and Harriman discussed as early as 2010 their function in artificial LH antennae.[48] You et al. looked at BODIPY-based photosensitizers for photodynamic therapy,[49] Chujo et al. discussed their use as advanced luminescent materials,[50] Boyle et al. examined their use as light active material components.[51]

[47] C. McCusker, J. B. Carroll and V. M. Rotello, *Chem. Commun*., **2005**, 996-998.
[48] R. Ziessel and A. Harriman, *Chem. Commun.,* **2011**, *47*, 611–631.
[49] S. G. Awuah and Y. You, *RSC Adv*., **2012**, *2*, 11169–11183.
[50] K. Tanaka and Y. Chujo, *Macromol. Rapid Commun*., **2012**, *33*, 1235–1255.
[51] M. Benstead, G. H. Mehl and R. W. Boyle, *Tetrahedron*, **2011**, 67, 3573–3601.

Chapter 2:

Objectives

2. Objectives

This PhD thesis intended to address three different topics: the design and synthesis of (1) sensors for the detection of trivalent cations in different media; (2) chemosensors and/or chemodosimeters to detect selectively nerve agent mimics avoiding acid interferences and (3) their hydrolysis to clean the contaminated areas.

The project related to the trivalent cation detection involves receptors based on fluorogenic probes. The aim consists in the synthesis and characterisation of new chromo-fluorogenic derivatives containing aminoethoxy moieties to coordinate trivalent cations. It is expected a low fluorescence in the free ligand due to PET promoted by the lone pair of the nitrogen atom, and fluorescence should recover upon cation detection.

In the project concerning the nerve agent mimics detection, the proposal consists in the design of molecules capable to detect selectively nerve agent mimics over other possible interfering species.

1. *Design and synthesis of BODIPY chemodosimeters for G-type nerve agents*: through the design, synthesis and characterization of BODIPY derivatives containing different reactive sites in electronic isolation, where they could react with the relevant species giving a different response and discriminating between the different nerve agent mimics and over possible interferents such as acid media or other related organophosphorus compounds, in order to avoid false positive or negative responses. Applicability "in-the-field" and real-time monitoring will be developed.
2. *Design and synthesis of BODIPY-complexes for detection of V-type nerve agents by a displacement mechanism:* the idea is to use one of the compounds for the trivalent cation coordination to obtain some BODIPY-complexes. The target agent will coordinate the metal centre, with concomitant change of the optical properties.

To study the use of supramolecular-based organocatalysts to promote a feasible and easy nerve agent hydrolysis.

Chapter3:

Selective Detection of Trivalent Cations

3.1 Introduction

Detecting cations is of great interest to many scientists, including chemists, biologists, clinical biochemists and environmentalists. Among these cations, triple-charged metal cation detection is of significant importance because of its crucial role in a wide range of environmental and human health areas and in living organism. [1] For example, Iron in its trivalent form is an essential element for many

[1] a) J. Mao, L. Wang, W. Dou, X. Tang, Y. Yan and W. Liu, *Org. Lett*., **2007***, 9*, 4567-4570. b) S. H. Kim, S. H. Choi, J. Kim, S. J. Lee, D. T. Quang and J. S. Kim, *Org. Lett*., **2009***, 12*, 560-563. c) Y. Lu, S. Huang, Y. Liu, S. He, L. Zhao and X. Zeng; *Org. Lett*., **2011***, 13*, 5274-5277.

organisms acting as a cofactor in several enzymatic reactions and it is involved in both electron transfer and oxygen transport.

Either deficiency or overdose levels of Fe^{3+} within the body have been associated with increasing incidence of certain cancers and dysfunction of certain organs, such as the heart, pancreas, and liver.[2] Aluminium is the most abundant metallic element in the earth's crust and is extensively used in our daily life, such as storage and cooking utensils which results in a moderate increase in the Al^{3+} concentration in food. In recent years, it has been recognized that excessive intake of Al^{3+} leads to a wide range of diseases, such as Alzheimer's disease, osteoporosis, colic, rickets, gastrointestinal problems, anemia, headache, memory loss and aching muscles.[3] Trivalent chromium is one of the most important heavy metal elements, it is a necessary trace element in human nutrition; Cr^{3+} adversely affects cellular structures and function and plays an important role in the metabolism of carbohydrates, lipids, proteins and nucleic acids.[4] Cr^{3+} overdose causes disturbance in glucose levels while its deficiency can cause diabetes and cardiovascular disease.[5] Thus, there is a need to develop strategies capable of detecting the presence of trivalent cation ions in environmental and biological samples.

One efficient way to detect cations is through the use of optical (both chromogenic and fluorogenic) molecular probes, which show a shift in color upon the cation recognition. The change in the characteristic absorption and/or emission band of the sensor is used to quantify the detection process, in terms of binding constant, stoichiometry of the resultant complex, selectivity and sensitivity, etc. Among various designs, the most widely used one consists of a signalling unit covalently linked through a spacer to the receptor.[6] Within the

[2] a) T.A. Rouault, *Nat. Chem. Biol*., **2006**, *2*, 406-414. b) D. Galaris, V. Skiada and A. Barbouti, *Cancer Letters*, **2008**, *266*, 21–29.

[3] a) G. D. Fasman, *Coord. Chem. Rev*., **1996**, *149*, 125-165. b) P. Nayak, *Environ. Res*., **2002**, *89*, 101-115. c) G. Berthon, *Coord. Chem. Rev*., **2002**, *228*, 319-341.

[4] A. K. Singh, V. K. Gupta and B. Gupta, *Anal. Chim. Acta*, **2007**, *585*, 171-178.

[5] J.B. Vincent, *Nutr. Rev*., **2000**, *58*, 67-72.

[6] a) N. Kaur and S. Kumar, *Tetrahedron*, **2011**, *67*, 9233-9264. b) K. Kaur, R. Saini, A. Kumar, V. Luxami, N. Kaur, P. Singhans S. Kumar, *Coord. Chem. Rev*., **2012**, *256*, 1992-2028. c) D. Sareen, P. Kaur and K. Singh, *Coord. Chem. Rev*., **2014**, *265*, 125-154.

large variety of molecules utilized as chemosensors, dyes constitute one of the most significant library of molecules owing to the diversity in their structural type as well as the physico-chemical characteristics. Besides their application in several fields of chemistry, biochemistry, biology, etc…;[6a,7] the extensive use of dyes in the field of chemosensing could be attributed to its ease use, their availability in sufficient quantities and the different classes of chromophores. As a consequence of cation recognition, the electronic conjugation of the chromophore is modulated, changing the position and/or the intensity of the absorption and/or emission band.

In the past few years many sensors have been reported for the detection of transition and p-block metal cations.[8] Czarnik and coworkers reported a pioneering work regarding fluorescent chemosensors for Pb^{2+} in 1996.[9] 2- and 9-anthracene derivatives bearing the *N*-methylthiohydroxamate ligand (**1** and **2**) were prepared, which exhibited strongly quenched fluorescence due to the photo-induced electron transfer (PET). Complexation of 2-derivative **1** with Pb^{2+} resulted in rapid metal ion-catalyzed hydrolysis. Whereas complexation of 9-derivative **2** with Pb^{2+} induced a 13-fold fluorescence enhancement at pH 9, which can be attributed to the steric protection of the thiocarbonyl group by two peri hydrogens (figure 3.1).

[7] a) A. T. Peters, H. S. Freeman, *Colour Chemistry. The Design and Synthesis of Organic Dyes and Pigments*. Elservier Science Publishers Ltd. **1991**. b) X. Qian, Y. Xiao, Y. Xu, X. Guo, J. Quian and W. Zhu, *Chem. Commun*., **2010**, *46*, 6418-6436.

[8] H. N. Kim, W. X. Ren, J. S. Kim and J. Yoon, *Chem. Soc. Rev*., **2012**, *41*, 3210–3244.

[9] M. Y. Chae, J. Yoon and A. W. Czarnik, *J. Mol. Recognit*., **1996**, *9*, 297-303.

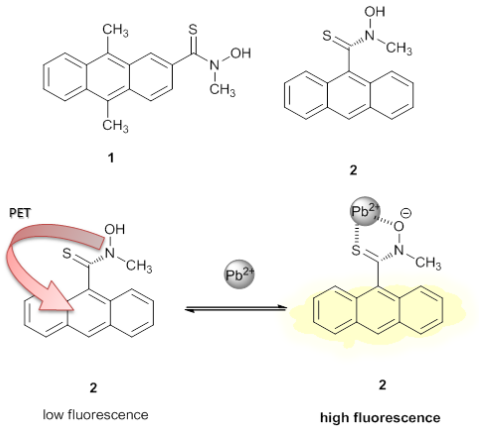

Figure 3.1. Scheme of a 9-anthracene derivative for Pb^{2+} detection.

More recently, Kim´s group reported a tren-spaced rhodamine and pyrene fluorophore **3**, as an Hg^{2+} and Cu^{2+} selective fluorogenic sensor that modulated pyrene excimer emission.[10] The complexation of **3** with Hg^{2+} induced the spirolactam ring opening and exhibited dynamic excimer emission. The coordination of Cu^{2+} with the pyrene amide group induced a static excimer emission. The different binding mode between Hg^{2+} and Cu^{2+} was elucidated from DFT (density functional theory) calculation and competition experiment.

[10] M. H. Lee, G. P. Kang, J. W. Kim, S. Y. Ham and J. S. Kim, *Supramol. Chem*., **2009**, *21*, 135-141.

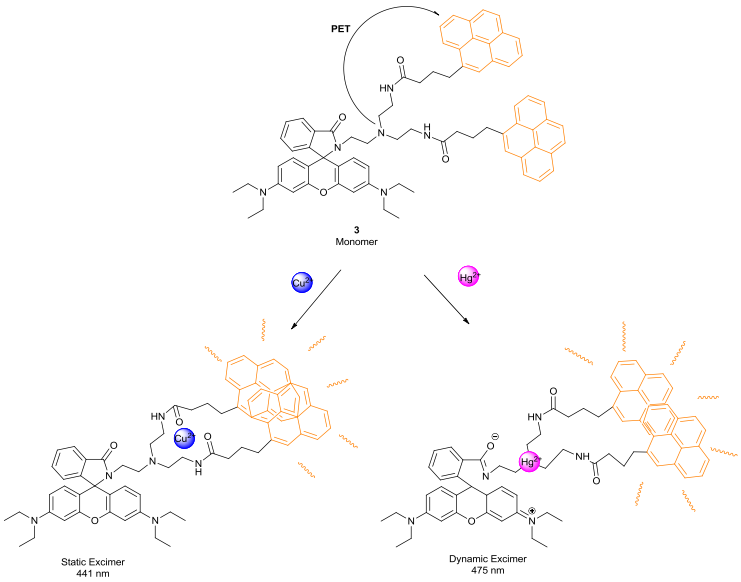

Figure 3.2. Schematic representation of Hg^{2+} and Cu^{2+} detection by excimer formation.

Even though there are a large number of chemosensors for divalent transition metal cation, very few probes have been synthesized to the detection of triple-charged metal cations; and a single sensor which can detect all these trivalent ions[11] (Al^{3+}, Cr^{3+} and Fe^{3+}) selectively over the other divalent and monovalent ions has scarcely studied, and even less in aqueous environments.

[11] a) Z. Zhou, M. Yu, H. Yang, K. Huang, F. Li, T. Yi and C. Huang, *Chem. Commun*., **2008**, 3387–3389. b) Z. Li, W. Zhao, Y. Zhang, L. Zhang, M. Yu, J. Liu and H. Zhang, *Tetrahedron*, **2011**, *67*, 7096-7100.

3.2 Objectives

Taking into account the biological significance and environmental importance of trivalent ions (especially Al^{3+}, Cr^{3+} and Fe^{3+}); we decided to design new sensors for their detection. In the following section, the synthesis, characterization and sensing properties of chemosensors for the selective detection of triple-charged metal ions in both organic media and aqueous environments is reported.

Specifically our aims were:

- ✓ Design and synthesis of chemosensors featured by two conjugated parts: a reactive site, with the ability to detect only the target trivalent analytes and a dye with tunable chromo-fluorogenic properties.
- ✓ Characterization of these new prepared molecules by the usual techniques (Nuclear Magnetic Resonance, High Resolution Mass Spectrometry….) before and after the reaction with the target analyte.
- ✓ Study the chromo-fluorogenic behavior of the synthesized chemosensors with the selected trivalent analytes.
- ✓ Evaluation of the reactivity of chemosensors in presence of different species, to test their applicability as selective sensor for the selected species.
- ✓ Study the detection applicability in aqueous environments.

3.3 Chemosensors Design

The aim was to obtain selective response to trivalent cations over common interferences. The "*Binding site–signalling subunit"* approach was selected for the chemosensor design by their versatility and major control of selectivity.

The detection system was designed in such a way that, upon coordination of trivalent cations in the binding site, a modulation of the absorption and/or emission band is induced, via energy or electron transfer process from the binding site to the chromo-fluorophore. Two different fluorophores were studied as signaling subunit. In a first approach, fluorescein was chosen by the group previous experience in using this fluorophore as signaling unit in sensing systems; but their photophysical properties are dependent on pH, that is why, for applicability in aqueous environments, the BODIPY-fluorophore was employed. Moieties containing N-electron-donor groups were chosen as binding site given their known capacity to coordinate metal cations, and involvement of the nitrogen in the coordination modulate the electronic properties of the sensor.

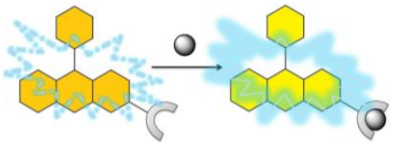

Figure 3.3. Sensing paradigm for the fluorogenic recognition of trivalent cations by using fluorescein derivative as signaling unit.

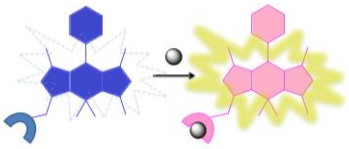

Figure 3.4. Sensing paradigm by using BODIPY derivative as signaling unit.

3.4 A new selective fluorogenic probe for trivalent cations.

A new selective fluorogenic probe for trivalent cations

Andrea Barba-Bon,[a,b,c,d] Ana M. Costero,[a,b] Salvador Gil,[a,b] Margarita Parra,[a,b] Juan Soto,[a,c], Ramón Martínez-Máñez,[a,c,d] and Felix Sancenón[a,c,d]

[a] Centro de Reconocimiento Molecular y Desarrollo Tecnológico (IDM),Unidad Mixta Universidad Politécnica de Valencia-Universitat de Valencia, Spain

[b] Departamento de Química Orgánica, Universitat de Valencia, Dr. Moliner, 50, 46100 Burjassot (Valencia), Spain.

[c] Departamento de Química, Universidad Politécnica de Valencia Camino de Vera s/n, 46022, Valencia, Spain

[d] CIBER de Bioingeniería, Biomateriales y Nanomedicina (CIBER-BBN)

Received: *18 th November 2011*
Published online: *23rd January 2012*

Chem. Commun., ***2012****, 48, 3000-3002.*

A new selective chromo-fluorogenic probe for Fe^{3+}, Cr^{3+} and Al^{3+} is reported. Detection limits are in the µM range and the fluorogenic sensing ability could be observed to the naked eye when illuminated with UV-light. No response is observed with divalent cations.

The design and synthesis of new chemosensors for transition and p-block metal cations remain an important subject in the field of supramolecular chemistry because of their impact on the environment and human health.[1-3] Even though a large number of chemosensors for divalent transition metal cations have been described, very few studies have been devoted to the development of organic probes that are sensitive to triple-charged metal cations.[4-6] However, trivalent cations have important biological properties and are directly involved in the cell function where there is a critical control of M^{3+} levels.[7] For instance, the trivalent form of chromium is an essential element in human nutrition and has a huge impact on the metabolism of carbohydrates, fats, proteins and nucleic acids as it can activate certain enzymes and stabilise proteins and nucleic acids. Cr^{3+} deficiency has been reported to disturb glucose levels and lipid metabolism.[8,9] At the same time, it is an environmental pollutant that causes concern in industry and agriculture.[9-11] Fe^{3+} is not only the most abundant transition metal in cellular systems, but is of outstanding biological importance given its presence in numerous enzymes and proteins. Iron is critically involved in both electron transfer reactions and oxygen transport due to its adequate redox potentials and its high affinity for oxygen. Finally, it is well-known that Al^{3+} is abundantly found in nature, causes drinking water contamination and can be toxic to humans in excessive amounts. Many symptoms of aluminium toxicity mimic those of Alzheimer's disease and osteoporosis. Moreover, gastrointestinal problems, interference with Ca^{2+} metabolism, decreased liver and kidney function can be caused by aluminium toxicity.[12-14] Thus, there is a pressing need to develop chemical sensors capable of detecting the presence of trivalent cations ions in environmental and biological samples.

The literature reveals that considerable efforts have been made in the last few decades to design new fluorogenic chemosensors. Sensors based on ion-induced changes in fluorescence are especially suitable as they are easy to use and usually give an instantaneous response with high sensitivity.[15-17] Moreover in this field, the design of probes displaying changes in optical properties through a "turn-on" response is much preferred for designing efficient sensors than those showing a "turn-off" response. Some Fe^{3+},[18-20] and Al^{3+} [21-24] selective fluorogenic probes have been reported yet, surprisingly, very few sensors for Cr^{3+} have been described in the literature.[9,25] Consequently, the design of new probes bearing suitable multidentate chelating units, which can potentially sense these metal ions, is a timely area of research. Given our interest in developing new chemosensing systems,[26] we report herein a new probe based on a derivative of fluorescein for the detection of trivalent cations Fe^{3+}, Al^{3+} and Cr^{3+}. In all cases a remarkable enhancement of the fluorescence emission in acetonitrile was observed.

Fluorescent probe **1** (vide infra) was based on the well-known fluorophore fluorescein and has been used herein for the selective detection of trivalent cations. This choice was supported by our previous experience in using fluorescein as a signalling unit in different sensing systems.[27,28] Fluorescein is one of the most commonly used fluorophores due to its high molar absorptivity, large fluorescent quantum yields and high photostability. However, fluorescein's photophysical properties are strongly dependent on pH, which is why our preliminary studies were carried out in organic media (acetonitrile).

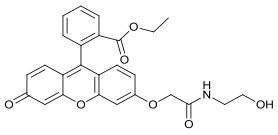

Figure 1. Ligand **1**.

The synthesis of **1**, Fig. 1, began with a Fischer esterification of fluorescein to fix the open form of the lactone ring. The coordinating moiety was then built from the hydroxyl group by alkylation with bromoacetic acid tert-butyl ester and subsequent trifluoroacetic acid-mediated deprotection. Both steps proceeded

easily, as previously described.[29] 2-Hydroxyethylamine was introduced by esterification of the BOC-protected derivative under optimized conditions.[30] BOC-deprotection was performed with trifluoroacetic acid to provide, through a rearrangement, the most thermodynamically stable compound **1** (44% overall yield) (see ESI). The spectroscopic properties of **1** were evaluated in acetonitrile solution. As shown in Fig. 2, **1** exhibits maximal absorptions at 352 (ε = 6.62 x 10^3 M^{-1} cm^{-1}), 430 (ε = 1.80 x 10^4 M^{-1} cm^{-1}), 453 (ε = 2.00 x 10^4 M^{-1} cm^{-1}) and 484 (ε = 1.10 x 10^4 M^{-1} cm^{-1}) nm in accordance with the presence of the fluorescein moiety, which is responsible for probe **1**'s pale yellow colour. Upon addition of chromium (0–2 equiv.), the absorbance at 484 nm decreases gradually and simultaneously, and a new significant absorption band developed at 437 nm (ε = 4.33 x $10^4 M^{-1}cm^{-1}$ for Cr^{3+} and ε = 5.05 x 10^4 M^{-1} cm^{-1} for Fe^{3+}). A similar effect was observed in the presence of Fe^{3+} (see ESI). Moreover, absorbance at 437 nm remained constant in the presence of more than 1 equiv. of Fe^{3+} or Cr^{3+}, strongly suggesting the formation of 1 : 1 ligand-to-metal complexes. This was also demonstrated via the corresponding Job's plots for both the **1**-Fe^{3+} and **1**-Cr^{3+} systems.

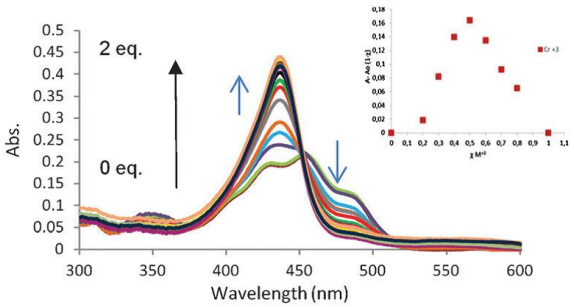

Figure 2. UV-vis spectra of ligand **1** (10^{-5} M) upon titration of Cr^{3+} (0–2 equiv.) in CH_3CN. Inset: stoichiometry determination by the Job's plot from UV-vis data.

Ligand **1** (10^{-5}M) exhibited practically no fluorescence (λ_{exc}= 453 nm) in the 450–520 nm range, whereas a significant enhancement of emission at 475 nm emerged after addition of Fe^{3+} or Cr^{3+} (see ESI). This band showed a linear enhancement with an increased cation concentration for ratios [cation]/[ligand] up to 1. A further increase of the cation concentration did not lead to any further emission enhancement. Probe **1** showed excellent selectivity for Al^{3+}, Fe^{3+} and Cr^{3+} ions over the relevant competing metal ions. The enhancement of fluorescence

allowed detection limits to reach the micromolar range (vide infra). These fluorogenic results are in full agreement with the UV-vis data. When similar studies were carried out with Al^{3+}, similar changes in both UV-vis and fluorescence to those found in the presence of Fe^{3+} and Cr^{3+} were also observed (see ESI). However for this cation, the formation of a 2:1 ligand-to-metal complex was determined. This 2:1 stoichiometry observed for **1** in the presence of Al^{3+}, in contrast to the 1:1 stoichiometry found for Fe^{3+} and Cr^{3+}, could be related to the smaller size of the former (ionic radius 0.50 Å for Al^{3+} versus 0.69 Å and 0.64 Å for Cr^{3+} and Fe^{3+}, respectively), which precluded an efficient coordination of Al^{3+} with only one ligand molecule. However, size could not be the only crucial factor as Liu and colleagues have developed selective fluorescent chemosensors, based on Rhodamine, that show different stoichiometries for complexation of Fe^{3+} and Cr^{3+}.[31] Moreover, complexation constants were determined from the corresponding UV-vis and fluorescence titration curves using the Spectfit program.[32] The log β values for the equilibria **1** + M^{3+} ↔ $[M(\mathbf{1})]^{3+}$ for Cr^{3+} and Fe^{3+}, and for the equilibrium 2 **1** + Al^{3+} ⇌ $[Al(\mathbf{1})_2]^{3+}$ are included in Table 1. Detection limits were evaluated and determined from the equation DL = *K* x Sb_1/S, where *K* = 3, Sb_1 is the standard deviation of the blank solution and *S* is the slope of the calibration curve[33] (see ESI). These values are also depicted in Table 1.

Table 1. Complexation constants and DL for **1** with trivalent cations.

Cation	Log β UV	Log β fluorescence	Detection limit (UV)/ μM	Detection limit (Fluor.)/ μM
Cr^{3+}	3.5 ± 0.8	4.2 ± 0.2	2.5	0.5
Fe^{3+}	5.3 ± 0.3	5.1 ± 0.2	0.6	0.3
Al^{3+}	9.71 ± 0.07	9.81 ± 0.03	0.3	0.2

A detailed analysis of the UV-vis absorption spectrum of **1** in the presence of other metal cations was carried out. As shown in Fig. 3, the addition of 1 equiv. of Li^{+}, Cu^{2+}, Cd^{2+}, Zn^{2+}, Co^{2+}, Ni^{2+}, Fe^{2+}, and Hg^{2+} had no noticeable effect on the fluorescence emission at 475 nm. This is in contrast with the strong enhancement of the emission intensity upon addition of Fe^{3+}, Cr^{3+} and Al^{3+}. Competitive

experiments in the presence of the above-mentioned metal cations also demonstrate the selective response of **1** to Fe^{3+} or Cr^{3+} or Al^{3+}. Probe **1**'s fluorogenic sensing ability could be observed by the naked eye when acetonitrile solutions of **1** in the presence of Fe^{3+} or Cr^{3+} or Al^{3+} were illuminated with 254 nm UV-light via the enhancement of a clearly observed pale blue emission (see Fig. 3, bottom). Quantum yields of 0.07, 0.10 and 0.16 were determined for the Cr^{3+}, Fe^{3+} and Al^{3+} complexes, respectively (using fluorescein, 0.1 M NaOH, ϕ = 0.85, as standard). The quantum yield difference is high enough to discriminate between these cations at concentrations higher than 5 μM. The fluorescence intensity decreases with an increase in the water content, however this could also be useful for the discrimination of the different cations. Thus, the Al^{3+} complex still remains fluorescent after addition of 4% water, whereas quenching of the fluorescence for A Cr^{3+} and Fe^{3+} complex was observed when more than 2% and 1% water, respectively, were added.

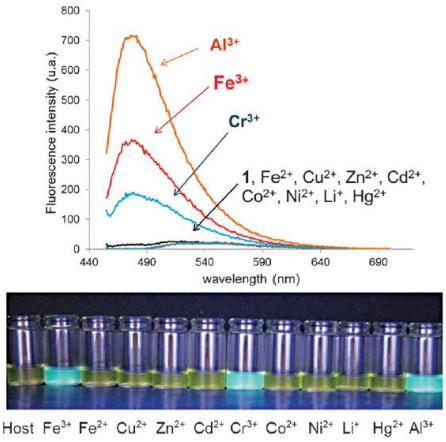

Figure 3. (top) Fluorescence spectra of **1** (10^{-5} M) upon addition of 1 equiv. of Fe^{3+}, Fe^{2+}, Cu^{2+}, Zn^{2+}, Cd^{2+}, Co^{2+}, Ni^{2+}, Li^{+}, Hg^{2+}, Cr^{3+} and Al^{3+} in CH_3CN (λ_{exc} = 437 nm). (bottom) Visual changes (λ_{exc} = 254 nm) observed for **1** in the presence of different metal cations.

The ^1H NMR spectra of ligand **1** recorded in CD_3CN upon the addition of increasing concentrations of Al^{3+} showed significant spectral changes (see ESI). The most important shifts of the signals of **1** were observed in the xanthene moiety, especially the α protons to the carbonyl group at 6.25 and 6.39 and the ortho-protons to the lateral chain at 7.19 and 6.95 ppm, which underwent a significant

downfield shift upon the addition of Al^{3+}. On the other hand, the singlet signal at 4.67 ppm displayed a similar behavior, with a downfield shift of 0.3 ppm. There were no appreciable changes in the peak positions of the ethylene chain next to the amide group. These data strongly suggest the direct involvement of the xanthene moiety and the lateral chain for Al^{3+} coordination. In order to suggest a complexation model for the 1 : 1 complexes, complementary NMR studies with Ru^{3+}, which showed to form 1 : 1 complexes with ligand **1**, were carried out (see ESI). The similarity of the spectra modifications, with those observed with Al^{3+}, suggests that the same groups are involved in both kinds of complexes.

In summary, we report herein the synthesis and characterization of a new probe for the fluorogenic detection of trivalent cations Fe^{3+}, Cr^{3+} and Al^{3+}. The choice of the fluorescein group allowed the optical detection of these ions, whereas the probe remained silent in the presence of monovalent and divalent cations such as Li^{+}, Cu^{2+}, Cd^{2+}, Zn^{2+}, Co^{2+}, Ni^{2+}, Fe^{2+} and Hg^{2+}. The acetonitrile solutions of **1** in the presence of Fe^{3+}, Cr^{3+} and Al^{3+} resulted in an associated ‘‘turn-on’’ response via the formation of the corresponding metal complexes. This chelation-enhanced fluorescence might be attributed to the change in polarity of the dye by increase of the donor–acceptor electronic delocalization after complexation. Fe^{3+} and Cr^{3+} were found to form 1 : 1 ligand-to-metal complexes with **1**, whereas the formation of 2 : 1 complexes was observed for Al^{3+}. A discrimination based on the fluorescence response according to the amount of water in solution can be envisaged.

AECID (A/026355109), DGICYT (projects MAT2009-14564-C01 and MAT 2009-14564-C04-3) and Generalitat Valenciana (project PROMETEO/2009/016) are gratefully acknowledged. A.B.B. thanks MICINN for a pre-doctoral FPI fellowship.

Notes and references

1 Q. Zhao, F. Li and C. Huang, *Chem. Soc. Rev*., 2010, **39**, 3007-3030.

2 A. V. Tsukanov, A. D. Dubonosov, V. A. Bren and V. I. Minkin, *Chem. Heterocyclic Comp.,* 2008, **44**, 899-923.

3 L. Prodi, F. Balletta, M. Mantalti and N. Zaccheroni, *Coord. Chem. Rev*., 2000, **205**, 59-83.

4 E. B. Veale and T. Gunnlaugsson, *Annu. Rep. Prog. Chem., Sect. B: Org. C,* 2010, **106**, 376-390.

5 A. V. Legin, D. O. Kirsanov, V. A. Babain, A. V. Borovoy and R. S. Herbst, *Anal. Chim. Acta*, 2006, **572**, 243-247.

6 D. O. Kirsanov, A. V. Legin, V. A. Babain and Y. G. Vlasov, Russ. *J. Appl. Chem*., 2005, **78**, 568-573.

7 T. Kawano, T. Kadono, T. Furuichi, S. Muto and F. Lapeyrie, *Biochem. Biophys. Res. Commun*., 2003, **308**, 35-42.

8 H. Arakawa, R. Ahmad, M. Naoni and H.-A. Tajmir-Riahi, *J. Biol. Chem*., 2000, **275**, 10150-10153.

9 H. Wu, P. Zhou, J. Wang, L. Zhao and C. Duan, *New J. Chem.*, 2009, **33**, 653-658.

10 V. Geraldes, M. Mihalma, M. N. Pinho, A. Aril, H. Ozqunoy,B. O. Bitlishi and O. Savi, *Pol. J. Environ. Stud*., 2009, **18**, 353-357.

11 O. F. H. Cobos, J. F. A. Londono and L. C. F. Garcia, *Dyna*, 2009, **160**, 107-119.

12 S. G. Lambert, J.-A. M. Taylor, K. L. Wegener, S. L. Woodhouse, S. F. Lincoln and A. D. Ward, *New J. Chem*., 2000, **24**, 541-546.

13 D. Maity and T. Govindaraju, *Chem. Commun*., 2010, **46**, 4499-4501.

14 Y. S. Jang, B. Yoon and J.-M. Kim, *Macromol. Res*., 2011, **19**, 97-99.

15 M. Wang, G. Zhong, D. Zhong, D. Zhu and B. Z. Tang, *J. Mater.Chem*., 2010, **20**, 1858-1867.

16 L.-J. Fan, Y. Zhang, C. B. Clifford, S. E. Angell, M. F. L. Parker,B. R. Flynn and W. E. Jones, *Coord. Chem. Rev.,* 2009, **253**, 410-422.

17 V. Amendola, L. Fabbrizzi, F. Forti, M. Licchelli, C. Manglano, P. Pallancini, A. Poggi, A. Sacchi and A. Taglieti, *Coord. Chem. Rev*., 2006, **250**, 273-299.

18 K. M. Orcutt, W. S. Jones, A. McJonald, A. Schrock and K.J. Wallace, *Sensors*, 2010,**10,** 1326-1337.

19 S. Fakih, M. Podinovskaia, X. Kong, H. L. Collins, V. E. Schoible and R. C. Hider, *J. Med. Chem.*, 2008, **51**, 4539-1445.

20 Z. Jiang, L. Tang, F. Shao, G. Zheng and P. Lu, *Sens. Actuators, B*, 2008, **134**, 414-418.

21 M. Daity and T. Govindaraju, *Chem. Commun.,* 2010, **46**, 4499-4501.

22 X. Jiang, B. Wang, Z. Yang, Y. Liu, T. Li and Z. Liu, *Inorg. Chem. Commun*., 2011, **14**, 1224-1227.

23 T. Ma, M. Dong, Y. Dong, Y. Wang and Y. Peng, *Chem.–Eur. J.*, 2010, **16**, 10313-10318.

24 L. Wang, W. Qin, X. Tang, W. Dou, W. Liu, Q. Teng and X. Yao, *Org. Biomol. Chem*., 2010, **8**, 3751-3757.

25 (a) Y.Wan, Q. Guo, X. Wang and A. Yia, *Anal. Chim. Acta*, 2010, **665**, 215; (b) M. Sarkar, S. Banthia and A. Samanta, *Tetrahedron Lett*., 2006, **47**, 7575-7578.

26 (a) S. Royo, R. Martínez-Mañez, F. Sancenó n, A. M. Costero, M. Parra and S. Gil, *Chem. Commun*., 2007,**46**, 4839-4847; (b) A.M. Costero, M. Parra, S. Gil, R. Gotor, P. M. E. Mancini, R. Martínez-Mañez, F. Sancenón and S. Royo, *Chem.–Asian J*., 2010, **5**, 1573-1585; (c) E. Climent, A. Martí, S. Royo, R. Martínez-Mañez, M. D.Marcos, F. Sancenón, J. Soto, A. M. Costero, S. Gil and M. Parra, *Angew. Chem., Int. Ed*., 2010, **49**, 5945-5948; (d) S. Royo, A. M. Costero, M. Parra, S. Gil, R. Martínez-Mañez and F. Sancenón, *Chem.–Eur. J*., 2011, **17**, 6931-6934; (e) Y. Salinas, E. Climent, R. Martínez-Mañez, F. Sancenón, M. D. Marcos, J. Soto, A. M. Costero, S. Gil, M. Parra and A. Pérez, *Chem. Commun*., 2011, **47**, 11885-11887.;(f) R. Gotor, A. M. Costero, S. Gil, M. Parra, R. Martínez-Mañez and F. Sancenón, *Chem.–Eur J.,* 2011, **17**, 11994-11997.

27 (a) A.M. Costero, J. V. Colomer, S. Gil and M. Parra*, Eur. J. Org. Chem*., 2009, **22**, 3673-3677; (b) A. M. Costero, M. Parra, S. Gil, J. V. Colomer and A. Martí, *Sens. Lett*., 2010, **8**, 818-823.

28 (a) E. Climent, R. Martínez-Mañez, F. Sancenón, M. D. Marcos, J. Soto, A.Maquieira and P. Amorós, *Angew. Chem., Int. Ed*., 2010,**49**, 7281-7283.; (b)M. Comes, E. Aznar, M. Moragues, M. D. Marcos, R. Martínez-Mañez, F. Sancenón, J. Soto, L. A. Villaescusa, L. Gil and P. Amorós, *Chem.–Eur. J.,* 2009, **15,** 9024-9033.

29 J. Lohse, P. E. Nielsen, N. Hawit and O. Dahl, *Bioconjugate Chem*., 1997, **8**, 199-203.

30 R. S. Klausen and E. N. Jacobsen, *Org. Lett*., 2009, **11**, 887-890.

31 J. Mao, L. Wang, W. Dou, X. L. Tang, Y. Yan and W. S. Liu, *Org. Lett*., 2007, **9**, 4567-4570.

32 SPECFIT/32TM GLOBAL ANALYSIS SYSTEM v.3.0, Spectrum Associates (Marlborough, MA, USA). www.bio-logic.info/rapidkinetics/ specfit.html.

33 M. Zhu, M. Yuan, X. Liu, J. Xu, J. Lv, C. Huang, H. Liu, Y. Li, S. Wang and D. Zhu, *Org. Lett*., 2008, **10**, 1481-1484.

Supporting Information

A new selective fluorogenic probe for trivalent cations

Andrea Barba-Bon, Ana M. Costero,
Salvador Gil, Margarita Parra, Juan Soto,
Ramón Martínez-Máñez, and Felix Sancenón

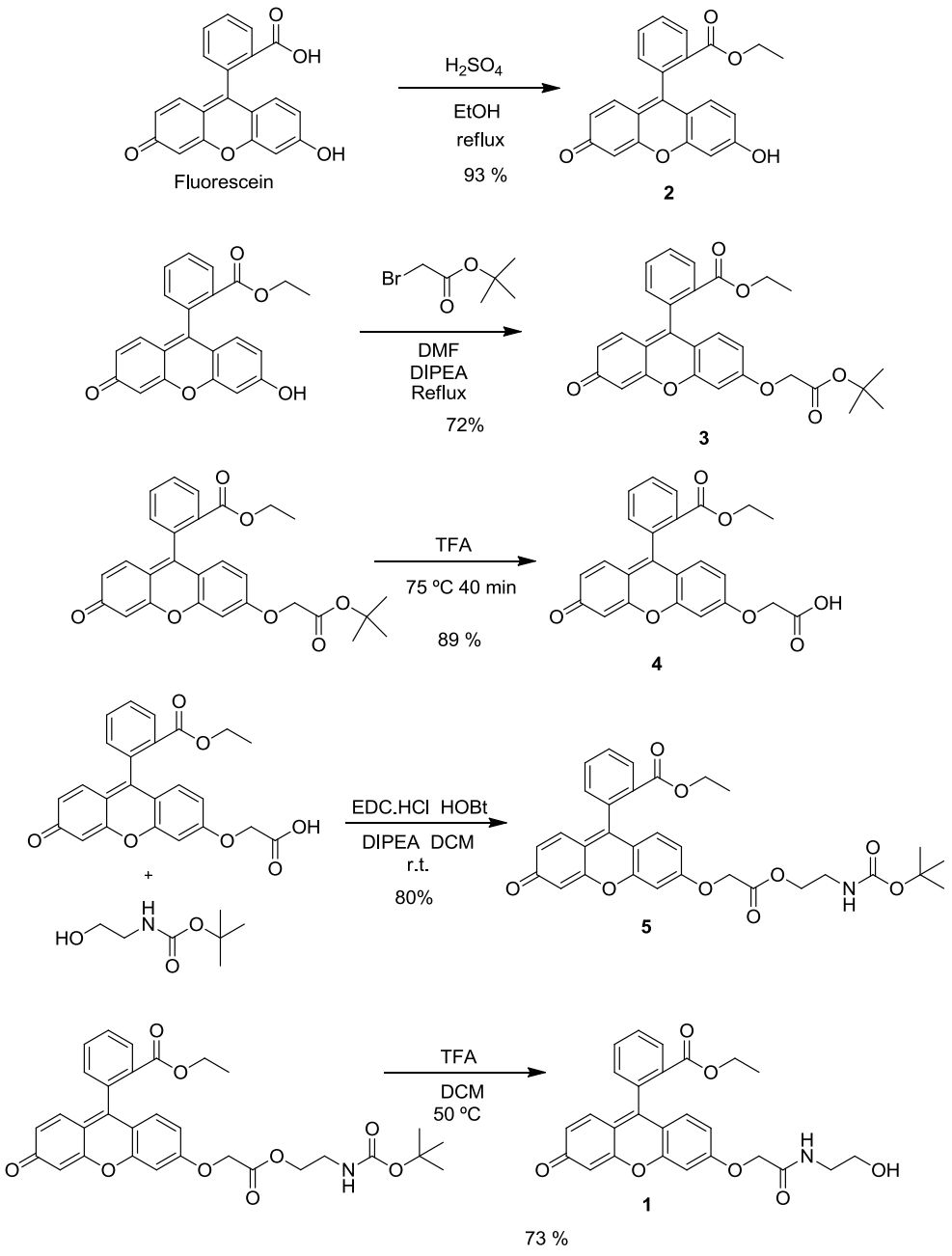

Figure SI-1. Scheme for the synthesis of **1**

EXPERIMENTAL PROCEDURES

Fluorescein ethyl ester (2)

H_2SO_4 (15 mL) was added dropwise to the solution of fluorescein (10.00 g, 30.09 mmol) in EtOH (200 mL) at room temperature. After stirring at reflux for 18 h, EtOH was evaporated under reduced pressure and the resulting mixture was diluted with CH_3Cl. Solid $NaHCO_3$ was added to the solution until gas evolution ceased. A heterogeneous mixture was filtered, and the organic phase was evaporated. The precipitate was dissolved in boiling 96% EtOH (400 mL); by boiling the volume was reduced to approximately 100 mL. Standing overnight at -20°C gave 9.201 g (93%) of fluorescein ethyl ester, orange-brown crystals with a green lustre. ^{1}H NMR (300 MHz, DMSO) δ 8.06 (dd, *J* = 7.7, 1.1 Hz, 1H), 7.78 (td, *J* = 7.5, 1.5 Hz, 1H), 7.69 (td, *J* = 7.6, 1.4 Hz, 1H), 7.39 (dd, *J* = 7.5, 1.0 Hz, 1H), 6.49 (d, *J* = 8.0 Hz, 1H), 6.47 (s, 1H), 6.13 (d, *J* = 2.1 Hz, 1H), 6.10 (d, *J* = 2.1 Hz, 1H), 6.05 (d, *J* = 2.1 Hz, 2H), 3.93 (q, *J* = 7.1 Hz, 3H), 0.84 (t, *J* = 7.1 Hz, 3H).^{13}C-NMR(75 MHz, DMSO): δ 13.6; 60.85; 103.56; 115.02; 129.98; 130; 130.53, 130.69, 133.03; 133.58; 150.52, 155.98; 165.06. $[M+H]^+$ Calc. for $C_{22}H_{17}O_5$: 361.1031; Found: 361.1076.

6-O-(*tert*-butoxycarbonylmethyl) fluorescein ethyl ester (3)

Fluorescein ethyl ester (5.80 g, 16 mmol) and bromoacetic acid *tert*-butyl ester (3.9 g, 20 mmol) in a mixture of DMF (20 mL) and diisopropylethylamine (10 mL) were refluxed at 100°C for 1 h. The reaction mixture was taken up in ethyl acetate (100 mL) and extracted with saturated $NaHCO_3$ (100 mL). The organic phase was washed with brine (150 mL) and dried over $MgSO_4$ to be filtered and concentrated *in vacuo* to yield a dark orange tar. It was dissolved in warm diethyl ether (80 mL) and then reduced, by boiling, to 40 mL. Standing overnight at -20°C, the orange solid that formed was filtered off and washed with ether to yield 5.46 g (72%). ^{1}H NMR (300 MHz, DMSO) δ 8.20 – 8.16 (m, 1H), 7.86 (td, *J* = 7.5, 1.5 Hz, 1H), 7.77 (td, *J* = 7.6, 1.4 Hz, 1H), 7.50 (dd, *J* = 7.5, 1.0 Hz, 1H), 7.19 (d, *J* = 2.1 Hz, 1H), 6.93 – 6.83 (m, 2H), 6.79 (t, *J* = 8.3 Hz, 1H), 6.39 (dd, *J* = 9.7, 1.9 Hz, 1H), 6.24 (d, *J* = 2.0 Hz, 1H), 4.86 (s, 2H), 4.03 – 3.88 (m, 2H), 1.42 (s, 9H), 0.91 – 0.81 (m, 3H). ^{13}C-

NMR (75 MHz, DMSO): δ 13.69; 28.05; 61.26; 65.35; 82.01; 101.79 104.49; 113.26; 114.80; 121.18; 129.06; 130.05; 130.53, 130.64, 130.70; 133.08; 133.48; 150.06, 153.28; 158.27; 265.31; 165.01; 167.46; 184.03. $[M+H]^+$ Calc. for $C_{28}H_{27}O_7$: 475.1712; Found: 475.1757.

6-O-(carboxymethyl) fluorescein ethyl ester (4)

6-O-(*tert*-butoxycarbonylmethyl) fluorescein ethyl ester (1.90 g, 4 mmol), in trifluoroacetic acid (9.9 mL), was refluxed at 75°C for 40 min. Most trifluoroacetic acid was removed under reduced pressure, and a trifluoroacetate of the product was precipitated with diethyl ether and filtered off. It was dissolved in boiling diethyl ether (25 mL) and then reduced to 10 mL. Overnight standing at -20°C produced yellow crystals, which were filtered off and washed with ether: yield 1.49 g (89%).^{1}H NMR (300 MHz, DMSO) δ 8.23 (dd, *J* = 7.7, 1.1 Hz, 1H), 7.89 (td, *J* = 7.5, 1.4 Hz, 1H), 7.81 (td, *J* = 7.6, 1.4 Hz, 1H), 7.55 – 7.50 (m, 1H), 7.37 (s, 1H), 7.07 – 6.97 (m, 3H), 6.64 (dd, *J* = 9.6, 2.0 Hz, 1H), 6.58 (d, *J* = 1.9 Hz, 1H), 4.96 (s, 2H), 4.03 – 3.88 (m, 2H), 0.87 (t, *J* = 7.1 Hz, 3H). ^{13}C- NMR (75 MHz, DMSO): δ 13.71; 61.39; 65.05; 101.68; 104.44; 113.66; 117.10; 130.85; 131.14, 133.16; 169.62. $[M+H]^+$ Calc. for $C_{24}H_{19}O_7$: 419.1086; Found: 419.1131.

2-((*tert*-butoxycarbonyl)amino)ethoxy6-O-(carbonylmethyl) fluorecein ethyl ester (5)

EDC·HCl (331.6 mg, 1.73 mmol) and HOBt (235 mg, 1.73 mmol) in DCM (5 mL) were stirred for 2 minutes. DIPEA (418 µL, 2.4 mmol) was added dropwise, followed by 6-O-(carboxymethyl) fluorecein ethyl ester (660 mg, 1.57 mmol). Tert-buthyl-2-hydroxyethylcarbamate (281.8 mg, 1.73 mmol) was added in one portion, the flask was sealed with a rubber septum and allowed to stir under N_2 for 24 hours. The reaction was diluted with DCM (10 mL) and washed twice with 0.5 M hydrochloric acid (2 x 5 mL). The acidic aqueous layer was extracted with DCM (20 mL), the combined organic layers were washed with saturated, aqueous sodium bicarbonate (20 mL) and brine (15 mL). The organic layer was dried over $MgSO_4$, filtered and concentrated *in vacuo* to yield 440 mg (80%) of orange solid with a green lustre, which was sufficiently pure to use in the subsequent step. ^{1}H

NMR (300 MHz, DMSO) δ 8.20 (d, *J* = 7.6 Hz, 1H), 7.87 (t, *J* = 7.2 Hz, 1H), 7.79 (t, *J* = 7.4 Hz, 1H), 7.52 (d, *J* = 6.7 Hz, 1H), 7.27 (d, *J* = 10.6 Hz, 1H), 7.01 (t, *J* = 5.8 Hz, 1H), 6.94 (d, *J* = 9.0 Hz, 1H), 6.84 (dd, *J* = 13.5, 9.3 Hz, 2H), 6.40 (d, *J* = 9.9 Hz, 1H), 6.24 (s, 1H), 4.98 (d, *J* = 8.1 Hz, 2H), 4.13 (t, *J* = 5.6 Hz, 2H), 3.97 (dd, *J* = 7.0, 3.5 Hz, 2H), 3.17 (dd, *J* = 18.7, 5.4 Hz, 2H), 1.37 (d, *J* = 2.6 Hz, 9H), 0.88 (t, *J* = 7.0 Hz, 3H). ^{13}C NMR (75 MHz, DMSO) δ 13.66;28.53; 30.98; 43.01; 55.19; 60.42; 61.24; 64.20; 65.36; 78.26; 101.76; 104.98; 113.96; 115.27; 117.40; 129.31; 130.32; 130.91; 133.39; 133.79; 150.19; 153.68; 156.05; 158.68; 162.47; 165.25; 168.28; 184.32. $[M+H]^+$ Calc. for $C_{31}H_{32}NO_9$: 562.2032; Found: 562.1532.

2-aminoethoxy 6-O-(carbonylmethyl) fluorecein ethyl ester (1)

2-((*tert*-butoxycarbonyl)amino)ethoxy 6-O (carbonylmethyl) fluorecein ethyl ester (200 mg, 0.36 mmol) was dissolved in DCM (3 mL). TFA (890 µL) was added dropwise and the reaction was heated under reflux for 72 hours.

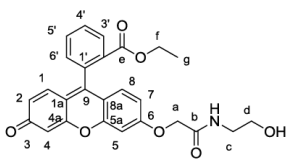

1M NaOH was added dropwise until pH 7. The solution was extracted with DCM (2 x 5mL), and then the organic layer was washed with brine (5 mL) and dried over $MgSO_4$, filtered, and concentrated *in vacuo* to yield the desired product (121 mg, 73%) as a light orange solid. IR (neat solid) υ 3310 (OH + NH), 1684 (CO_2Et), 1652 (C=O), 1635 (Amide I), 1539 (Amide II) cm^{-1}; ^{1}H NMR (300 MHz, DMSO) δ 8.16 (dd, *J* = 7.4, 3.4 Hz, 1H, H-3'), 8.15 (t, *J* = 5.8 Hz, NH), 7.86 (td, *J* = 7.5, 1.5 Hz, 1H, 5'), 7.77 (td, *J* = 7.6, 1.4 Hz, 1H, H-4'), 7.50 (dd, *J* = 7.5, 1.1 Hz, 1H, H-6'), 7.19 (d, *J* = 2.3 Hz, 1H, H-5), 6.95 (dd, *J* = 8.8, 2.3 Hz, 1H, H-7), 6.88 (d, *J* = 8.8 Hz, 1H, H-8), 6.81 (d, *J* = 9.7 Hz, 1H, H-1), 6.39 (dd, *J* = 9.7, 1.9 Hz, 1H, H-2), 6.25 (d, *J* = 1.9 Hz, 1H, H-4), 4.72 (t, J = 6.0 Hz, OH), 4.67 (s, 2H, Ha), 4.02 – 3.86 (m, 2H, Hf), 3.43 (dd, *J* = 11.4, 5.9 Hz, 2H, Hd), 3.20 (q, *J* = 5.9 Hz, 2H, Hc), 0.87 (t, *J* = 7.1 Hz, 3H, Hg). ^{13}C NMR (75 MHz, DMSO) δ :13.72 (Cg); 41.61 (Cc); 59.94 (Cd); 61.27 (Cf); 67.62 (Ca); 101.73 (C-5); 105.00 (C-4); 114.30 (C-7); 115.15 (C-8a); 117.34 (C-1a); 129.30 (C-8); 129.8 (C-2); 130.29 (C-4'); 130.40 (C-1); 130.77 (C-6'); 130.9 (C-3'); 131.06 (C-2'); 133.40 (C-1'); 133.82 (C-5'); 150.25 (C-9); 153.65 (C-5a); 158.67 (C-4a); 162.57 (C-6), 165.29 (Ce); 167.14 (Cb); 184.29 (C3). $[M+H]^+]^+$ Calc. for $C_{26}H_{24}NO_7$: 462.1533;

Found: 462.2008. *Anal*. Calcd. for $C_{26}H_{24}NO_7$: C, 67.67; H, 5.02; N, 3.04. Found: C, 67.95; H 5.04; N, 3.02.

***tert*-Butyl-2-hydroxyethylcarbamate.**

2-aminoethanol (2.04 mL, 34 mmol) was dissolved in 1M NaOH solution (100 mL) and the mixture was stirred. A separate solution of BOC_2O (8.89 g, 40.8 mmol) in 1,4-Dioxane (50 mL) was added to the reaction. The solution was stirred for 48 hours. The reaction was quenched with water and the solution was extracted with ethyl acetate (3 x 75 mL), the organic layer was washed with brine (75 mL) and dried over $MgSO_4$, filtered, and concentrated *in vacuo* to yield the Tert-buthyl-2-hydroxyethylcarbamate (4.06 g, 74%) as a light yellow oil. ^{1}H NMR (300 MHz, $CDCl_3$) δ 5.51 (s, 1H), 3.96 (s, 1H), 3.34–3.23 (m, 2H), 2.97 – 2.85 (m, 2H), 1.12 (s, 9H).

Spectrocopic data for Ligand 1.

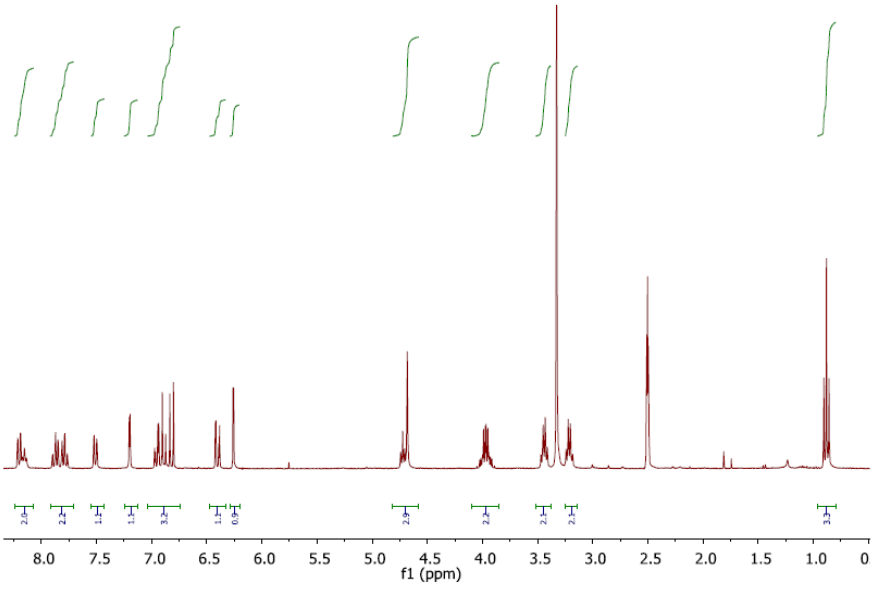

Figure SI-2. ^{1}H NMR of chemosensor **1**.

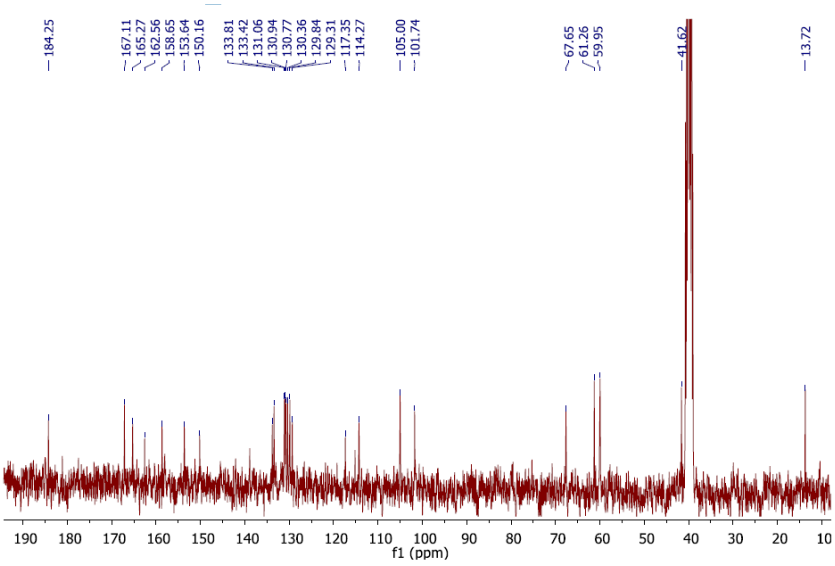

Figure SI-3. ^{13}C NMR of Ligand **1**.

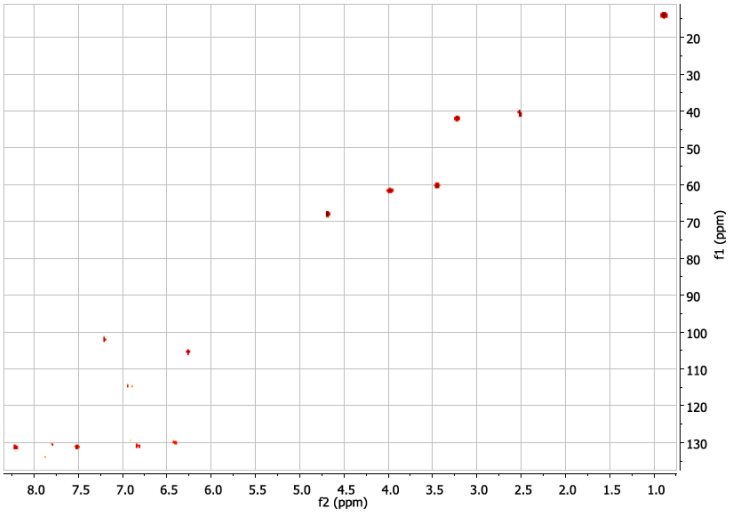

Figure SI-4. ^{13}C-^{1}H HSQC NMR of Ligand **1**.

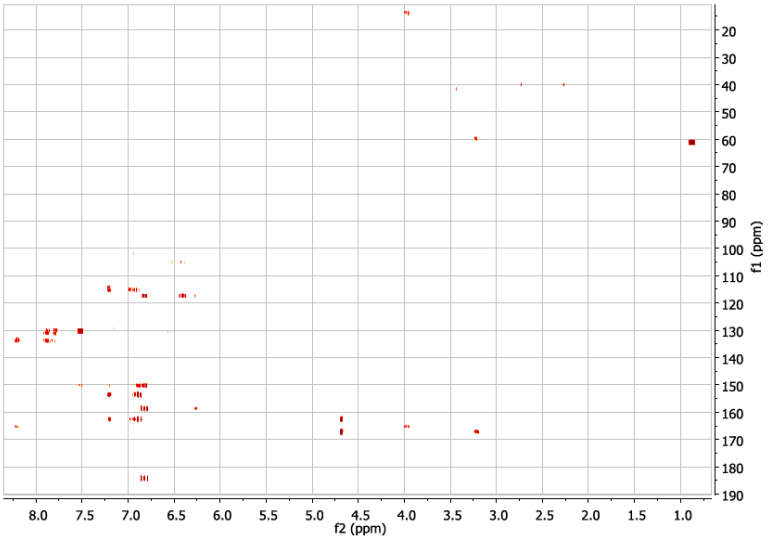

Figure SI-5. ^{13}C-^{1}H HMBC NMR of Ligand **1**.

Titration experiments

The binding constants of ligand **1** towards trivalent cations were evaluated by UV–vis and fluorescence titrations in acetonitrile. Typically, the 10^{-5} M solutions of the receptors in acetonitrile (3 mL) were titrated by adding 0.1 equiv. aliquots of the envisaged cations in CH_3CN and by registering the UV–vis or fluorescence spectrum after each addition. The log Kc value was calculated by fitting all the spectrophotometric titration curves with the SPECFIT program [32].

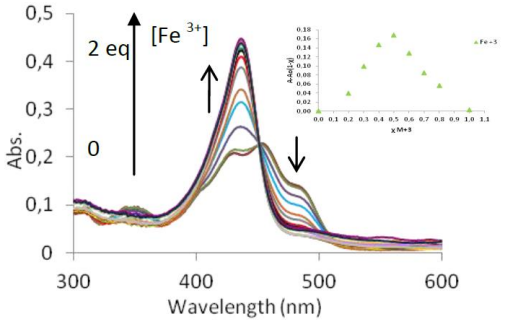

Figure SI-6. UV-vis spectra of ligand **1** (10^{-5} M) upon titration of Fe^{3+} (0-2 equiv.) in CH_3CN. Inset: absorbance of **1** at 437 nm as a function of the [cation]/[ligand] ratio.

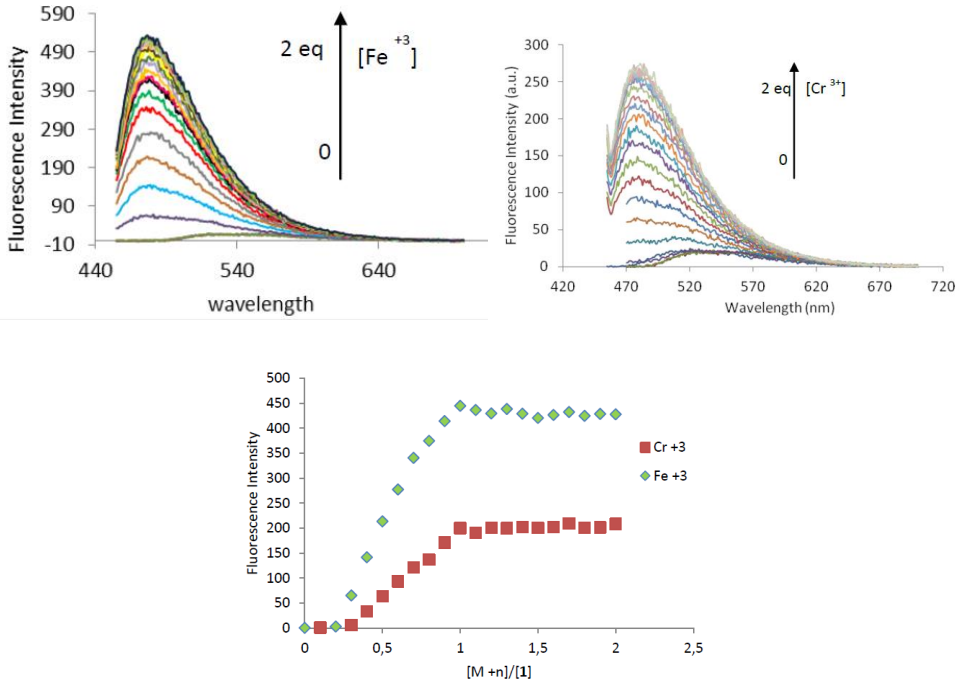

Figure SI-7. Fluorescence titration spectra of **1**(10^{-5} M) upon titration with Fe^{3+} and Cr^{3+} in CH_3CN (λ_{exc} = 437nm). Graphic of fluorescence intensity versus Fe^{3+} and Cr^{3+} concentration.

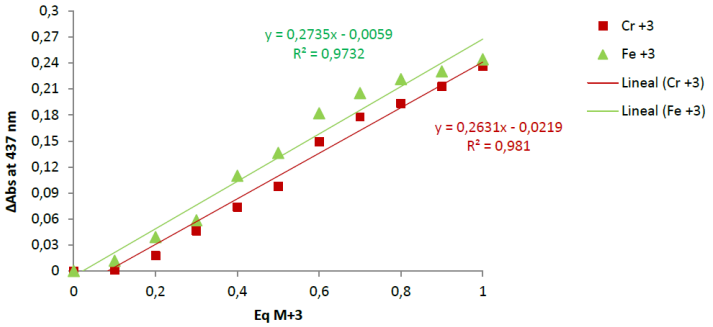

Figure SI-8. A plot of ($A-A_o$) vs. cations concentrations at 437 nm in CH_3CN at room temperature.

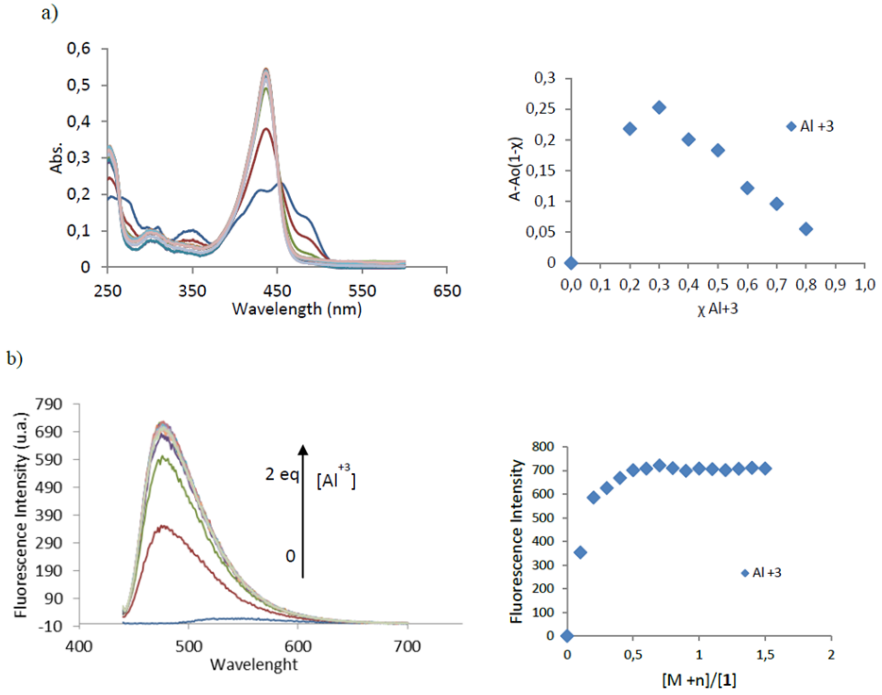

Figure SI-9. (a) UV-vis spectra of ligand **1** (10^{-5} M) upon titration of Al^{3+} (0-2 equiv.) in CH_3CN. Inset: Stoichiometry determination by the Job's plot yielded from UV-vis absorption; (b) Fluorescence titration spectra of ligand **1**(10^{-5} M) upon titration with Al^{3+} in CH_3CN (λ_{exc} = 437 nm) and graphic of fluorescence intensity versus Al^{3+} concentration.

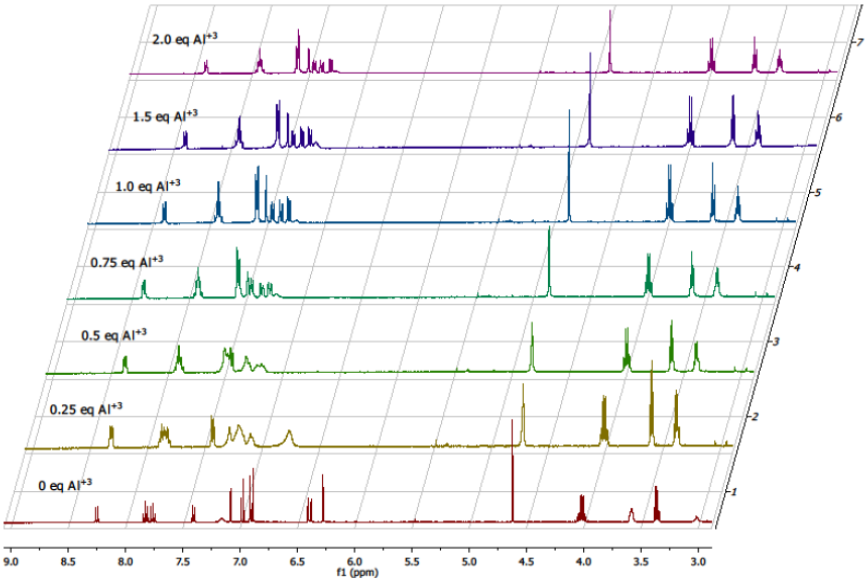

Figure SI-10. ^{1}H NMR spectra of Ligand **1** and Ligand **1** + 0.25, 0.50, 0.75, 1.0, 1.5, 2.0 eq. of Al^{3+} in CD_3CN from the bottom to the top respectively.

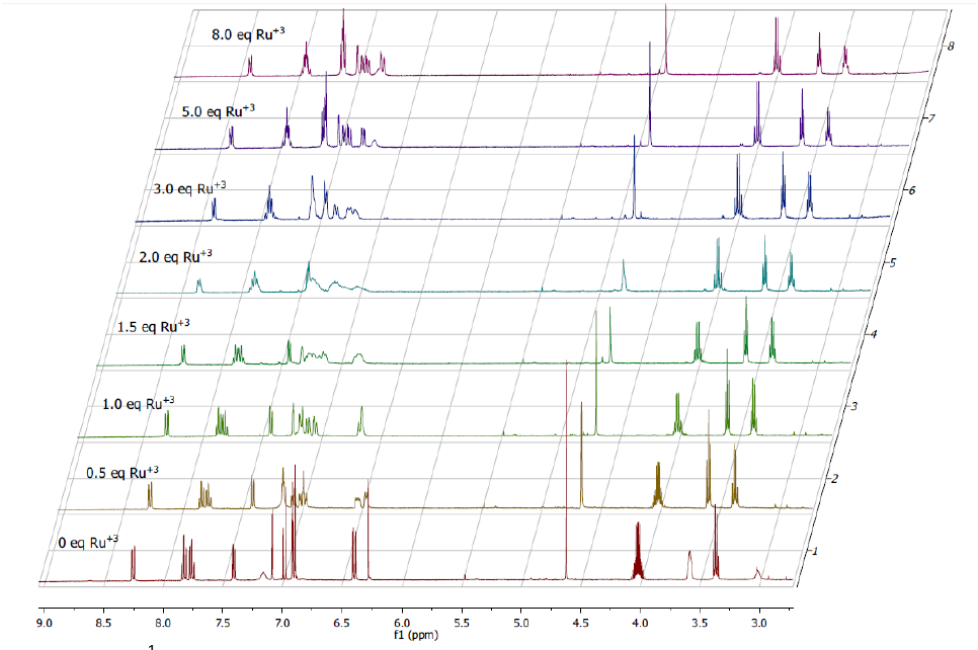

Figure SI-11. ^{1}H NMR spectra of Ligand **1** and Ligand **1** + 0.50, 1.0, 1.5, 2.0, 3.0, 5.0 and 8.0 eq. of Ru^{3+} in CD_3CN from the bottom to the top respectively

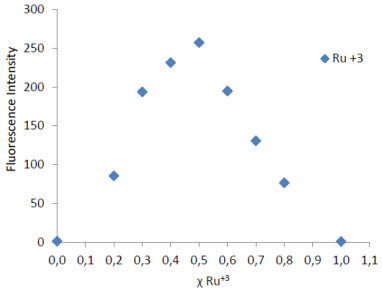

Figure SI-12. Stoichiometry determination of **1**·Ru^{3+} complex by the Job's plot yielded from fluorescence.

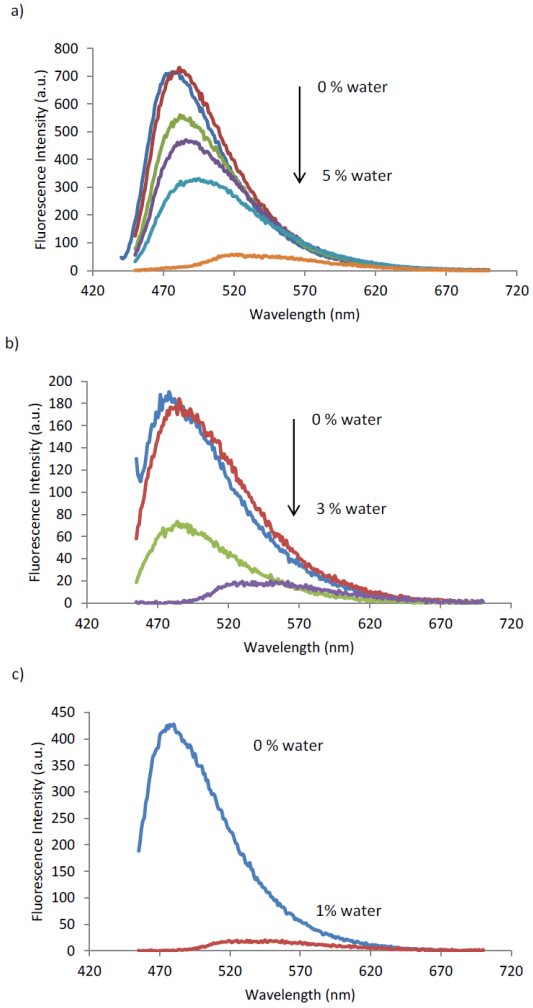

Figure SI-13. Fluorescence spectra (λ_{ex} = 437 nm) of **1** measured with 1 eq. of Al^{3+} (a), Cr^{3+} (b) and Fe^{3+} (c) in CH_3CN in the presence of 0-5 % water.

3.5 Off-on BODIPY-based chemosensors for selective detection of Al^{3+} and Cr^{3+} versus Fe^{3+} in aqueous media.

Off-on BODIPY-based chemosensors for selective detection of Al^{3+} and Cr^{3+} versus Fe^{3+} in aqueous media

Andrea Barba-Bon,[a,] Laura Calabuig,[b] Ana M.Costero,[ab] Salvador Gil,[ab] Ramón Martínez-Máñez[ac] and Felix Sancenón[ac]

[a] Centro de Reconocimiento Molecular y Desarrollo Tecnológico (IDM),Unidad Mixta Universidad Politécnica de Valencia-Universitat de Valencia, Spain

[b] Departamento de Química Orgánica, Universitat de Valencia, Dr. Moliner, 50, 46100 Burjassot ,Valencia, Spain.

[c] Departamento de Química, Universidad Politécnica de Valencia Camino de Vera s/n, 46022, Valencia, Spain.

Received: *19 th November 2013*

Published online: *20 rd January 2014*

RSC Adv., ***2014***, *4, 8962-8965.*

Two new off–on BODIPY-based chemosensors that are highly sensitive for trivalent cations in aqueous solutions are described. Compound 2 exhibits selective sensing of Al^{3+} and Cr^{3+} *versus* Fe^{3+} through two different channels (UV-vis and fluorescence).

The design of new probes for transition and p-block metal cations is an important subject within the field of supramolecular chemistry because of their impact on the environment and human health. In this area, although a number of chemosensors for divalent transition metal cations have been described, there are a relatively small number of probes able to selectively respond to triple-charged metal cations[1] and even less in aqueous environments.[2] However, trivalent cations have important properties and play significant roles in different fields. For instance chromium is an essential element in human nutrition and has a huge impact on the metabolism of carbohydrates, fats, proteins and nucleic acids and has been reported to disturb glucose levels and lipid metabolism.[3] On the other hand Fe^{3+} also plays a key role in many biochemical processes at the cellular level and it is indispensable for most organisms, and both its deficiency and overload can induce various disorders.[4,5] Finally, it is well-known that Al^{3+} plays important roles in cells and environmental food chains and for instance was found to kill fishes in acidified water and cause damages to the central nerve system of human beings.[6] Therefore, the design of new probes for the simple and easy detection of these metal cations in a number of different situation is of much interest.

Based in these concepts, and bearing in mind our interest in the design of chemosensors, we report herein two new probes (**1** and **2**, see Scheme 1) based in dipyrromethene boron difluoride (BODIPY) scaffold, for a simple optical detection of trivalent cations. BODIPY dyes are a class of well-known fluorophores with widespread applications as fluorescent probes due to their valuable characteristics, such as high molar absorption coefficients and high quantum yields leading to intense absorption and fluorescence bands.[7] In this context, although a large number of BODIPY dyes have been designed and prepared for

detecting metal cations, [8] very few examples display sensing features in aqueous solutions.[9]

Probe **1** was synthesized through a bicondensation of *N*-methyl-*N*-(2-hydroxyethyl)-4-aminobenzaldehyde and 2,4-dimethylpyrrole in the presence of trifluoroacetic acid (TFA) as catalyst,[10] followed by oxidation with *p*-chloranil. The boron difluoride bridge was introduced by treatment with boron trifluoride diethyl etherate ($BF_3{\cdot}Et_2O$) in the presence of triethylamine (TEA). For the synthesis of probe **2**, the BODIPY derivative **I** was prepared from 2,4-dimethylpyrrole and benzaldehyde (see ESI) following the same procedure as above.[10] Condensation of **I** and *N*-methyl-*N*-(2-hydroxyethyl)-4-aminobenzaldehyde in benzene in presence of acetic acid and piperidine[7b,11] yielded **2**.

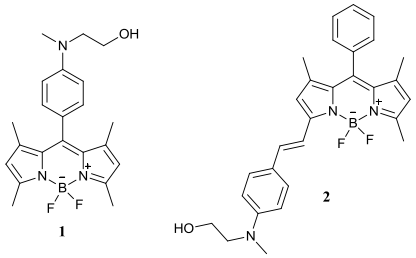

Scheme 1. Chemical structure of the BODIPY derivatives **1** and **2**.

Probe **1** shows in water : CH_3CN (80 : 20 v/v) an intense absorption band at 490 nm (ε = 77600 cm^{-1} M^{-1}) yet it is scarcely fluorescent (ϕ = 0.002 using aqueous fluorescein as reference).[12] This low emission is tentatively attributed to a photo-electron transfer (PET) from the lone pair of the amino group to the photo-excited BODIPY group.[13] Fig. 1 shows the fluorescence spectrum (λ_{exc} = 480 nm) of **1** alone and in the presence of 1 equiv. of different metal cations. Addition of Fe^{2+}, Cu^{2+}, Zn^{2+}, Cd^{2+}, Co^{2+}, Ni^{2+}, Li^{+}, Hg^{2+} and Ru^{3+} did not modify the emission of **1**, whereas trivalent cations Al^{3+}, Fe^{3+} and Cr^{3+} led to a very remarkable enhancement of the fluorescence emission (ϕ_{Al} = 0.29; ϕ_{Fe} = 0.17; ϕ_{Cr} = 0.24) at 515 nm.

Moreover, no colour modulations in the presence of metal cations were found for **1**. This was an expected result bearing in mind the presence of methyl groups in the pyrrole units that most likely impose a twist position of the phenyl ring that

interrupts the conjugation between the *N*-methyl-*N*-(2-hydroxyethyl) coordination site and the signaling unit.[14]

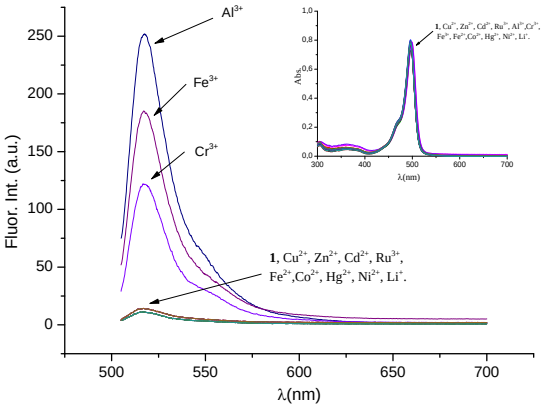

Figure 1. Fluorescence emission spectra of **1** (10^{-5} M) upon addition of 1 eq. of Fe^{3+}, Fe^{2+}, Cu^{2+}, Zn^{2+}, Cd^{2+}, Co^{2+}, Ni^{2+}, Li^{+}, Hg^{2+}, Ru^{3+}, Cr^{3+} and Al^{3+} in water : CH_3CN (80 : 20 v/v) (λ_{ex} = 480 nm). Inset: UV-Vis spectra of **1** (10^{-5} M) upon addition of 1 eq. of the different cations in water: CH_3CN (80: 20 v/v).

In contrast, the signaling unit and binding site in probe **2** are electronically connected and therefore changes both in colour and emission were found (vide infra). In water : CH_3CN (40 : 60 v/v), **2** exhibited a strong absorbance with a maximum at 603 nm (ε = 38400 M^{-1} cm^{-1}). This band is bathochromically shifted by *ca*. 100 nm when compared with the parent BODIPY fluorophore due to the styryl extension at the α-position. Moreover probe **2** was poorly fluorescent (λ_{exc} = 530 nm, ϕ = 0.007) most likely due to an efficient ICT quenching of the excited state of the BODIPY-chromophore from the electron-donating amino moiety.

Addition of Fe^{2+}, Zn^{2+}, Cd^{2+}, Co^{2+}, Ni^{2+}, Li^{+}, Cu^{2+}, Hg^{2+}, Ru^{3+} or Fe^{3+} to solutions of **2** in water : CH_3CN (40 : 60 v/v) did not induce any change neither in the UV-Vis nor in the fluorescence spectra. By contrast, in the presence of the trivalent cations Cr^{3+} and Al^{3+} the colour of the solutions changed dramatically from blue to pink due to the appearance of a new band at 560 nm (see Fig. 2). Probe **2** also shows some colour change in the presence of Fe^{3+} but only when CH_3CN alone or mixtures with a maximum of 8% water were used. Interestingly probe **2** also displays a

remarkable strong fluorescence emission at 563 nm in water : CH_3CN (40 : 60 v/v) upon addition of the metal cations Cr^{3+} and Al^{3+} (ϕ_{Al} = 0.33; ϕ_{Cr} = 0.30).

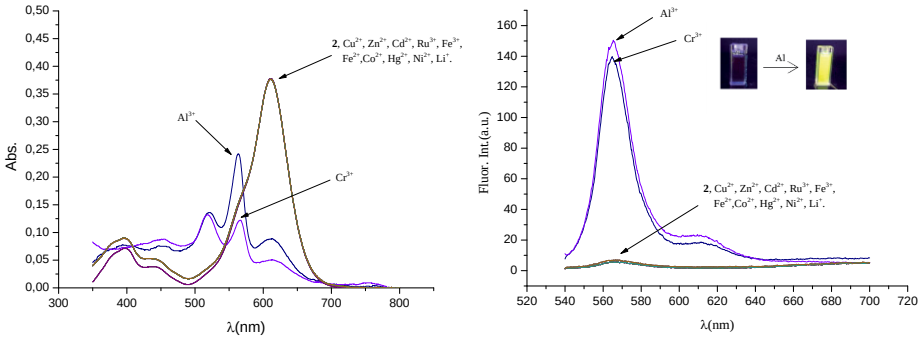

Figure 2. UV-Vis spectra (a) and fluorescence emission spectra (λ_{ex} = 530 nm) (b) of **2** (10^{-5} M) upon addition of 1 eq. of Fe^{3+}, Fe^{2+}, Cu^{2+}, Zn^{2+}, Cd^{2+}, Co^{2+}, Ni^{2+}, Li^{+} , Hg^{2+},Cr^{3+} and Al^{3+} in water : CH_3CN (40 : 60 v/v).

Furthermore in competitive experiments it was found that probes **1** and **2** respond to the presence of Al^{3+}, Cr^{3+} and Fe^{3+} (for **1**) and to Al^{3+} and Cr^{3+} (for **2**) in the presence of Hg^{2+}, Li^{+}, Na^{+}, K^{+}, Ag^{+}, Ca^{2+}, Mg^{2+}, Ni^{2+}, Zn^{2+}, Cd^{2+}, Fe^{2+}, Co^{2+} and Cu^{2+} cations. In addition, limits of detection (LOD) were determined from the equation LOD = *K* x Sb_1/S, where *K* =3, Sb_1 is the standard deviation of the blank solution and *S* is the slope of the calibration curve.[15] The obtained results were 0.14, 019 and 0.10 μM for Al^{3+}, Cr^{3+} and Fe^{3+} respectively with ligand **1** and 0.08 and 0.18 μM for Al^{3+} and Cr^{3+} with ligand **2** using in both cases emission measurements. Moreover LOD of 0.18 and 0.52 μM were calculated for Al^{3+} and Cr^{3+} using **2** from UV-vis titrations.

Titration experiments of **1** and Fe^{3+}, Cr^{3+} and Al^{3+} in water: CH_3CN (80: 20 v/v) (by fluorescence spectroscopy) and of **2** with Cr^{3+} and Al^{3+} in water: CH_3CN (40: 60 v/v) (by either UV-Vis or fluorescence) were carried out in order to determine the complexation constants by using the software Specfit program.[16] As an example Fig. 3 shows the fluorescence titration of **1** with Al^{3+}.

A stepwise addition of Al^{3+} led to an enhancement of the band at 515 nm, which is saturated upon the addition of 1 equiv. of Al^{3+}, strongly, suggesting the formation of 1 : 1 ligand-to-metal complexes. This was also demonstrated via the

corresponding Job's plot and MS. The same stoichiometry was observed for Cr^{3+} and Fe^{3+} with **1**.

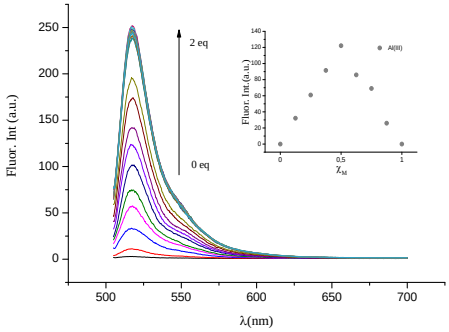

Figure 3. Fluorescence response ($\lambda_{exc.}$ = 480 nm) for **1** (10^{-5} M) to increasing amounts of Al^{3+} in water : CH_3CN (80 : 20 v/v). The inset shows the corresponding Job plot.

Moreover, similar fluorescence titration studies with **2** also indicated the formation of 1 : 1 ligand-to-metal complexes with the trivalent metal cations Cr^{3+} and Al^{3+}. Moreover UV-vis spectroscopy titrations with **2** also resulted in similar results (see Table 1).

Table 1 Complexation constants for probes **1** and **2** with trivalent cations for the formation of 1 : 1 ligand-to-metal complexes.

	Ligand **1**[a]	Ligand **2**[b]	
Cation	log K[c]	log K[d]	log K[c]
Al^{3+}	5.9 ± 0.2	5.9 ± 0.7	5.2 ± 0.3
Cr^{3+}	6.5 ± 0.3	5.3 ± 0.6	5.6 ± 0.3
Fe^{3+}	4.8 ± 0.2	-	-

[a] Determined in water : CH_3CN (80 : 20 v/v). [b] Determined in water : CH_3CN (40 : 60 v/v).
[c] Determined by UV-vis titrations. [d] Determined by fluorescence titrations.

All these results are consistent with a sensing mechanism in which the metal cations form complexes with **1** and **2** via coordination with the *N*-methyl-*N*-(2-hydroxyethyl) moiety. The interaction of the cation with the lone pair on the nitrogen atom in **1** results in an inhibition of the PET process giving rise to the observed enhancement of the fluorescence emission. On the other hand, the binding of the cation with the lone pair on the nitrogen atom in **2** results in a reduction of the electron-donating ability of the nitrogen atom of *N*-methyl-*N*-(2-

hydroxyethyl)-styryl group which is in conjugation to the BODIPY core, thus suppressing the ICT process causing the blue shift of the absorption spectrum band and an enhancement of the fluorescence.

To confirm the proposed sensing mechanism, ^{1}H NMR experiments were carried out. Thus, ^{1}H NMR spectra of ligand **1** free and the presence of different amounts of Al^{3+} were recorded in CD_3CN (Fig. 4). The most important modifications of the signals of **1** after complexation were observed in the phenyl moiety (7.10 and 6.84 ppm) which underwent a significant downfield shift upon the addition of Al^{3+} (0.52 and 0.90 ppm respectively). The change is especially important in the *ortho*-protons to the amino group. On the other hand the methylene group that in the free ligand appears at 3.44 ppm show a downfield shift of 0.20 ppm and the signal corresponding to the hydroxymethylene protons, at 3.58 ppm, displayed a different behavior with an upper field shift of 0.18 ppm. Finally, there were no changes in the protons of the pyrrole units (at 6.15 ppm). These data strongly suggest the direct involvement of the amino group in the Al^{3+} coordination.

A similar behavior was observed with ligand **2** (see ESI†) upon addition of Al^{3+}. Remarkable changes were observed in the *N*-methyl-*N*-(2-hydroxyethyl) styryl group, especially in the *ortho*-protons to the amino group. On the other hand, changes in the protons of the pyrrole units and phenyl moiety in the 8 position of the BODIPY were negligible.

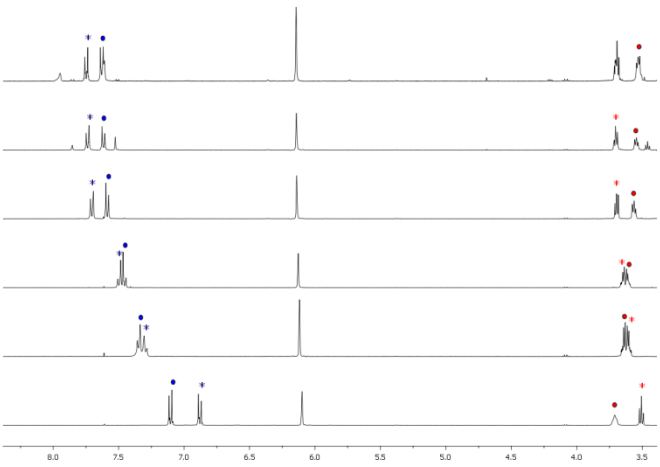

Figure 4. ^{1}H-NMR spectra of **1** and **1** + increasing amounts of Al^{3+} in CD_3CN.

Conclusions

In summary, we have successfully synthesized and characterized two BODIPY-based probes which show a "turn-on" response with trivalent cations of interest whereas the probe remained silent in the presence of competitive cations (Hg^{2+}, Li^{+}, Na^{+}, K^{+}, Ag^{+}, Ca^{2+}, Mg^{2+}, Ni^{2+}, Zn^{2+}, Cd^{2+}, Fe^{2+}, Co^{2+}, Ru^{3+}, Fe^{2+} and Cu^{2+}). This sensing behavior is highly selective and it is observed in mixed aqueous solutions. Compound **1** can be only used in fluorescence studies whereas compound **2** gives sensing response through two different channels, UV-vis and fluorescence. The observed colour change or enhanced fluorescence emission can be attributed to the binding of M^{3+} to the 2-aminoethanol moiety which reduces the electron-donating ability of the nitrogen atom conjugated to the BODIPY core. Finally, selective sensing of Al^{3+} and Cr^{3+} versus Fe^{3+} was observed with ligand **2**.

Acknowledgements

Financial support from the Spanish Government (Project MAT2012-38429-C04) and the Generalitat Valencia (Project PROMETEO/2009/016) is gratefully acknowledged. A.B.B. thanks for a pre-doctoral FPI fellowship.

Notes and references

1 (a) R. Kramer, *Angew. Chem., Int. Ed*., 1998, **37**, 772–773; (b) L. Fabbrizzi and A. Poggi, *Chem. Soc. Rev*., 1995, **24**, 197– 202; (c) Y. Wu, X. Peng, B. Guo, J. Fan, Z. Zhang, J. Wang, A. Cui and Y. Gao, *Org. Biomol. Chem*., 2005, **3**, 1387–1392; (d) X. Peng, J. Du, J. Fan, J. Wang, Y. Wu, J. Zhao, S. Sun and T. Xu, *J. Am. Chem. Soc.,* 2007, **129**, 1500–1501; (e) X. Chen, Y. Zhou, X. Peng and J. Yoon, *Chem. Soc. Rev.*, 2010, **39**, 2120–2135; (f) A. Barba-Bon, A. M. Costero, S. Gil, M. Parra, J. Soto, R. Martinez-Mañez and F. Sncenón, *Chem. Commun*., 2012, **48**, 3000–3002.

2 (a) C.-H. Chen, D.-J. Liao, C.-F. Wan and A.-T. Wu, *Analyst*, 2013, **138**, 2527–2530; (b) S.-D. Liu, L.-W. Zhang and X. Liu, *New J. Chem*., 2013, **37**, 821–826; (c) S.-R. Liu and S.-P. Wu, *Sens. Actuators, B,* 2012, **171**, 1110–1116.

3 (a) H. Arakawa, R. Ahmad, M. Naoni and H.-A. Tajmir-Riahi, *J. Biol. Chem.,* 2000, **275**, 10150–10153; (b) H. Wu, P. Zhou, J. Wang, L. Zhao and C. Duan, *New J. Chem*., 2009, **33**, 653– 658.

4 (a) P. Aisen, M. Wessling-Resnick and E. A. Leibold, *Curr. Opin. Chem. Biol*., 1999, **3**, 200–206; (b) R. S. Eisenstein, *Annu. Rev. Nutr*., 2000, **20**, 627–662.

5 (a) N. C. Andrews, *N. Engl. J. Med*., 1999, **341**, 1986–2195; (b) D. Touati, *Arch. Biochem. Biophys*., 2000, **373**, 1–6.

6 S. Garcia-Medina, A. C. Razo-Estrada, L. M. Gomez-Olivan, A. Amaya-Chavez, E. Madrigal-Buijaidar and M. Galar-Martinez, *Fish Physiol. Biochem*., 2010, **36**, 875–882.

7 (a) A. Loudet and K. Burgess, *Chem. Rev*., 2007, **107**, 4891– 4932; (b) G. Ulrich, R. Ziessel and A. Harriman*, Angew. Chem., Int. Ed*., 2008, **47**, 1184–1201.

8 (a) D. Wang, Y. Shiraishi and T. Hiari*, Tetrahedron Lett*.,2010, **51**, 2545–2549; (b) X. Xie and Y. Qin, *Sens. Actuators, B*, 2011, **156**, 213–217; (c) D. Wang, Y. Shiraisi and T. Hirai, *Chem. Commun*., 2011, **47**, 2673–2675; (d) H. B. Sun, S. J. Liu, T. C. Ma, N. N. Song, Q. Zhao and W. Huang, *New J. Chem.,* 2011, **35**, 1194–1197; (e) H. Son, J. H. Lee, Y. R. Kim, S. Han, X. Liu, J. Jaworski and H. Jung, *Analyst,* 2012, **137**, 3914–3916.

9 (a) M. Wang, J. Wang, W. Xue and A. Wu, *Dyes Pigm*., 2013, **97**, 475–480; (b) T. Hirata, T. Terai, T. Komatsu, K. Hanaoka and T. Nagano, *Bioorg. Med. Chem. Lett*., 2011, **21**, 6090–6093; (c) S. Zhu, J. Zhang, J. Janjanam, G. Vegesna, F.-T. Luo, A. Tiwari and H. Liu*, J. Mater. Chem. B,* 2013, **1**, 1722–1728.

10 (a) M. Baruah, W. Qin, N. Basari´e, W. M. De Borggraeve and N. Boens, *J. Org. Chem*., 2005, **70**, 4152–4157; (b) Y. Ikawa, S. Moruyama and H. Furuta, *Anal. Biochem*., 2008, **378**, 166–170.

11 N. Saki, T. Din and E. U. Akkaya, *Tetrahedron,* 2006, **62**, 2721– 2725.

12 J. Umberger and V. K. LaMer, *J. Am. Chem. Soc*., 1945, **67**, 1099–1109.

13 A. P. de Silva, H. Q. N. Gunaratne, T. Gunnlaugsson, A. J. M. Huxley, C. P. McCoy, J. T. Rademacher and T. E. Rice, *Chem. Rev.*, 1997, **97**, 1515–1566.

14 M. Kollmannsberger, T. Gareis, S. Heinl, J. Breu and J. Daub, *Angew. Chem., Int. Ed*., 1997, **36**, 1333–1335.

15 M. Zhu, M. Yuan, X. Liu, J. Xu, J. Lv, C. Huang, H. Liu, Y. Li,S. Wang and D. Zhu, *Org. Lett*., 2008, **10**, 1481–1484.

16 *SPECFIT/32TM GLOBAL ANALYSIS SYSTEM v.3.0*, Spectrum Associates, Marlborough, MA, USA, http://www.biologic. info/rapidkinetics/specfit.html.

Supporting Information

Off-on BODIPY-based chemosensors for selective detection of Al^{3+} and Cr^{3+} versus Fe^{3+} in aqueous media

Andrea Barba-Bon, Laura Calabuig, Ana M.Costero, Salvador Gil, Ramón Martínez-Máñez and Felix Sancenón

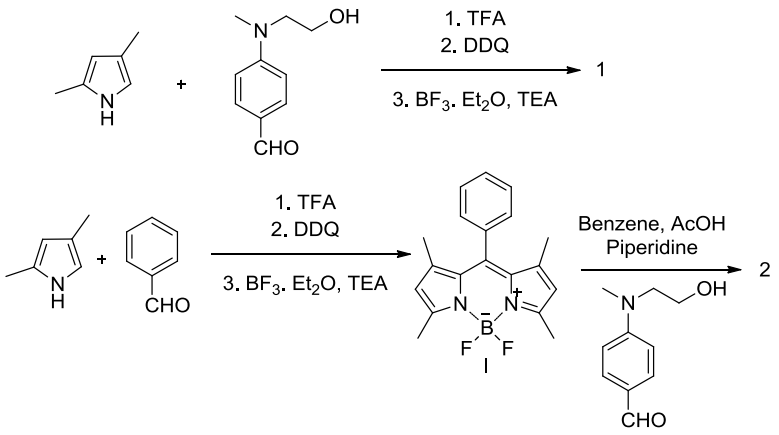

Scheme SI-1. Synthetic routes for BODIPY dyes **1** and **2**.

Experimental section

General remarks

CH_2Cl_2 and CH_3CN were distilled from P_2O_5 under Ar prior to use. Benzene was distlled from CaH_2 under Ar proir to use. All other solvents and starting materials were purchased from comercial sources when available, and were used without purification. Colum chromatography was performed on silica gel.^{1}H NMR, ^{13}C NMR (300 MHz) spectra were determined on a Bruker AV 300 spectrometrer. Chemical shifts are reported in parts per million (ppm), calibrated to the solvent peak set.

Synthesis and characterization of BODIPY derivatives

4,4-difluoro-8-(4-((2-hydroxyethyl)(methyl)amino)phenyl)-1,3,5,7-tetramethyl -4-bora-3a,4a-diaza-s-indacene. (**1**)

2,4-Dimethylpirrole (2.2 mL; 21.3 mmol) and *N*-methyl-*N*-(2-hydroxyethyl)-4-aminobenzaldehyde (1.90 g; 10.65 mmol) were dissolved in 80 mL of CH_2Cl_2. Trifluoroacetic acid (82 µL; 1.06 mmol) was added, and the solution was stirred at room temperature for 50 min. A solution of DDQ (2,3-dichloro-5,6-dicyano-*p*-

benzoquinone, 2.61 g; 10.65 mmol) in CH_2Cl_2 (15 mL) was added. Stirring was continued for 50 min, followed by the addition of 20 mL of triethylamine. After stirring for 30 min, $BF_3.OEt_2$ (29 mL) was added. The mixture was stirred for 75 min at rt. After the evaporation of the solvents under reduced pressure, the crude product was purified by silica gel column chromatography with AcOEt/Hexane (2:1) to give the compound **1** as red crystals in 36% yield (1.528 g). ^{1}H NMR (300 MHz, DMSO) δ 7.10 – 7.01 (m, 2H), 6.84 (t, *J* = 5.8 Hz, 2H), 6.15 (s, 2H), 4.73 (t, *J* = 5.3 Hz, 1H), 3.58 (q, *J* = 5.8 Hz, 2H), 3.44 (t, *J* = 6.0 Hz, 2H), 2.98 (s, 3H), 2.43 (s, 6H), 1.45 (d, *J* = 8.5 Hz, 6H).^{13}C NMR (75 MHz, DMSO) δ 154.41 , 149.96 , 143.04 , 128.88 , 120.95 ,112.08, 58.38, 54.54, 41.43, 38.97, 14.64 HRMS (EI): m/z (%) calc for $C_{22}H_{26}BF_2N_3O$: 398.2107 $[M+1]^+$ found: 398.2225. UV-Vis (CH_3CN) λ_{max} 496.5 nm.

4, 4-difluoro-1,3,5,7-tetramethyl-8-phenyl-4-bora-3a, 4a-diaza-s-indacene. (**I**)
2,4-Dimethylpirrole (1.0 mL; 10 mmol) and benzaldehyde (0.5 mL; 5 mmol) were dissolved in 50 mL of CH_2Cl_2. Trifluoroacetic acid (39 µL; 0.5 mmol) was added, and the solution was stirred at room temperature for 50 min. A solution of DDQ (1.2 g; 5 mmol) in CH_2Cl_2 was added. Stirring was continued for 50 min, followed by the addition of 10 mL of triethylamine. After stirring for 30 min, $BF_3{\cdot}OEt_2$ (10 mL) was added. The mixture was stirred for 45 min at room temperature. After the evaporation of solvents under reduced pressure, the crude product was purified by silica gel column chromatography with AcOEt/Hexane (1:2) to give the compound **I** as green crystals in 40 % yield. ^{1}H NMR (300 MHz, $CDCl_3$) δ 7.49 (d, *J* = 1.8 Hz, 1H), 7.47 (t, *J* = 2.4 Hz, 2H), 7.30 – 7.26 (m, 2H), 5.98 (s, 2H), 2.56 (s, 6H), 1.37 (s, 6H). UV-Vis (CH_3CN) λ_{max} 507 nm; emission (CH_3CN) λ_{max} 516 nm.

(E)-4,4-difluoro-5-(4-((2-hydroxyethyl)(methyl)amino)styryl)-1,3,7-trimethyl-8-phenyl-4-bora-3a,4a-diaza-s-indacene.(**2**)
Compound **I** (600 mg; 1.85 mmol) and *N*-methyl-*N*-(2-hydroxyethyl)-4-aminobenzaldehyde (330 mg; 1.85 mmol) were dissolved in a mixture of benzene (80 mL), acetic acid (5.3 mL) and piperidine (5.8 mL; 59.2 mmol). Any water formed during the reaction was removed azeotropically by heating in a Dean-

Stark apparatus for 3 h. The reaction mixture was concentrated under reduced pressure and then subjected to silica gel column chromatography with AcOEt/Hexane (2:1) to yield the desired product **2** as blue crystals in 43 % yield (387 mg). ^{1}H NMR (300 MHz, DMSO) δ 7.55(dd, *J* = 9 Hz, 3H), 7.47 (d, *J* = 16.4 Hz, 1H), 7.41 (d, *J* = 9 Hz, 2H), 7.38(dd, *J* = 7.0, 2.6 Hz, 2H), 7.22 (d, *J* = 16.3 Hz, 1H), 6.91 (s, 1H), 6.76 (d, *J* = 9.0 Hz, 2H), 6.11 (s, 1H), 4.75 (t, *J* = 5.3 Hz, 1H), 3.58-3.52 (m, 2H), 3.47 (d, *J* = 4.8Hz, 2H), 3.01 (s, 3H), 2.45 (s, 3H), 1.37 (s, 3H), 1.32 (s, 3H). ^{13}C NMR (126 MHz, DMSO) δ 155.58 153.63 152.41,150.51, 150.37 , 143.29 , 141.86 ,140.44 ,139.44 , 138.73 , 138.28 , 137.75 , 134.37 , 132.51 ,132.37 , 130.54 ,130.05 ,129.77 ,129.50 , 129.08 , 128.18 , 123.11 , 120.36 , 118.28 , 112.30 ,112.10 ,112.24 ,111.89 , 58.12 , 53.91 ,41.02 , 39.10 , 30.65 ,14.25 , 14.18 , 13.77 . HRMS (EI): m/z (%) calc for $C_{29}H_{30}BF_2N_3O$: 486.2824 $[M+1]^+$ found: 486.2541. UV-Vis (CH_3CN) λ_{max} 601 nm.

Spectroscopic Measurements

Metal cations (Fe^{+3}, Fe^{+2} Cu^{+2}, Zn^{+2}, Cd^{+2}; Co^{+2}, Ni^{+2}, Li^{+}, Hg^{+2},Cr^{+3} ,Al^{+3}, Na^{+}, K^{+}, Ca^{2+}, Mg^{2+} and Ag^{+}) as nitrate or perchlorate salts were used to obtain solutions of concentration of 10^{-3} M in CH_3CN. Uv-Vis spectra were recorded using a Shimadzu UV-2600 spectrometer. Fluorescence spectra were recorded using a Varian Cary Eclipse fluorometer. Titrations were performed by adding aliquots of M^{+3} (10^{-3} M in CH_3CN) in a solution of ligand (**1** and **2**) (10^{-5} M) in water : CH_3CN (80 : 20 v/v for **1** and 40:60 v/v for **2**). The relative fluorescence quantum yields were obtained by comparing the area under the corrected emission spectrum of test sample with that of a solution of Fluorescein (0.1 M in NaOH ϕ= 0,85).[1]

Competition experiments

Firstly, a solution of ligand (**1** or **2**) (10^{-5} M) in water:CH_3CN (80:20 v/v for **1** and 40:60 v/v for **2**) was mixed with 5 equivalents of various metal ions (Cu^{2+}, Zn^{2+}, Cd^{2+},Ru^{3+}, Fe^{2+}, Co^{2+}, Ni^{2+}, Li^{+}, Hg^{2+},Na^{+}, K^{+}, Ca^{2+}, Mg^{2+} and Ag^{+}) followed by adding 1 eq. of Al^{3+}, Fe^{3+} or Cr^{3+}. Even in presence of other metal ions, Al^{3+}, Fe^{3+} and Cr^{3+} ($Al^{3}$and Cr^{3+} with **2**) could still coordinate with the ligand and cause a strong response.

^{1}H NMR spectroscopic titrations

A Bruker AV400 NMR spectrometer was used to measure the ^{1}H NMR shifts of the complexes. NMR titrations were performed by adding aliquots of Al^{+3} (10^{-1} M in CD_3CN) in to a solution of **1** (or **2**) (1.26×10^{-2} M) in CD_3CN.

LOD determination

To the corresponding receptor in water/acetonitrile (10^{-5}M) increasing amounts of the corresponding cation (in acetonitrile) were added. The Uv-vis and fluorescence spectra were recorded in 1-cm path length cells at 25°C (termostatted). Representation of absorbance/ fluorescence at the appropriate wavelength vs. concentration of cation allowed the detection limit to be calculated.

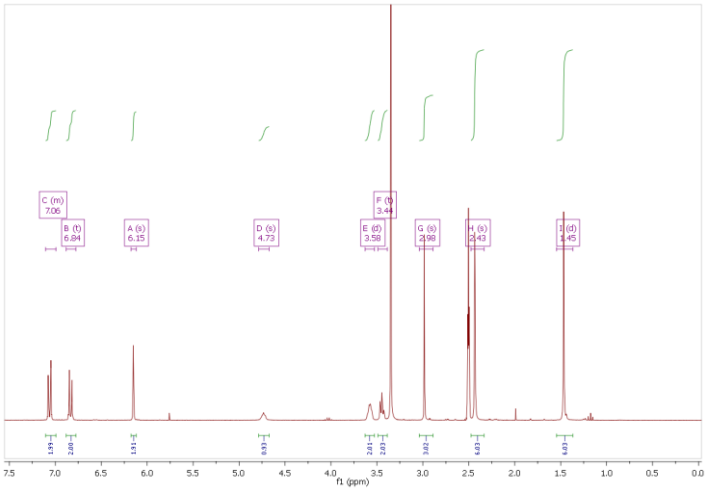

Figure SI-1. ^{1}H NMR spectrum of compound **1** (DMSO)

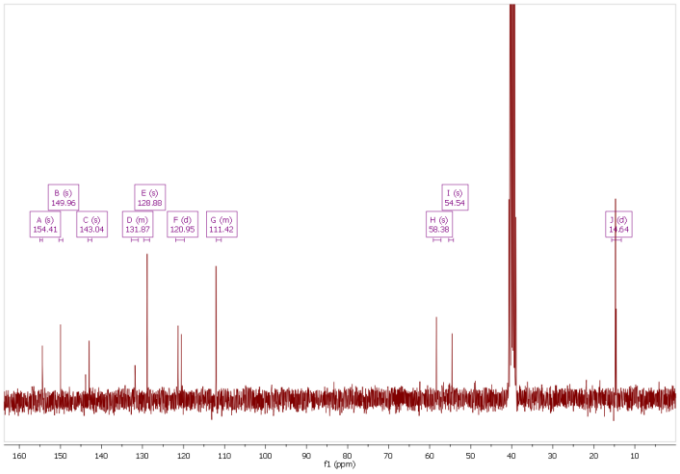

Figure SI-2. ^{13}C NMR spectrum of compound **1** (DMSO)

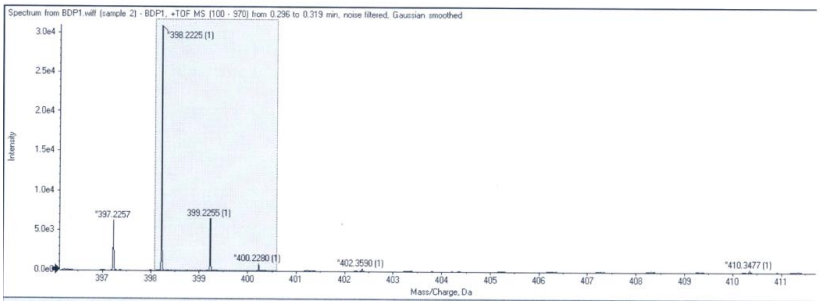

Figure SI-3. MS of compound **1**

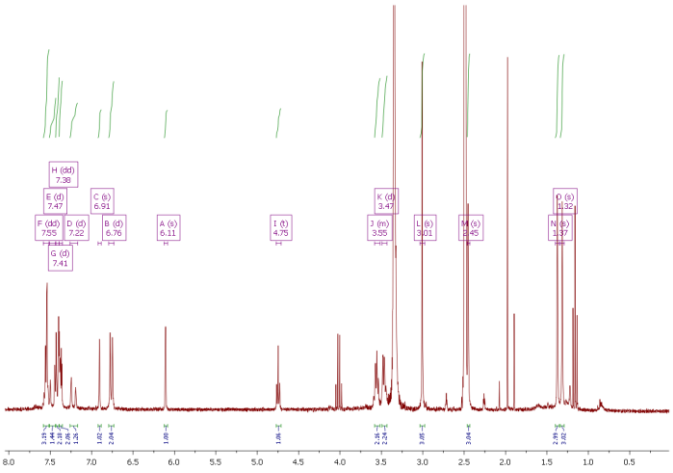

Figure SI-4. ^{1}H NMR spectrum of compound **2** (DMSO)

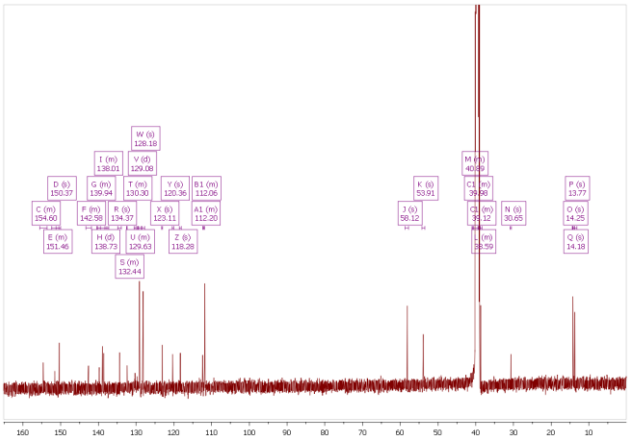

Figure SI-5. ^{13}C NMR spectrum of compound **2** (DMSO)

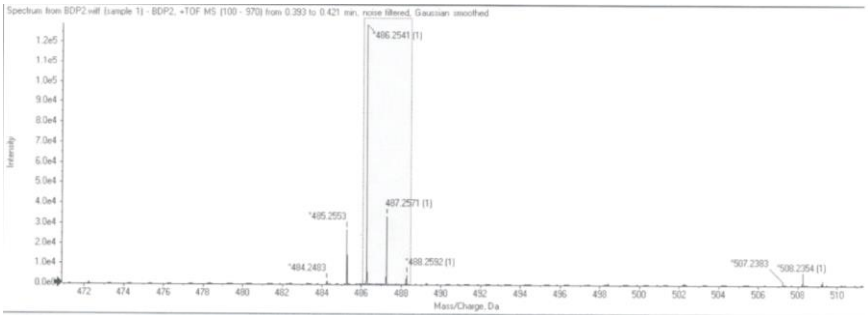

Figure SI-6. MS of compound **2**

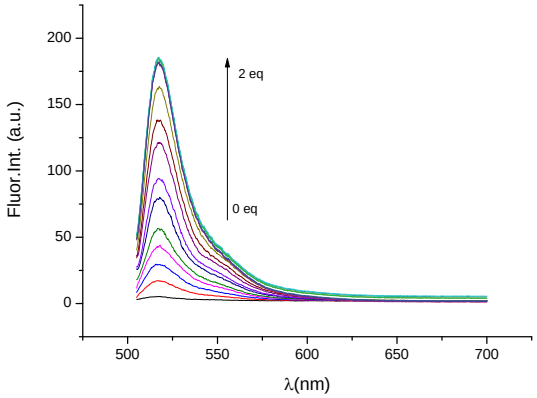

Figure SI-7. Fluorescence titration (λ_{ex} = 480 nm) of **1** (10^{-5} M) with Fe^{3+} in water : CH_3CN (80:20 v/v).

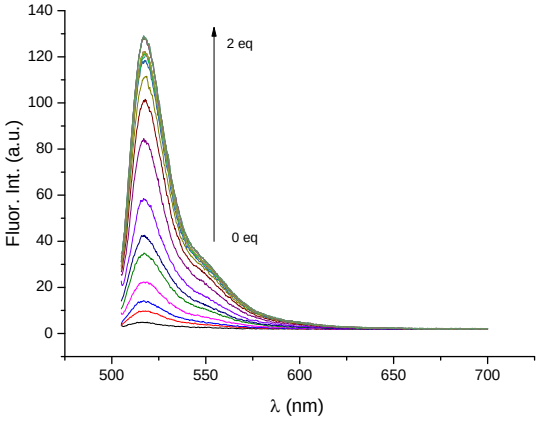

Figure SI-8. Fluorescence titration (λ_{ex} = 480 nm) of **1** (10^{-5} M) with Cr^{3+} in water : CH_3CN (80:20 v/v).

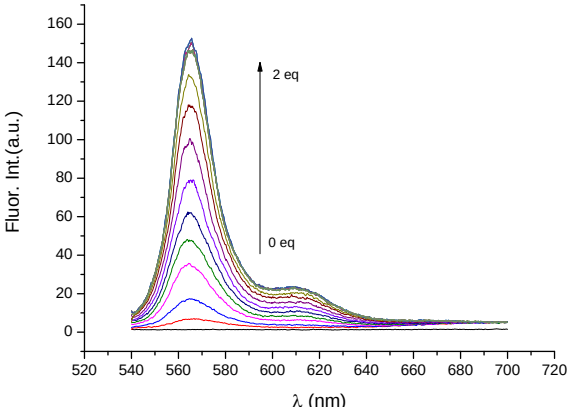

Figure SI-9. Fluorescence titration (λ_{ex} = 530 nm) of **2** (10^{-5} M) with Cr^{3+} in water : CH_3CN (40:60 v/v).

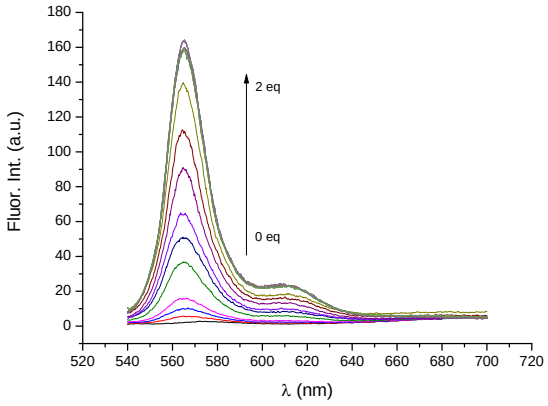

Figure SI-10. Fluorescence titration (λ_{ex} = 530 nm) of **2** (10^{-5} M) with Al^{3+} in water:CH_3CN (40:60 v/v).

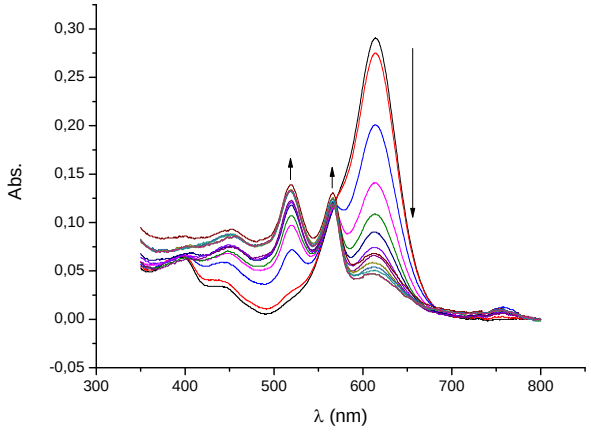

Figure SI-11. UV titration of **2** (10^{-5} M) with Cr^{3+} in water:CH_3CN (40:60 v/v).

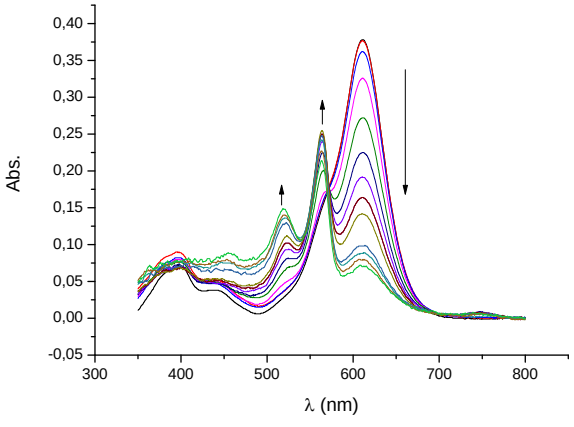

Figure SI-12. UV titration of **2**(10^{-5} M) with Al^{3+} in water: CH_3CN (40:60 v/v).

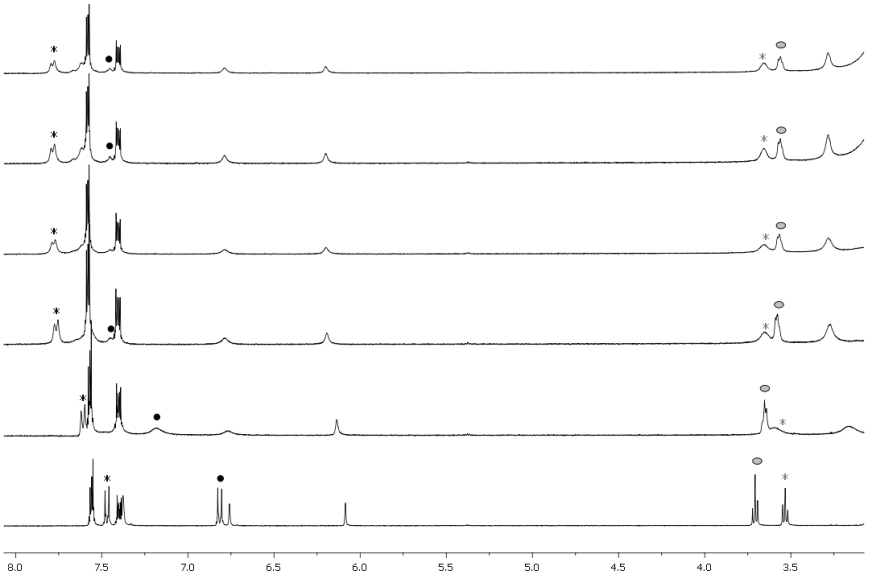

Figure SI-13. ^{1}H NMR spectra of compound **2** alone and in the presence of increasing amounts of Al^{3+} in CD_3CN.

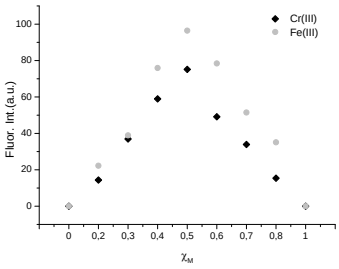

Figure SI-14. Job´s Plot of **1** from fluorescence data.

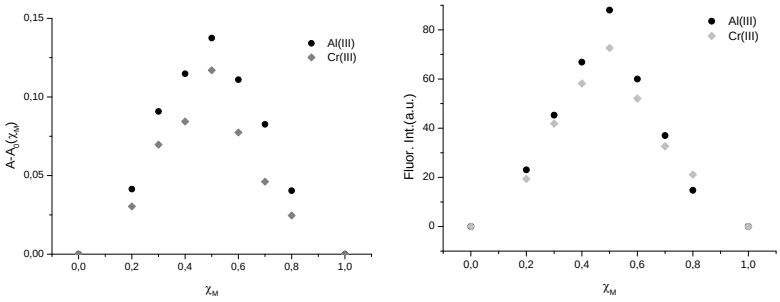

Figure SI-15. Job´s Plot of **2** from Uv-Vis data (left) and fluorescence data (right)**.**

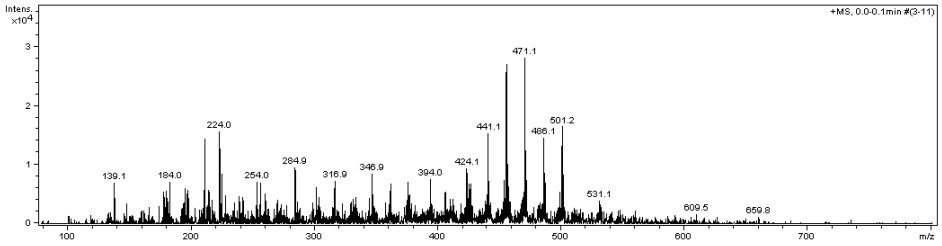
Intens.
x10^4
+MS, 0.0-0.1min #(3-11)
471.1
224.0
441.1
501.2
486.1
284.9
139.1
184.0
254.0
316.9
346.9
394.0
424.1
531.1
609.5
659.8
m/z

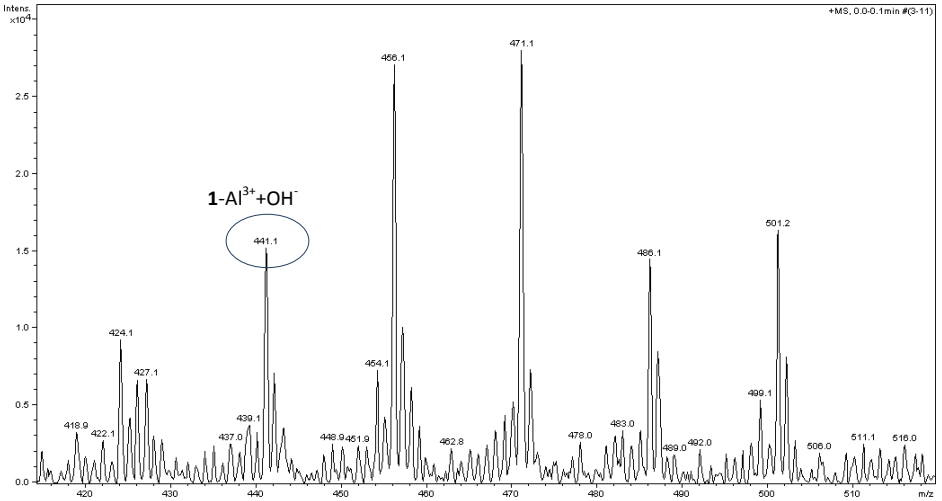
Intens.
x10^4
+MS, 0.0-0.1min #(3-11)
466.1
471.1
1-Al3++OH-
441.1
501.2
486.1
424.1
427.1
454.1
499.1
418.9
422.1
439.1
437.0
448.9
451.9
462.8
478.0
483.0
489.0
492.0
506.0
511.1
516.0
m/z

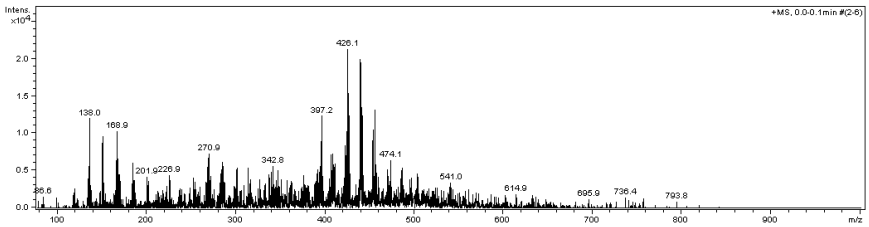
Intens.
x10^4
+MS, 0.0-0.1min #(2-6)
426.1
138.0
168.9
397.2
270.9
342.8
474.1
201.9
226.9
541.0
614.9
695.9
736.4
793.8
m/z

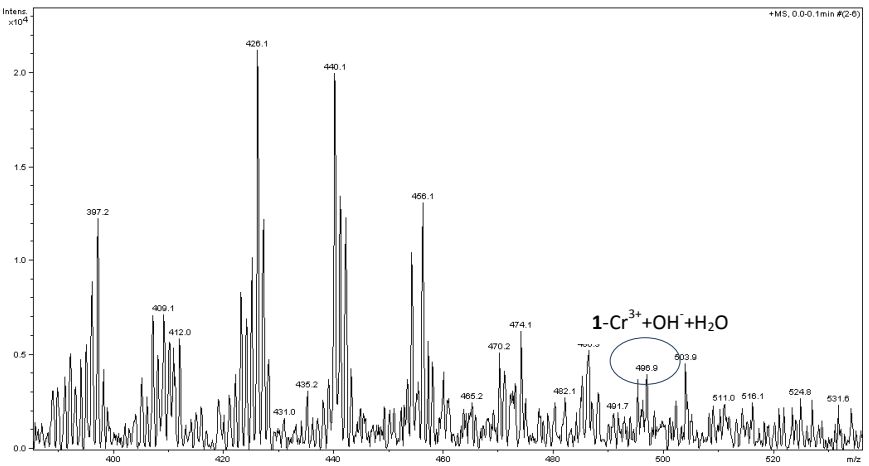
Intens.
x10^4
+MS, 0.0-0.1min #(2-6)
426.1
440.1
456.1
397.2
409.1
412.0
474.1
1-Cr3++OH-+H2O
470.2
496.9
503.9
435.2
431.0
465.2
482.1
491.7
511.0
516.1
524.8
531.6
m/z

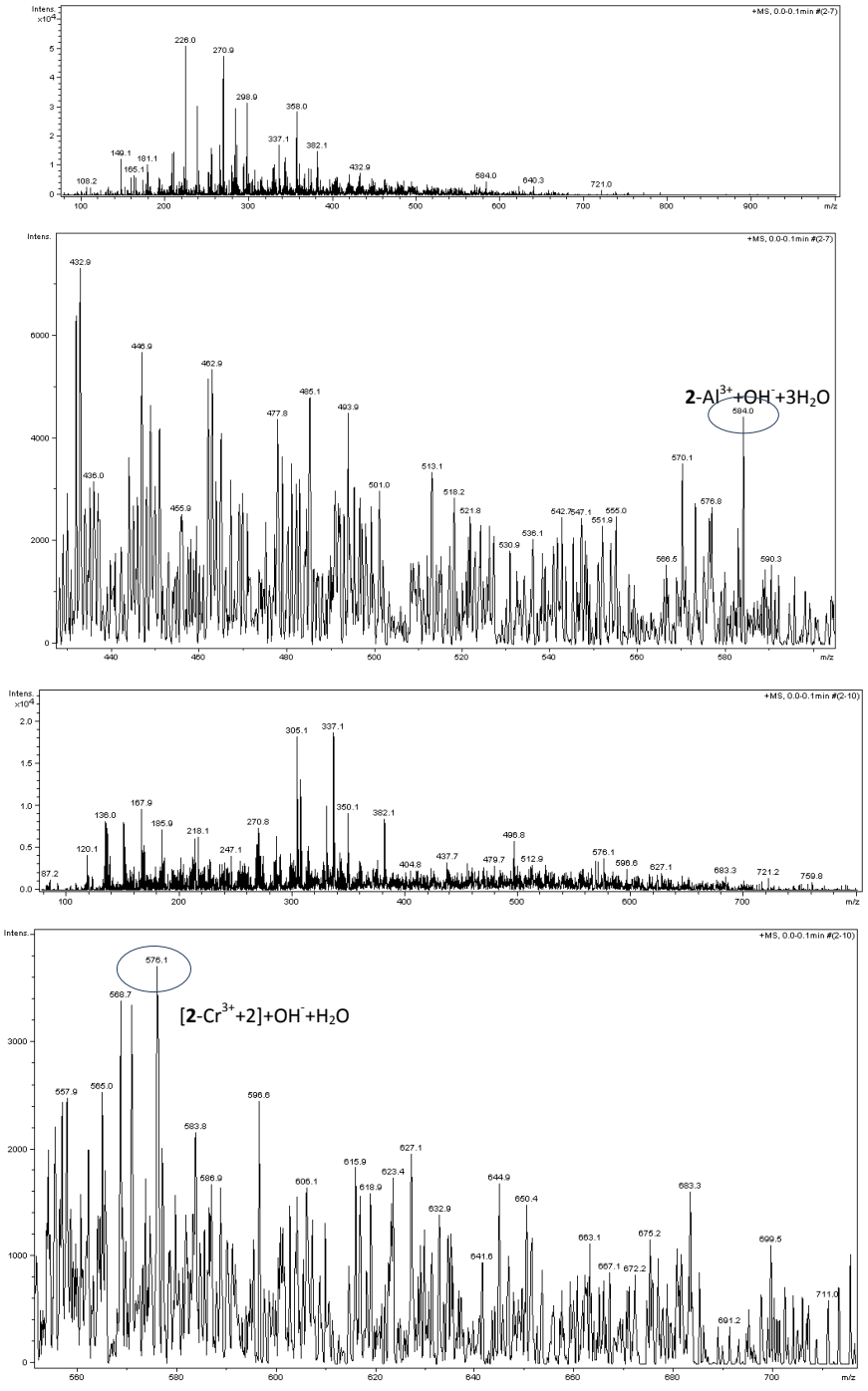

Figure SI-16. MS data of complexes formed with **1** and **2** and Al^{3+} and Cr^{3+} showing a 1:1 stoichiometry

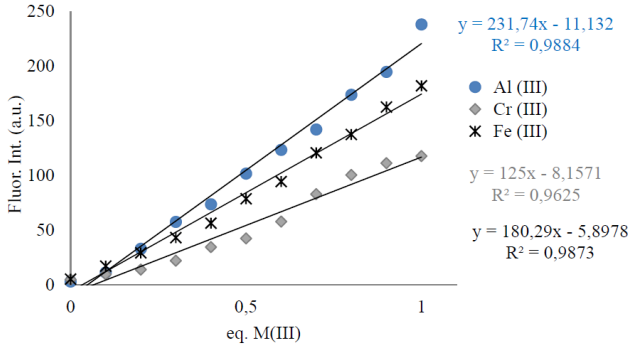

Figure SI-17. A plot of **1** vs. cations concentration at 560 nm in CH_3CN : water (80 : 20 v/v).

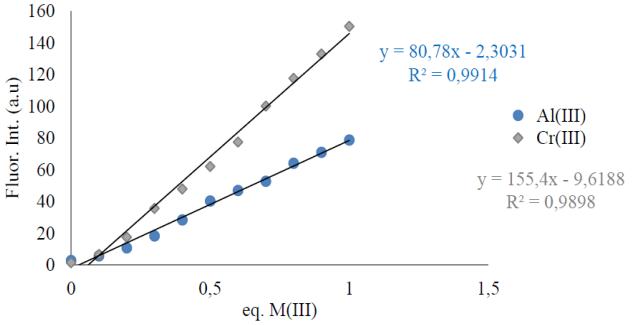

Figure SI-18. A plot of **2** vs. cations concentration at 563 nm in CH_3CN : water (40 : 60 v/v).

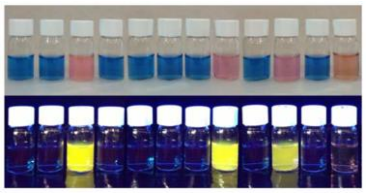

Figure SI-19. Color change (top, under ambient light) and fluorescence response (bottom, irradiated with 254 nm by using a UV lamp) of acetonitrile solutions of **2** in the presence of different metal cations. (**2**, Hg^{2+}, Al^{3+}, Li^{+}, Ni^{2+}, Zn^{2+}, Cd^{2+}, Cr^{3+}, Fe^{2+}, Fe^{3+}, Co^{2+} and Cu^{2+}).

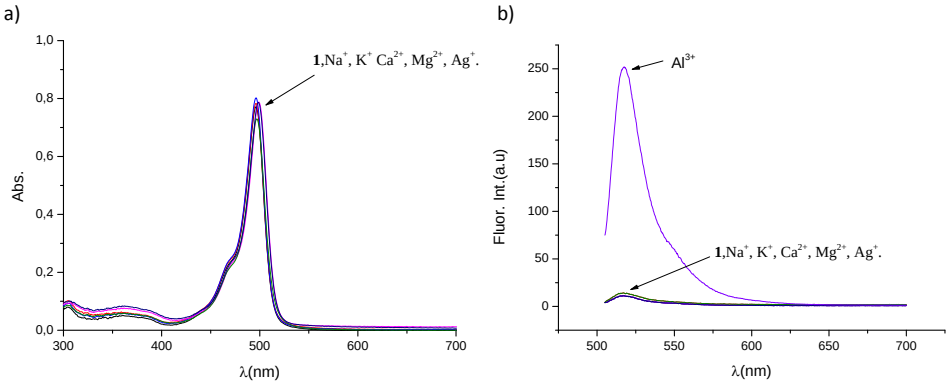

Figure SI-20. UV-Vis spectra a) and fluorescence emission spectra (λ_{ex} = 480 nm) b) of **1** (10^{-5} M) upon addition of 10 eq of Na^+, K^+, Ca^{2+}, Mg^{2+}, Ag^+ and 1 eq of Al^{3+} in water:CH_3CN (80:20 v/v).

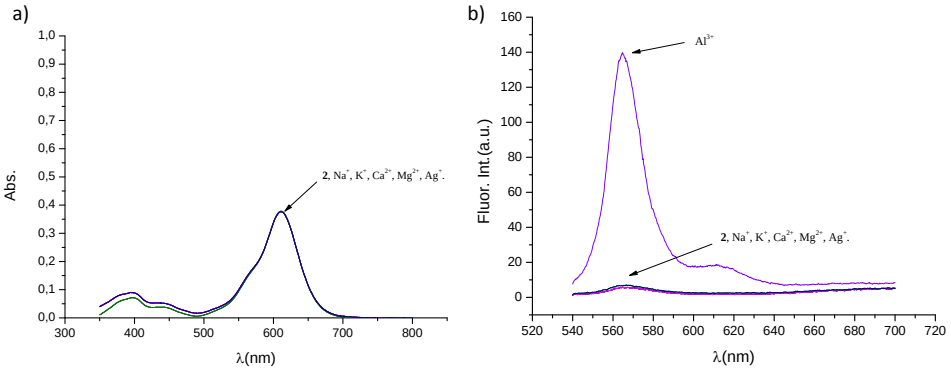

Figure SI-21. UV-Vis spectra a) and fluorescence emission spectra (λ_{ex} = 530 nm) b) of **2** (10^{-5} M) upon addition of 10 eq of Na^+, K^+, Ca^{2+}, Mg^{2+}, Ag^+ and 1 eq of Al^{3+} in water:CH_3CN (40:60 v/v).

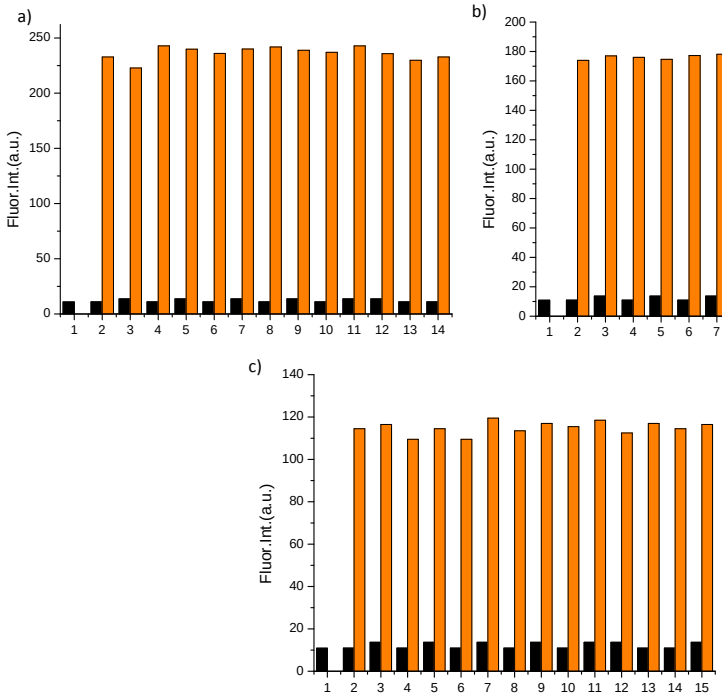

Figure SI-22. The fluorescent response of **1** (10^{-5} M in water : CH_3CN; 40:60 v/v) (λ_{ex} = 480nm; λ_{em} = 515nm) in the presence of a) Al^{3+}; b) $Fe^{3+}$and c) Cr^{3+} and the interfering ions. The black bars represent the addition of 5 eq. appropriate metal ions to a solution of **1**. The orange bars represent the subsequent addition of 1 eq. a) Al^{3+}; b) $Fe^{3+}$and c) Cr^{3+} to the above solution. 1-15 represent, **1**, Cu^{2+}, Zn^{2+}, Cd^{2+},Ru^{3+}, Fe^{2+}, Co^{2+}, Ni^{2+}, Li^{+}, Hg^{2+},Na^{+}, K^{+}, Ca^{2+}, Mg^{2+} and Ag^{+}.

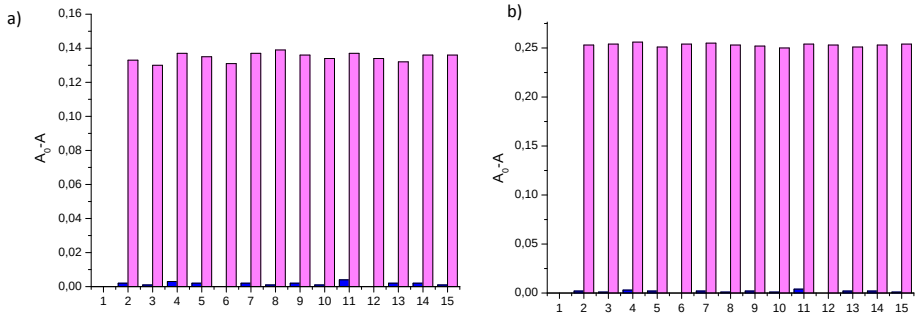

Figure SI-23. The Uv-Vis. response of **2** (10^{-5} M in water : CH_3CN; 20 : 80 v/v) in the presence of a) $Al^{3+}$and b) Cr^{3+} and the interfering ions. The blue bars represent the addition of 5 eq. appropriate metal ions to a solution of **2**. The magenta bars represent the subsequent addition of 1 eq. a) $Al^{3+}$and b) Cr^{3+} to the above solution. 1-15 represent, **2**, Cu^{2+}, Zn^{2+}, Cd^{2+},Ru^{3+}, Fe^{2+}, Co^{2+}, Ni^{2+}, Li^{+}, Hg^{2+},Na^{+}, K^{+}, Ca^{2+}, Mg^{2+} and Ag^{+}.

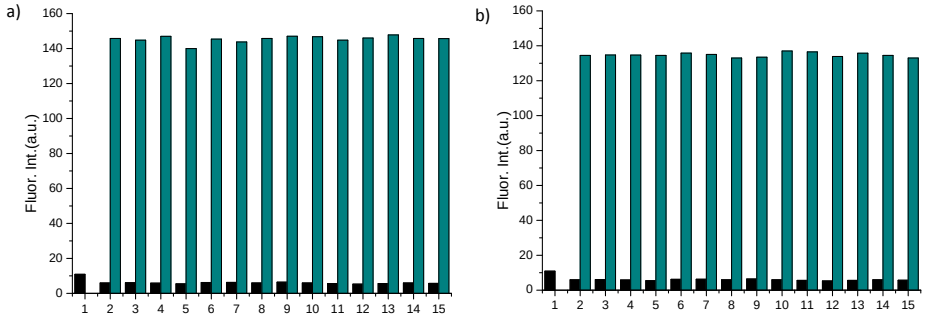

Figure SI-24. The fluorescent response of **2** (10^{-5} M in water : CH_3CN; 20:80 v/v) (λ_{ex} = 530nm; λ_{em} = 563nm) in the presence of a) $Al^{3+}$and b) Cr^{3+} and the interfering ions. The black bars represent the addition of 5 eq. appropriate metal ions to a solution of **2**. The blue bars represent the subsequent addition of 1 eq. a) $Al^{3+}$and b) Cr^{3+} to the above solution. 1-15 represent, **2**, Cu^{2+}, Zn^{2+}, Cd^{2+}, Ru^{3+}, Fe^{2+}, Co^{2+}, Ni^{2+}, Li^{+}, Hg^{2+},Na^{+}, K^{+}, Ca^{2+}, Mg^{2+} and Ag^{+}.

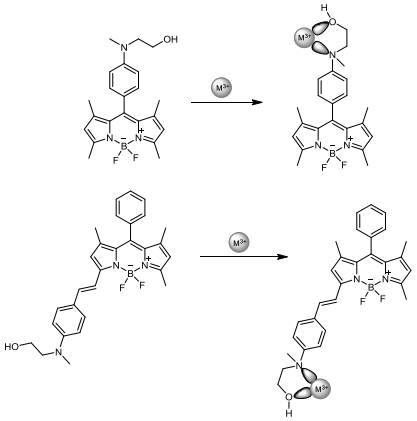

Scheme SI-2. Proposed interaction of compounds **1** and **2** with trivalent cations.

Reference: 1**.** J. Umberger and V. K. LaMer, J. *Am. Chem. Soc*., 1945, **67**, 1099-1109.

Chapter 4:

Detection of G-type Nerve Agents

4.1 Introduction

The expression “Chemical Warfare Agent” (CWAs), first used in 1917, refers to all tactical war assets with the use of incendiary mixtures, smokes and irritating, vesicant, poisonous or asphyxiating gases.[1]

[1] a) J. K. Smart, *Medical Aspects of Chemical and Biological Warfare-Textbook of Military Medicine*. b) R.T. Delfino, T.S. Ribeiro and J.D. Figueroa-Villar, *J. Braz. Chem. Soc.,* **2009**, 3, 407-428.

Military CWAs can be classified in several categories, according to the nature of their use, their persistence in the field and their physiological action.[2] Most common CWAs are generally divided in:

(i) *Vesicants*: mustard gases ($ClCH_2CH_2XCH_2CH_2Cl$; X = O,S,NR).
(ii) *Pulmonary Toxicants*: Phosgene ($COCl_2$) and diphosgene ($Cl_3COCOCl$).
(iii) *Cyanides*: Hydrogen cyanide (HCN) and cyanogen cyanide.
(iv) *Incapacitating agents*: tear gases (chloroacetophenone, bromoacetone…) and vomiting gases (chloropicrin…).
(v) *Neurotoxic Agents*: which are also known as nerve agents or nerve gases (Tabun, Sarin, VX….).

Neurotoxic Agents (nerve agents), the focus of this thesis, are among the most toxic synthetic compounds and, along with vesicants constitute the major of the modern chemical arsenals.

Neurotoxic chemical warfare agents are essentially organophosphorus compounds (OPs), they are derivatives of phosphoric or phosphonic acids and contain two alkyl groups (R and OR´) and a leaving group. The nerve agents are traditionally divided into the G- and V-agents; in the case of G-agents the leaving group is often a fluorine atom, (exceptionally in Tabun which is cyanide). The V-agents are phosphonothioates of the O-P type in which the leaving group is linked to phosphorus through sulphur atom, except for VG which is a phosphorothioate [3](see figure 4.1). Some physical, chemical and toxicological properties of nerve agents are summarized on table 4.1.

The OPs nerve agents primarily addressed in this chapter include the G-series (Tabun, Sarin and Soman) whereas V-series will be studied in the following chapter. Due to the grave toxicity of the nerve agents, various comparatively innocuous and readily available molecules are frequently used in the laboratory

[2] a) W. S. Angerson, *Chemical and Biological Warfare Agents*, RAND Reports, **2000**. b) D. R. Walt and D. R. Franz, *Anal. Chem.*, **2000**, 72, 738A-746A.
[3] A. Watson, D. Opresko, R. Young, V. Hauschild, J. King and K. Bakshi, Chapter 6: *Organophosphate Nerve Agents* in *Handbook of Toxicology of Chemical Warfare Agents*.

studies (DCP, DCNP and DFP).[4] These compounds (hereafter referred as *simulants*, *mimics* or *surrogates*) have similar reactivity but lack the acute toxicity; they are less expensive as well.

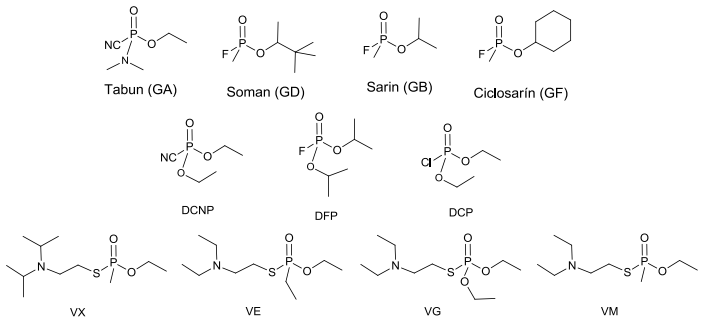

Figure 4.1. Chemical structures of G-nerve agents, their simulants and V-type agents.

Table 4.1. Physical, chemical and toxicological properties of the principal nerve agents.

Property	**Tabun (GA)**	**Sarin (GB)**	**Soman (GD)**	**VX**
Molecular weight (Da)	162.3	140.1	182.2	267.4
Boiling point (°C)	230	158	198	298
Melting point (°C)	-49	-56	-80	-20
Vapor pressure (mmHg)	0.037 (20°C)	2.1 (20°C)	0.40 (25°C)	0.0007(20°C)
Vapor density (relative to air)	5.6	4.9	6.3	9.2
Liquid density (g/mL at 25 °C)	1.08	1.10	1.02	1.01
Volatility (mg/m^3 at 25 °C)	610	22000	3900	10.5
Solubility in water (25 °C)	9.8 g *per* 100g	miscible	2.1 g *per* 100g	miscible
Persistence on soil	1-1.5 days	2-24 h	≈persistent	2-6 days
LCt_{50} in humans (mg min/m^3)	400	100	50	10
LD_{50} in humans(mg *per* 70kg)[a]	1000	1700	350	6-10

[a] percutaneous. Source: reference 1b, 3 and 5

Neurotoxic agents are able to enter the human body by inhalation or through the skin and they attack the nervous system. The action of OPs results from their effects on enzymes, particularly esterases.[5] Acetylcholinesterase (AChE) inhibition

[4] K. Kim, O.G. Tsay, D.A. Atwood and D.G. Churchill , *Chem. Rev*., **2011**, 111, 5345-5403.
[5] T.C. Marrs, R.L. Maynard and R.R. Sidell, *Chemical warfare Agents: Toxicology and Treatment*, (2nd Edition), **2007**, John Wiley & Sons, Ltd.

is the most well-know mode of action of nerve agents. Inhibition occurs through the irreversible binding of organophosphates to the catalytic site of the enzyme[6] (which comprises a catalytic triad of serine, histidine and glutamic acid residues, and other important features of the enzyme are a "gorge" connecting the active site to the surface of the protein and a periferical anionic site).[1b,4] AChE is an enzyme that hydrolyzes acetylcholine (ACh); the binding of AChE with ACh results in acetylation of the serine at the active site of the enzyme, with loss of the choline moiety[7] (see Scheme 4.1a).

The mechanism of AChE inhibition with nerve agents is analogous to the reaction of the enzyme with ACh, except for the reaction in with the leaving group of the nerve agents is lost, so the enzyme becomes phosphorylated instead of acetylated[5,8] (see Scheme 4.1b). The phosphorylated enzyme can no longer hydrolyze acetylcholine, leading to the accumulation of this molecule in cholinergic receptors and consequent continuous stimulation of the nerve fiber, resulting in hypersecretion, bronchoconstriction, miosis, muscular twitching, mental confusion, convulsive seizures, paralysis, respiratory distress and eventually death.[9]

[6] a) A. Friboulet, F. Rieguer, D. Godou, G. Amitai and P. Taylor; *Biochemistry,* **1990**, 29, 914-920. b) T.M. Shit, R.K. Kan and J.H. McDonough, *Chem. Biol Interact*., **2005**, 157, 293-303.
[7] S. M. Somani, *Chemical Warfare Agents*, Academic Press, San Diego, (**1992**).
[8] A. Ordertlinch, D. Barack, C. Kronman, N. Ariel, Y. Segall, B. Velan and A. Shafferman, *J. Biol. Chem.,* **1996**, *271*, 11953-11962.
[9] a) T. C. Marrs, *Pharmacol. Ther.,* **1993**, *58*, 51-66. b) F. R. Sidell and J. Borak, *Ann. Emerg. Med.,* **1992**, *21*, 865-871.

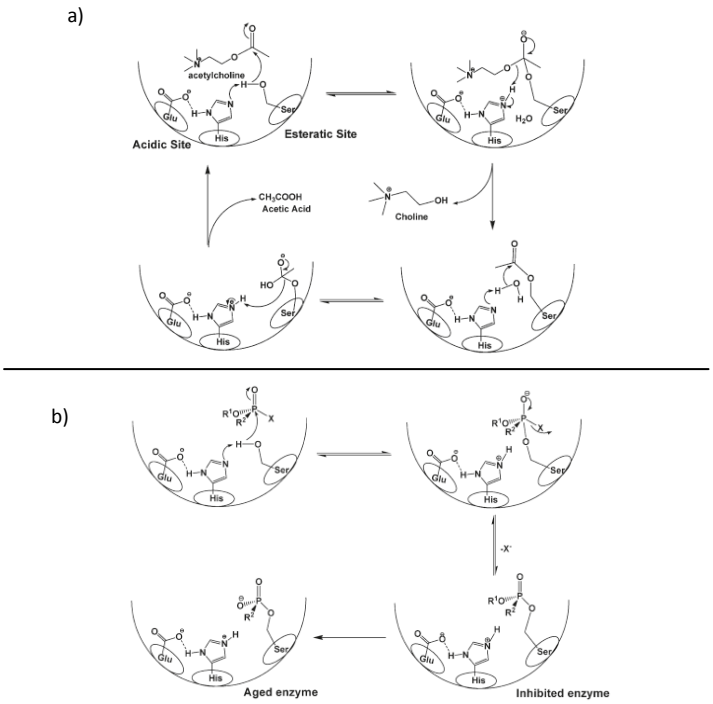

Scheme 4.1. a) Mechanism of Ach hydrolysis by AChE. b) AChE inhibition by Organophosphates.[4]

Due to the latent dangers of nerve agent species (extreme toxicity, easy production and ready accessibility relative to more conventional weapons) there is a need to have adequate sensing protocols. Intense research efforts have been directed to develop sensitive and selective protocols to detect nerve gases.[4,10] Recently many methods for detecting nerve agents are continually being developed and optimized, which include ion mobility spectrometry, mass spectrometry, NMR spectroscopy, enzyme sensors, polymers and gels.[11] These methods do not afford convenient access to appropriate selectivity and/or are not

[10] a) S. Royo, R. Martínez-Máñez, F. Sancenón, A. M. Costero, M. Parra and S. Gil, *Chem. Commun*., **2007**, *46,* 4830-4847. b) D. Ajami and J. Rebek*, Org. Biomol. Chem*., **2013**, *11*, 3936-3942. c) M.R. Sambrook and S. Notam, *Chem. Soc. Rev*., **2013**, *42*, 9251-9267.

[11] a) T. J. Henderson, *Anal. Chem*., **2002**, *74*, 191-198. b) D. Du, J. Wang, J. N. Smith, C. Timchalk and Y. H. Lin, *Anal. Chem.,* **2009**, *81*, 9314-9320. c) L. Louise-Leriche, E. Paunescu, G. Saint-Andre, R. Baati, A. Romieu, A. Wagner and P. Y. Renard, *Chem. Eur. J.,* **2010,** *16*, 3510-3523. d) P. Prashant and S. S. Seo, *Int. J. Polym. Anal. Charact.,* **2009**, *14*, 481-492. f) J. P. Walker and S. A. Asher, *Anal. Chem*., **2005**, *77*, 1596-1600. e) S. Clavaguera, A. Carella, L. Caillier, C. Celle, J. Pecaut, S. Lenfant, D. Vuillaume and J. P. Simonato, *Angew. Chem., Int. Ed*., **2010**, *49*, 4063-4066.

convenient/portable and simply enough for real-time monitoring. More convenient are the chromogenic and fluorescent sensing methods because they are very sensitive, allow detection in real-time and are easy to access by the unassisted eye[12] thus, they are not expensive, allowing its application for an individual use.

There are a variety of chemical systems that involve selective color/fluorescent changes as an indication of the presence of nerve agents. J. Rebek *et al.* reported a family of compounds for nerve agent simulant DCP detection[13] (figure 4.2). In the molecular system shown prior to nucleophilic attack, the tertiary amino lone pair of the probe is engaged electronically via photoinduced electron transfer (PET) with the delocalized pyrenyl system. Upon addition of DCP, this lone pair achieves intramolecular ring closure and removes the PET quenching mechanism pathway allowing for natural pyrenyl fluorescence.

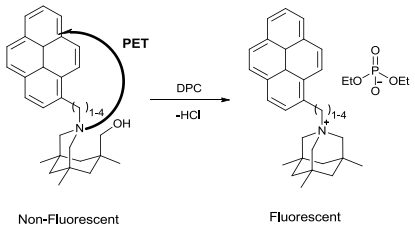

Figure 4.2. The Rebek group system.

A. M. Costero *et al*. developed chemosensors able to detect nerve agent mimics.[14] The authors designed colorimetric probes where 2-(2-(dimethylamino)-phenyl)ethanol derivatives play the role of binding site due to the ability of hydroxyl moiety to react with phosphate compounds to yield quaternary ammonium salts. In the presence of DCP, the selected derivative (azo- and stilbene- derivatives) undergoes a cyclation reaction which results in a hypsochromic shift (see figure 4.3).

[12] Y. J. Jang, O.G. Tsay, D. P. Murale, J. A. Jeong, A. Segev and D.G. Churchill*, Chem. Commun.,* **2014**, *50*, 7531-7534.
[13] T. J. Dale and J. Rebek, *J. Am. Chem. Soc.*, **2006**, *128*, 4500-4501.
[14] a) A. M. Costero, S. Gil, M. Parra, P. M. E. Mancini, R. Martinez- Mañez, F. Sancenon and S. Royo, *Chem. Commun*, **2008**, *45*, 6002-6004. b) A. M. Costero, M. Parra, S. Gil, R .Gotor, P. M. E. Mancini, R. Martinez-Mañez,F. Sancenon and S. Royo, *Chem. Asian J.*, **2010**,*5*, 1573-1585.

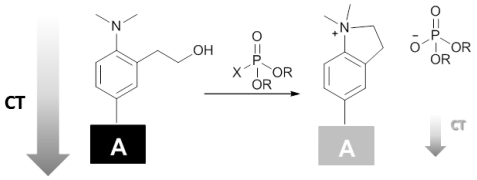

Figure 4.3. The Costero group system.

S. Han published a detection method based on a Lossen rearrangement of Rhodamine–hydroxamate in the presence of diethyl chlorophosphate, under alkaline conditions.[15] BESThio fluorescent probe based on fluorescein can be used for the direct detection of nerve agents possessing a thiocholine leaving group.[16]

A. Akthakul *et al*. developed a sensor containing the Nile Red dye.[17] The device demonstrates over an order of magnitude increase in vapor sensitivity for the Sarin simulant DMMP when inorganic oxides were used as a quencher. An organogel containing a 2-(2'-hydroxyphenyl)benzoxazole group was synthesized and tested for detection of nerve agent simulant.[18]

Notwithstanding the interest in the design on probes for nerve agent detection; the reported examples have some limitations to avoid: i) false positives or negative responses in presence of non-toxic compounds (acids or hydrolysis-products) and/or ii) the probes are non-specific/unable to determine the specific identity of the agent.

[15] S. F. Han; Z.W. Xue., Z. Wang, T.B. Wen, *Chem. Commun*., **2010**, *46*, 8413-8415.
[16] X. Y. Zheng, K. Okolotowicz, B. L. Wang, M. MacDonald, J. R. Cashman and J. Zhang, *Chem. Biol. Interact*., **2010**, *187*, 330-334.
[17] A. Akthaku, N. Maklakov and J. White, *Anal. Chem*., **2010**, *82,* 6487-6494.
[18] T.H. Kim; D. G. Kim; M. Lee and T. S. Lee , *Tetrahedron,* **2010,** *66*, 1667-1672.

4.2 Objectives

Bearing in mind the danger regarding nerve agents and the limitation of existing systems we considered the possibility of design different improved systems for the chromo-/fluorogenic detection of nerve agent simulants. Thus, the main objective of this chapter is the design and development of new BODIPY-dyes to detect the nerve agent simulant in the presence of interfering species (avoiding false positive/negative responses) and the possibility of distinguish between the agents.

Particularly, our aims were:

- ✓ Design and synthesis of new BODIPY-dyes for the selective detection of nerve agent simulants.
- ✓ Study the chromo-fluorogenic behavior of the synthesized BODIPY-dyes in absence/presence of the nerve agent simulants.
- ✓ Evaluation of the behavior of BODIPY-dyes in presence of interfering species, and different media, to test their applicability as selective sensor for the selected species.
- ✓ Development of different test strips for their application in real-time monitoring.

4.3 Chemosensors Design

The main focus was to prepare a family of BODIPY-dyes with structural variations for the detection of nerve agent simulant avoiding acid interferences. In this case the "*chemodosimeter"* approach was selected for the probes design because it commonly involves the rupture/formation of covalent bond with remarkable chemical modifications, leading to notable spectroscopic modulations.

In the first part of the study, two potential reactive sites were included in the chemodosimeter design, one hydroxyl group suitable to react with electrophilic phosphorus atom and a basic pyridine to interact with acids, in order to discriminate among the nerve agent mimics and the acidic response. In the second part, three possible reactive sites were included, one hydroxyl group to react with electrophilic phosphorus atom; a carbonyl group for its known capacity to react with cyanide and a triisopropylsilyl group that is expected to react with fluoride.

Moreover, a dual optical response with both chromogenic and fluorogenic response were searched. Thus, a strong conjugation in the molecular structure and donor/acceptor moieties were used to favor internal charge transfer character.

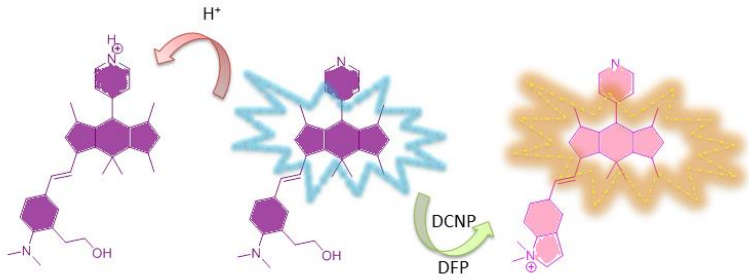

Figure 4.4. Outline for the chromo-fluorogenic sensing paradigm.

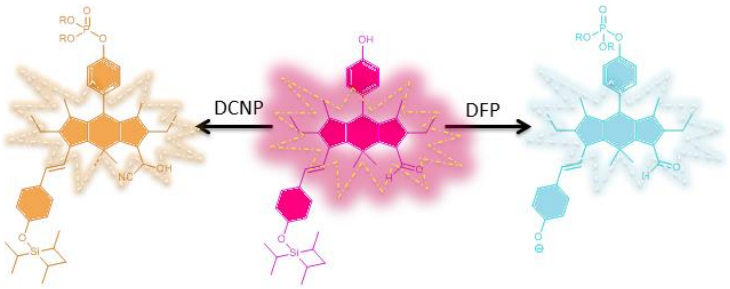

Figure 4.5. Schematic representation of the sensing paradigm for selective detection of DCNP and DFP.

4.4 Highly Selective Detection of Nerve-Agent Simulants with BODIPY Dyes.

Highly Selective Detection of Nerve-Agent Simulants with BODIPY Dyes

Andrea Barba-Bon, [ab] *Ana M.Costero,* [a] *Salvador Gil,* [a] *Anthony Harriman* [c] *and Felix Sancenón* [b]

[a] *Centro de Reconocimiento Molecular y Desarrollo Tecnológico (IDM), Universidad de Valencia, Dr. Moliner, 50, 46100 Burjassot ,Valencia, (Spain).*

[b] *Centro de Reconocimiento Molecular y Desarrollo Tecnológico (IDM), Universidad Politécnica de Valencia, Camino de Vera s/n, 46022 Valencia, (Spain).*

[c] *Molecular Photonics Laboratory, School of Chemistry, Bedson Building, Newcastle University, Newcastle upon Tyne, NE17RU (UK).*

Received: *15 th November 2013*

Published online: *3 th April 2014*

Chem. Eur.J., ***2014****, 20, 6339-6347.*

Abstract

Two chromo-fluorogenic probes, each based on the boron dipyrromethene core, have been developed for the detection of nerve agent mimics. These chemosensors display both a color change and a significant enhancement of fluorescence in the presence of diethylcyanophosphonate (DCNP) and diisopropylfluorophosphate (DFP). No interference from other organo-phosphorus compounds or acids has been observed. Two portable chemosensor kits have been developed and tested to demonstrate its practical application in real-time monitoring.

Introduction

Nerve agents are among the most important and lethal classes of chemical-warfare agents (CWAs). Nerve agents such as Sarin, Soman or Tabun are organophosphonate derivatives, in which the phosphorus atom is electrophilic by nature and can bind easily with the hydroxy group of the serine unit of the acetylcholinesterase enzyme (AChE). This reaction renders the enzyme non-functional,[1] thus resulting in acetylcholine accumulation in the synaptic junctions that hinders muscle relaxation.[2] Because of the extreme toxicity, facile production and ready accessibility relative to more conventional weapons, there is always the possibility of CWA attack by military regimes and terrorist organizations. As a consequence, intense research effort has been directed to the development of sensitive and selective analytical protocols for their detection. Several approaches have been proposed, including the use of an enzymatic assay,[3] ion-mobility spectroscopy,[4] lanthanide luminescence,[5] electrochemistry,[6] photonic crystals,[7] micro-cantilevers,[8] and optical-fibre arrays.[9] However, at least one of the following limitations is prevalent in each of these protocols: low response, lack of specificity, limited selectivity, poor sensitivity, operation complexity, nonportability, difficulties in real time monitoring and false positive readings.

The development of chromogenic and fluorogenic probes has gained increased interest in recent years to overcome these limitations.[10] Colorimetric and fluorimetric detection are particularly appealing as they are low-cost systems

capable of performing quantitative analysis with widespread technologies. These techniques also offer the possibility of detecting analytes with the "naked-eye". Notwithstanding the intrinsic interest in the design of such probes, the reported examples have certain limitations; the most important being the false positive or negative responses in the presence of non-toxic compounds such as acids.[11] Buffered solutions have been used to curtail this problem, but even under these conditions acids are important competitive agents that interfere with the sensing experiments.[10d,12] Therefore, we have been stimulated to design systems capable of discriminating between the target molecule and acidic media.

Taking the above concept into consideration and following our interest in the development of probes for the detection of nerve agents,[10c,11c,13] we report herein the use of Boron dipyrromethene (BODIPY) dyes as signaling systems for the selective detection of these chemicals (Scheme 1). It is widely recognized that BODIPY dyes are excellent fluorophores with widespread applications as probes in natural and artificial systems. These probes possess valuable characteristics, such as intense absorption and fluorescence transitions in the visible-spectral region, high molar-absorption coefficients and fluorescence quantum yields, and good stability towards thermal and photochemical degradation.[14]

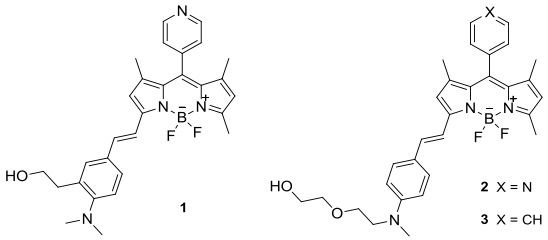

Scheme 1. Molecular formulae of target compounds **1** and **2** and control compound **3**.

Results and Discussion

Design of the sensory agents

Traditionally, the development of chromo- and fluorogenic probes relies on the design of two components: 1) a binding or reactive site and 2) a chromo-

fluorogenic trigger. For the fluoro-colorimetric event, we selected the BODIPY core due to the properties cited above. Probes **1** and **2** (Scheme 1) were designed that contain two chemo-sensing moieties to avoid acid interference. Firstly, there is a nucleophilic hydroxyl group that provides a suitable reactive site for electrophilic phosphorus atoms,[10c,11c,15] such as those functionalities likely to persist in nerve agents. Secondly, each chromophore is equipped with a basic pyridine moiety that is known to react with acid.[16] The intention is to keep these two units in electronic isolation where they can react with the relevant species in solution, thus giving a disparate response to the trapping of each reagent and discriminating between the target and acid. In addition, the corresponding phenyl derivative **3** was prepared for control experiments because this compound lacks the acid-sensitive *meso*-pyridine residue.

Our research group has previously reported the use of 2-[2-(dimethylamino)phenyl]ethanol moieties in the detection of nerve agents.[10c,11c] The nucleophilic hydroxyl group is easily phosphorylated by the nerve agent, thus forming a phosphoester, which is displaced in a second step by the attack of the nitrogen atom to give a five-membered-ring quaternary ammonium salt (Scheme 2a). Following these earlier results, we decided to explore the use of both 2-[2-(dimethylamino)phenyl]ethanol (**1**) and 2-2-{2-[methyl(phenyl)-amino]ethoxy}ethanol (**2**) as reactive units for the quantitative detection of nerve agents. In a first step, the hydroxyl group was phosphorylated to form a phosphoester intermediate that undergoes rapid intramolecular *N*-alkylation to afford the corresponding cation (Scheme 2). The change in the electronic distribution promoted by these processes allows the colorimetric and/or fluorescent detection of nerve agents.

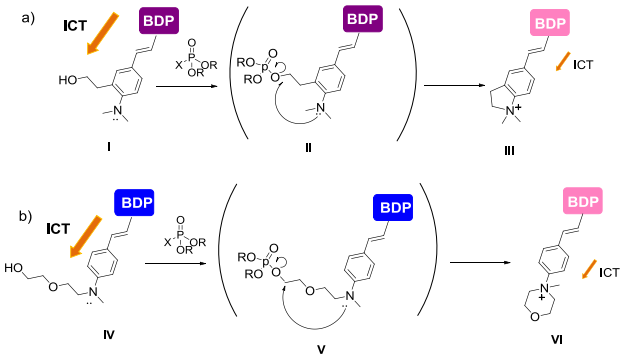

Scheme 2. Proposed outline for the chromo-fluorogenic sensing paradigm. ICT= internal charge transfer.

A crucial feature of any successful analytical protocol is the prevention of false positives produced by other species, such as acidic media. Consequently, we made a deliberate attempt to design chemosensors capable of discriminating between nerve agents and acidic interferences. To achieve this goal, we introduced the pyridine moiety at the *meso*-position (see Scheme 1). It has been demonstrated previously that the fluorescence emission of pyridyl-BODIPY can be quenched reversibly by protonation of the pyridine N-atom.[17] This simple strategy introduces the necessary functionality to avoid false positives caused by adventitious acid contaminants. In fact, the pyridine moiety is more basic than the terminal amino group and will be the first point of reaction in the presence of acid, thus triggering the characteristic signal response (i.e., little effect on the absorption profile but a significant change in fluorescence intensity). On the other hand, generation of the cyclic ammonium salt is the most favorable reaction in the presence of the nerve agent, thereby giving rise to the accompanying change of color. The system was designed in such a way that even in the presence of both species (i.e., nerve agent and acid) a response will be reported.

Synthesis of the probes

Reagents **1** and **2** were synthesized by using the Knoevenagel condensation on BODIPY **4** according to previously reported procedures.[14b,18] Thus, **4** in benzene was condensed with the corresponding aldehyde in the presence of acetic acid and piperidine (Scheme 3).

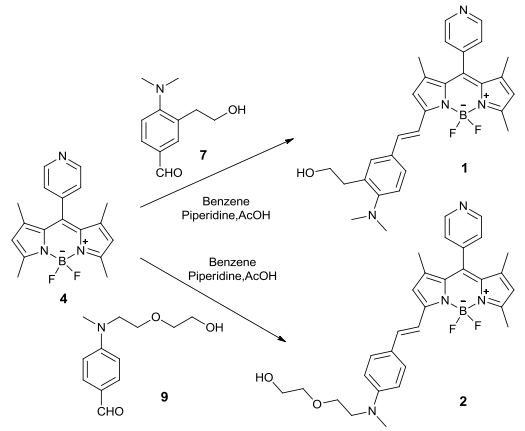

Scheme 3. Synthetic protocol used for preparation of probes **1** and **2**.

Prior to this work, the starting compound **4** was synthetized according to a reported procedure[14b,19] by condensation of 2,4-dimethylpyrrole with 4-pyridinecarboxaldehyde in the presence of trifluoroacetic acid (TFA) as a catalyst, followed by oxidation with *p*–chloranil (Scheme 4). The boron difluoride bridging unit was introduced by treatment with boron trifluoride diethyl etherate ($BF_3.Et_2O$) in the presence of triethylamine (TEA).

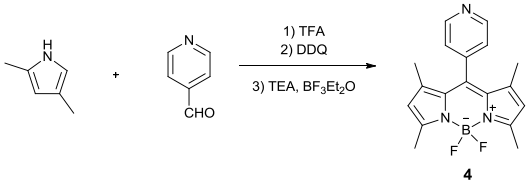

Scheme 4. Synthetic protocol used for preparation of compound **4**.
DDQ = 2,3-dichloro-5,6-dicyano-*para*-benzoquinone.

Preparation of aldehyde **7** necessitated a three-step synthesis (Scheme 5). Thus 2-(2-aminophenyl)ethanol was transformed into 2-[2-(dimethylamino) phenyl]ethanol (**5**) by reaction with iodomethane. This amino compound was subsequently converted to the corresponding bromoderivative **6** by reaction with *N*-bromosuccinimide catalyzed with ammonium acetate. In turn, the latter reagent was lithiated with *n*BuLi and then converted into the formyl derivative **7** by reaction with *N,N*-dimethylformamide (DMF).

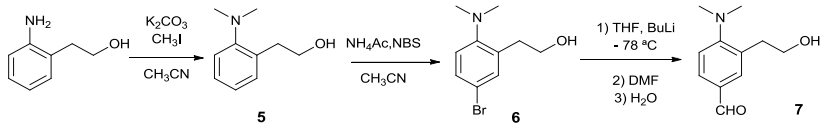

Scheme 5. Synthetic protocol used for preparation of aldehyde **7**.NBS = *N*-bromosuccinimide.

The synthesis of aldehyde **9** was achieved following a two-step procedure starting from 4-[(2-hydroxyethyl)(methyl)-amino]benzaldehyde (Scheme 6). The first step consists of tosylation with *para*-toluenesulfonyl chloride in dichloromethane in the presence of triethylamine. The obtained derivative **8** was treated with ethylene glycol to give the required 4-{[2-(2-hydroxyethoxy)ethyl](methyl) amino}benzaldehyde. By following the same procedure, the important control compound **3** was prepared from 8-phenyl-1,3,5,7-tetramethyl-Bodipy and aldehyde **9**.

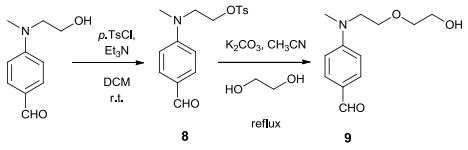

Scheme 6. Synthetic protocol used for the preparation of aldehyde **9**.Ts = para-toluenesulfonyl.

Spectroscopic properties

Figure 1 shows the absorption and fluorescence spectra recorded for **1** and **2** in acetonitrile (10^{-5} M). The absorption spectral profiles are reminiscent of those characterized for various related BODIPY dyes,[20,21] with an intense transition seen at approximately λ = 570 nm and 610 nm for **1** and **2**, respectively, and both spectra exhibited a shoulder at shorter wavelength (*ca.* λ = 530 nm). The fluorescence spectra display a small Stokes shift with good mirror symmetry, as is often the case with BODIPY dyes.[20-21] The emission maxima are in the range of λ = 575-620 nm.

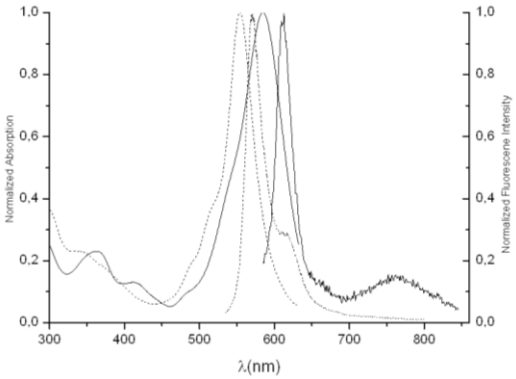

Figure 1. Normalized absorption and fluorescence spectra (λ_{ex} = 530 nm) recorded for **1** (·····) and **2** (—) in CH_3CN.

The effect of the solvent on the spectroscopic properties of **1** and **2** were investigated at room temperature; the electronic absorption and emission spectra recorded for **1** in several solvents are shown in Figure 2 (see the Supporting Information for **2**) and the photophysical data collected for both compounds are listed in Table 1.

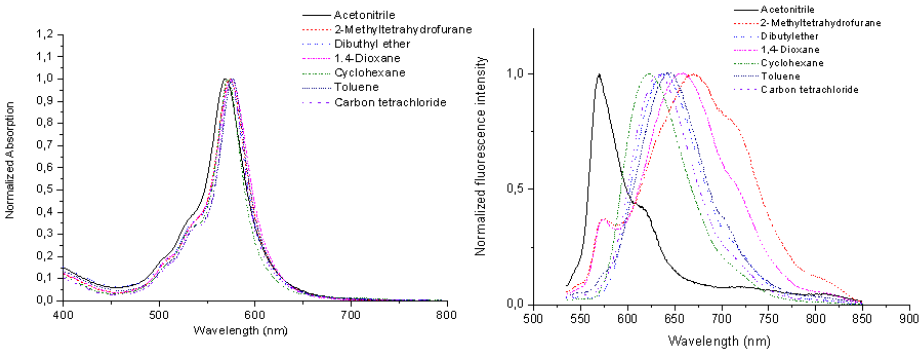

Figure 2. Enlargement of the main absorption peak (left) and fluorescence emission peak (right) of **1** in several solvents to emphasize the solvatochromic shifts. The intensities in this figure are normalized to the same value at the wavelength of maximum intensity.

In all solvents studied, two absorption peaks are seen clearly with relatively narrow spectral bandwidths. The lower energy band is assigned to the 0-0 band of a strong S_0-S_1 transition, with the maximum ranging from λ = 570 nm to 577 for **1** and from λ = 608 nm to 617 nm for **2**. The (more- or less-pronounced) shoulder on

the high-energy side of the main band is attributed to the 0-1 vibrational band of the same transition. The S_0-S_1 transition of the BODIPY core seems to possess some small degree of charge-transfer character due to the presence of the styryl group because the absorption maximum shows a slight sensitivity towards solvent polarity. In contrast, the emission energies of **1** and **2** are much more sensitive to the solvent polarity. On increasing the solvent polarity, a significant redshift is observed. The fluorescence quantum yields ϕ are weak; which is explained in terms of efficient charge transfer from the appended amino-alcohol moieties to the styryl-BODIPY core.[22] Compound **3** (10^{-5} M in acetonitrile) exhibits an absorption peak at λ = 598 nm (ε = 8400 M^{-1} cm^{-1}) and is essentially non-fluorescent at room temperature (See the supporting Information).

Table 1. Photophysical properties recorded for BODIPY compounds **1**- **2** in several solvents.

Probe	Solvent	λ_{abs} (max/nm)	λ_{em} (max/nm)	$\Delta\nu$[a]	ε (M^{-1} cm^{-1})	ϕ[b]
1	acetonitrile	569.4	575	171	30800	0.0141
	MTHF	573	668.2	2481	36100	0.1888
	Dibutyl ether	573	637	1753	33400	0.2802
	1,4-Dioxane	575	657.4	2177	32600	0.2506
	Cyclohexane	572	622.4	1415	33100	0.3732
	Toluene	577	640.8	1725	35000	0.0662
	CCl_4	574	632.8	1618	36000	0.3217
2	acetonitrile	607.5	616	227	62100	0.002
	MTHF	611	675.5	1562	57200	0.068
	Dibutyl ether	609.5	651	1045	34100	0.075
	1,4-Dioxane	607.5	663.3	1384	16800	0.073
	Cyclohexane	607.5	636.1	740	45100	0.140
	Toluene	616	655.5	978	50600	0.050
	CCl_4	609	642.86	864	35900	0.078

[a] Stokes shift. [b] Quantum yields were calculated using Rhodamine B in ethanol (Φ_{EtOH} = 0.49) as standard .MTHF = 2-methyltetrahudrofuran.

Sensing capability

Analytical studies were carried out with diethylcyanophosphonate (DCNP) and diisopropylfluorophosphate (DFP) in acetonitrile (Scheme 7). Given the extreme toxicity of the nerve agents, Sarin, Soman and tabun,[1a] the control compounds DCNP and DFP were used as models for the design of indicators and sensing systems. In general, these controls have similar reactivity but lack the acute toxicity.

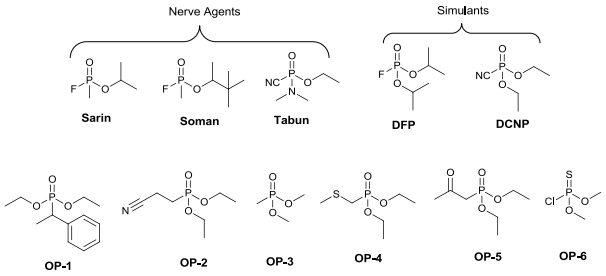

Scheme 7. Molecular formulae of nerve agents and different organophosphorus derivatives.

As a first step, studies were carried out with **2** in acetonitrile solution (10^{-5} M). Typically, the addition of DCNP and/or DFP resulted in a blueshift (from λ = 608 to 560 nm) of the absorption band (a color modulation from blue to pink, which is easily detected with the naked eye; Figure 4) and a dramatic enhancement and blueshift for the fluorescence, which now appears at λ = 570 nm.Comparable behaviour was observed on the addition of DCNP and DFP to solutions of **1** in acetonitrile; namely, a blueshift (from λ = 569 to 558 nm) of the absorption band (a color modulation from purple to pink; see the Supporting Information). There is also the accompanying dramatic emission enhancement and blueshift to λ = 575 nm with increasing DCNP/DFP concentration. (Figure 5)

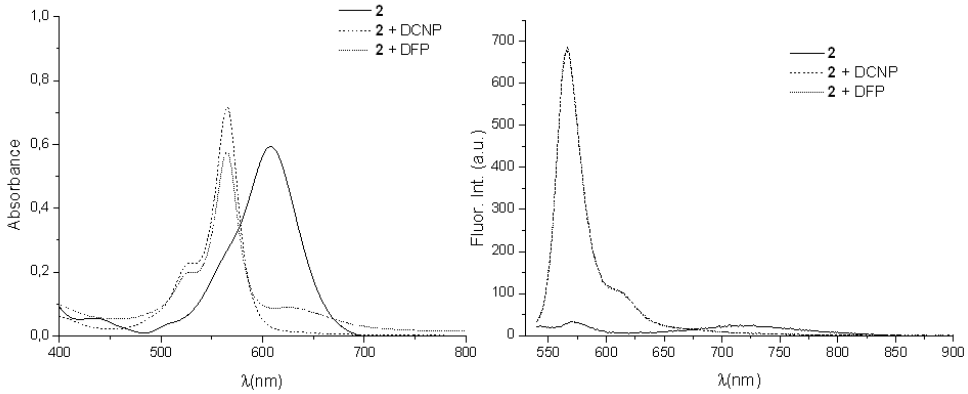

Figure 3. Absorption (left) and fluorescence (right) spectra (λ_{ex} = 530 nm) recorded for **2** (10^{-5} M in CH_3CN) alone and in the presence of DCNP or DFP.

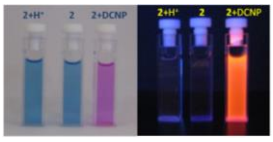

Figure 4. Visual changes observed for **2** in the presence of acid or DCNP; under daylight (left) and irradiation conditions at λ = 254nm (right).

The color changes are ascribed to intramolecular *N*-alkylation to give a five-membered ring quaternary ammonium salt in **1** and the corresponding morpholino cation in **2** (see Scheme 2). The effect of this transformation is to switch off the electron-donating ability of the tertiary amino group, thus leading to loss of the charge-transfer character.

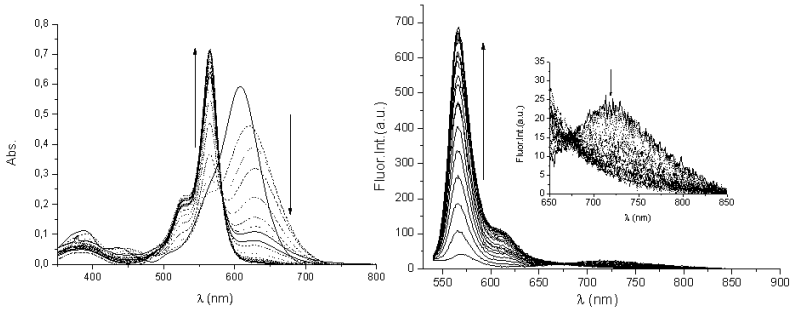

Figure 5. Absorption (left) and fluorescence (right) response (λ_{ex} = 530 nm) of **2** (10^{-5} M in CH_3CN) to the successive addition of incremental amounts of DCNP (inset spectra: amplification of the weak band at λ = 725 nm).

The observation of the weak BODIPY emission (ϕ= 0.014 and 0.002 for **1** and **2,** respectively) before cyclization is strong testament for such an intramolecular charge transfer from the amino group. The revival of the vibronic-structured emission band together with the emission enhancement (ϕ= 0.22 and 0.23 for **1** and **2**, respectively, after recognition) is in good accord with this hypothesis.

To evaluate the applicability of these BODIPY dyes for the detection of nerve-agent simulants, the limits of detection (LOD) were determined by using the equation: LOD = K x Sb_1/S, where K = 3, Sb_1 is the standard deviation of the blank solution, and S is the slope of the calibration curve.[23] Both dyes showed lower LOD values for DCNP than for DFP, which is in agreement with the trend observed by using other chromo-reagents (Table 2).[10e,24] Compound **2** showed a somewhat lower LOD than **1**. This difference in response is ascribed to the easier cyclization of the phosphorylated derivative of **1** relative to the restricted conformation that occurs with **2**. In dye **1**, the nucleophilic nitrogen atom and the phosphorylated hydroxyl group are connected by two aromatic carbon atoms in a plane, which imposes a restricted conformation to the ethyl chain that contains the phosphate group and promotes intramolecular cyclization.

Table 2. Derived limit of detection (LOD) for dyes **1** and **2**.

Probe	Simulant	LOD UV (ppm)	LOD Fluor. (ppm)
1	DCNP	0,28	0,10
	DFP	0,43	0,39
2	DCNP	4,52	4,01
	DFP	7,35	6,10

Finally, the reactivity of **1** and **2** towards DCNP was studied in different media (Table 3). A similar behavior was observed in all cases; on the addition of DCNP, a blueshift of the absorption band (a color modulation from purple to pink or blue to pink for compounds **1** and **2**, respectively) and a dramatic emission enhancement was observed.

Table 3. Photophysical properties of BODIPY dye **1** and **2** in several solvents alone and in the presence of DCNP.

	Compound	λ_{abs} (nm)	λ_{em} (nm)	$\varepsilon(M^{-1} cm^{-1})$	$\Phi^{[a]}$
Acetonitrile	**1**	569.4	575.0	30800	0.014
	1 + DCNP	558.6	575.0	33000	0.218
	2	607.5	616.0	62100	0.002
	2 + DCNP	565.5	568.9	76500	0.231
MTHF	**1**	573.0	668.2	36100	0.189
	1 + DCNP	562.0	577.0	40700	0.403
	2	611.3	675.5	57200	0.068
	2 + DCNP	568.9	569.5	63400	0.374
Dibutyl ethet	**1**	573.0	637.0	33400	0.280
	1 + DCNP	561.5	576.0	36540	0.399
	2	609.5	651.0	34100	0.075
	2 + DCNP	571.0	570.1	62800	0.392
1,4-Dioxane	**1**	575.0	657.4	32600	0.250
	1 + DCNP	563.0	577.8	36800	0.437
	2	607.5	663.3	16800	0.073
	2 + DCNP	569.3	570.4	65900	0.405
Toluene	**1**	577.0	640.8	35000	0.062
	1 + DCNP	566.0	576.0	35300	0.387
	2	616.0	655.5	50600	0.05
	2 + DCNP	570.0	578.3	65300	0.398
Carbon	**1**	574.5	638.2	36000	0.321
tetrachloride	**1** + DCNP	565.0	576	40100	0.402
	2	609.0	642.8	35900	0.078
	2 + DCNP	568.4	572.8	60100	0.381
Water/Acetonotrile	**1**	570.4	575.3	30500	0.016
(3:1)	**1** + DCNP	560.4	576	34000	0.210
	2	609.0	618.5	59100	0.002
	2 + DCNP	569.5	570.6	61500	0.284

[a] Quantum yields were calculated using Rhodamine B in ethanol (ϕ_{EtOH} = 0.49) as standard.

Competing reagents

As expected, addition of protons to solutions of **1** and **2** (10^{-5} M) in CH_3CN results in extinction of fluorescence from the BODIPY unit, but without marked changes in the corresponding absorption spectra. This behavior demonstrates that protonation takes place on the pyridine moiety because the addition of protons to

the control compound **3** induces a drastic blue shift of its absorption band and a dramatic enhancement of emission. These latter effects are well explained in terms of protonation at the terminal amino group. It is notable that these same changes are not observed in buffered media (see the Supporting Information). To further confirm the crucial importance of the pyridine moiety to avoid false readings, competitive studies were carried out. For this purpose, DCNP and DFP were added to a solution containing the dye in acidified media. In all cases, a clear color change could be observed by the naked eye. The reactivity with other organophosphorus compounds (Scheme 7) was also studied under comparable conditions. However, it proved impossible to detect any change in the absorption or fluorescence spectral profiles or intensities recorded for **1** and **2,** (see the Supporting Information). Such behaviour indicates that there is no reaction between the fluorescent dye and these particular phosphate derivatives.

Table 4. Photophysical properties recorded for the BODIPY dyes **1** and **2** alone and in the presence of both the nerve-agent simulant and acid.

Compound	λ_{abs} (nm)	ε (M^{-1} cm^{-1})	λ_{em} (nm)	$\phi^{[a]}$
1	569	30800	575	0.014
1 + DCNP	559	33000	575	0.218
1 + DFP	559	32800	575	0.197
1+ HCl	569	30800	610	$6 \cdot 10^{-6}$
2	608	62100	616	0.002
2 + DCNP	565	76500	567	0.231
2+ DFP	565	61400	569	0.230
2+ HCl	608	62100	725	$8 \cdot 10^{-6}$

[a] Quantum yields were calculated using Rhodamine B in ethanol (ϕ_{EtOH} = 0.49) as standard.

Development of a chemo-sensor kit

Having demonstrated the sensing capability of the new BODIPY dyes, we decided to take a further step and extend their applicability to real-time monitoring. Thus, two different test strips for the colorimetric (and fluorescent) detection of nerve agent simulants in the gas phase were developed.

To this end, hydrophobic polyethylene oxide films and silica gel plates containing probes **1** and **2** were prepared. In a typical assay, the films or plates were placed

into a container holding the nerve-agent simulant (30 ppm introduced as an aerosol). Alternatively, the strips were exposed to solutions containing DCNP, DFP and/or acid in acetonitrile. A similar chromogenic behavior was noted in both the solution and the gas phase; typically, this constitutes a color modulation from purple to pink and an increase in fluorescence for the strips containing probe **1**. Similar behavior was noted with **2** in the presence of DCNP and DFP. Critically, the strips remained fluorescent. No change in strip color was observed in the presence of acid.

Figure 6. Silica gel plate of **1** (10^{-3} M) (center) in the presence of acid (left) and DCNP (right).

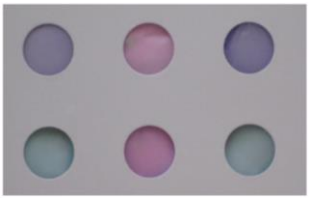

Figure 7. The polyethylene oxide membranes of **1** (top) and **2** (bottom) in the absence and presence DCNP (30 ppm) and HCl (50 ppm) vapors (from left to right).

Conclusion

We have report herein two BODIPY derivatives for the chromo- and fluorogenic detection of nerve-agent simulants. The reaction of **1** or **2** with DCNP or DFP results in phosphorylation of a hydroxyl group. In a second step, the reaction leads to an intramolecular *N*-alkylation, thus giving a five-membered-ring quaternary ammonium salt in **1** and the corresponding morpholino cation in **2**. These transformations are evidenced by a significant blueshift for the lowest-energy absorption transition, which is easily detected by the naked eye. There is an accompanying escalation in the fluorescence yield, which is made more

remarkable by the shift from the far-red to the blue region. A critical feature of these new reagents is that they are less prone to false readings in the presence of acids because preferential protonation on the pyridine moiety protects the terminal aniline unit. In consequence, the sensing mechanism is still working in the presence of acids, thus avoiding a false negative response. In addition, the signaling abilities are retained in the solid state, allowing the development of simple colorimetric tests for the presence of nerve-agent simulants in gaseous and liquid phases. To the best of our knowledge, the dyes reported herein are the first such probes to display the necessary discrimination between nerve agents and acidic residues.

Experimental Section

General remarks

CH_2Cl_2 and CH_3CN were distilled from P_2O_5 under Ar prior to use. Benzene was distlled from CaH_2 under Ar proir to use. THF was distilled from Na/benzophenone under Ar prior to use. All the other solvents and starting materials were purchased from comercial sources where available and were used without purification. Silica gel 60 F254 (Merk) plates were used for TLC analysis. Colum chromatography was performed on silica gel (60, 40-63 Å). ^{1}H and ^{13}C NMR (300 MHz) spectra were determined on a Bruker AV 300 spectrometrer. Chemical shifts are reported in parts per million (ppm), calibrated to the solvent-peak set. High-resolution mass spectra were recorded in the positive-ion mode with a VG-AutoSpec mass spectrometer.

Synthesis and characterization of BODIPY derivatives:

2-[2-(dimethylamino) phenyl] ethanol (5): A mixture of 2-(2-aminophenyl) ethanol (2 mL; 15.2 mmol) and K_2CO_3 (4.4 g, 32.4 mmol) in CH_3CN (60 mL) was stirred at room temperature for 40 min. Iodomethane (1.99 mL, 30.4 mmol) was added dropwise to the reaction mixture, which was heated to reflux for 3

h. The suspension was filtered, and the resulting solid was washed with CH_3CN. The filtered solution was concentrated under vacuo and re-dissolved in CH_2Cl_2. The resulting solution was extracted with water, and the organic layer was washed with brine, dried over anhydrous $MgSO_4$ and concentrated in vacuo to yield **5** (2.157 g, 86.3 %) as a brown oil. ^{1}H NMR (300 MHz, $CDCl_3$) δ 7.25–7.10 (m, 3H), 7.04 (m, 1H), 5.20 (t, *J* = 2.0 Hz, 1H), 3.82 (m, 2H), 2.98 (t, *J* = 6 Hz, 2H), 2.66 (s, 6H). HRMS (EI): m/z (%) calc for $C_{10}H_{16}NO$: 166.215 $[M+1]^+$ found: 166.232.

2-[5-bromo-2-(dimethylamino)phenyl]ethanol (6): 2-[2-(dimethylamino) phenyl]ethanol (**5**) (1.05 g, 6.36 mmol) and NH_4OAc (5.21 g, 6.74 mmol) were dissolved in CH_3CN (50 mL). *N*-bromosuccinimide (1.2 g, 6.68 mmol) was added to the reaction mixture, which was stirred at room temperature. After completion of the reaction, as indicated by TLC analysis the mixture was concentrated in vacuo and extracted with CH_2Cl_2:H_2O (1:1). The organic portion was separated from the extract, dried and concentrated to yield **6** (1.456 g, 94 %) as a dark-orange oil. ^{1}H NMR (300 MHz, $CDCl_3$) δ 7.28–7.19 (m, 2H), 6.97 (m, 1H), 3.79 (m, 2H), 2.90 (m, 2H), 2.59 (s, 6H). HRMS (EI): m/z (%) calc for $C_{10}H_{15}BrNO$: 245.119 $[M+1]^+$ found: 245.128.

4-(dimethylamino)-3-(2-hydroxyethyl) benzaldehyde (7): A solution of bromide **6** (350 mg, 1.43 mmol) in anhydrous THF (10 mL) was cooled to -78 °C under Ar. *n*-BuLi (2 mL, 3.16 mmol) in hexane (1.6 M) was added dropwise with stirring to the reaction mixture, which was warmed to 0°C. After stirring 30 min. at this temperature, dry dimethylformamide (122 µL, 1.57 mmol) was added at -78°C. The resulting mixture was allowed to warm to room temperature and stirred at room temperature for 3h. Water was added and the reaction mixture was extracted with CH_2Cl_2 and water. The separated organic layer was dried over anhydrous $MgSO_4$, filtered, concentrated and purified by column chromatography on silica gel with ethyl acetate/ hexane (1:1) as eluent to afford aldehyde **7** (258 mg, 93.4%) as yellow oil. ^{1}H NMR (300 MHz, $CDCl_3$) δ 9.75 (s, 1H) 7.66–7.54 (m, 2H), 7.06 (t, *J* = 7.6 Hz ,1H), 3.79 (t, *J* =6.4 Hz, 2H), 2.92 (m, *J* = 6.4 Hz, 2H), 2.70 (s, 6H). HRMS (EI): m/z (%) calc for $C_{11}H_{16}NO_2$: 194.240 $[M+1]^+$ found: 194.242.

5,5-difluoro-1,3,7,9-tetramethyl-10-(pyridin-4-yl)-5H-dipyrrolo[1,2-c:2',1'-f][1,3,2]diazaborinin-4-ium-5-uide (4)*:* 2,4-Dimethylpirrole (2 mL, 19.42 mmol) and 4-pyridinecarboxaldehyde (0.9 mL, 9.24 mmol) were dissolved in 150 mL of anhydrous CH_2Cl_2 (150 mL). Trifluoroacetic acid (50 µL; 0.5 mmol) was added, and the solution was stirred at room temperature for 50 min. A solution of DDQ (2.27 g, 9.24 mmol) in CH_2Cl_2 was added. Stirring was continued for 50 min, followed by the addition of triethylamine (20 mL). After stirring for 30 min, $BF_3.OEt_2$ (20 mL) was added to the reaction mixture, which was stirred for 2h at room temperature. After the evaporation of the solvents under reduced pressure, the crude product was purified by column chromatography on silica gel with AcOEt/hexane (1:1) as eluent to give the BODIPY derivative **4** (1.15g, 38%) as red crystals. ^{1}H NMR (300 MHz, $CDCl_3$) δ 8.71 (dd, *J* = 4.3 Hz and 1.6 Hz, 2H), 7.24 (dd, *J* = 4.3 Hz and 1.6 Hz, 2H), 5.94 (s, 2H), 2.49 (s, 6H), 1.34 (s, 6H).^{13}C NMR (75 MHz, $CDCl_3$) δ 157.1, 151.1, 144.0, 142.9, 138.1, 130.6, 123.7, 122.2, 15.1, 15.0 HRMS (EI): m/z (%) calc for $C_{18}H_{19}BF_2N_3$: 326.1635 $[M+1]^+$ found: 326.1641. UV-Vis (CH_3CN): λ_{max}= 500.4; λ_{em}= 510 nm.

(E)-7-(4-(dimethylamino)-3-(2-hydroxyethyl)styryl)-5,5-difluoro-1,3,9-trimethyl-10-(pyridin-4-yl)-5H-dipyrrolo[1,2-c:2',1'-f][1,3,2]diazaborinin-4-ium-5-uide(1): BODIPY derivative **4** (100 mg, 0.3 mmol) and aldehyde **7** (60 mg, 0.3 mmol) were dissolved in a mixture of benzene (30 mL), acetic acid (862.5 µL) and piperidine (950 µL, 9.6 mmol). Any water formed during the reaction was removed azeotropically by heating in a Dean-Stark apparatus for 14 h. The reaction mixture was concentrated under reduced pressure and then subjected to column chromatography on silica gel with AcOEt/Hexane (2:1) to yield the desired dye **1** (42 mg, 26.6 %) as purple crystals. ^{1}H NMR (300 MHz, $CDCl_3$) δ 8.73 (d, *J* = 4.8 Hz, 2H) 7.51 (d, *J* = 15.8 Hz, 1H), 7.39 (d, *J* = 8.2 Hz, 1H), 7.32 (d, *J* = 2.0 Hz, 1H), 7.27 (dd, *J* = 4.8, 1.6 Hz, 2H), 7.12 (dd, *J* = 15.4, 8.3 Hz, 2H), 6.55 (s, 1H), 5.97 (s, 1H), 3.86–3.75 (m, 2H), 2.99 (dd, *J* = 9.9, 4.4 Hz, 2H), 2.69 (s, 6H), 2.54 (s, 3H), 1.39 (s, 3H), 1.36 (s, 3H).^{13}C NMR (75 MHz, $CDCl_3$) δ 155.5, 153.5, 150.3, 149.8, 144.0, 142.3, 139.8, 138.6, 134.5, 132.0, 129.9, 129.6, 123.9, 120.9, 118.4, 114.1, 112.1, 61.8, 47.5, 39.1, 21.5, 15.0,

14.5. HRMS (EI): m/z (%) calc for $C_{29}H_{31}BF_2N_4O$: 501.2632 $[M+1]^+$ found: 501.2627. UV-Vis (CH_3CN): λ_{max}= 569.4; λ_{em}= 575 nm.

2-((4-formylphenyl)(methyl)amino)ethyl 4-methylbenzenesulfonate (8):A solution of 4-[(2-hydroxyethyl)(methyl)amino]benzaldehyde (1 g, 5.6 mmol) and Et_3N (1.15 mL, 7.3 mmol) in anhydrous CH_2Cl_2 (50 mL) was stirred for 10 min. at room temperature. *para*-Toluenesulfonyl chloride (1.6 g, 8.4 mmol) was added and the reaction mixture, which was stirred for 22 h. The reaction mixture was extracted with a saturated $NaHCO_3$. The organic phase was dried over anhydrous $MgSO_4$, filtered and concentrated under reduced pressure and then subjected to column chromatography on silica gel with AcOEt/Hexane (1:1) to yield the desired product **8** (862 mg, 46%) as pale yellow solid. ^{1}H NMR (300 MHz, $CDCl_3$) δ 9.57 (s, 1H) 7.50 (m, 4H), 7.07 (m, *2*H), 6.42 (t, *J* = 5.8 Hz, 2H), 4.08 (t, *J* = 5.5 Hz, 2H), 3.54 (t, *J* = 5.5 Hz, 2H) 2.79 (s, 3H), 2.20 (s, 3H). HRMS (EI): m/z (%) calc for $C_{17}H_{20}NO_4S$: 334. 2124 $[M+1]^+$ found: 334.2104.

4-((2-(2-hydroxyethoxy)ethyl)(methyl)amino)benzaldehyde (9): K_2CO_3 (332 mg, 2.4 mmol) was added to ethylene glycol (35 µL, 0.6 mmol) dissolved in dry CH_3CN (30 mL). The white suspension was refluxed for 1h and then compound **8** (200 mg, 0.6 mmol) in dry CH_3CN (10 mL) was added dropwise over 60 minutes. Subsequently the reaction was heated to reflux for 16 h. The suspension was filtered, and the solvent was removed by evaporation. The crude was purified by column chromatography on silica gel with AcOEt/Hexane (3:2 to 5:1) as eluent to obtain aldehyde **9** (74.6 mg, 53 %) as yellow precipitate.^{1}H NMR (300 MHz, $CDCl_3$) δ 9.66 (s, 1H) 7.66 (m, 2H), 6.67 (m, 2H), 3.63 (m, 6H), 3.49 (m, 2H), 3.04 (s, 3H). HRMS (EI): m/z (%) calc for $C_{12}H_{18}NO_3$: 224.1283 $[M+1]^+$ found: 224.1208.

(E)-5,5-difluoro-7-(4-((2-(2-hydroxyethoxy)ethyl)(methyl)amino)styryl)-1,3,9-trimethyl-10-(pyridin-4-yl)-5H-dipyrrolo[1,2-c:2',1'-f][1,3,2]diazaborinin-4-ium-5-uide (2): BODIPY derivative **4** (36.5 mg; 0.11 mmol) and aldehyde **9** (29.1 mg, 0.13 mmol) were dissolved in a mixture of benzene (16 mL), acetic acid (317 µL) and piperidine (350 µL, 3.52 mmol). Any water formed during the reaction was removed azeotropically by heating in a Dean-Stark apparatus for 4 h. The reaction

mixture was concentrated under reduced pressure and then subjected to column chromatography on silica gel with AcOEt as eluent to yield the desired dye **2** (13.3 mg, 33%) as blue crystals. ^{1}H NMR (300 MHz, $CDCl_3$) δ 8.77 (dd, *J* = 4.4, 1.5 Hz, 2H), 7.49 (m, 3H), 7.34 (dd, *J* = 4.4, 1.6 Hz, 2H), 7.20 (s, 1H), 6.72 (d, *J* = 8.7 Hz, 2H), 6.62 (s, 1H), 5.99 (s, 1H), 3.70 (m, 4H), 3.62 (m, 2H), 3.56 (m, 2H), 3.06 (s, 3H), 2.59 (s, 3H), 1.45 (s, 3H), 1.41 (s, 3H).^{13}C NMR (75 MHz, $CDCl_3$) δ 155.6, 153.5, 150.2, 149.8, 144.2, 142.3, 140.1, 138.6, 134.6, 132.1, 130.0, 129.6, 123.9, 120.9, 118.4, 113.8, 112.1, 72.5, 68.6, 61.8, 52.2, 42.5, 21.5, 14.3, 14.2. HRMS (EI): m/z (%) calc for $C_{30}H_{34}BF_2N_4O_2$: 531.2742 $[M+1]^+$ found: 531.2748. UV-Vis (CH_3CN): λ_{max}= 607.5; λ_{em}= 642.9 nm.

(E)-5,5-difluoro-7-(4-((2-(2-hydroxyethoxy)ethyl)(methyl)amino)styryl)-1,3,9-trimethyl-10-phenyl-5H-dipyrrolo[1,2-c:2',1'-f][1,3,2]diazaborinin-4-ium-5-uide

(3)*:* 8-phenyl-1,3,5,7-tetramethyl-BODIPY (42,7 mg, 0,11 mmol) and aldehyde **9** (29.1 mg, 0.13 mmol) were dissolved in a mixture of benzene (15 mL), acetic acid (315 µL) and piperidine (325 µL, 3.3 mmol). Any water formed during the reaction was removed azeotropically by heating in a Dean-Stark apparatus for 5 h. The reaction mixture was concentrated under reduced pressure and then purified by column chromatography on silica gel with ethyl acetate/ hexane (3:1) as eluent to yield the desired dye **3** (6,4 mg,11 %) as blue crystals. ^{1}H NMR (300 MHz, $CDCl_3$) δ 7.43 (d, *J* = 8.7 Hz, 3H), 7.40 (d, *J* = 1.9 Hz, 2H), 7.28 – 7.21 (m, 3H), 7.16 (s, 1H), 6.63 (d, *J* = 8.9 Hz, 2H), 6.52 (s, 1H), 5.90 (s, 1H), 3.67 – 3.59 (m, 4H), 3.55 (d, *J* = 5.2 Hz, 2H), 3.52 – 3.47 (m, 2H), 3.02 (d, *J* = 16.3 Hz, 3H), 2.52 (s, 3H), 1.94 (s, 3H), 1.35 (s, 3H), 1.31 (s, 3H).^{13}C NMR (75 MHz, $CDCl_3$) δ 156.5, 154.6, 151.2, 148.5, 145.2, 143.3, 141.1, 139.5, 135.3, 133.1, 130.5, 127.7, 124.9, 121.9, 119.3, 115.05, 113.1, 110.4, 109.4, 73.4, 69.5, 62.8, 53.2, 40.1, 22.4, 15.7, 15.1.

Spectroscopic Studies

All the solvents were purchased at spectroscopic grade from Aldrich Chemicals Co., were used as received, and were free of fluorescent impurities. The absorption and fluorescence spectra were recorded using a Hitachi U3310 spectrophotometer and a Hitachi F4500 spectrofluorimeter, respectively. Fluorescence quantum yields were measured at room temperature in N_2-purged

solution of the corresponding solvent relative to Rhodamine B (ϕ_{EtOH} = 0.49)[25] at λ = 525 nm.

General Procedure for Detection-limit determinations

Increasing amounts of the corresponding simulant solutions (in acetonitrile) were added to the corresponding receptor in acetonitrile (10^{-5} M). The Uv/Vis and fluorescence spectra were recorded in cells with a path length of 1 cm at 25 °C (termostatted). Representation of absorbance/ fluorescence at the appropiate wavelength versus concentration of simulant allowed the detection limit to be calculated.

Membrane Preparation

Polyethylene oxide (2 g, Mw = 400,000 Dalton) was slowly added to a solution of **1** or **2** (2 mg) in dichloromethane (40 mL). The mixture was stirred until a highly viscous mixture was formed. This mixture was poured into a glass plate (40 cm^2) and kept in a dry atmosphere for 24 h.

Silica gel plate Preparation

The strip was prepared by immersing the silica gel plate into the acetonitrile solution of **1** or **2** (10^{-3} M) and then dried in air.

Acknowledgements

We thank the Spanish Government (MAT2012-38429-C04-02) for support. A.B.B. acknowledges the award of a predoctoral FPI fellowship. SCSIE (Universidad de Valencia) is gratefully acknowledged for all the equipment employed. Dr. S. Royo is thanked for support with some of the synthetic chemistry.

Keywords: boron • fluorescent probes • neurological agents • phosphorylation • sensors

References

1 (a) S. M. Somani, *Chemical Warfare Agent*, Academic Press, San Diego**, 1992**; (b) C. H. Gunderson, C. R. Lehmann, F. R. Sidell and B. Jabbari, *Neurology*, **1992**, *42*, 946-950.

2 (a) Silver, *The Biology of Cholinesterases*, Elsevier, New York, **1974**, 449-488; (b) P. Taylor, in *The Pharmacological Basis of Therapeutics,* 10th ed. (ed: J. G. Hardman, L. E. Limbird, A. G. Gilman,) McGraw-Hill, New York, **2001**, 175-191.

3 (a) A. J. Russell, J. A. Berberich, G. F. Drevon and R. R. Koepsel, *Annu. Rev. Biomed. Eng*., **2003**, *5*, 1–27; (b) J. A. Ashley, C.-H. Lin, P. Wirsching and K. D. Janda *Angew. Chem., Int. Ed*., **1999**, *38*, 1793-1795.

4 E. Steiner, S. J. Klopsch, W. A. English, B. H. Clowers, H. H. Hill, *Anal. Chem.,* **2005**, *77*, 4792-4796.

5 (a) J.-C. G. Bunzli and C. Piguet, *Chem. Soc. Rev.,* **2005**, *34*, 1048-1077; (b) B. Zhao, X. Y. Chen, P. Cheng, D.-Z. Liao, S.-P. Yan and Z. H. Jiang, *J. Am. Chem. Soc*., **2004**, *126*, 15394-15395.

6 (a) M. A. K. Khan, Y. T. Long, G. Schatte, H. B. Kraatz, *Anal. Chem*. **2007**, *79*, 2877-2882; (b) O. V. Shulga, C. Palmer, *Anal. Bioanal. Chem*. **2006**, *385*, 1116-1121; (c) G. Liu, Y. Lin, *Anal. Chem.* **2006**, *78*, 835-843; (d) G. Liu, Y. Lin*, Anal. Chem*. **2005**, *77*, 5894-5902.

7 (a) W. He, Z. Liu, X. Du, Y. Jiang, D. Xiao, *Talanta*, **2008**, *76*, 698-704; (b) J. P. Walker, K. W. Kimble, S. A. Asher, *Anal. Bioanal. Chem.* **2007**, *389*, 2115-2118; c) J. P. Walker, S. A. Asher, *Anal. Chem.* **2005***, 77*, 1596-1600.

8 (a) G. Zuo, X. Li, P. Li, T. Yang, Y. Wang, Z. Chen, S. Feng, *Anal. Chim. Acta* **2006**, *580*, 123-125; (b) C. Karnati, H. Du, H. F. Ji, X. Xu, Y. Lvov, A. Mulchandani, P. Mulchandani, W. Chen, *Biosens. Bioelectron***. 2007**, *22*, 2636-2640.

9 M. J. Aernecke, D. R. Walt, *Sens. Actuators B* **2009**, *142*, 464-473.

10 (a) M. Burnworth, S. J. Rowan and C. Weder, *Chem. Eur. J.,* **2007**, *13*, 7828-7836; (b) N. A. Rakow, A. Sen, M. C. Janzen, J. B. Ponder and K. S. Suslick, *Angew. Chem., Int. Ed.,* **2005**, *44*, 4528-4532; (c) A. M. Costero, S. Gil, M. Parra, P. M. E. Mancini, R. Martinez-Mañez, F. Sancenon and S. Royo, *Chem. Commun*., **2008**, 6002-6004 (d) T. J. Dale and J. Rebek, *Angew. Chem., Int. Ed*., **2009**, *48*, 7850-7852. (e) S. B. Nagale, T. Sternfeld and D. R. Walt, *J. Am. Chem. Soc*., **2006**, *128*, 5041-5048;(f) W.-M. Xuan, Y.-T. Cao, J.-H. Zhou and W. Wang *Chem. Commun*., **2013**, *49*, 10474-10476; (g) S. Han, Z. Xue, Z. Wang and T. B. Wen, *Chem. Commun.,* **2010**, *46*, 8413-8415;(h) S. Clavaguera, A. Carella, L. Caillier, C. Celle, J. Pecaut, S. Lenfant, D. Vuillaume and J.-P. Simonato, *Angew. Chem.,* **2010**, *122*,4157-4160 ;*Angew. Chem., Int. Ed*, **2010,** 49, 4063-4066.

11 (a) S.-W. Zhang and T.M. Swager *J. Am. Chem. Soc.,* **2003**, *125*, 3420-3421; (b) K. J. Wallace, J. Morey, W. M. Lynch and E. V. Anslyn *New J. Chem*., **2005**, *29*, 1469-1474; (c) K. A. Van, D. C. Heath and R. S. Pilato, *J. Am. Chem. Soc*., **1998**, *120*, 12359-12360.

12 (a) D. Parker, *Coord. Chem. Rev*., **2004,** *205*, 109-130; (b) F. Ilhan, D. S. Tyson and M. A. Meador, *Chem. Mater.*, **2004**, *16*, 2978-2980; (c) A. M. Costero, M. Parra, S. Gil, R. Gotor, P. M. E. Mancini, R. Martinez-Mañez, F. Sancenon and S. Royo, *Chem. Asian J.,* **2010**, *5*, 1573-1585.

13 (a) S. Royo, R. Gotor, A. M. Costero, M. Parra, S. Gil, R. Martinez-Mañez and F. Sancenon. *New J. Chem*., **2012**, *36*, 1485-1489; (b) A. Marti, A. M. Costero, P. Gaviña, S. Gil, M. Parra, M. Brotons-Gisbert and J. F. Sanchez-Royo, *Eur. J. Org. Chem*. **2013**, 4770–4779.

14 (a) A. Loudet and K. Burgess, *Chem. Rev.,* **2007**, *107*, 4891-4932; (b) G. Ulrich, R. Ziessel and A. Harriman, *Angew. Chem., Int. Ed***., 2008**, *47,* 1184-1201.

15 (a) X. Wu, Z. Wu and S. Han *Chem. Commun*., **2011**, *47*, 11468-11470; (b) Z. Wu, X. Wu, Y. Yang, T.-b. Wen and S. Han *Bioorg. Med. Chem. Lett*. **2012**, *22*, 6358-6361.

16 M. A. H. Alamiry, A. Harriman, L. J. Mallon, G. Ulrich and R. Ziessel, *Eur. J. Org. Chem.,* **2008**, 2774-2782.

17 A. Harriman, L. J. Mallon, G. Ulrich and R. Ziesel, *Chem-Phys Chem*, **2007**, *8*, 1207-1214.

18 N. Saki, T. Din and E. U. Akkaya, *Tetrahedron* **2006**, *62,* 2721-2725

19 (a) M. Baruah, W. Qin, N. Basarié, W. M. DeBorggraeve and N. Boens, *J.Org.Chem*., **2005**, *70*, 4152-4157; (b) Y. Ikawa, S. Moruyama and H. Furuta*, Anal. Biochem.,* **2008**, *378*, 166-170.

20 (a) W. Qin; M. Baruah; W. M. De Borggraeve and N. Boens, *J. Photochem. Photobiol. A: Chem*. **2006**, *183*, 190-197. (b) X. Peng, J. Du, J. Fan, J. Wang, Y. Wu, J. Zhao, S. Sun and T. Xu, T. *J. Am. Chem. Soc*. **2007**, *129*, 1500-1501.

21 (a) W. Qin, T. Rohand, W. Dehaen, J. N. Clifford, K. Driesen, D. Beljonne, B. Van Averbeke, M. Van der Auweraer and N. Boens, *J. Phys. Chem. A,* **2007**, *35*, 8589-8597; (b) Z. Yin, A. Yiu-Yan, K. Man-Chung, C. H. Tao, B. Li, C. T. Poon, L. Vivian and W. W. Yam, *Dalton Trans.,* **2012**, *41*, 11340-11350.

22 (a) T. Cheng, T. Wang, W. Zhu, X. Chen, Y. Yang, Y. Xu and X. Qian, *Org. Lett.,* **2011**, *13*, 3656-3660; (b) T. Cheng, T. Wang, W. Zhu, Y. Yang, B. Zeng, Y. Xu and X. Qian, *Chem. Commun.*, **2011**, *47*, 3915-3918.

23 M. Zhu, M. Yuan, X. Liu, J. Xu, J. Lv, C. Huang, H. Liu, Y. Li, S. Wang and D. Zhu, *Org. Lett.,* **2008**, *10*, 1481-1484.

24 S. Royo, R. Martinez-Mañez, F. Sancenon A. M. Costero, M. Parra and S. Gil, *Chem. Commun*., **2007**, *46*, 4830-4847.

25 K. G. Casey and E. L. Quitevis, *J. Phys. Chem*., **1998**, *92*, 6590–6594.

Supporting Information

Highly Selective Detection of Nerve-Agent Simulants with BODIPY Dyes

Andrea Barba-Bon, Ana M.Costero,
Salvador Gil, Anthony Harriman and
Felix Sancenón

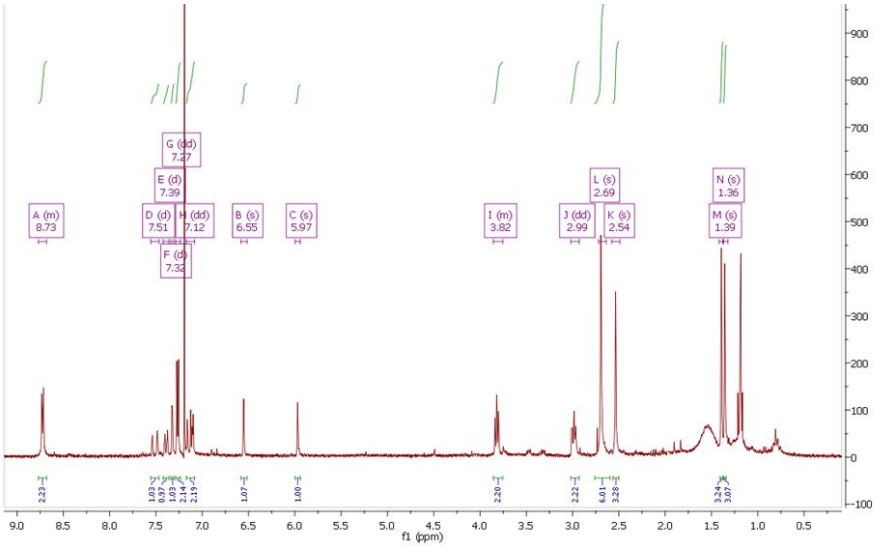

Figure SI-1. ^{1}H NMR spectrum of compound **1** ($CDCl_3$)

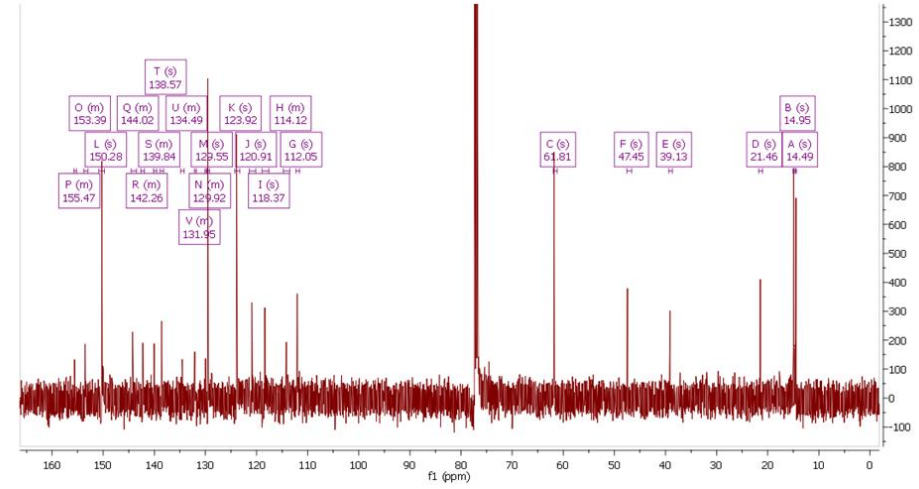

Figure SI-2. ^{13}C NMR spectrum of compound **1** ($CDCl_3$)

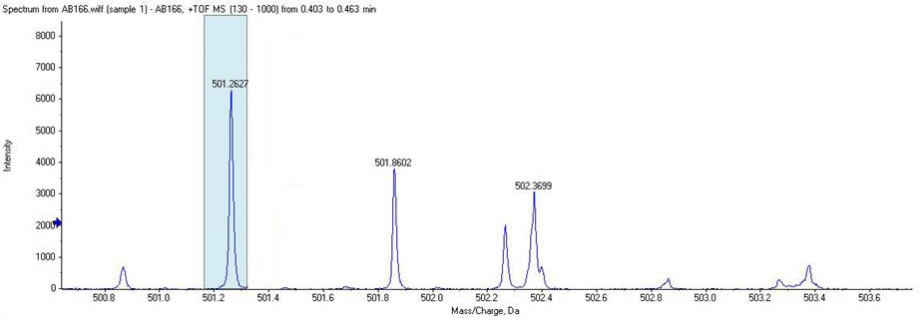

Figure SI-3. MS of compound **1**

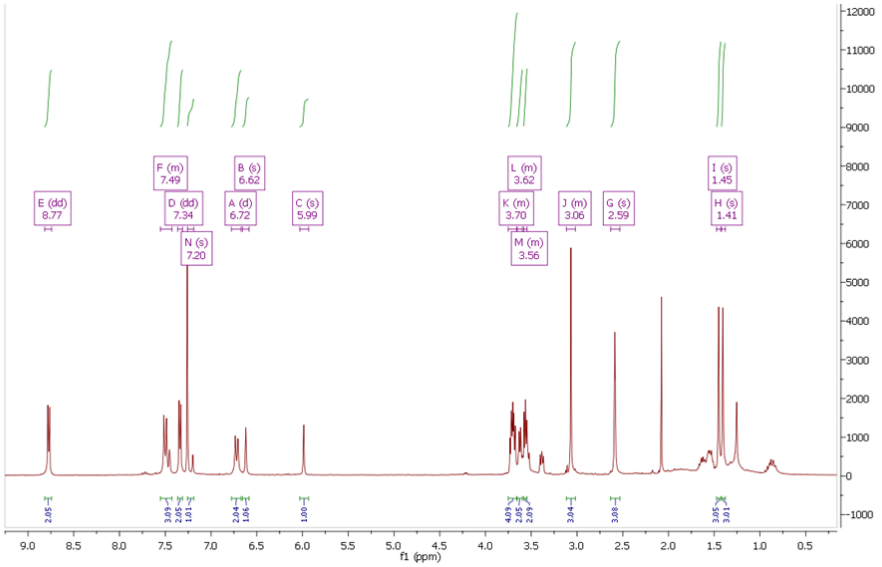

Figure SI-4. ^{1}H NMR spectrum of compound **2** ($CDCl_3$)

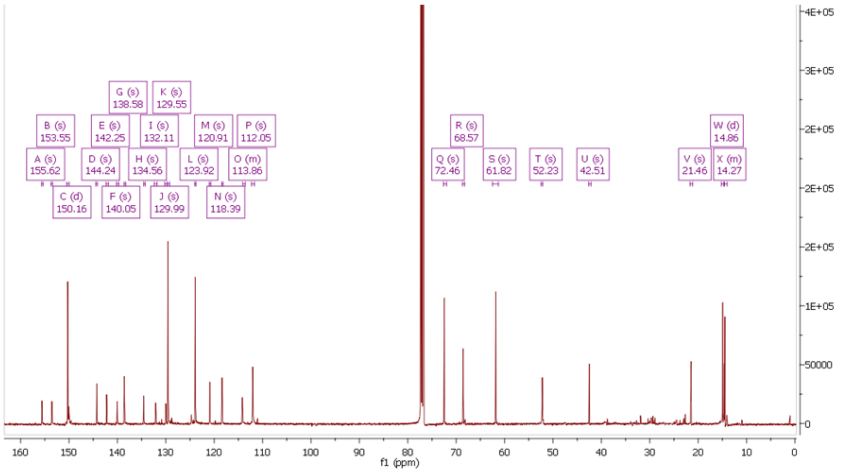

Figure SI-5. ^{13}C NMR spectrum of compound **2** ($CDCl_3$)

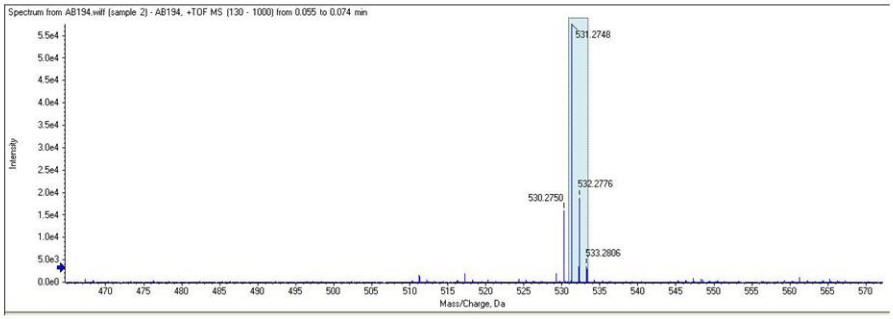

Figure SI-6. MS of compound **2**

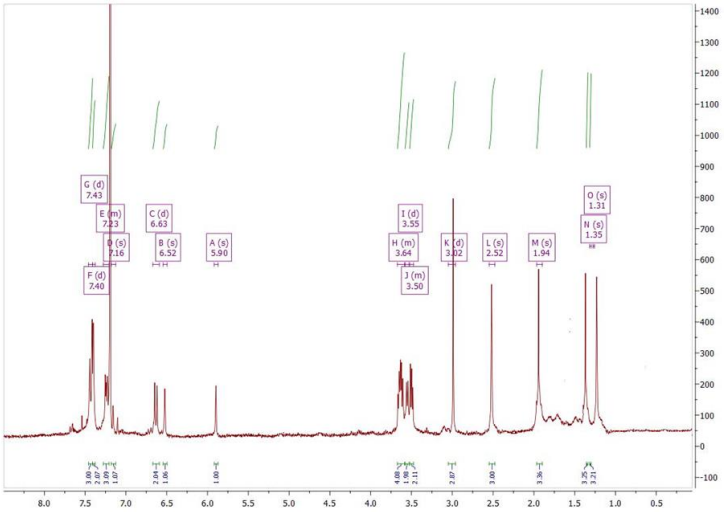

Figure SI-7. ^{1}H NMR spectrum of compound **3** ($CDCl_3$)

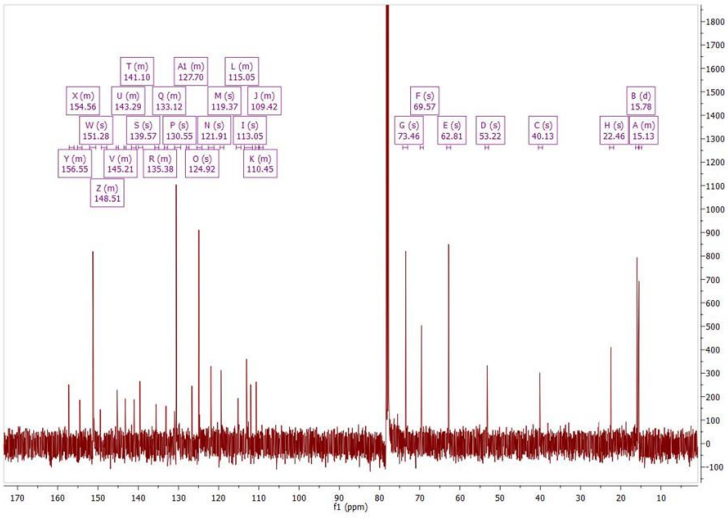

Figure SI-8. ^{13}C NMR spectrum of compound **3** ($CDCl_3$).

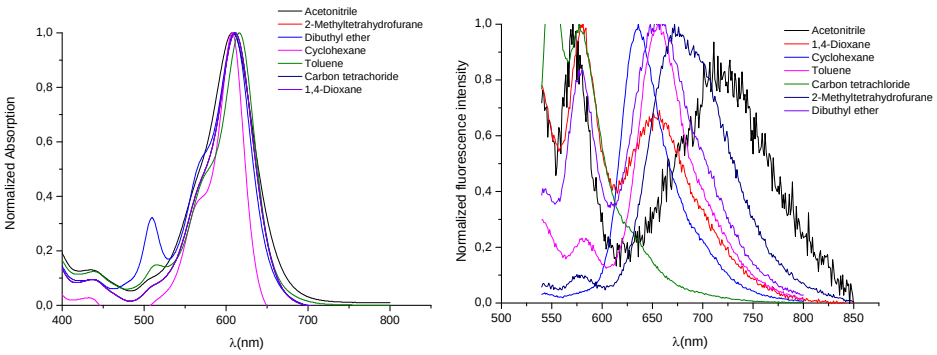

Figure SI-9. Enlargement of the main absorption peak (left) and fluorescence emission peak (right) of **2** in several solvents to emphasize the solvatochromic shifts. The intensities in this figure are normalized to the same value at the wavelength of maximum intensity.

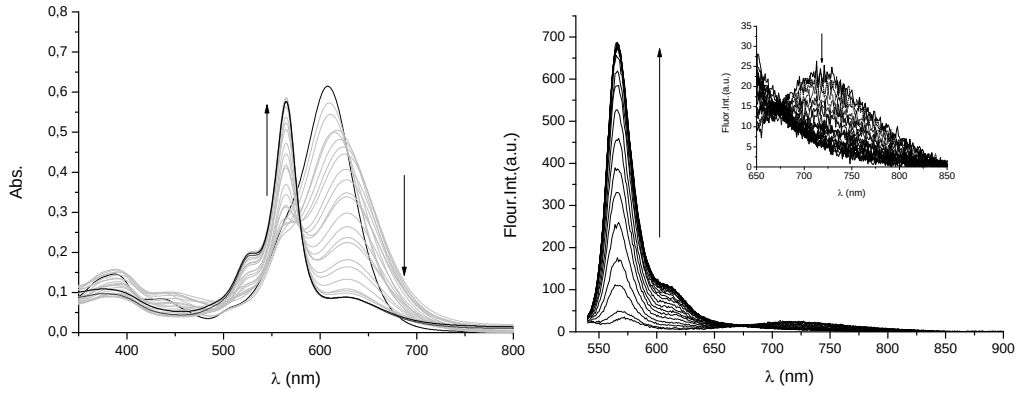

Figure SI-10. (left) Uv-vis and (right) and fluorescence response (λ_{ex} = 530 nm) of **2** (10^{-5} M in CH_3CN) in presence of increasing amount of DFP (inset spectra: amplified the small band at 725 nm).

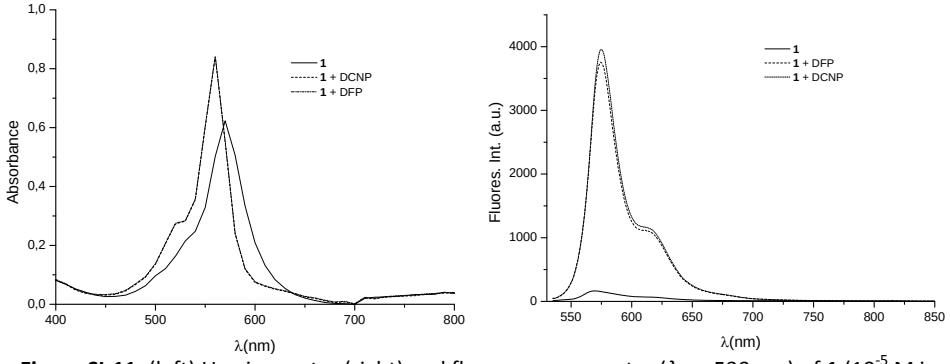

Figure SI-11. (left) Uv-vis spectra (right) and fluorescence spectra (λ_{ex} = 530 nm) of **1** (10^{-5} M in CH_3CN) alone and in presence of DCNP and DFP.

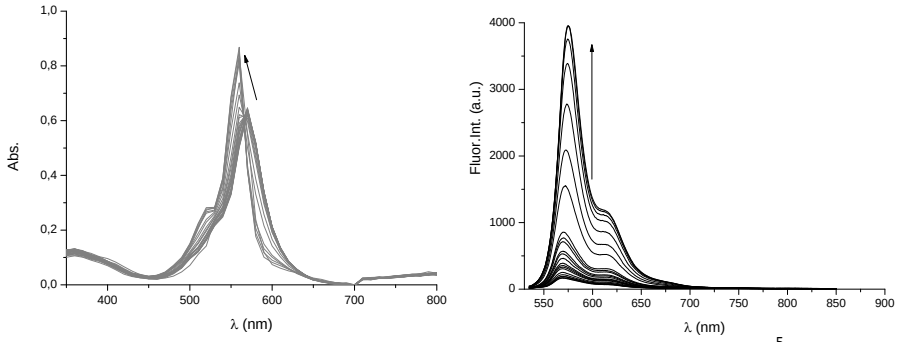

Figure SI-12. Uv-vis (Left) and fluorescence (right) (λ_{ex} = 530 nm) response for **1** (10^{-5} M in CH_3CN) in presence of increasing amount of DCNP.

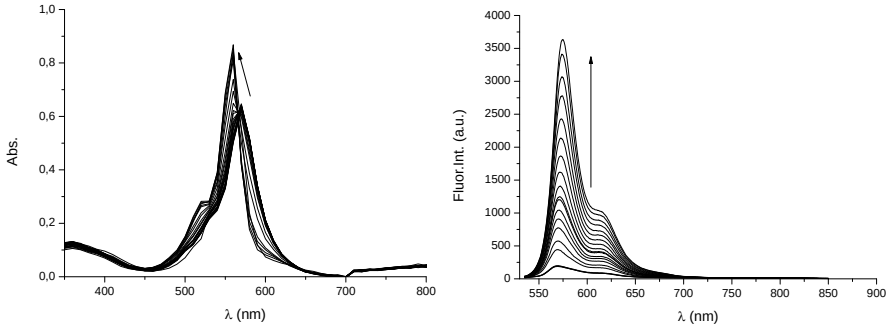

Figure SI-13. Uv-vis (Left) and fluorescence (right) (λ_{ex} = 530 nm) response for **1** (10^{-5} M in CH_3CN) in presence of increasing amount of DFP.

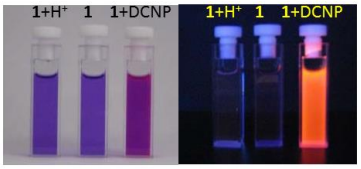

Figure SI-14. Visual changes observed for **1** in the presence of acid or DCNP; under day-light (left hand panel) and under irradiation at 254 nm (right hand panel).

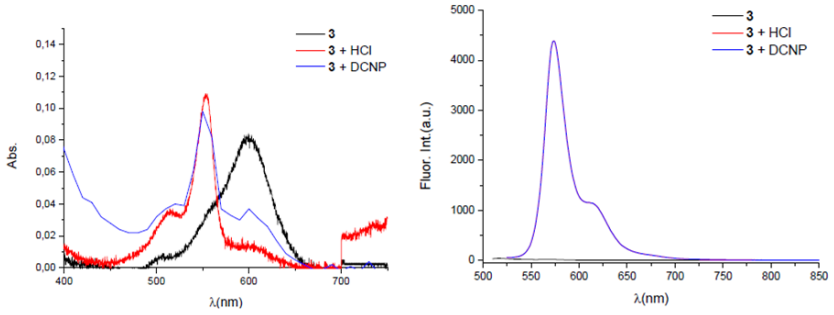

Figure SI-15. Absorption (left hand panel) and fluorescence (right hand panel) spectra (λ_{ex} = 520 nm) recorded for **3** (10^{-5} M in CH_3CN) alone and in presence of acid and DCNP.

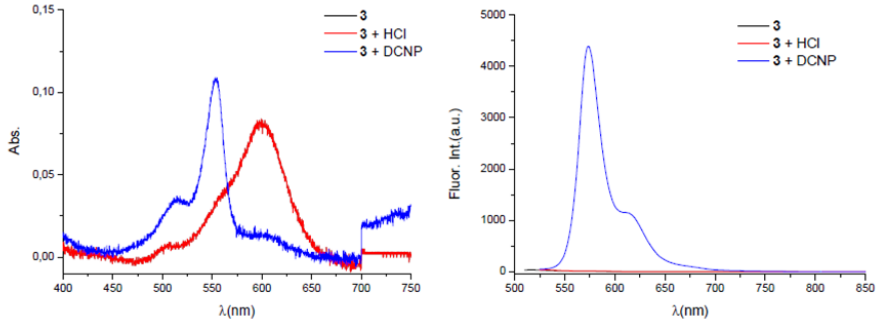

Figure SI-16. Absorption (left hand panel) and fluorescence (right hand panel) spectra (λ_{ex} = 520 nm) recorded for **3** (10^{-5} M in CH_3CN: MOPS (1:3); pH = 7.01) alone and in presence of acid and DCNP.

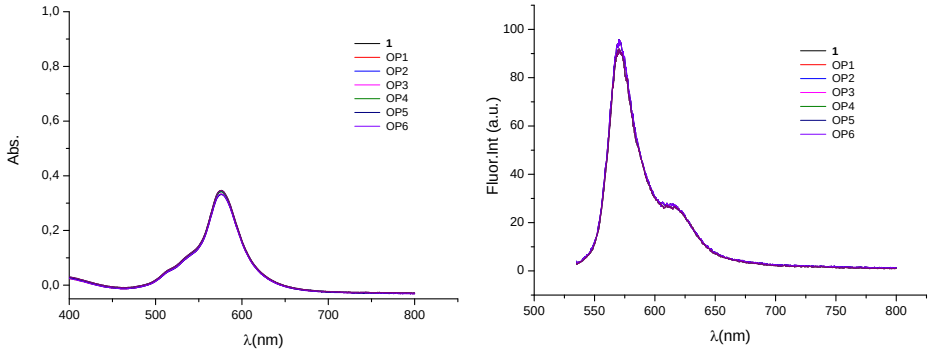

Figure SI-17. (left) Uv-vis and (Right) Fluorescence spectra (λ_{ex} = 530 nm) of **1** (10^{-5} M in CH_3CN) alone and in presence of interferents (OP1-OP6).

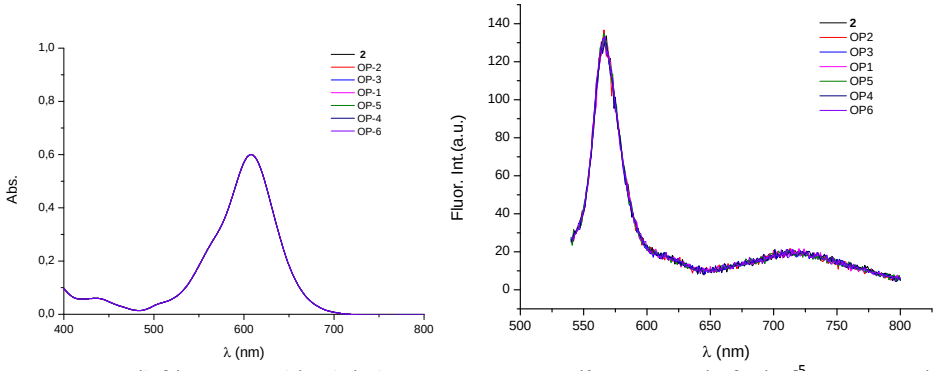

Figure SI-18. (left) Uv-vis and (Right) Fluorescence spectra (λ_{ex} = 530 nm) of **2** (10^{-5} M in CH_3CN) alone and in presence of interferents (OP1-OP6).

4.5 Selective chromo-fluorogenic detection of DFP (a Sarin and Soman mimic) and DCNP (a Tabun mimic) with a unique probe based on a boron dipyrromethene (BODIPY) dye.

Selective chromo-fluorogenic detection of DFP (a Sarin and Soman mimic) and DCNP (a Tabun mimic) with a unique probe based on a boron dipyrromethene (BODIPY) dye.

Andrea Barba-Bon, [ab] *Ana M.Costero,* [ab] *Salvador Gil,* [ab] Ramón Martínez-Máñez, [acd] *and Felix Sancenón* [acd]

[a] *Centro de Reconocimiento Molecular y Desarrollo Tecnológico (IDM). Unidad Mixta Universidad de Valencia-Universidad Politécnica de Valencia, Spain.*
[b] *Departamento de Química Orgánica. Universidad de Valencia, Doctor Moliner 50, 46100, Burjassot, Valencia, Spain.*
[c] *Departamento de Química. Universidad Politécnica de Valencia, Camino de Vera s/n, 46022, Valencia, Spain.*
[d] *CIBER de Bioingeniería Biomateriales y Nanomedicina (CIBER-BBN).*

Received: *23rd June 2014*
Published online: *13th September 2014*

Org. Biomol. Chem., **2014**, *12*, 8745-8751.

A novel colorimetric probe (**P4**) for the selective differential detection of DFP (a Sarin and Soman mimic) and DCNP (a Tabun mimic) was prepared. Probe **P4** contains three reactive sites; i.e. (i) a nucleophilic phenol group able to undergo phosphorylation with nerve gases, (ii) a carbonyl group as a reactive site for cyanide; and (iii) a triisopropylsilyl (TIPS) protecting group that is known to react with fluoride. The reaction of **P4** with DCNP in acetonitrile resulted in both the phosphorylation of the phenoxy group and the release of cyanide, which was able to react with the carbonyl group of **P4** to produce a colour modulation from pink to orange. In contrast, phosphorylation of **P4** with DFP in acetonitrile released fluoride that hydrolysed the TIPS group in **P4** to yield a colour change from pink to blue. Probe **P4** was able to discriminate between DFP and DCNP with remarkable sensitivity; limits of detection of 0.36 and 0.40 ppm for DCNP and DFP, respectively, were calculated. Besides, no interference from other organophosphorus derivatives or with presence of acid was observed. Besides, the sensing behaviour of **P4** was retained when incorporated into silica gel plates or onto polyethylene oxide membranes, which allowed the development of simple test strips for the colorimetric detection of DCNP and DFP in the vapour phase. **P4** is the first probe capable of colorimetrically differentiating between a Tabun mimic (DCNP) and a Sarin and Soman mimic (DFP).

Introduction

Nerve agents are an extremely toxic class of organophosphorus compounds that are included in the group of chemical warfare agents. Nerve agents are especially dangerous because they are able to interfere with nervous system action through their reactivity with esterase enzymes in general, and with acetylcholinesterase (AChE) in particular. Nerve agents phosphorylate the serine hydroxyl group at the active site of AChE, [1] which is also involved in the binding of acetylcholine (the natural enzyme substrate). However, the interaction of the nerve agent with AChE is stronger than that with acetylcholine, and the entire process results in acetylcholine accumulation,

which produces neuromuscular paralysis and eventually death.[2]

Given their easy production, extreme toxicity and possible use by military regimes and terrorist attacks, intense research efforts have been directed to develop sensitive and selective protocols to detect nerve gases. Several remarkable methodologies have been proposed, including the use of enzymatic assays,[3] ion mobility spectroscopy,[4] lanthanide luminescence,[5] electrochemistry,[6] photonic crystals,[7] micro-cantilevers,[8] optical-fibre arrays,[9] and nanomaterials such as nanotubes or nanowires.[10] These protocols usually contain at least one of the following limitations: low response, lack of specificity, limited selectivity, poor sensitivity, operation complexity, non-portability, difficulties in real-time monitoring and false-positive readings.

As an alternative to these procedures, the development of chromogenic and fluorogenic probes has recently gained increasing interest.[11] Colorimetric detection is particularly appealing as it is low-cost and offers the possibility of detecting analytes *at site* and to the "naked-eye". In these studies, nerve gas simulants such as diethylcyanophosphate (DCNP) and diisopropylfluorophosphate (DFP), are habitually used (see Scheme 1). These compounds show similar reactivity to real nerve agents Sarin, Soman and Tabun, but lack their severe toxicity (see Scheme 1).

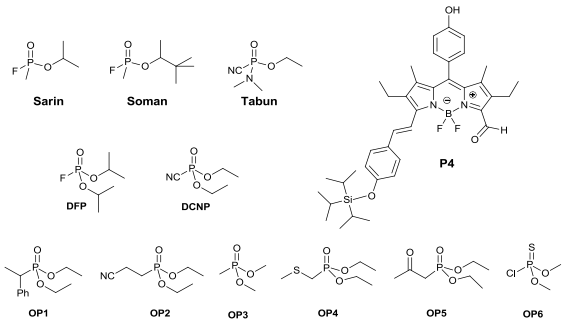

Scheme 1. Chemical structures of nerve agents (Sarin, Soman and Tabun), their simulants (DFP and DCNP), selected organophosphates (OP1-OP6) and probe **P4**.

Most reported chromo-fluorogenic probes rely on the electrophilic reactivity of nerve gases and their binding to suitable nucleophiles. However some have

certain shortcomings, e.g., detection in solution, but not in the gas phase, as well as serious interference from acids. The reactions used in these probes are non-specific and the reported dye-based probes usually display the same optical response to all nerve gases and are unable to determine the specific identity of the nerve agent. Individual detection of Sarin, Soman or Tabun is proving important; for instance, poisonings with nerve agents are typically treated by administering atropine and certain oximes.[1c] Atropine antagonises the action of acetylcholine at muscarinic receptors, while oximes reactivate inhibited AChE by cleaving the ester formed by nerve gases with the serine hydroxyl group. There is some experimental evidence which indicates that some oximes are ineffective for certain nerve agents, which suggests the importance of distinguishing certain agents within this family of lethal chemicals for appropriate antidote use upon exposure to nerve agents.[12] Very few examples display the specific detection of one of the agents.[13] Idded there are certain probes capable of selectively detecting the Tabun mimic DCNP and the Sarin and Soman mimic DFP. As far as we know, there are no reported examples able to distinguish one from the other using a unique probe.

After taking the above concept into account and following our interest in developing probes for the selective detection of nerve agents[11a,13,14] we report herein a simple molecule (**P4**, see Scheme 1) that has been designed to respond differentially to Tabun and Sarin/Soman, in addition to being insensitive to acid interference.[14c] A clear colour modulation was observed in both solution and the gas phase.

Results and discussion

Probe design

A typical chromo- and/or fluorogenic probe combines a selective analyte recognition site with a colorimetric/fluorescent reporter, which translates the binding event into a colour/fluorescence output signal. As a chromo-fluorogenic reporter, in this study we selected a boron dipyrromethene

(BODIPY) core for its robustness against light and chemicals, good solubility, resistance to self-aggregation in solution, excitation/emission wavelengths in the visible spectral region (≥ 500 nm), and its usually high molar absorption coefficients and fluorescence quantum yields.[15] The BODIPY core in probe **P4** was also equipped with three reactive sites; i.e. (i) a nucleophilic phenol group (in the *meso*-position), able to react with electrophilic phosphorus atoms, such as those in nerve agents; (ii) a carbonyl group, which is a reactive site for cyanide (a specific by-product of Tabun);[16] (iii) a triisopropylsilyl (TIPS) protecting group, known to react with fluoride[17] (a specific by-product of Sarin and Soman). Moreover, all these reactions were expected to occur with significant colour and fluorescence modulation. In addition, BODIPY derivatives **P1, P2** and **P3**, lacking some of those reactive sites, were also prepared and used in the control experiments (see Scheme 2).

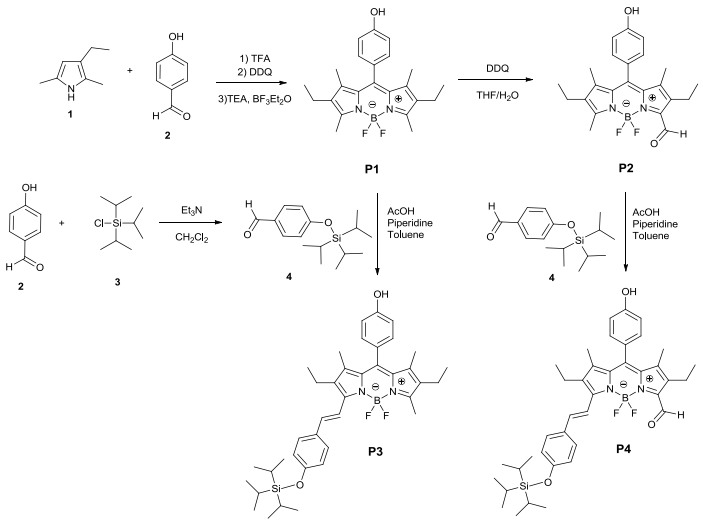

Scheme 2. Synthesis of probe **P4** and compounds **P1**, **P2** and **P3**.

Synthesis and spectroscopic characterisation of the probe

Probe **P4** was prepared following the pathway described in Scheme 2. Firstly, compound **P1** was synthesized according to published procedures[18] by the condensation of 3-ethyl-2,4-dimethylpyrrole (**1**) with 4-hydroxybenzaldehyde

(**2**) in the presence of trifluoroacetic acid (TFA) as a catalyst, followed by oxidation with 2,3-dichloro-5,6-dicyano-p-benzoquinone (DDQ). The boron difluoride bridging unit was introduced by treatment with boron trifluoride diethyl etherate in the presence of triethylamine. The selective DDQ oxidation of the methyl group at position 3 of compound **P1** was used to confer the corresponding aldehyde **P2**.[19] Compounds **P3** and **P4** were synthesized using a Knoevenagel-type[15b] reaction between **P1** or **P2** with aldehyde **4** in the presence of acetic acid and piperidine.[17]

In a first step, the spectroscopic behaviour of probe **P4** was studied. Figure 1 shows the absorption and fluorescence spectra for **P4** in acetonitrile. The absorption profile of this derivative was reminiscent of those reported for several related BODIPY dyes,[20,21] with an intense transition at 591 nm (log ε = 4.92) and a shoulder on the short wavelength side (*ca.* 550 nm). The electronic absorption maxima at 591 nm can be attributed to the 0-0 band of a strong S_0-S_1 transition, while the second maximum or shoulder at higher energy can be attributed to the 0-1 vibrational transition. The fluorescence spectrum of **P4** displayed a small Stokes shift with good mirror symmetry (λ_{ex} = 555 nm, λ_{em} = 625 nm, ϕ = 0.52), similarly to other BODIPY dyes.[20,21] The spectroscopic characteristics of compounds **P1**-**P3** were also studied and are detailed in the Supporting Information.

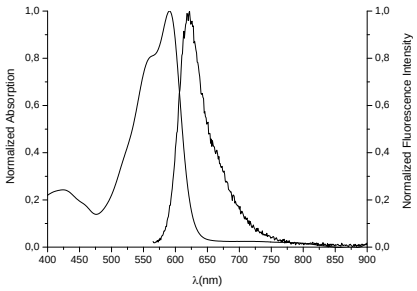

Figure 1. Normalised absorption and fluorescence (λ_{ex} = 555 nm) spectra of probe **P4** in acetonitrile (c = 1.0 x 10^{-5} mol dm^{-3}).

Chromo-fluorogenic response against nerve agent mimics

The chromogenic behaviour of the acetonitrile solutions of probe **P4** was

tested in the presence of DFP and DCNP (see Figure 2). Addition of DCNP to **P4** induced a marked decrease in the band centred at 591 nm, and the appearance of new bands at 515 and 560 nm concomitantly with a clear colour change from bright pink to orange (see the inset in Figure 2). In contrast, a very different chromogenic response was observed when DFP reacted with **P4**. In this case, a major bathochromic shift of the visible absorption band of **P4** from 590 to 715 nm was observed. This bathochromic shift was reflected in a colour modulation from bright pink to light blue (see the inset in Figure 2).

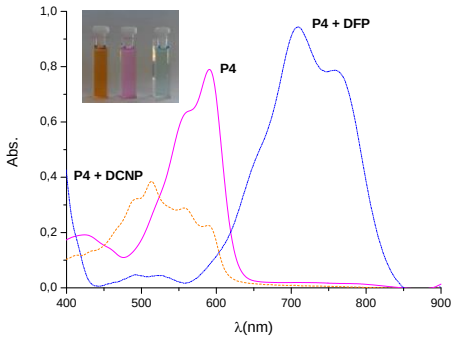

Figure 2. Visible spectra of **P4** in acetonitrile (1.0 x 10^{-5} mol dm^{-3}) alone and in the presence of 1 eq. of DFP and DCNP. The inset shows the colour changes observed, from left to right: **P4**+DCNP, **P4** and **P4**+DFP.

The different chromogenic response observed upon the addition of DCNP and DFP to **P4** was related with the release of CN^- and F^- anions upon the phosphorylation of the phenol moiety of **P4**. Cyanide (the unique by-product from the Tabun simulant DCNP) reacted with the carbonyl group at the 3-position of the BODIPY core of **P4** to yield an electron-rich cyanohydrin (see Scheme 3) moiety. Fluoride (the unique by-product from the Sarin and Soman simulant DFP) also induced the hydrolysis of the TIPS-protective group. The deprotection reaction generated a strong intramolecular charge transfer (ICT) donor phenoxide ion in full conjugation with the BODIPY core, which would reduce the energy gap for the S_0-S_1 transition, and thus resulted in a large red shift in absorbance.

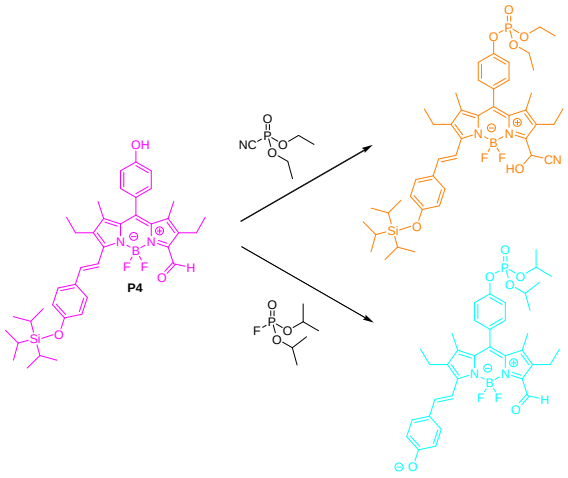

Scheme 3. Mechanism for the chromogenic response observed for probe **P4** in the presence of DCNP and DFP.

This mechanism was confirmed with the experiments carried out with control compounds **P1**, **P2** and **P3**. The addition of both simulants to **P1** induced negligible changes in the UV-visible spectrum. This behavior was expected as the unique phosphorylation of the nucleophilic phenol group was not anticipated to induce colour variations. For **P2**, only the addition of DCNP induced a hypsochromic shift of the absorption band from 517 nm to 489.7 nm (due to phosphorylation and the further cyanide addition to the carbonyl). With **P3,** only DFP was able to yield a bathochromic shift of the visible band from 580 to 703 nm (due to phosphorylation and the further fluoride-induced hydrolysis of the TIPS protecting group). See Supporting Information for additional details.

Excitation of the acetonitrile solutions of **P4** at 555 nm induced emission at 625 nm (quantum yield of 0.52) (see Figure 1). Addition of both DCNP and DFP induced emission quenching (see Supporting Information) due to the phosphorylation of the nucleophilic phenol group (at the *meso*-position) of **P4** and the subsequent generation of electron donor moieties (a cyanohydrin with DCNP and a phenolate anion when DFP was added). Moreover, the photophysical parameters of probes **P1**-**P4** in other solvents other than acetonitrile in the presence and absence of DCNP and DFP are also found in the Supporting Information.

Other titration experiments of **P4** with DCNP and DFP allowed us to calculate the corresponding limits of detection (LOD) using the equation: LOD = *K* x Sb_1/S, where K = 3, Sb_1 is the standard deviation of the blank solution, and S is the slope of the calibration curve.[22] Lower LOD values were found for DCNP than for DFP, which is in agreement with the trend observed using other chromogenic reagents (see Table 1).[13,23]

Table 1. Limits of detection for DCNP and DFP using probe **P4**.

Simulant	UV-visible (ppm)	Fluorescence (ppm)
DCNP	0.91	0.36
DFP	0.95	0.40

One fundamental study into the development of probes for nerve agents is the role played by the possible interferents or false-positive outcomes produced by other species. Bearing this concept in mind, the reactivity of probe **P4** with other organo-phosphorus compounds (OP1-OP6 in Scheme 1) and an acid medium was also studied under comparable conditions. Nevertheless, it was not possible to detect a change in absorption or in the fluorescence profiles of the probe (see Supporting Information). Such behavior indicates that there was no reaction between **P4** and these particular phosphate derivatives and acids, thus rendering **P4** a suitable selective probe for the detection of nerve gases.

Encouraged by the selective response observed with **P4**, and in order to extend its applicability to real-time monitoring, we decided to take another step. In this context, two different test strips were developed for the colorimetric detection in both solution and the gas phase of the nerve agent mimics. To this end, hydrophobic polyethylene oxide films and silica gel plates containing probe **P4** were prepared (see Experimental Section for details).

In a typical assay, films or plates were placed into a container holding the nerve agent simulant (30 ppm introduced as an aerosol). Alternatively, strips were exposed to acetonitrile solutions containing DCNP or DFP (10 ppm). Similar chromogenic behaviour was noted in both the solution and the gas

phase (see Figure 3). As seen, a colour modulation from purple to orange (in the presence of DCNP) and to light blue (when DFP was present) was observed. Limits of detection in the gas phase assays were determined, being lower for the polyethylene oxide membranes (1.61 ppm and 1.12 ppm for DCNP and DFP respectively) than for silica gel plates (2.57 ppm and 3.36 ppm for DCNP and DFP respectively).

To complete the study, the strips containing **P4** were introduced into a container with the saturated vapours of organo-phosphorus derivatives (OP1-OP6) and acid medium for 24 h. However, no change in the colour of the strips was observed.

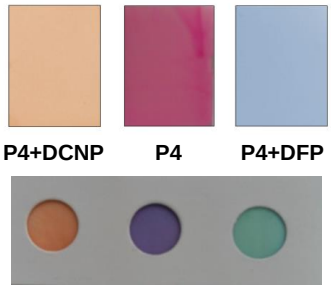

Figure 3. Silica gel plate (up) and polyethylene oxide membrane (down) of **P4** in the presence of the DCNP and DFP vapours (30 ppm).

Conclusions

We report herein a simple probe (**P4**) based on a BODIPY derivative which is able to colorimetrically distinguish the presence of the Tabun mimic DCNP from the Sarin and Soman mimic DFP. In particular, the reaction of probe **P4** with DCNP or DFP resulted in the phosphorylation of the phenoxy group, with the subsequent release of a fluoride (for DFP) or cyanide (for DCNP) anion. In the presence of DCNP, further cyanide nucleophilic addition of the probe to the carbonyl group resulted in a hypsochromic shift of the absorption band concomitantly with a colour change from pink to orange. In contrast when DFP was used, the released fluoride anion was able to hydrolyse the TIPS group of the probe to yield a highly coloured phenoxide anion with a charge transfer band located in the NIR region. Probe **P4** was highly selective and allowed

discrimination between DFP and DCNP with remarkable sensitivity.The signalling abilities of **P4** were also retained when incorporated into silica gel plates or onto polyethylene oxide membranes, which allowed the development of simple test strips for the colorimetric detection of DCNP and DFP in the liquid or the vapour phase. To the best of our knowledge, **P4** is the first reported probe capable of showing a different colour change in the presence of the Tabun mimic DCNP and the Sarin and Soman mimic DFP. We believe that this, or similar probes, may open up new routes to help design highly selective kits for "in-the-field" real-time monitoring applications of nerve gases with operational simplicity.

Experimental section

General remarks

CH_2Cl_2 and CH_3CN were distilled from P_2O_5 under Ar prior to use. Benzene and toluene were distilled from CaH_2 under Ar prior to use. THF was distilled from Na/benzophenone under Ar prior to use. All the other solvents and starting materials were purchased from commercial sources where available, and were used without purification. Silica gel 60 F254 (Merck) plates were used for TLC. Column chromatography was performed on silica gel (60, 40-63 μm). ^1H NMR (300 MHz), ^{13}C NMR spectra were determined in a Bruker AV 300 spectrometer. Chemical shifts are reported in parts per million (ppm), calibrated to the solvent peak set. High-resolution mass spectra were recorded in the positive ion mode with a VG-AutoSpec mass spectrometer.

Synthesis of P1

3-Ethyl-2,4-Dimethylpyrrole (**1**, 2 mL, 14.8 mmol) and 4-hydroxybenzaldehyde (**2**, 0.86 g, 7.06 mmol) were dissolved in anhydrous CH_2Cl_2 (150 mL). Trifluoroacetic acid (27 μL, 0.35 mmol) was added and the solution was stirred at room temperature for 50 min. A solution of DDQ (2,3-dichloro-5,6-dicyano-p-benzoquinone, 1.6 g, 7.06 mmol) in CH_2Cl_2 was added. Stirring was

continued for 50 min, followed by the addition of triethylamine (16 mL). After stirring for 30 min, $BF_3.OEt_2$ (16 mL) was added. The mixture was stirred for 4 h at room temperature. After evaporating solvents under reduced pressure, the crude product was purified by silica gel column chromatography with AcOEt/hexane (1:2) to give **P1** (778 mg) as red crystals in a 28% yield. ^{1}H NMR (300 MHz, $CDCl_3$) δ 7.11 (dd, *J* = 8.8 Hz and 2.3 Hz, 2H), 6.93 (dd, *J* = 8.8 Hz and 2.3 Hz, 2H), 2.51 (s, 6H), 2.29 (q, *J* = 7.6 Hz, 4H), 1.35 (s, 6H), 0.98 (t, *J* = 7.6 Hz, 6H).^{13}C NMR (75 MHz, $CDCl_3$) δ 156.17, 153.54, 140.20, 138.48, 132.71,131.17, 129.64, 127.9, 115.62, 17.07,14.62,12,49, 11.85. HRMS (EI): m/z (%) calc for $C_{23}H_{28}BF_2N_2O$: 397.2263 $[M+1]^+$ found: 397.2251. UV-Vis (CH_3CN λ_{max}/nm) 520.0; emission (CH_3CN λ_{max}/nm) 535.9.

Synthesis of P2

To a degassed solution of **P1** (200 mg, 0.50 mmol) in THF/H_2O (15/0.15 mL), a solution of DDQ (553 mg, 1.99 mmol) in THF (6 mL) was added drop-wise at 0°C. The reaction mixture was stirred from 0^{o}C to room temperature overnight. The reaction mixture was concentrated under reduced pressure and then subjected to silica gel column chromatography with AcOEt/hexane (1:3) to give **P2** (126 mg) as orange crystals in a 60.8% yield. ^{1}H NMR (300 MHz, $CDCl_3$) δ 10.37 (s, 1H) 7.11 (dd, *J* = 8.7 Hz and 2.3 Hz, 2H), 7.01 (dd, *J* = 8.7 Hz and 2.3 Hz, 2H),2.71 (q, *J* = 7.4 Hz,2H) 2.64 (s, 3H), 2.36 (q, *J* = 7.4 Hz, 2H), 1.45 (s, 3H), 1.36(s, 3H), 1.03(s, 3H).^{13}C NMR (75 MHz, $CDCl_3$) δ 187.71, 166.65, 157.86, 144.58, 142.83, 139.85, 138.10, 137.81, 136.72, 134.84, 133.41, 129.63, 126.56, 116.90, 18.05, 17.51, 14.74, 14.47, 14.08, 12.96, 11.08. HRMS (EI): m/z (%) calc for $C_{23}H_{26}BF_2N_2O_2$: 411.2055 $[M+1]^+$ found: 411.2058. UV-Vis (CH_3CN λ_{max}/nm) 517.0; emission (CH_3CN λ_{max}/nm) 545.0.

Synthesis of 4

Triisopropylsilyl chloride (**3**, 5.8 mL, 27.06 mmol) was added to a heterogeneous mixture of 4-hydroxybenzaldehyde (**2**, 3 g, 24.6 mmol) and triethylamine (6.9 mL, 49.2 mmol) in CH_2Cl_2 (100 mL) at room temperature. After stirring for 1 h, the yellow solution was quenched by methanol and

stirred for another 10-minute period. The reaction mixture was diluted with CH_2Cl_2 and washed with water and brine, and was dried ($MgSO_4$) and concentrated under reduced pressure to yield **5** (6.22 g, 91 %) as a light orange oil. ^{1}H NMR (300 MHz, $CDCl_3$) δ 9.83 (s, 1H), 7.73(d, *J* = 8.2 Hz ,2H), 6.92 (d, *J* = 8.2 Hz ,2H) , 1,23 (m, 3H), 1.07 (m, 9H), 1.04 (m, 9H).^{13}C NMR (75 MHz, $CDCl_3$) δ190.87, 131.40, 120.60, 18.16,12.78. HRMS (EI): m/z (%) calc for $C_{16}H_{27}O_2Si$: 279.1780 $[M+1]^+$ found: 279.1774.

Synthesis of P3

P1 (200 mg, 0.51 mmol) and aldehyde **4** (170 mg, 0.61 mmol) were dissolved in a mixture of toluene (140 mL), acetic acid (700 µL) and piperidine (700 µL). Any water formed during the reaction was removed azeotropically by heating in a Dean-Stark apparatus for 15 h. The reaction mixture was concentrated under reduced pressure and then subjected to silica gel column chromatography with AcOEt/hexane (1:2) to yield **P3** (10 mg) as purple crystals in a 30% yield**.** ^{1}H NMR (300 MHz, $CDCl_3$) δ 7.59 (d, *J* = 16.8 Hz, 1H), 7.48 (d, *J* = 8.5 Hz, 2H), 7.14 (d, *J* = 8.5 Hz, 2H), 6.96 (m, 2H), 6.83 (d, *J* = 8.5 Hz, 2H), 6.77 (d, J = 16.8 Hz, 1H),2.76 (m,2H), 2.69 (m, 2H), 2.21 (s, 3H), 2.09 (s, 3H), 1.50 (s, 3H), 1.40 (s, 3H), 1.29(s, 3H), 1.22(m, 3H), 1.18(s, 9H), 1.16(s, 9H). ^{13}C NMR (75 MHz, $CDCl_3$) δ 156.20, 139.24,133.48, 132.82, 132.25, 132.13, 130.43, 129.95, 129.86, 129.75, 128.91, 128.77,128.18, 120.90, 120.10, 118.00, 116.07, 115.72, 115.58, 24.75, 22.70, 18.32, 17.91, 17.12, 14.57, 14.12, 12.65, 11.95, 11.61. HRMS (EI): m/z (%) calc for $C_{39}H_{52}BF_2N_2O_2Si$**:** 657.3859 $[M+1]^+$ found: 657.7277 UV-Vis (CH_3CN λ_{max}/nm) 580.0; emission (CH_3CN λ_{max}/nm) 600.2.

Synthesis of P4

In a 250 mL round-bottomed flask equipped with a Dean-Stark trap and a reflux condenser, aldehyde **4** (163 mg, 0.58 mmol) was dissolved in benzene (50 mL), acetic acid (400 µL) and piperidine (400 µL). The reaction mixture was stirred at reflux temperature and then a solution of **P2** (120 mg, 0.29 mmol) in benzene (40 mL) was added drop-wise. Any water formed during the reaction

was removed azeotropically by heating in a Dean-Stark apparatus for 1 h. The reaction mixture was concentrated under reduced pressure and then subjected to silica gel column chromatography with AcOEt/hexane (1:2) to yield **P4** (40 mg) as dark purple crystals in a 20% yield**.** ^{1}H NMR (300 MHz, $CDCl_3$) δ 10.46 (s, 1H), 7.69 (d, *J*=16.5 Hz, 1H), 7.55 (dd, *J* = 8.7 Hz and 3.3 Hz, 2H), 7.50 (d, *J*=16.5 Hz, 1H),7.16 (m, 2H), 7.04 (m,2H), 6.92 (dd, *J* = 10.4 Hz and 8.6 Hz, 2H), 2.69 (dq, *J* = 22.6 Hz and 7.5 Hz, 4H), 2.17 (s, 3H), 1.46 (s, 3H), 1.35 (s, 3H), 1.26 (m, 3H), 1.17(s, 3H), 1.14 (m, 18H). ^{13}C NMR (75 MHz, $CDCl_3$) δ 186.01, 158.99, 157.85, 157.14, 156.68, 143.94, 141.25, 139.65, 137.08, 134.24, 133.52, 130.01, 129.77, 129.68, 129.43, 121.20, 120.46, 116.84, 116.30, 115.92, 29.70, 18.49, 17.79, 14.35, 13.69, 12.69, 12.33, 10.77. HRMS (EI): m/z (%) calc for $C_{39}H_{50}BF_2SiN_2O_3$: 671.3652 $[M+1]^+$ found: 671.3643. UV-Vis (CH_3CN λ_{max}/nm) 591.0; emission (CH_3CN λ_{max}/nm) 626.1.

Spectroscopic studies

All the solvents were purchased at spectroscopic grade from Aldrich Chemicals Co., used as received, and were found to be free of fluorescent impurities. Absorption and fluorescence spectra were recorded using a Shimadzu UV-2600 spectrophotometer and a Varian Cary Eclipse spectrofluorimeter, respectively. Fluorescence quantum yields were measured at room temperature in the N_2-purgued solution in relation to rhodamine B (ϕ_{EtOH} = 0.49)[24] at 525 nm for **P1** and **P2**; and rhodamine 101 + 0.01% HCl (ϕ_{EtOH} = 1.0)[25] at 554 nm for **P3** and **P4** as standards. The fluorescence quantum yields were calculated from Eq. (1).[26] Here, F denotes the integral of the corrected fluorescence spectrum, A is the absorbance at the excitation wavelength, and n is the refractive index of the medium.

$$\phi_{exp} = \phi_{ref}\frac{F\{1-exp(-A_{ref}ln10)\}n^2}{F_{ref}\{1-exp(-A\,ln10)\}n_{ref}^2} \quad (1)$$

Limits of detection measurements

Increasing quantities of the nerve agent mimics (DFP or DCNP) dissolved in acetonitrile were progressively added to a solution of **P4** (1.0×10^{-5} mol dm^{-3}) in the same solvent. The UV-visible and fluorescence spectra were recorded in

1-cm path length cells at 25°C. Representation of Δ of absorbance or fluorescence at the appropriate wavelength vs. concentration of simulant allowed the limit of detection to be calculated.

Silica gel plates preparation

The strip was prepared by immersing the silica gel plate into an acetonitrile solution of **P4** (1.0×10^{-3} mol dm^{-3}) and then dried in air.

Polymeric membrane preparation

Polyethylene oxide (2 g, Mw 400,000 Dalton) was slowly added to a solution of **P4** (2 mg) in CH_2Cl_2 (40 mL). The mixture was stirred until a highly viscous mixture was formed. This mixture was poured into a glass plate (40 cm^2) and kept in a dry atmosphere for 24 h.

Acknowledgements

We thank the Spanish Government (MAT2012-38429-C04) for support. A.B.B. acknowledges the award of a pre-doctoral FPI fellowship. SCSIE (Universidad de Valencia) is gratefully acknowledged for all the equipment employed.

Notes and references

1 (a) S. M. Somani, *Chemical Warfare Agent*, Academic Press, San Diego**,** 1992; (b) C. H. Gunderson, C. R. Lehmann, F. R. Sidell and B. Jabbari, *Neurology*, 1992, **42**, 946-950.(c) J. A. Vale, P. Rice and T. C. Marrs, *Chemical Warfare Agents: Toxicology and Treatment,* ed. T. C. Marrs, R. L. Maynard and F. R. Sidell, John Wiley & Sons, Chichester, 2007.

2 (a) A. Silver, *The Biology of Cholinesterases*, Elsevier, New York, 1974, 449–488; (b) P. Taylor, in *The Pharmacological Basis of Therapeutics*, 10th. ed. (ed: J. G. Hardman, L. E. Limbird, A. G. Gilman,) McGraw-Hill, New York, 2001, 175–191.

3 (a) A. J. Russell, J. A. Berberich, G. F. Drevon and R. R. Koepsel, *Annu. Rev. Biomed. Eng*., 2003, **5**, 1–27; (b) J. A. Ashley, C. -H. Lin, P. Wirsching and K. D. Janda *Angew. Chem., Int. Ed.*, 1999, **38***,* 1793-1795.

4 E. Steiner, S. J. Klopsch, W. A. English, B. H. Clowers, H. H. Hill, *Anal. Chem*., 2005, **77**, 4792-4796.

5 (a) J. -C. G. Bunzli and C. Piguet, *Chem. Soc. Rev*., 2005, **34**, 1048-1077; (b) B. Zhao, X. Y. Chen, P. Cheng, D. -Z. Liao, S. -P. Yan and Z. H. Jiang, *J. Am. Chem. Soc*., 2004, **126**, 15394-15395.

6 (a) M. A. K. Khan, Y. T. Long, G. Schatte, H. B. Kraatz, *Anal. Chem*. 2007, **79**, 2877-2882; (b) O. V. Shulga, C. Palmer*, Anal. Bioanal. Chem*. 2006, **385**, 1116-1121; (c) G. Liu, Y. Lin, *Anal. Chem*. 2006, **78**, 835-843; (e) K. A. Joshi, M. Prouza, M. Kum, J. Wang, J. Tang, R. Haddon, W. Chen, A. Mulchandani, *Anal. Chem*. 2006, **78**, 331-336; (f) G. Liu, Y. Lin, *Anal. Chem*. 2005, **77**, 5894-5902.

7 (a) W. He, Z. Liu, X. Du, Y. Jiang, D. Xiao, *Talanta*, 2008, **76**, 698-704; (b) J. P. Walker, K. W. Kimble, S. A. Asher, *Anal. Bioanal. Chem*. 2007, **389**, 2115-2118; c) J. P. Walker, S. A. Asher, *Anal. Chem.* 2005, **77**, 1596-1600.

8 (a) G. Zuo, X. Li, P. Li, T. Yang, Y. Wang, Z. Chen, S. Feng, *Anal. Chim. Acta* 2006, **580***,* 123-125; (b) C. Karnati, H. Du, H. F. Ji, X. Xu, Y. Lvov, A. Mulchandani, P. Mulchandani, W. Chen, *Biosens. Bioelectron***.** 2007, **22**, 2636-2640.

9 M. J. Aernecke, D. R. Walt, *Sens. Actuators B* 2009, **142**, 464-473.

10 (a) F. Wang, H. Gu, T. M. Swager, *J Am Chem Soc* 2008, **130**, 5392-5393; (b) S. Claveguera, N. Raoul, A. Carella, M. Delalande, C. Celle, J. –P. Simonato, *Talanta* 2011, **85**, 2542-2545; (c) S. Claveguera, A. Carella, L. Caillier, C. Celle, J. Pécaut, S. Lenfant, D. Vuillaume, J. –P. Simonato, *Angew Chem Int Ed* 2010, **49**, 4063-4066; (e) O. S. Kwon, S. J. Park, J. S. Lee, E. Park, T. Kim, H. –W. Park, S. A. You, H. Yoon, J. Jang, *Nano Lett* 2012, **12**, 2797-2802; (f) L. Wei, D. Shi, P. Ye, Z. Dai, H. Chen, C. Chen, J. Wang, L. Zhang, D. Xu, Z. Wang, Y. Zhang, *Nanotechnology* 2011, **22**, 425501-425507.

11 (a) A. M. Costero, S. Gil, M. Parra, P. M. E. Mancini, R. Martínez-Máñez, F. Sancenón and S. Royo, *Chem. Commun*., 2008, 6002-6004; (b) S. Royo, R. Martínez-Máñez, F. Sancenón A. M. Costero, M. Parra and S. Gil, *Chem. Commun*., 2007, 4839-4847; (c) T. J. Dale and J. Rebek, *Angew. Chem., Int. Ed*., 2009, **48**, 7850-7852; (d) S. Han, Z. Xue, Z. Wang and T. B. Wen*, Chem. Commun.*, 2010, **46**, 8413-8415; (e) L. Ordronneau, A. Carella, M. Pohanka and J. -P. Simonato, *Chem. Commun*, 2013, **49**, 8946-8948; (f) W. -M. Xuan, Y. -T. Cao, J. -H. Zhou and W. Wang, *Chem. Commun*., 2013, **49**, 10474-10476; (g) G. H. Dennison, M. R. Sambrook and M. R. Johnston, *Chem. Commun*, 2014, **50**, 195-197.

12 (a) F. Worek, H. Thiermann, L. Szinicz and P. Eyer, *Biochem. Pharmacol.*, 2004, **68,** 2237-2248. (b) F. Brandhuber, M. Zengerle, L. Porwol, A. Bierwisch, M. Koller, G. Reiter, F. Worek and S. Kubik, *Chem. Commun*, 2013, **49**, 3425-3427.

13 (a) S. Royo, A. M. Costero, M. Parra, S. Gil, R. Martínez-Máñez and F. Sancenón, *Chem. Eur. J*. 2011, **17**, 6931 – 6934; (b) R. Gotor, A. M. Costero, M. Parra, S. Gil, R. Martínez-Máñez and F. Sancenón, *Chem. Eur. J*. 2011, **17**, 11994 – 11997.

14 (a) I. Cadel, A. Bernardos, E. Climent, M.D. Marcos, R. Martínez-Máñez, F. Sancenón, J. Soto, A. Costero, S. Gil, M. Parra, *Chem. Commun*. 2011, **47**, 8313-8315; (b) E. Climent,

A. Martí, S. Royo, R. Martínez-Máñez, M.D. Marcos, F. Sancenón, J. Soto, A.M. Costero, S. Gil, M. Parra, *Angew. Chem. Int. Ed*., 2010, **49**, 5945-5948; (c) A. Barba-Bon, A. M. Costero, S. Gil, A. Harriman and F. Sancenón. DOI: 10.1002/chem.201304475.

15 (a) G. Ulrich, R. Ziessel and A. Harriman*, Angew. Chem., Int. Ed***.,** 2008, **47***,* 1184-1201. (b) N. Boens, V. Leen and W. Dehaen, *Chem. Soc. Rev.*, 2012, **41**, 1130-1172.

16 S. Madhu, S. K. Basu, S Jadhav and M. Ravikanth, *Analyst*, 2013, **138**, 299–306.

17 O. A. Bozdemir, F. Sozmen, O. Buyukcakir, R. Guliyev, Y. Cakmak and E. U. Akkaya, *Org. Lett.*, 2010, **12**, 1400-1403.

18 (a) G. Ulrich and R. Ziessel, *Tetrahedron Lett*., 2004, **45**, 1949–1953; (b) G. Ulrich and R. Ziessel, *J.Org. Chem*., 2004, **69**, 2070-2083.

19 A. Haefele, C. Zedde, P. Retailleau, G. Ulrich and R. Ziessel, *Org. Lett.,* 2010, **12**, 1672-1675.

20 (a) W. Qin, M. Baruah, W. M. De Borggraeve and N. Boens, *J. Photochem. Photobiol. A: Chem*. 2006, **183**, 190-197; (b) X. Peng, J. Du, J. Fan, J. Wang, Y. Wu, J. Zhao, S. Sun and T. Xu, T. *J. Am. Chem. Soc.* 2007, **129**, 1500-1501.

21 (a) Y. Chen, L. Wan, D. Zhang, Y. Bian and J. Jiang, *Photochem. Photobiol. Sci.,* 2011**, 10**, 1030-1038; (b) Z. Yin, A. Yiu-Yan, K. Man-Chung, C. H. Tao, B. Li, C. T. Poon, L. Vivian and W. W. Yam, *Dalton Trans*., 2012, **41**, 11340-11350.

22 M. Zhu, M. Yuan, X. Liu, J. Xu, J. Lv, C. Huang, H. Liu, Y. Li, S. Wang and D. Zhu, *Org. Lett*., 2008, **10**, 1481-1484.

23 S. B. Nagale, T. Sternfeld and D. R. Walt, *J. Am. Chem. Soc.,* 2006, **128**, 5041-5048.

24 K. G. Casey and E. L. Quitevis, *J. Phys. Chem.*, 1988, **92**, 6590-6594.

25 T .Karstens and K. Kobs, *J. Phys. Chem.*, 1980, **84**, 1871-1872.

26 P. Didier, G. Ulrich, Y. M´ely and R. Ziessel, *Org. Biomol. Chem*., 2009, **7**, 3639–3642.

Supporting Information

Selective chromo-fluorogenic detection of DFP (a Sarin and Soman mimic) and DCNP (a Tabun mimic) with a unique probe based on a boron dipyrromethene (BODIPY) dye.

Andrea Barba-Bon, Ana M. Costero, Salvador Gil, Ramón Martínez-Máñez, *and Félix Sancenón*

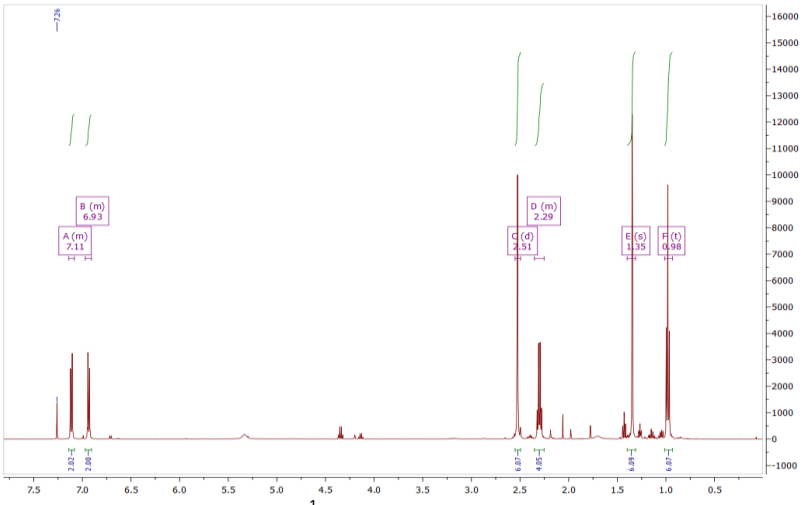

Figure SI- 1. ^{1}H NMR spectrum of **P1** ($CDCl_3$).

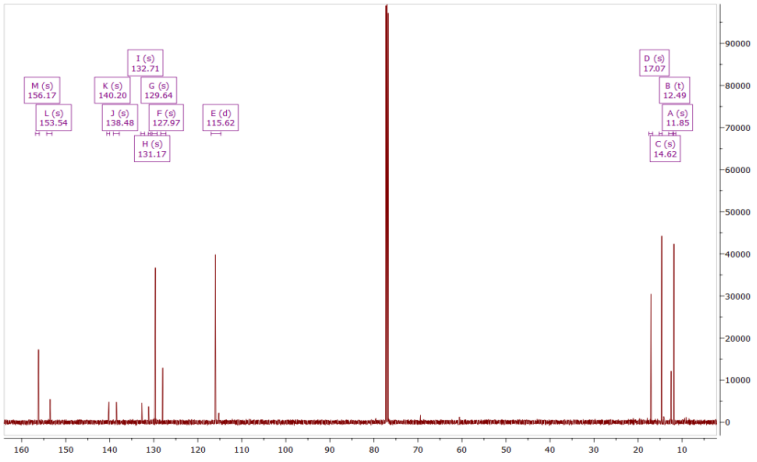

Figure SI- 2. ^{13}C NMR spectrum of **P1** ($CDCl_3$).

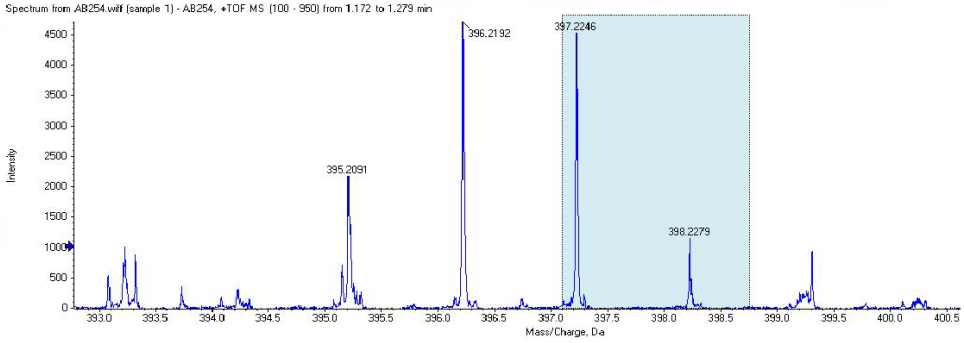

Figure SI- 3. MS of **P1**.

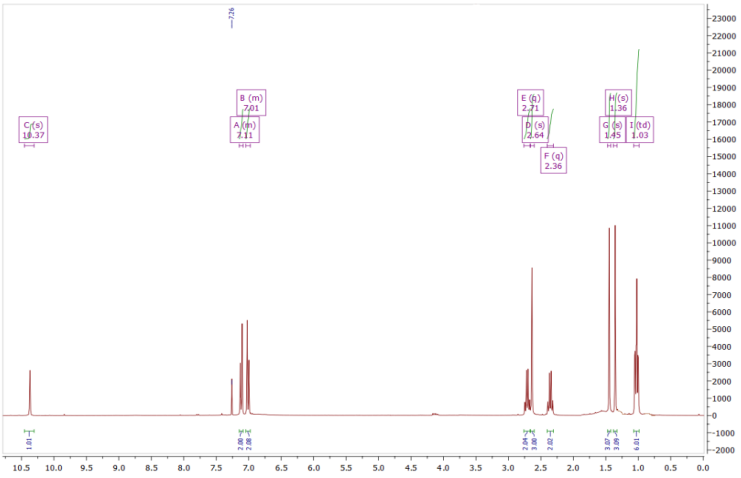

Figure SI-4. ^{1}H NMR spectrum of **P2** ($CDCl_3$).

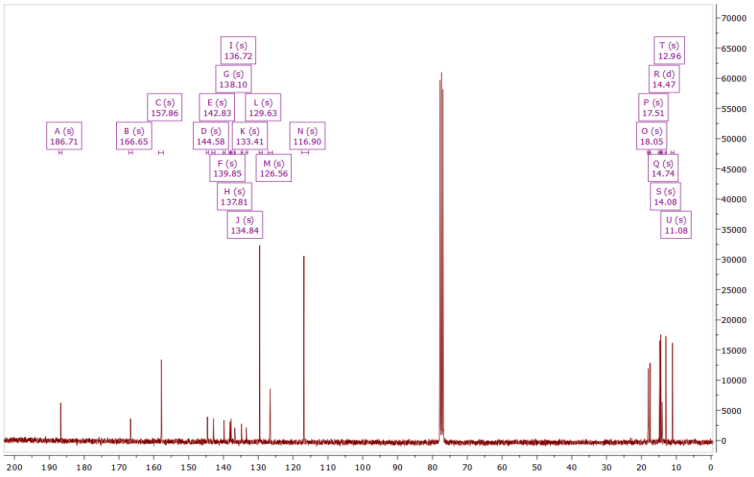

Figure SI- 5. ^{13}C NMR spectrum of **P2** ($CDCl_3$).

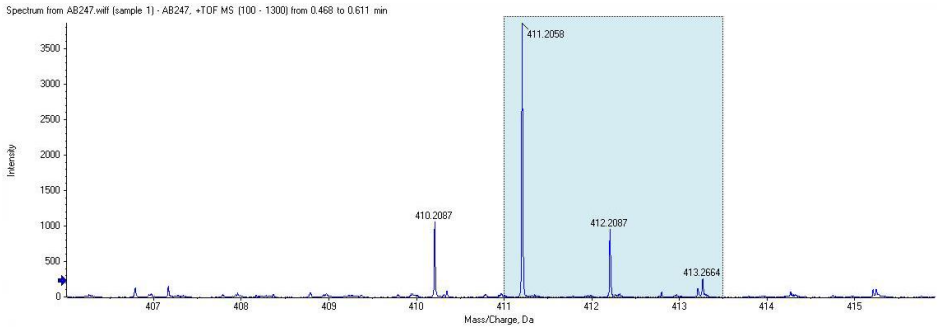

Figure SI-6. MS of **P2**.

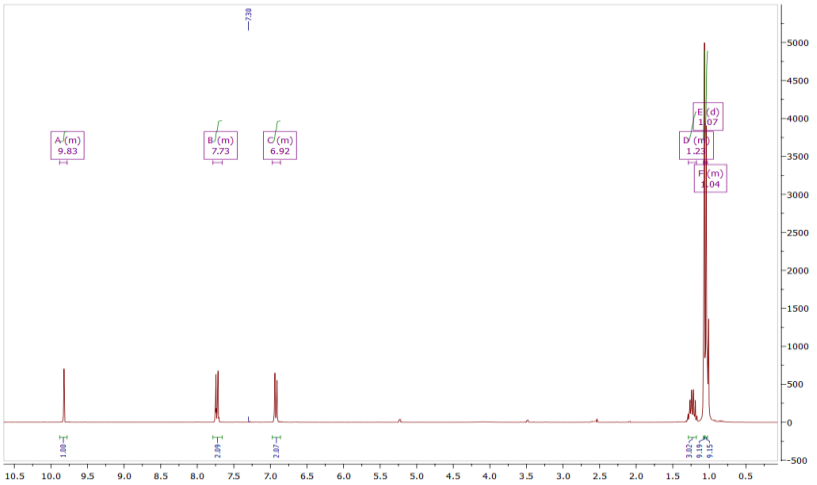

Figure SI- 7. ^{1}H NMR spectrum of aldehyde **4** ($CDCl_3$).

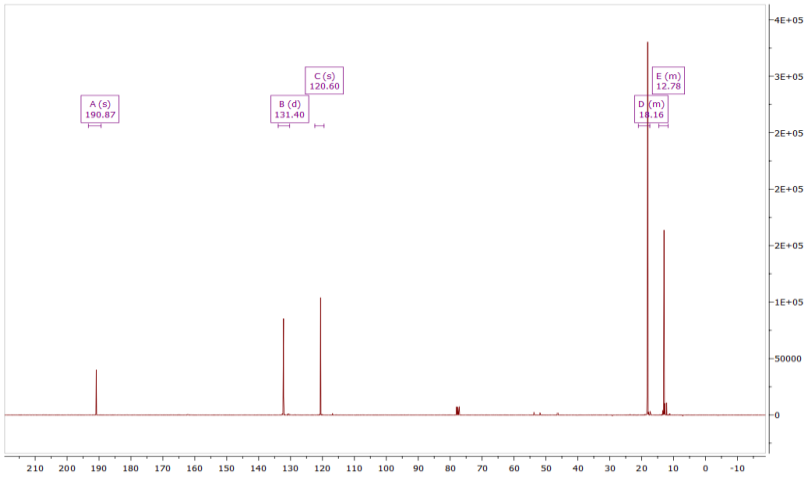

Figure SI-8. ^{13}C NMR spectrum of aldehyde **4** ($CDCl_3$).

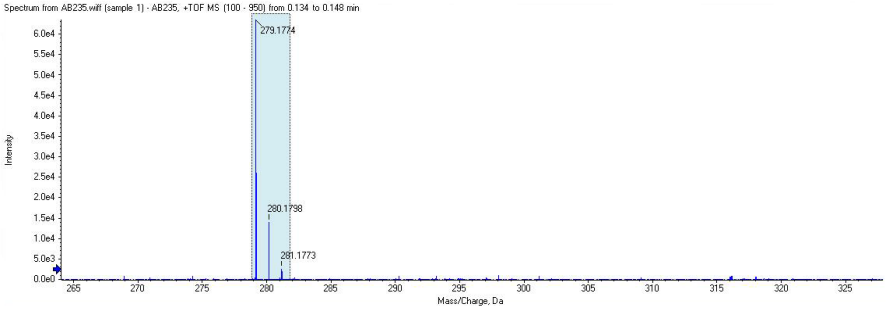

Figure SI- 9. MS of aldehyde **4**.

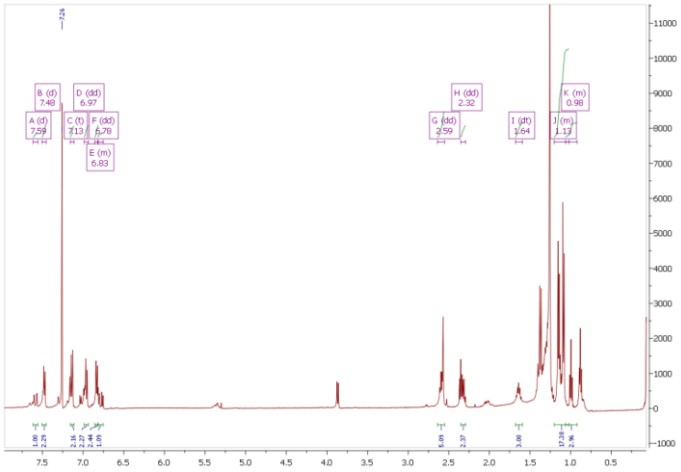

Figure SI-10. ^{1}H NMR spectrum of **P3** ($CDCl_3$).

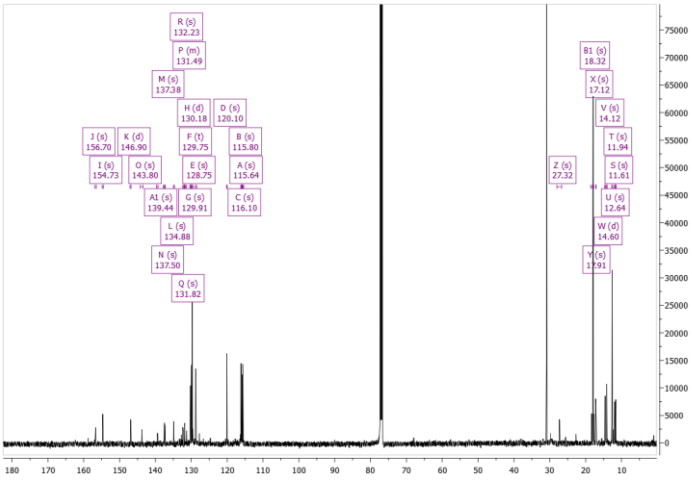

Figure SI-11. ^{13}C NMR spectrum of **P3** ($CDCl_3$).

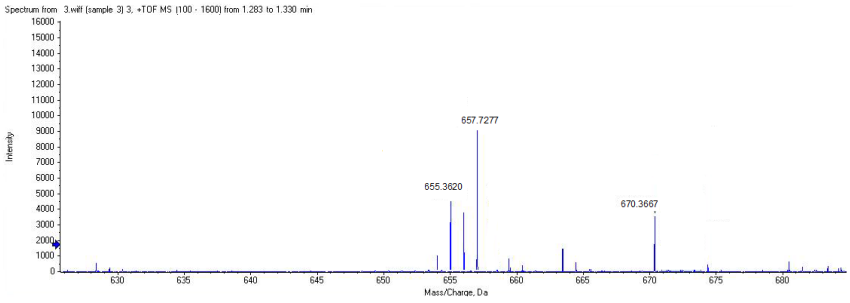

Figure SI-12. MS of **P3**.

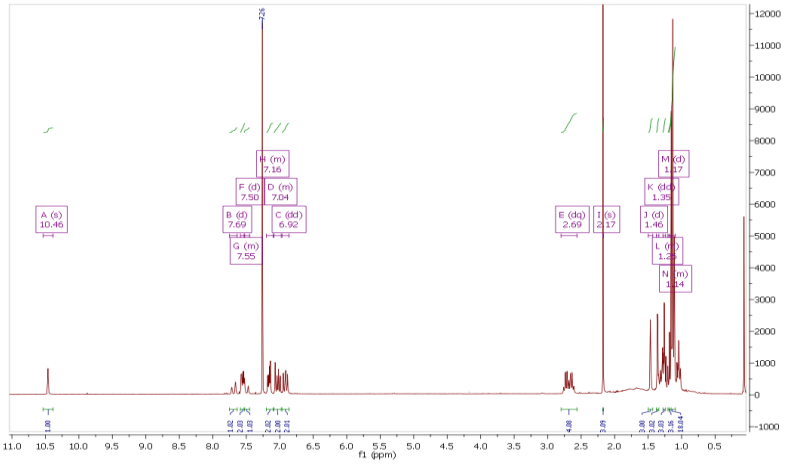

Figure SI-13. ^{1}H NMR spectrum of **P4** ($CDCl_3$).

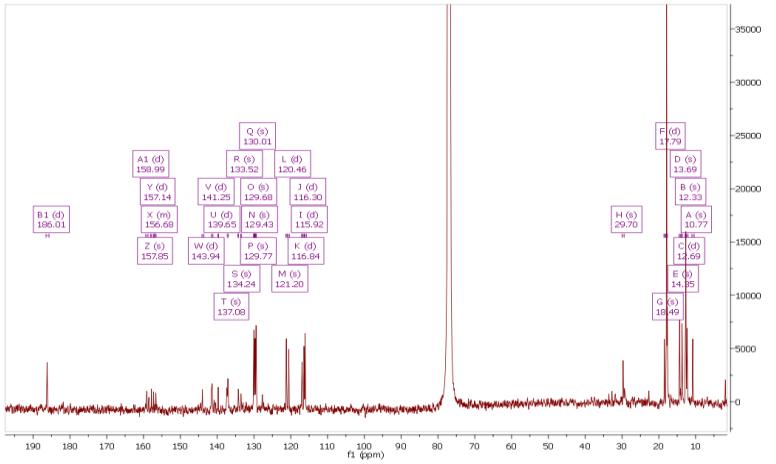

Figure SI-14. ^{13}C NMR spectrum of **P4** ($CDCl_3$).

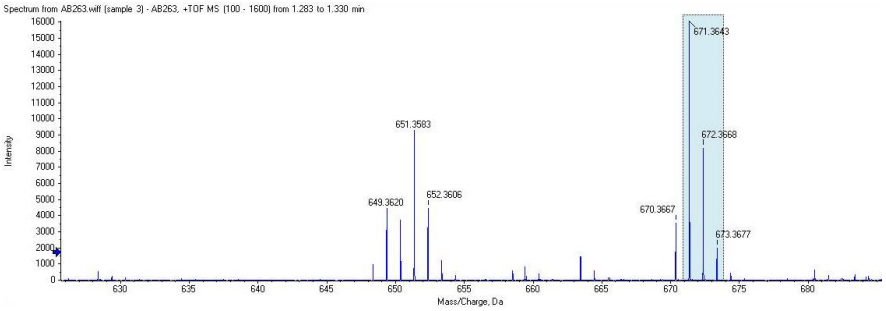

Figure SI-15. MS of **P4**.

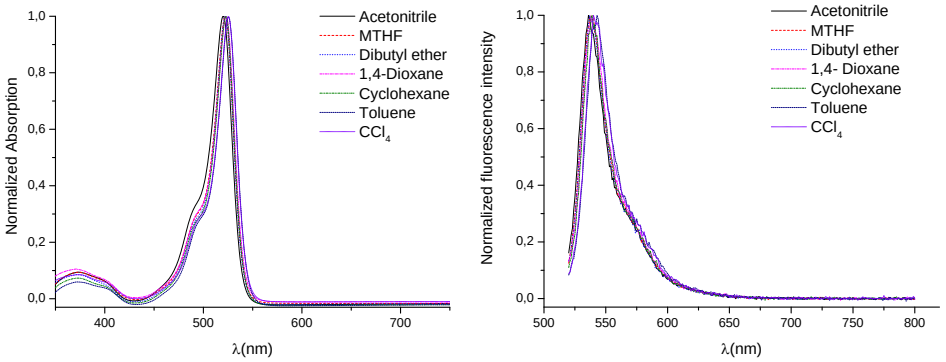

Figure SI-16. Absorption (left) and fluorescence emission (right) spectra of **P1** in different solvents. The intensities in this figure are normalized to the same value at the wavelength of maximum intensity.

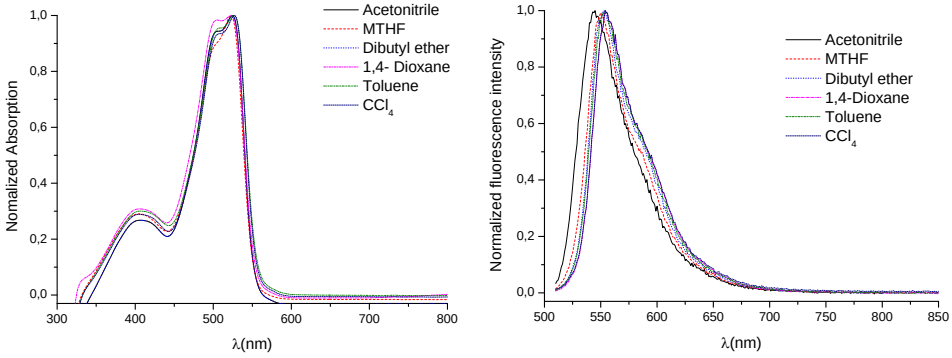

Figure SI-17. Absorption (left) and fluorescence emission (right) spectra of **P2** in different solvents. The intensities in this figure are normalized to the same value at the wavelength of maximum intensity.

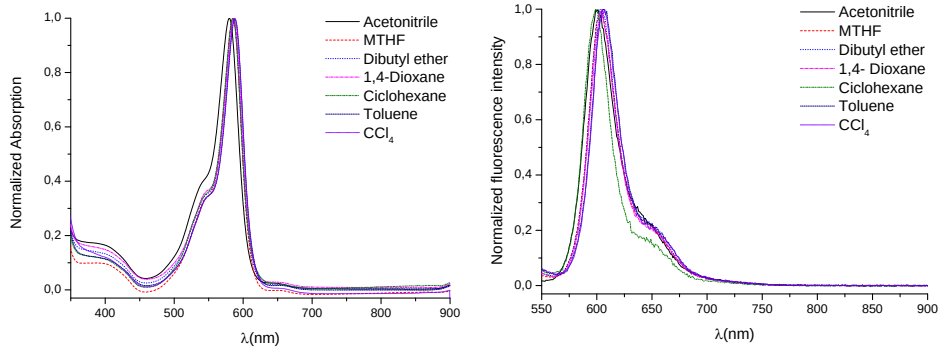

Figure SI-18. Absorption (left) and fluorescence emission (right) spectra of **P3** in different solvents. The intensities in this figure are normalized to the same value at the wavelength of maximum intensity.

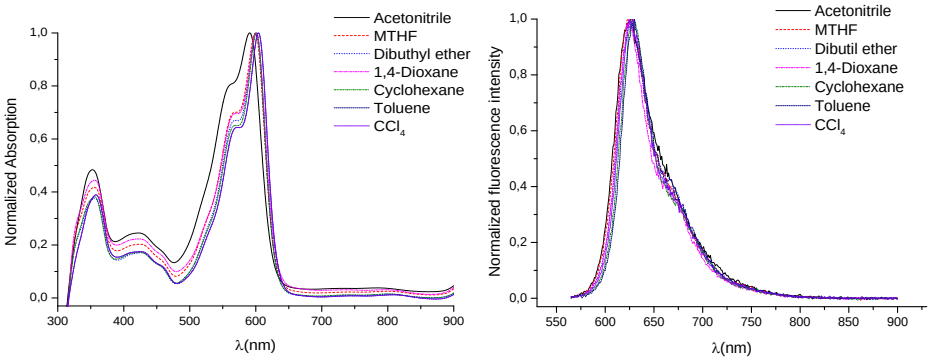

Figure SI-19. Absorption (left) and fluorescence emission (right) spectra of **P4** in different solvents. The intensities in this figure are normalized to the same value at the wavelength of maximum intensity.

Table SI-1. Photophysical parameters of compounds **P1**-**P4** in different solvents.

Probe	Solvent	λ_{abs}(max/nm)	λ_{em}(max/nm)	$\Delta\upsilon$ [a] (cm^{-1})	log ε	ϕ [b]
P1	Acetonitrile	520.0	535.9	570	5.00	0.62
	MTHF	522.0	540.0	638	4.98	0.61
	Dibutyl ether	522.0	537.0	535	5.03	0.63
	1,4-Dioxane	523.0	538.0	533	4.98	0.63
	Cyclohexane	523.5	538.9	545	5.06	0.55
	Toluene	525.5	542.9	609	5.01	0.60
	CCl4	525.5	540.1	514	5.04	0.57
P2	Acetonitrile	517.0	545.0	993	4.87	0.46
	MTHF	522.5	549.8	950	4.92	0.53
	Dibutyl ether	524.5	552.9	979	4.93	0.47
	1,4-Dioxane	522.5	552.9	1022	4.90	0.48
	Cyclohexane	-[c]	-	-	-	-
	Toluene	526.5	554.0	943	4.89	0.53
	CCl4	527.0	552.8	886	4.99	0.54
P3	Acetonitrile	580.0	600.2	580	4.87	0.60
	MTHF	585.0	603.8	490	4.85	0.62
	Dibutyl ether	585.0	603.3	519	4.92	0.62
	1,4-Dioxane	586.5	603.8	489	4.87	0.65
	Cyclohexane	585.0	598.9	518	4.43	0.56
	Toluene	588.0	605.8	499	4.83	0.62
	CCl4	588.5	604.8	460	4.87	0.59
P4	Acetonitrile	591.0	624.8	915	4.92	0.52
	MTHF	599.0	625.9	717	4.88	0.54
	Dibuthyl ether	600.5	627.3	711	5.00	0.54
	1,4-Dioxane	600.5	628.0	729	4.95	0.58
	Cyclohexane	601.0	624.8	634	4.98	0.57
	Toluene	604.0	627.9	633	4.91	0.58
	CCl_4	604.1	629.9	680	5.02	0.56

[a] Stokes shift

[b] Quantum yields were calculated using rhodamine B in ethanol (ϕ_{EtOH} = 0.49) for **P1** and **P2** and Rhodamine 101 in ethanol + 0.01% HCl (ϕ_{EtOH} = 1.0) for **P3** and **P4** as standard.

[c] **P2** was not soluble in Cyclohexane.

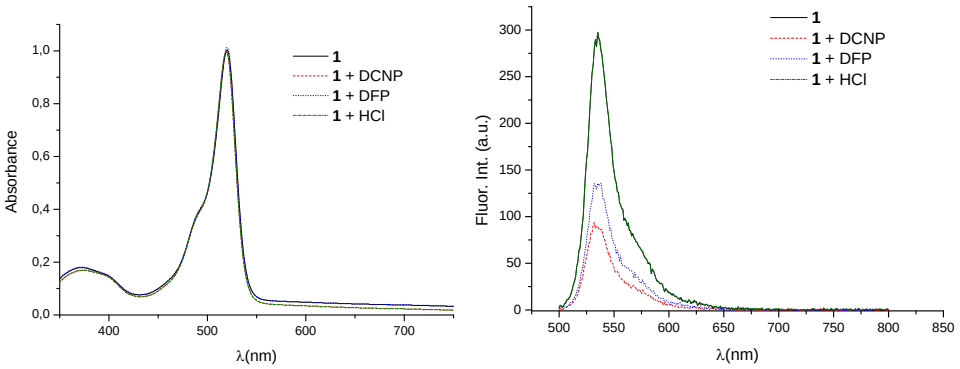

Figure SI-20. Absorption spectra (left) and fluorescence (right) spectra (λ_{ex} = 490 nm) of **P1** (1.0 x 10^{-5} mol dm^{-3} in CH_3CN) alone and in the presence of DCNP, DFP and acid media.

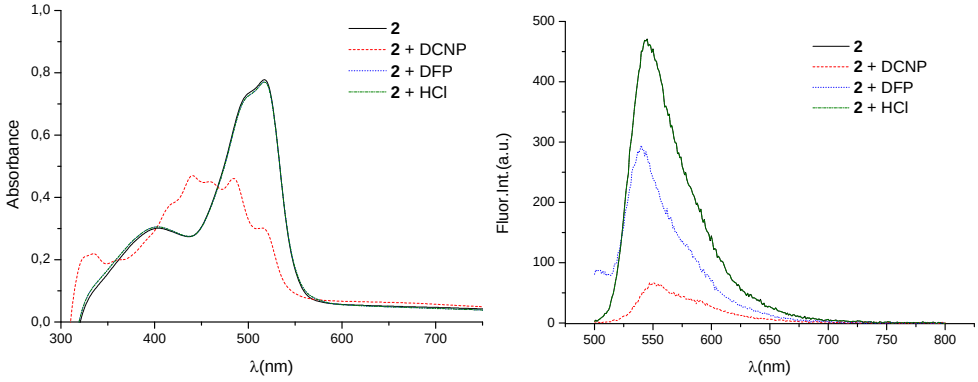

Figure SI-21. Absorption spectra (left) and fluorescence (right) spectra (λ_{ex} = 490 nm) of **P2** (1.0 x 10^{-5} mol dm^{-3} in CH_3CN) alone and in the presence of DCNP, DFP and acid media.

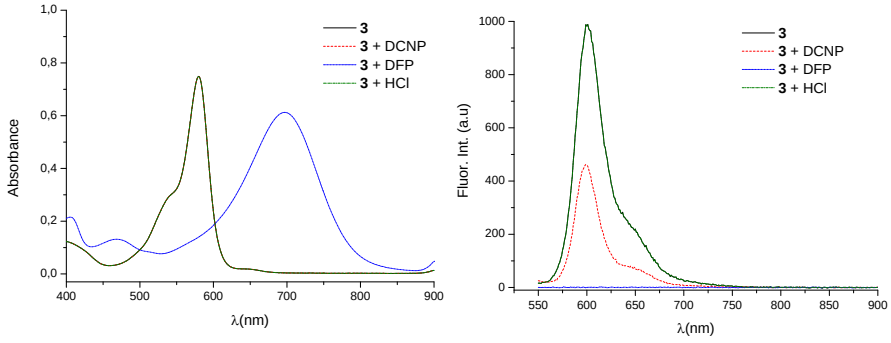

Figure SI-22. Absorption spectra (left) and fluorescence (right) spectra (λ_{ex} = 540 nm) of **P3** (1.0 x 10^{-5} mol dm^{-3} in CH_3CN) alone and in the presence of DCNP, DFP and acid media.

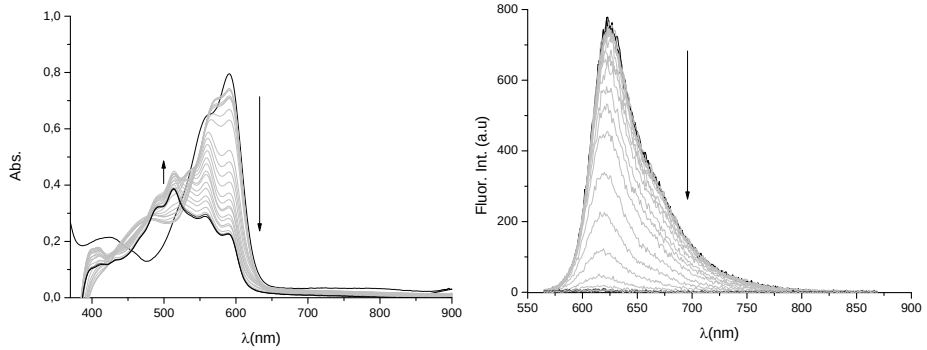

Figure SI-23. Absorption (left) and fluorescence (right) response (λ_{ex} = 555 nm) of **P4** (1.0 x 10^{-5} mol dm^{-3} in CH_3CN) to incremental amounts of DCNP.

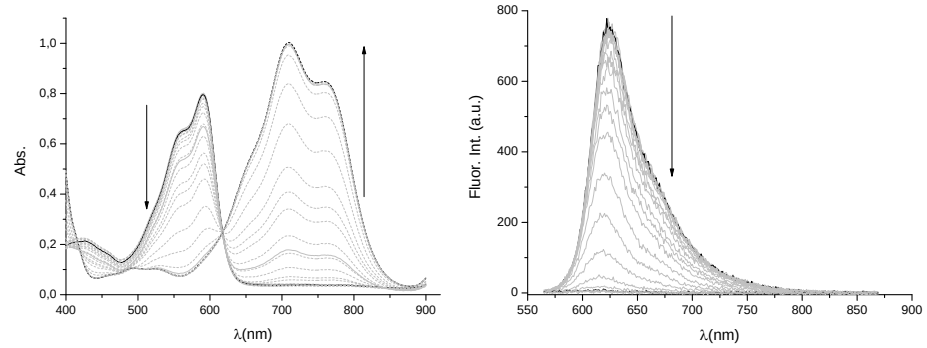

Figure SI-24. Absorption (left) and fluorescence (right) response (λ_{ex}=555 nm) of **P4** (1.0 x 10^{-5} mol dm^{-3} in CH_3CN) to incremental amounts of DFP.

Table SI-2. Photophysical parameters of **P4** in different solvents alone and in presence of DCNP.

						DCNP			
Dye	Solvent	λ_{abs} (nm)	log ε	λ_{em} (nm)	$\phi^{[a]}$	λ_{abs} (nm)	log ε	λ_{em} (nm)	$\phi^{[a]}$
P4	Acetonitrile	591.0	4.92	624.8	0.52	515.0	4.56	625.0	$5{\cdot}10^{-4}$
	MTHF	599.0	4.88	625.9	0.54	522.0	4.45	625.9	$6{\cdot}10^{-4}$
	Dibutyl ether	600.5	5.00	627.3	0.54	523.0	4.81	624.7	$2{\cdot}10^{-4}$
	1,4-Dioxane	600.5	4.95	628.0	0.58	522.5	4.70	627.5	$1{\cdot}10^{-4}$
	Cyclohexane	601.0	4.98	624.8	0.57	521.5	4.37	625.3	$3{\cdot}10^{-4}$
	Toluene	604.0	4.91	627.9	0.58	525.5	4.69	626.7	$7{\cdot}10^{-4}$
	CCl_4	604.1	5.02	629.9	0.56	525.5	4.84	626.5	$2{\cdot}10^{-4}$

[a] quantum yields were calculated using Rhodamine 101 in ethanol + 0.01% HCl (ϕ_{EtOH} = 1.0) as standard.

Table SI-3. Photophysical parameters of **P4** in different solvents alone and in presence of DFP.

						DFP			
Dye	Solvent	λ_{abs} (nm)	log ε	λ_{em} (nm)	$\phi^{[a]}$	λ_{abs} (nm)	log ε	λ_{em} (nm)	$\phi^{[a]}$
P4	Acetonitrile	591.0	4.92	624.8	0.52	715.5	5.00	625.0	$5{\cdot}10^{-4}$
	MTHF	599.0	4.88	625.9	0.54	725.8	4.92	625.9	$6{\cdot}10^{-4}$
	Dibutyl ether	600.5	5.00	627.3	0.54	720.1	5.12	624.7	$2{\cdot}10^{-4}$
	1,4-Dioxane	600.5	4.95	628.0	0.58	718.9	5.01	627.5	$1{\cdot}10^{-4}$
	Cyclohexane	601.0	4.98	624.8	0.57	720.3	5.08	625.3	$3{\cdot}10^{-4}$
	Toluene	604.0	4.91	627.9	0.58	722.5	5.10	626.7	$7{\cdot}10^{-4}$
	CCl_4	604.1	5.02	629.9	0.56	722.9	5.09	626.5	$2{\cdot}10^{-4}$

[a] quantum yields were calculated using Rhodamine 101 in ethanol + 0.01% HCl (ϕ_{EtOH} = 1.0) as standard.

Table SI-4. Photophysical parameters of compounds **P1-P3** in different solvents, alone and in the presence of DCNP.

						DCNP			
Dye	Solvent	λ_{abs} (nm)	log ε	λ_{em} (nm)	$\phi^{[a]}$	λ_{abs} (nm)	log ε	λ_{em} (nm)	$\phi^{[a]}$
P1	Acetonitrile	520.0	5.00	535.9	0.62	520.0	5.00	535.9	0.23
	MTHF	522.0	4.98	540.0	0.61	522.0	4.99	540.1	0.24
	Dibutyl ether	522.0	5.03	537.0	0.63	522.0	5.03	537.1	0.24
	1,4-Dioxane	523.0	4.98	538.0	0.63	523.0	4.99	538.0	0.27
	Cyclohexane	523.5	5.06	538.9	0.55	523.5	5.06	538.9	0.20
	Toluene	525.5	5.01	542.9	0.60	525.5	5.00	542.9	0.30
	CCl_4	525.5	5.04	540.1	0.57	525.5	5.04	540.1	0.24
P2	Acetonitrile	517.0	4.87	545.0	0.46	489.7	4.66	549.6	0.14
	MTHF	522.5	4.92	549.8	0.53	487.5	4.75	547.6	0.09
	Dibutyl ether	524.5	4.93	552.9	0.47	490.5	4.81	553.9	0.07
	1,4-Dioxane	522.5	4.90	552.9	0.48	493.0	4.70	550.7	0.06
	Cyclohexane	-[b]	-	-	-	-	-	-	-
	Toluene	526.5	4.89	554.0	0.53	488.5	4.72	539.1	0.15
	CCl_4	527.0	4.99	552.8	0.54	472.0	4.69	556.0	0.04
P3	Acetonitrile	580.0	4.87	600.2	0.60	580.0	4.87	600.2	0.33
	MTHF	585.0	4.85	603.8	0.62	585.0	4.85	603.8	0.31
	Dibutyl ether	585.0	4.92	603.3	0.62	585.0	4.92	603.3	0.36
	1,4-Dioxane	586.5	4.87	603.8	0.65	586.5	4.87	603.8	0.34
	Cyclohexane	585.0	4.43	598.9	0.56	585.0	4.43	598.9	0.18
	Toluene	588.0	4.83	605.8	0.62	588.0	4.83	605.8	0.37
	CCl_4	588.5	4.87	604.8	0.59	588.5	4.87	604.8	0.32

[a] Quantum yields were calculated using Rhodamine B in ethanol (ϕ_{EtOH} = 0.49) for **P1** and **P2** and Rhodamine 101 in ethanol + 0.01% HCl (ϕ_{EtOH} = 1.0) for **P3** as standard.
[b] **P2** was not soluble in Cyclohexane.

Table SI-5. Photophysical parameters of compounds **P1-P3** in different solvents, alone and in the presence of DFP.

						DFP			
Dye	Solvent	λ_{abs} (nm)	log ε	λ_{em} (nm)	$\phi^{[a]}$	λ_{abs} (nm)	log ε	λ_{em} (nm)	$\phi^{[a]}$
P1	Acetonitrile	520.0	5.00	535.9	0.62	520.0	5.00	535.9	0.24
	MTHF	522.0	4.98	540.0	0.61	522.0	4.99	540.0	0.25
	Dibutyl ether	522.0	5.03	537.0	0.63	522.0	5.03	538.0	0.26
	1,4-Dioxane	523.0	4.98	538.0	0.63	523.0	4.99	538.0	0.29
	Cyclohexane	523.5	5.06	538.9	0.55	523.5	5.06	538.9	0.24
	Toluene	525.5	5.01	542.9	0.60	525.5	5.01	543.0	0.31
	CCl_4	525.5	5.04	540.1	0.57	525.5	5.04	540.1	0.25
P2	Acetonitrile	517.0	4.87	545.0	0.46	517.0	4.87	545.0	0.20
	MTHF	522.5	4.92	549.8	0.53	522.5	4.92	549.8	0.25
	Dibutyl ether	524.5	4.93	552.9	0.47	524.5	4.93	552.9	0.22
	1,4-Dioxane	522.5	4.90	552.9	0.48	522.5	4.90	551.9	0.21
	Cyclohexane	-[b]	-	-	-	-	-	-	-
	Toluene	526.5	4.89	554.0	0.53	526.5	4.89	554.0	0.27
	CCl_4	527.0	4.99	552.8	0.54	527.0	4.99	552.6	0.29
P3	Acetonitrile	580.0	4.87	600.2	0.60	697.0	4.77	-	-
	MTHF	585.0	4.85	603.8	0.62	686.0	4.63	-	-
	Dibutyl ether	585.0	4.92	603.3	0.62	585.0	4.92	-	-
	1,4-Dioxane	586.5	4.87	603.8	0.65	691.0	4.56	-	-
	Cyclohexane	585.0	4.43	598.9	0.56	690.0	4.29	-	-
	Toluene	588.0	4.83	605.8	0.62	679.0	4.68	-	-
	CCl_4	588.5	4.87	604.8	0.59	694.5	4.69	-	-

[a] Quantum yields were calculated using Rhodamine B in ethanol (ϕ_{EtOH} = 0.49) for **P1** and **P2** and Rhodamine 101 in ethanol + 0.01% HCl (ϕ_{EtOH} = 1.0) for **P3** as standard.
[b] **P2** was not soluble in Cyclohexane.

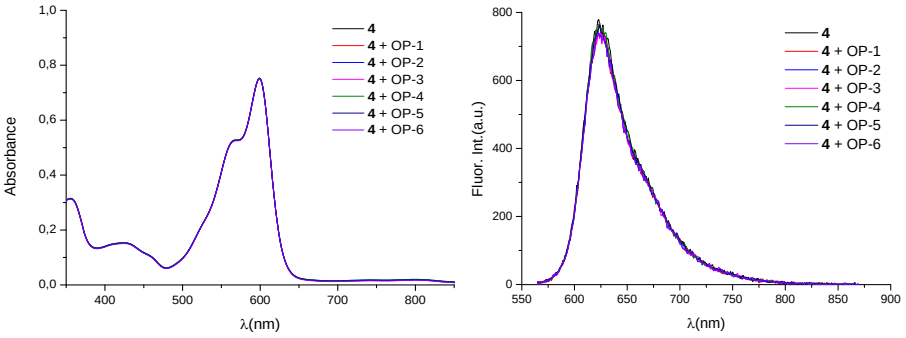

Figure SI-25. Absorbance (left) and fluorescence (λ_{ex} = 555 nm) (right) spectra of **P4** (1.0×10^{-5} mol dm^{-3} in CH_3CN) alone and in presence of organo-phosphorus derivatives (OP1-OP6).

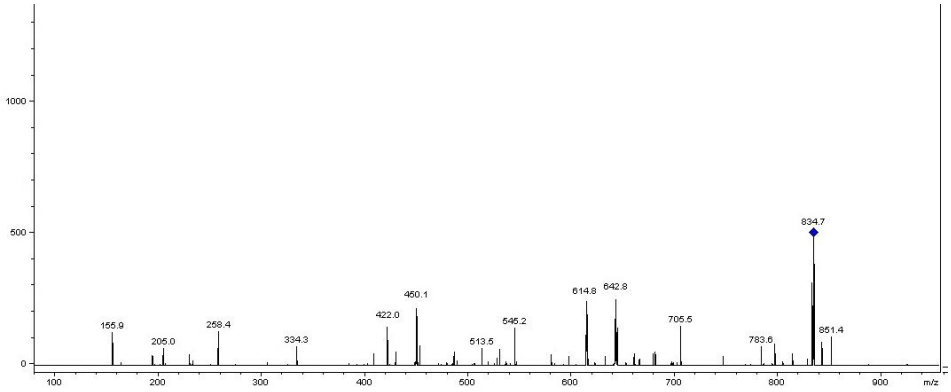

Figure SI-26. Mass Spectra of **P4** +DCNP; [M^++1] = 834.7

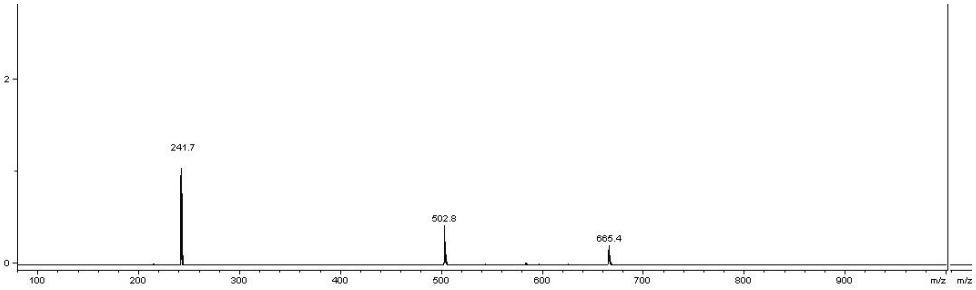

Figure SI-27.Mass Spectra of **P4** + DFP; [M^+-HCO+OH] = 655.4

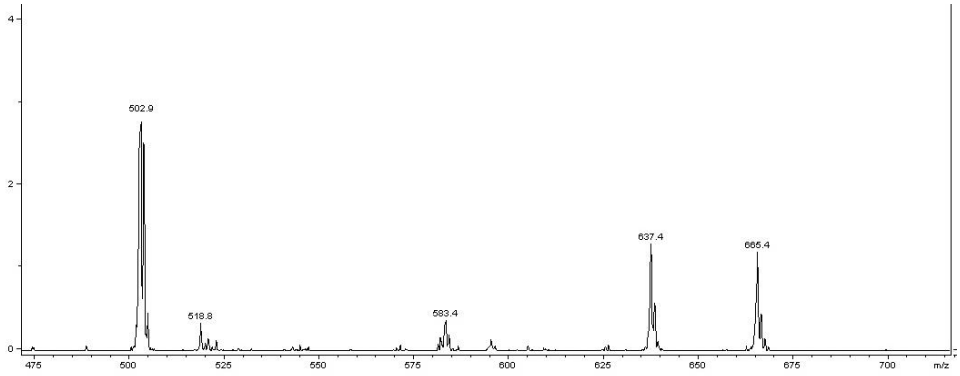

Figure SI-28.Mass Spectra of **P3** + DFP; [M^++2] = 655.4; [M^+-CO] = 637.4

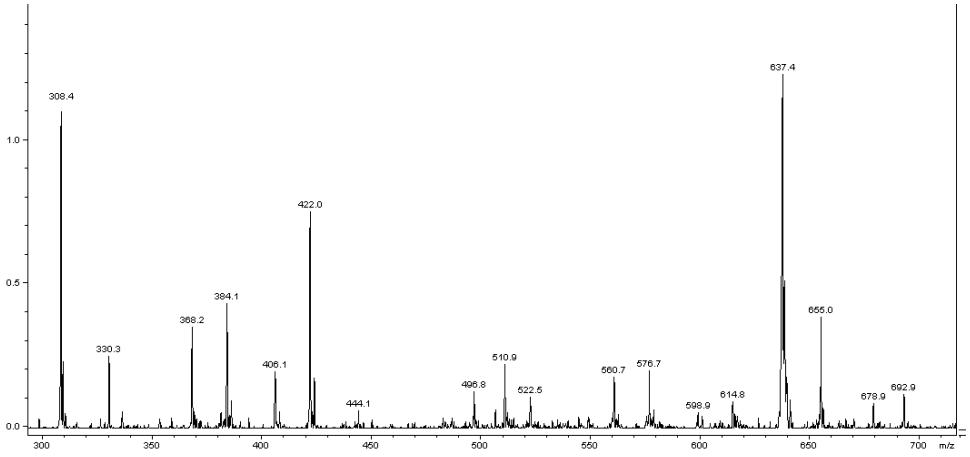

Figure SI-29.Mass Spectra of **P2** + DCNP; [M^++2 MeOH] = 637.4

Mass Spectra were determined in a Bruker ESQUIRE 3000 PLUS Ion-trap Mass Spectrometer.

Characteristics:

- Mass Spectrometer ion-trap is coupled to a high performance liquid chromatograph AGILENT 1100 (HPLC-MS).
- The equipment has an electrospray (ESI) source.
-Direct infusion of the sample.

Nebulizer: 10psi
Dry gas: 6 l / min
Dry temperature: 3250ºC
Target: 30000
Scan: 80-1000 m / z

Chapter 5:

Detection of V-type Nerve Agents

5.1 Introduction

Of the known weaponized nerve agents, the V-type agents are among the most toxic and persistents.[1] The V-agents are phosphonothioates of the P–O type in which the leaving group is linked to phosphorus through a sulfur atom, except for VG which is a phosphorothioate.

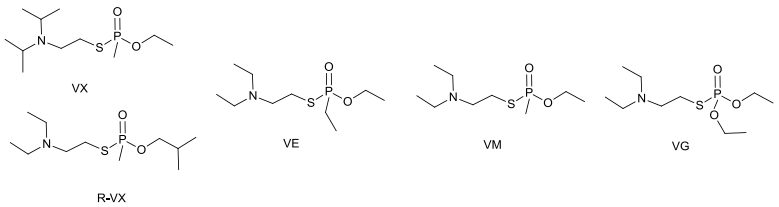

Figure 5.1. Chemical structures of V-nerve agents.

[1] a) Y. C. Yang, L. L. Szafrainec, W. T. Beaudry and D.K. Rohrbaugh, *J. Am. Chem. Soc.,* **1990**, *112*, 6621-6627. b) Y. C. Yang, J. A. Baker and J. R Ward, *Chem. Rev*., **1992**, *92*, 1729-1743.

In contrast to G-agents, V-agents possess a thiolo leaving group. The poorer hydrogen-bonding ability of sulfur derivative to oxygen and the lower electrophilicity of the phosphorus make V-agents much more stable and less volatile compared with G-series.[2] The extreme potential for acute toxicity of V-agents is due, in part; to their low volatily which allows them to persist indefinitely on common surfaces.[3] For instance, to an estimated lethal dermal exposure of 6 mg for an average human, contact with VX is approximately 200 times more toxic than Soman (GD) and 300 times more toxic than Sarin (GB).[4]

Cholinesterases (ChE) are well-known targets for organophosphates, and V-nerve agents are no exception. V-type agents inibhit AChE, thereby disrupting hydrolysis of the neurotransmitter Ach. The active site of AChE comprises a catalytic triad of serine, histidine and glutamic acid residues and other important features of the enzyme are a 'gorge' connecting the active site to the surface of the protein and a peripheral anionic site. V-agents phosphorylate the serine hydroxyl group in the active site of AChE[5] that is also involved in the binding of acetylcholine (the natural substrate of the enzyme). The interaction of the nerve agent with the AChE is stronger that with acetylcholine thus, the entire process resulting in accumulation of acetylcholine that produces neuromuscular paralysis and eventually death.[6] In the case of V-agents, at physiological pH (7.4) the tertiary amine (pK_a 8.4) is likely to be protonated and therefore cationic.[7] Binding of V-

[2] I. Cherny, P. J. Greisen, Y. Ashani, S. D. Khare, G. Oberdorfer, H. Leader, D. Baker and D. S. Tawfik, *ACS Chem. Biol.,* **2013**, *8*, 2394-2403.
[3] I. Columbus, D. Waysbort, I. Marcovitch, L. Yehezkel, D. M. Mizrahi, *Environ. Sci. Technol*., **2012**, *46*, 3921-3927.
[4] J. B. Leikin, R. G. Thomas, F. G. Walter, R. Klein and H. W. Meislin, *Crit. Care Med*., **2002**, *30*, 2346-2354.
[5] J. A. Vale, P. Rice and T. C. Marrs, *Chemical Warfare Agents: Toxicology and Treatment,* ed. T. C. Marrs, R. L. Maynard and F. R. Sidell, John Wiley & Sons, Chichester, **2007**
[6] a) S. M. Somani, *Chemical Warfare Agent*, Academic Press, San Diego**, 1992.** b) P. Taylor, in *The Pharmacological Basis of Therapeutics,* 10th ed. (ed: J. G. Hardman, L. E. Limbird, A. G.Gilman,) McGraw-Hill, New York, **2001**.
[7] A. Ordentlich, D. Barak, G. Sod-Moriah, D. Kaplan ,D. Mizrahi, Y. Segall, C. Kronman ,Y. Karton, A. Lazar, D. Marcus, B. Velan, and A. Shafferman, *Biochemistry*, **2004**, *43*, 11255-11265.

series is further stabilized by interactions between this quaternary ammonium group and the anionic site.

In addition to the phosphoryl functionality, the V-agents contain sulfide and tertiary amine groups for possible coordination to transition or lanthanide metal centers. Churchill and coworkers reported a comprehensive study on the possibility of mono- and bi-dentate coordination modes for the binding of a VX simulant to a range of metal ions.[8] The study describes six potential bidentate binding modes, and these are shown in Figure 5.2.

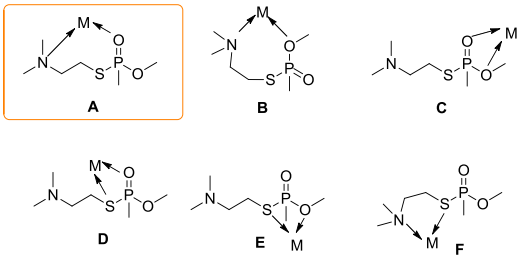

Figure 5.2. The six possible binding modes for V- surrogate with a metal center proposed by Churchill and co-workers.

For the cationic metal ions studied (Li^+, Na^+, K^+, Be^{2+}, Mg^{2+} and Ca^{2+}) the theoretical studies indicated the most stable binding mode was the seven-membered chelation mode (A) highlighted in figure 5.2 .

The high toxicity and environmental persistence of V-agents makes the development of novel detection methods particularly important, nonetheless the detection of V-type nerve agent degradation products has been reported,[9] but probes for V-agents are very unusual.

[8] I. Bandyopadhyay, M. J. Kim, Y. S. Lee and D. G. Churchill, *J. Phys. Chem. A,* **2006**, *110*, 3655–3661.
[9] a) W. Joseph, J. Zima, N. S. Lawrence and M. P. Chatrathi, *Anal. Chem*., **2004**, *76*, 4721-4726. b) O. V. Shulga, C. Palmer, *Anal. Bioanal. Chem*., **2006,** *385*, 1116–1123. c) J. S. Knaack, Y. Zhou, C. W. Abney, S. M. Prezioso, M. Magnuson, R. Evans, E. M. Jakubowski, K. Hardy and R. C. Johnson, *Anal. Chem*., **2012**, *84*, 10052−10057.

Recently, Denninston *et al.* reported the bidentate coordination of V-series agent with lanthanide ions.[10] Addition of VX or VG to 1,10-phenantroline nitrate Ln(III) complexes resulted in a quenching of the lanthanide luminescence emission. This is a result of ligand displacement by competitive binding thereby nullifying the antenna effect.

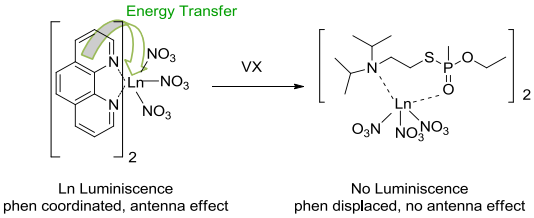

Figure 5.3. The bidentate coordination of VX proposed by Denninston and co-workers.

5.2 Objectives

Bearing in mind this example, the main objective of this chapter is the design and synthesis of new BODIPY-complexes that could be able to detect selectively V-type over G-type nerve agents, *via* a displacement of the ligand with the aim to obtain a colorimetric response.

Specially, our aims were:

- ✓ Design and synthesis of new BODIPY-complexes for the selective detection of V-type nerve agent surrogates.
- ✓ Study of the chromo/fluorogenic behavior of the synthesized complexes with the selected surrogates.
- ✓ Evaluation of the selectivity in presence of different G-type mimics.
- ✓ Testing the developed sensor with simulated samples with matrix.

[10] G. H. Dennison, M. R. Sambrook and M. R. Johnston, *Chem. Commun*., **2014**, *50*, 195-197.

5.3 Chemosensors Design

As have been mentioned above, metallic species are able to coordinate (in mono- and bi-dentate modes) V-type mimics. Bearing in mind this fact, along with our experience in the complexation and sensing of trivalent ions lead us to select Eu^{3+} and Au^{3+} BODIPY-complexes to detect V-surrogates by the *displacement assay* approach. This approach was selected because the coordination of the target molecule with the ion is expected to induce the release of the dye. A remarkable optical response is obtained because the color or emission of the signaling subunit in the sensing ensemble is different than those presented when it is free in solution.

The sensing paradigm by these complexes relies on displacement of a sensitizing BODIPY ligand by coordination of the trivalent cation with V-nerve agent mimic; a modulation In the optical properties of the BODIPY-ligand is expected.

Moiety containing N-electron-donor group was selected as binding site given its capacity to coordinate metal trivalent cations. Among them, Eu^{3+} and Au^{3+} were chosen by their ability to coordinate with V surrogates. In addition BODIPY core was selected as chromophore due to their know photophysical properties and their pH stability.

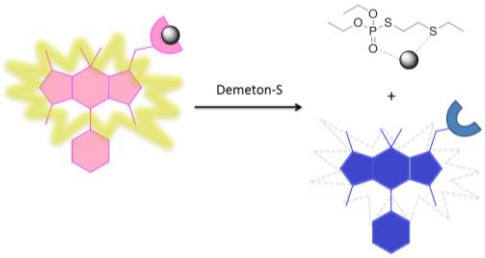

Figure 5.4. Sensing paradigm for the chromo-fluorogenic recognition of V-surrogate by using the *displacement assay* approach.

5.4 Chromo-fluorogenic BODIPY-complexes for selective detection of V-type nerve agent surrogates.

Chromo-fluorogenic BODIPY-complexes for selective detection of V-type nerve agent surrogate

Andrea Barba-Bon, [acd] *Ana María Costero,* [ab] *Salvador Gil,* [ab] *Felix Sancenón* [acd] *and Ramón Martínez-Máñez* [acd]

[a] *Centro de Reconocimiento Molecular y Desarrollo Tecnológico (IDM), Unidad Mixta Universidad Politécnica de Valencia- Universidad de Valencia, Spain.*

[b] *Departamento de Química Orgánica, Facultad de Ciencias Químicas, Universidad de Valencia, Dr. Moliner, 50, 46100 Burjassot ,Valencia, (Spain).*

[c] *Departamento de Química, Universidad Politécnica de Valencia, Camino de Vera s/n, 46022 Valencia, (Spain).*

[d] *CIBER de Bioingeniería, Biomateriales y Nanomedicina (CIBER-BBN).*

Received: *30 th July 2014*

Published online: *10th September 2014*

Chem. Commun., **2014,** *50*, 13289-13291.

Two new Eu^{3+} and Au^{3+} BODIPY-complexes capable of chromo-fluorogenically detecting micromolar concentrations of V-type nerve agent surrogates by a simple displacement assay are described.

Nowadays, the growing fear of possible attacks with chemical warfare agents (CWAs) by military regimes and terrorist organizations has thrown up a new challenge to develop sensitive and selective devices to monitor these extremely dangerous chemicals.[1] Within CWAs, nerve agents (classified in G- and V-series, see Scheme 1) represent an extremely toxic class of organophosphorus compounds that cause incapacitation and even death through inhibition of acetylcholinesterase (AChE) activity.[2] Nerve agents phosphorylate the serine hydroxyl group in the active site of AChE that is also involved in the binding of acetylcholine (the natural substrate of the enzyme).[3] The interaction of AChE with the nerve agent is stronger than with acetylcholine, the entire process resulting in accumulation of acetylcholine that causes neuromuscular paralysis and eventually death.[2] Moreover V-gases are low-volatile liquids with high boiling points and are much more persistent and toxic than nerve agents of the G-series. For example, compared with Sarin (GB), VX is estimated to be approximately twice as toxic by inhalation, ten times as toxic by oral administration, and approximately 170 times as toxic after skin exposure.[4]

Most common methods for monitoring the presence of nerve agents are based on the use of biosensors,[5] ion mobility spectroscopy[6] and electrochemical methods.[7] Moreover, recently the development of fluorogenic and chromogenic chemosensors has gained increasing interest as an alternative to these instrumental procedures.[8] Chromo-fluorogenic probes are especially appealing because they allow simple visual detection *in situ* or at site without any sample pretreatment or the use of complex equipment. However it is apparent from the literature that although a variety of chemosensors for the detection of G-type agents have been reported,[1,9] probes for V-type agents are still very rare.[10]

Due to the high toxicity of nerve agents, various comparatively innocuous and readily available molecules (usually named simulants, mimics or surrogates) are frequently used in research studies. In particular the organophosphorus

insecticide, demeton-S, has been used in this work as a surrogate of the highly toxic V-type nerve agents.[11] Moreover nerve gas simulants such as diethylcyanophosphate (DCNP), diisopropylfluorophosphate (DFP) and dimethyl methylphosphonate (DMMP) are usually used as simulants of the G-type nerve agents Sarin, Soman and Tabun. All these surrogates show similar reactivity to real nerve agents but lack their severe toxicity (see Scheme 1).

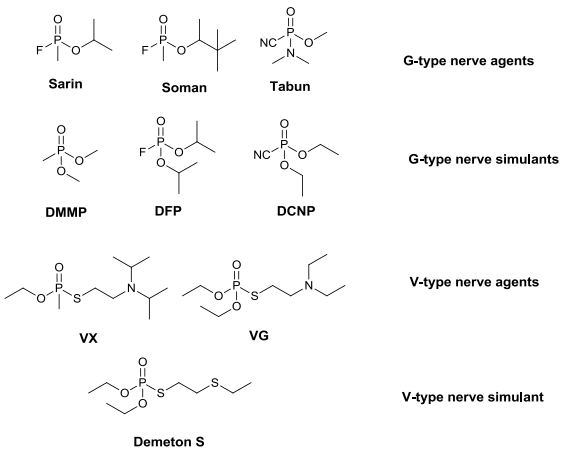

Scheme 1. Chemical structures of G-type and V-type agents and their simulants.

Following our interest in the development of chromo-fluorogenic probes for nerve agents,[12] we show herein two new BODIPY-complexes that are able to detect selectively the V-type nerve agents mimic demeton-S *versus* G-type nerve agents simulants (see Scheme 2). The design of the probe is based in the use of the BODIPY derivative **1** that is known to form 1:1 metal complexes with trivalent cations in a bidentate coordination mode.[13] It is also known that some metal cations such as Eu^{3+} and Au^{3+} coordinate well with V-nerve agents through the formation of mono[1,14] and bidentate complexes.[10] Based on these concepts, the sensing paradigm we report herein relies on the preparation of the **1**-Eu^{3+} and **1**-Au^{3+} complexes and on a demeton-S-induced demetallation that was expected to result in a significant chromo-fluorogenic response.

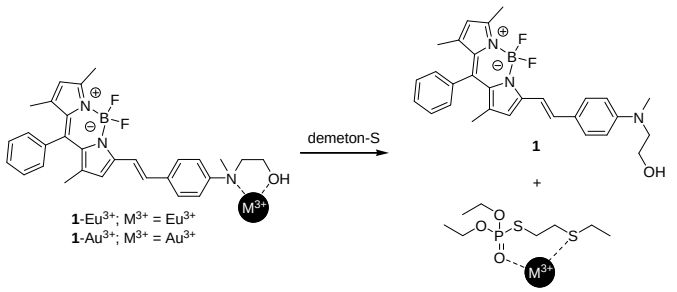

Scheme 2. Metal-complexes **1**-Eu^{3+} and **1**-Au^{3+}, and schematic outline of the sensing paradigm.

Complexes **1**-Eu^{3+} and **1**-Au^{3+} were prepared by simple mixing of the corresponding metal salt with **1** and further purification by recrystallization from EtOH-water mixtures (see ESI for details).[14c,15] Acetonitrile solutions of **1** showed an intense absorption band in the visible region centred at 600.5 nm responsible for the blue colour observed. Besides, solutions of **1** are nearly non-emissive (see Table 1) attributed to an efficient ICT quenching of the excited state of the BODIPY fluorophore from the electron-donating aniline group. In contrast **1**-Eu^{3+} and **1**-Au^{3+} were pink and presented strong emission bands (at 572.8 and 573.2 nm for **1**-Eu^{3+} and **1**-Au^{3+}, respectively) due to an inhibition of the quenching process, active in **1**, upon coordination with the metal cations (see Table 1). The formation of 1:1 complexes between **1** and Eu^{3+} and Au^{3+} was additionally confirmed through titration experiments in acetonitrile and from Job plot studies .^{1}H NMR studies were carried out to envisage the cation complexation mode (see ESI).

Table 1. Uv-vis absorption and fluorescence data of free ligand and their complexes (**1**/M^{3+} =1:1).

	λ_{abs} (nm)	log ε	λ_{em} (nm)	$\Phi^{[a]}$
1	600.5	4.96	570.0	< 0.001
1-Eu^{3+}	553.0	5.07	572.8	0.22
1-Au^{3+}	552.5	5.09	573.2	0.28

[a] Quantum yields were calculated using Rhodamine B in ethanol (Φ_{EtOH}=0.49)[16] as standard.

As a first step, the behaviour of **1**-Eu^{3+} in the presence of demeton-S was tested in acetonitrile. Addition of increasing quantities of demeton-S induced a progressive and marked decrease of the absorption at 553 nm and the appearance of a new band at 600.5 nm with a colour modulation from bright pink to blue, easily

detectable to the naked eye (see Figure 1). Besides, remarkable quenching of the emission band at 572.8 nm was also observed (see Figure 1). A very similar behaviour was observed upon addition of demeton-S to acetonitrile solutions of complex **1**-Au^{3+} (see ESI). The red-shifted bands, obtained upon addition of demeton-S to solutions of **1**-Eu^{3+} and **1**-Au^{3+}, that were identical to that of **1** alone, and the strong quenching observed were in agreement with a demetallation process as the mechanism of the observed optical modulation.

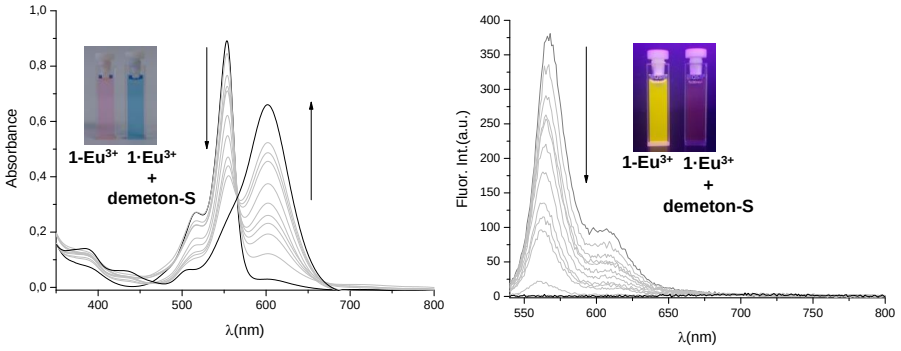

Figure 1. Absorption (left) and emission (right, λ_{exc} = 530 nm) titration of **1**-Eu^{3+} (1.0×10^{-5} M in acetonitrile) obtained upon the successive addition of incremental amounts of demeton-S.

In order to further study the sensing protocol, the association constants of Eu^{3+} and Au^{3+} cations with **1** were calculated from UV-vis titration experiments by using the Specfit program.[17] Logarithms of complexation constants for **1** with Eu^{3+} and Au^{3+} for the formation of the **1**-Eu^{3+} and **1**-Au^{3+} 1:1 complexes were 4.1 ± 0.5 and 4.2 ± 0.4, respectively from UV-vis titrations. Nearly similar stability constants for the formation of the complexes were determined from fluorescence experiments (i.e. log *K* = 4.6 ± 0.3 and 4.3 ± 0.4 for the formation of **1**-Eu^{3+} and **1**-Au^{3+}, respectively). On the other hand, log *K* for the displacement reaction (i.e. **1**-M^{3+} + demeton-S ⇄ **1** + demeton-S-M^{3+}) were also determined and amounted to 5.8 ± 0.5 and 6.6 ± 0.2 (from UV-vis) and 5.9 ± 0.4 and 6.7 ± 0.3 (from fluorescence) for Eu^{3+} and Au^{3+}, respectively. These studies demonstrated that Eu^{3+} and Au^{3+} showed stronger affinity for demeton-S than for **1** in agreement with the proposed sensing paradigm. Besides, Au^{3+} displayed a higher displacement

association constant with demeton-S than Eu^{3+} which is tentatively ascribed to the high affinity of Au^{+3} for sulfur-containing derivatives.[18]

Moreover from titration experiments of **1**-Eu^{3+} and **1**-Au^{3+} with demeton-S limits of detection (LOD) of 13.97 and 9.17 (from UV-vis) and 12.89 and 9.08 ppm (from fluorescence) were determined for **1**-Eu^{3+} and **1**-Au^{3+}, respectively.

Finally, in order to verify the selectivity of the method, similar experiments with probes **1**-Eu^{3+} and **1**-Au^{3+} were performed in the presence of the G-type nerve agent mimics DCNP, DFP and DMMP (see Figure 2). The results show that probes **1**-Eu^{3+} and **1**-Au^{3+} are highly selective to the presence of demeton-S, whereas G-type derivatives induced a very poor response even at concentrations as high as 500 ppm. The presence of G-type agents in the medium only gives negligible change in the response. Detection can be even carried out in the presence of 50% of water. (see ESI)

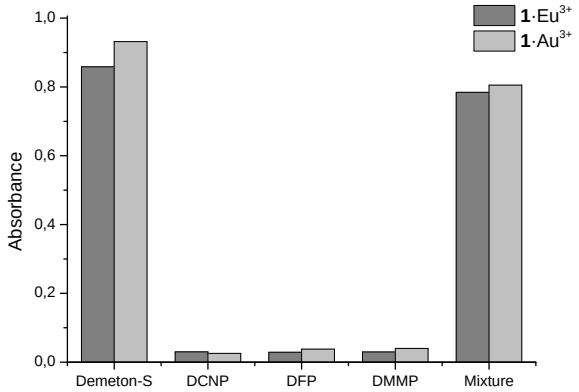

Figure 2. Absorbance (measured at 600.5 nm) of complexes **1**-Eu^{3+} and **1**-Au^{3+} in the presence of Demeton-S (100 ppm), DCNP, DFP and DMMP (500 ppm) (Mixture: DCNP+DFP+DMMP+Demeton-S).

In summary, Eu^{3+} and Au^{3+} complexes of the BODIPY-containing derivative **1** were prepared and their utility in the selective detection of the V-type nerve agent surrogate demeton-S demonstrated. The mechanism of detection occurs *via* the displacement of the BODIPY ligand by coordination of demeton-S with the metallic centre, resulting in colour modulation and fluorescence quenching which were observed easily to the naked eye. LOD in the 9-14 ppm range were determined. Probes **1**-Eu^{3+} and **1**-Au^{3+} are some of the very few examples

reported in the literature that are able to detect V-type nerve agent mimics. Moreover **1**-Eu^{3+} and **1**-Au^{3+} are easy to prepare and we believe they may inspire further research in the design of new probes that are able to chromo-fluorogenically and selectively detect V-type *versus* G-type nerve agent.

Financial support from the Spanish Government (Project MAT2012-38429-C04) and the Generalitat Valencia (Project PROMETEOII/2014/047) is gratefully acknowledged. A.B.B acknowledges the award of a pre-doctoral FPI fellowship. SCIE (Universidad de Valencia) is gratefully acknowledged for all the equipment employed.

Notes and references

1 K. Kim, O. G. Tsay, D. A. Atwood and D. G. Churchill, *Chem. Rev*., 2011, **111**, 5345-5403.

2 (a) S. M. Somani, *Chemical Warfare Agent*, Academic Press, San Diego**,** 1992**;** (b) P. Taylor, in The Pharmacological Basis of Therapeutics, 10th ed. (Ed: J. G. Hardman, L. E. Limbird, A. G.Gilman) McGraw-Hill, New York, 2001, 175-191.

3 J. A. Vale, P. Rice and T. C. Marrs, *Chemical Warfare Agents: Toxicology and Treatment,* (Ed. T. C. Marrs, R. L. Maynard and F. R. Sidell) John Wiley & Sons, Chichester, 2007.

4 R. Gupta, *Handbook of Toxicology of Chemical Warfare Agents,* Academic Press, London**,** 2009.

5 H. Wang, J. Wang, D. Choi, Z. Tang, H. Wu and Y. Lin, *Biosens. Bioelectron.*, 2009, **24**, 2377-2383.

6 E. Steiner, S. J. Klopsch, W. A. English, B. H. Clowers and H. H. Hill, *Anal. Chem*., 2005, **77**, 4792-4799.

7 M. A. K. Khan, Y. T. Long, G. Schatte and H. B. Kraatz, *Anal. Chem.*, 2007, **79**, 2877-2884.

8 (a) S. Royo, R. Martínez-Máñez, F. Sancenón, A. M. Costero, M. Parra, S. Gil, *Chem. Commun.*, 2007, **46**, 4839-4847; (b) B. D. de Greñu, D. Moreno, T. Torroba, A. Berg, J. Gunnars, T. Nilsson, R. Nyman, M. Persson, J. Pettersson, I. Eklind, P. Wästerby, *J. Am. Chem. Soc*., 2014, **136**, 4125-4128.

9 M. R. Sambrook and S. Notman, *Chem. Soc. Rev.,* 2013, **42**, 9251-9267

10 G. H. Dennison, R. Sambrook and M. J. Johnston, *Chem. Commun*., 2014, **50**, 195-197.

11 (a) K. A. Joshi, M. Prouza, M. Kum, J. Wang, J. Tang, R. Haddon, W, Chen and A. Mulchandani, *Anal. Chem*., 2006, **78**, 331-336; (b) A. Bazire, E. Gillon, O. Lockridge, V. Vallet and F. Nachon, *Toxicology in Vitro*, 2011, **25**, 754-759.

12 (a) A. M. Costero, S. Gil, M. Parra, P. M. E. Mancini, R. Martínez-Máñez, F. Sancenón and S. Royo, *Chem. Commun.,* 2008, **45**, 6002-6004; (b) S. Royo, R. Gotor, A. M. Costero, M. Parra, S. Gil, R. Martínez-Máñez, F. Sancenón, *New J. Chem.,* 2012, **36**, 1485-1489; (c) E. Climent, A. Martí, S. Royo, R. Martínez-Máñez, M.D. Marcos, F. Sancenón, J. Soto, A.M. Costero, S. Gil, M. Parra, *Angew. Chem. Int. Ed*., 2010, **49**, 5945-5948.; (d) A. Barba-Bon, A. M. Costero, S. Gil, A. Harriman and F. Sancenón, *Chem. Eur. J*., 2014, **20**, 6339-6347.

13 (a) A. Barba-Bon, A. M. Costero, S. Gil, M. Parra, J. Soto, R. Martínez-Máñez and F. Sancenón, *Chem. Commun.*, 2012, **48**, 3000-3002; (b) A. Barba-Bon, L. Calabuig, A. M. Costero, S. Gil, R. Martínez-Máñez and F. Sancenón, *RSC Adv*., 2014, **4**, 8962-8965.

14 (a) I. Bandyopadhyay, M. J. Kim, Y. S. Lee and D. G. Churchill, *J. Phys. Chem. A*, 2006, **110**, 3655-3661; (b) D. Knapton, M. Burnworth, S. J. Rowan and C. Weder, *Angew. Chem. Int. Ed*., 2006, **45**, 5825-5829; (c) S. Nadella, J. Sahoo, P. S. Subramanian, A. Sahu, S. Misha and M. Albrecht, *Chem. Eur. J*., 2014, **20**, 1-8.

15 L. Cao, M. C. Jennings and R. J. Puddephatt, *Inorg. Chem.*, 2007, **46**, 1361-1368.

16 K. G. Casey and E. L. Quitevis, *J. Phys. Chem.*, 1988, **92**, 6590-6594.

17 Specifit/32TM Global Analysis System v.3.0, Spectrum Associates, Marlborough, MA, USA, http://www.biologic.info/rapidkinetics/specfit.html.

18 T. Zou, C. T. Lum, S. S. -Y. Chui and C. M. Che, *Angew. Chem. Int. Ed*., 2013, **52**, 2930-2933.

Supporting Information

Chromo-fluorogenic BODIPY-complexes for selective detection of V-type nerve agent surrogate

Andrea Barba-Bon, Ana María Costero,
Salvador Gil, Felix Sancenón and
Ramón Martínez-Máñez

Experimental section

General remarks

CH_3CN was distilled from P_2O_5 under Ar prior to use. $NaAuCl_4$ was prepared by neutralization of an aqueous solution of $HAuCl_4$ with $NaHCO_3$. All the other solvents and starting materials were purchased from commercial sources where available, and were used without purification. ^{1}H-NMR (300 MHz), ^{13}C NMR spectra were determined in a Bruker AV 300 spectrometer. Chemical shifts are reported in parts per million (ppm), calibrated to the solvent peak set.

Synthesis of 1: Synthesis of *(E)-4,4-difluoro-5-(4-((2-hydroxyethyl)(methyl)amino)styryl)-1,3,7-trimethyl-8-phenyl-4-bora-3a,4a-diaza-s-indacene* has been reported previously.[1]

Synthesis of 1-Eu^{3+}: To a solution of **1** (243 mg, 0.50 mmol) in 30 mL of MeOH an aqueous solution of $Eu(NO_3)_2{\cdot}5H_2O$ (214 mg, 0.50 mmol) was added dropwise and the mixture was stirred for 3 h. at rt. The resulting bright pink reaction mixture was evaporated under reduced pressure. The solid was recrystallized from EtOH-water (1:1) to give **1**-Eu^{3+} (285 mg, 61 %).^{1}H-MNR (300 MHz; $CDCl_3$) δ 7.64 (dd, *J*=17.4, 9.0 Hz,4 H) , 7.43 (m, 3H) , 7.23 (m, 3H) , 7.10(d, *J*=16.4Hz, 1H), 6.54(s, 1H) ,5.99 (s, 1H), 3.86 (s,2H), 3.57 (s,2H), 3.20 (s,3H), 2.54 (s,3H), 1.34 (d, *J*=8.6 Hz, 6H). UV/vis (CH_3CN) λ_{max} = 553.0; λ_{em} = 572.8 nm.

Synthesis of 1-Au^{3+}: To a solution of $NaAuCl_4$ (150 mg, 0.40 mmol) in H_2O (20 mL), $NaHCO_3$ (35 mg, 0.40 mmol) and KPF_6 (150 mg, 0.82 mmol) was added. To this solution a solution of **1** (200 mg, 0.41 mmol) in MeOH (5 mL) was added dropwise. The product precipitated as a pink solid, which was separated by filtration and recrystallized from EtOH-water (1:1) to give **1**-Au^{3+} (170 mg, 47 %).^{1}H-MNR (300 MHz; $CDCl_3$) δ 7.71 (dd, *J*=17.4, 9.0 Hz,4 H) , 7.49 (m, 3H) , 7.30 (m, 3H) , 7.17(d, *J*=16.4Hz, 1H), 6.61(s, 1H) ,6.06 (s,1H), 3.93 (s,2H), 3.64 (s,2H), 3.27 (s,3H), 2.58 (s,3H), 1.38 (m,6H). UV/vis (CH_3CN) λ_{max} = 552.5; λ_{em} = 573.2nm.

Spectroscopic studies

Acetonitrile was purchased at spectroscopic grade from Aldrich Chemicals Co., used as received, and was found to be free of fluorescent impurities. Absorption and fluorescence spectra were recorded using a Shimadzu UV-2600 spectrophotometer and a Varian Cary Eclipse spectrofluorimeter, respectively. Fluorescence quantum yields were measured at room temperature in the N_2-purgued solution using rhodamine B (Φ_{EtOH} = 0.49)[2] at 525 nm as standard. The fluorescence quantum yields were calculated from Eq. (1).[3] Here, F denotes the integral of the corrected fluorescence spectrum, A is the absorbance at the excitation wavelength, and n is the refractive index of the medium.

$$\Phi_{exp} = \Phi_{ref} \frac{F\{1-exp(-A_{ref} ln10)\}n^2}{F_{ref}\{1-exp(-A\, ln10)\}n_{ref}^2} \quad (1)$$

Limits of detection measurements

Increasing amounts of demeton-S dissolved in acetonitrile were progressively added to 3.5 mL solutions of **1**-Eu^{3+} and **1**-Au^{3+} (1.0 x 10^{-5} M). The UV-visible and fluorescence spectra were recorded in 1-cm path length cells at 25°C. Representation of Δ of absorbance or fluorescence at the appropriate wavelength vs. concentration of simulant allowed the limit of detection to be calculated by using the equation (2) where K = 3; Sb_1 is the standard deviation of the blank solution and S is the slope of the calibration curve.[4]

$$LOD = K\frac{Sb_1}{S} \quad (2)$$

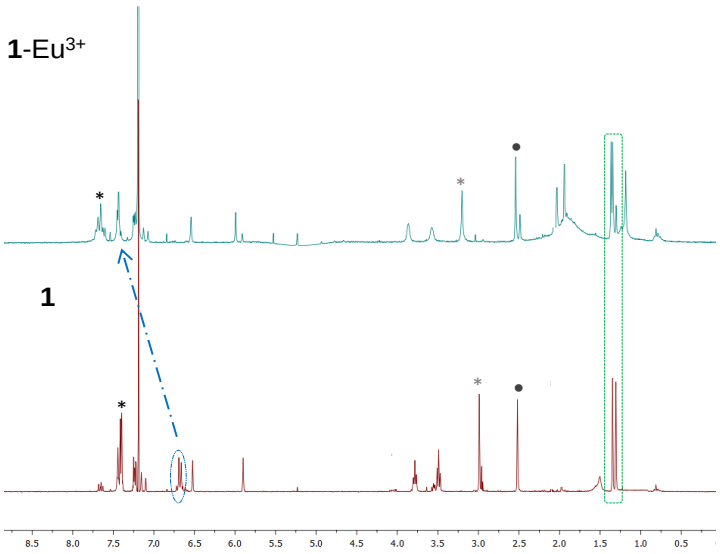

Figure SI-1. ^{1}H-NMR spectra of **1** (in $CDCl_3$) before and after complexation with Eu^{3+}.

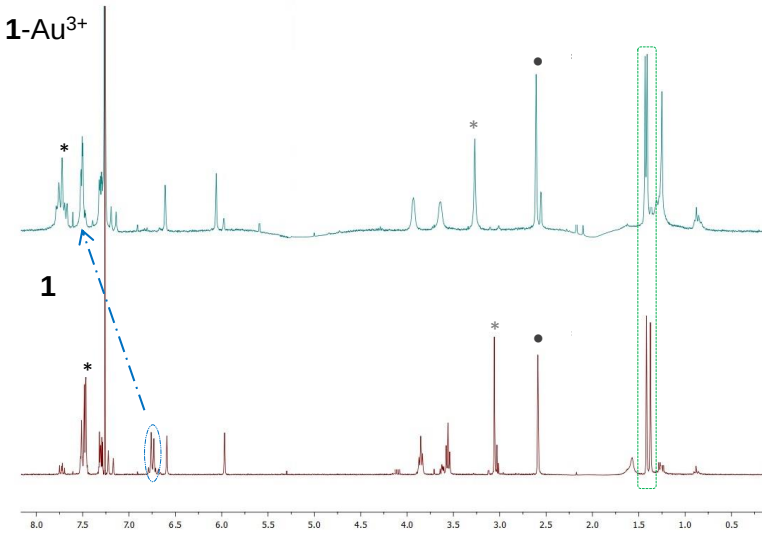

Figure SI-2. ^{1}H-NMR spectra of **1** (in $CDCl_3$) before and after complexation with Au^{3+}.

Structural proposal 1-Eu^{3+} and 1-Au^{3+}: ^{1}H NMR spectra of ligand **1** free and the presence of Eu^{3+} and Au^{3+} were recorded in $CDCl_3$. The most important modifications of the signals of **1** after complexation with Au^{3+} were observed in the phenyl moiety (7.48 and 6.74 ppm) which underwent a significant downfield

shift upon the addition of Eu^{3+} and Au^{3} (0.23 and 0.75 ppm respectively). The change is especially important in the *ortho*-protons to the amino group. On the other hand the methylene groups show a downfield shift around 0.1 ppm. A downfield displacement of 0.20 ppm in the methyl on the amino group is observed. Finally, there were no changes in the protons of the pyrrole units. These data strongly suggest the direct involvement of the amino group in the M^{3+} coordination. Similar behavior was observed for Eu^{3+}.

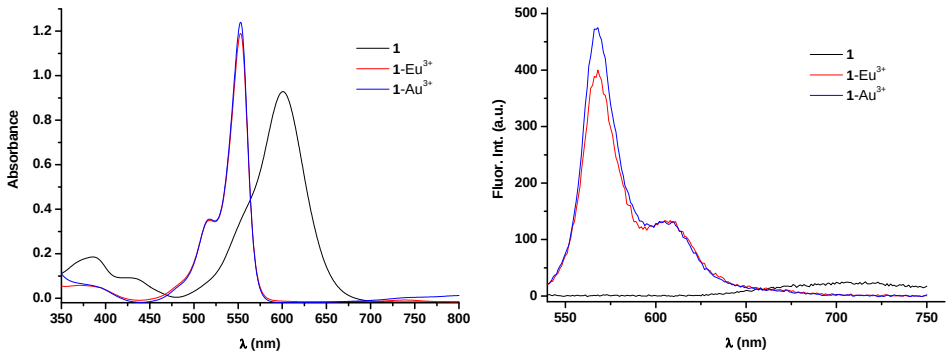

Figure SI-3. Absorption (left) and fluorescence (right) spectra (λ_{ex} = 530 nm) recorded for **1**, **1**-Eu^{3+} and **1**-Au^{3+} (1.0 x 10^{-5} M in CH_3CN).

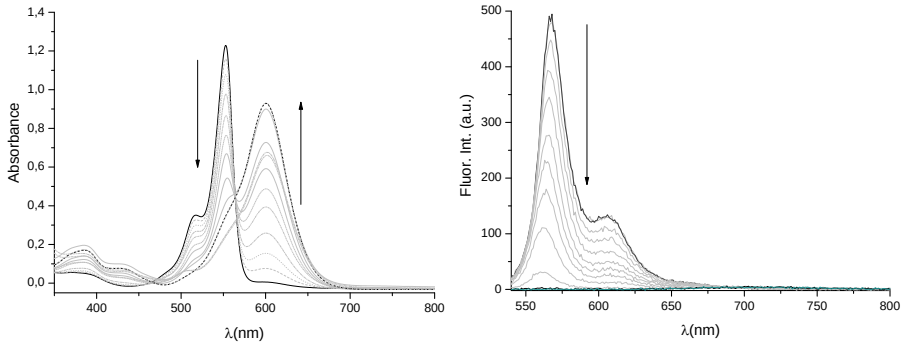

Figure SI-4. Absorption (left) and fluorescence (right) titration (λ_{ex} = 530 nm) of **1**-Au^{3+} (1.0 x 10^{-5} M in CH_3CN) upon addition of incremental amounts of demeton-S (1.0 x 10^{-4} M in CH_3CN).

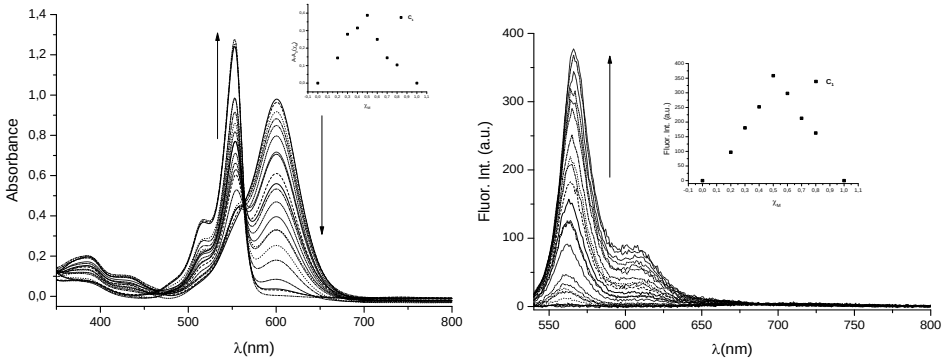

Figure SI-5. Absorption (left) and fluorescence (right) titration (λ_{ex} = 530 nm) of **1** (1.0 x 10^{-5} M in CH_3CN) upon addition of incremental amounts of Eu^{3+} used for association constants calculations. The inset shows the corresponding Job plot´s.

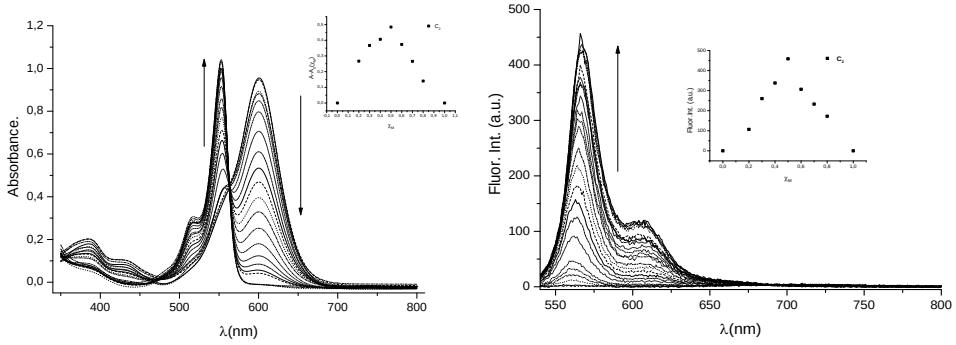

Figure SI-6. Absorption (left) and fluorescence (right) titration (λ_{ex} = 530 nm) of **1** (1.0 x 10^{-5} M in CH_3CN) upon addition of incremental amounts of Au^{3+}, used for association constants calculations. The inset shows the corresponding Job plot´s.

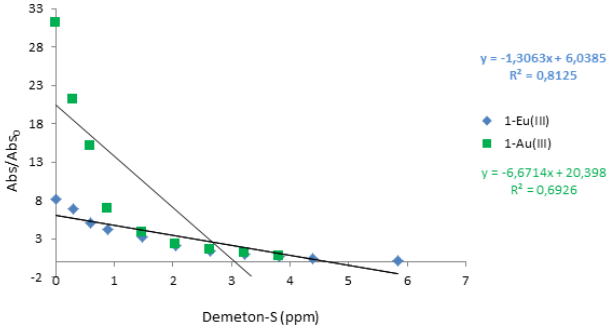

Figure SI-7. Abs/ Abs_0 of **1**-Eu^{3+} and **1**-Au^{3+} (1.0 x 10^{-5}M) versus increasing amounts of demeton-S at room temperature.

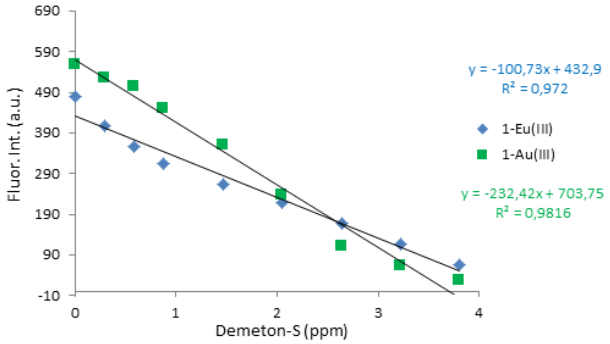

Figure SI-8. Fluorescence Intensity of **1**-Eu^{3+} and **1**-Au^{3+} (1.0 x 10^{-5}M) versus increasing amounts of demeton-S at room temperature.

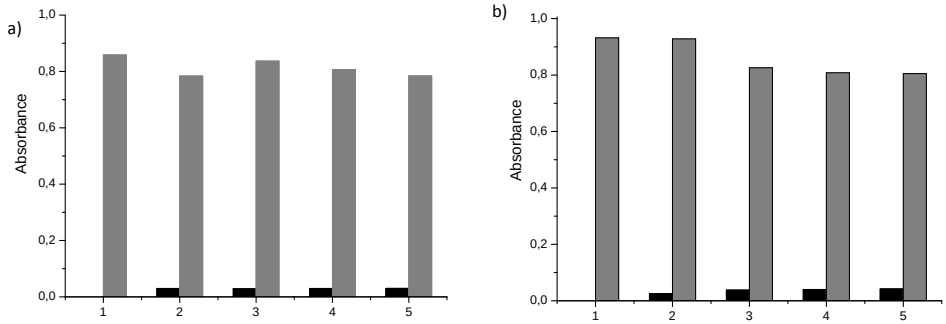

Figure SI- 9: Absorbance (measured at 600.5 nm) of a) **1**-Eu^{3+} and b) **1**-Au^{3+} in the presence of demeton-S and G-type derivatives. The black bars represent the addition of G-type derivatives (200 ppm) to the solution of **1**-M^{3+}. The grey bars represent the subsequent addition of demeton-S (100 ppm) to the above solution. 1-5 represent **1**-M^{3+}, DCNP, DFP, DMMP and DCNP + DFP + DMMP, respectively.

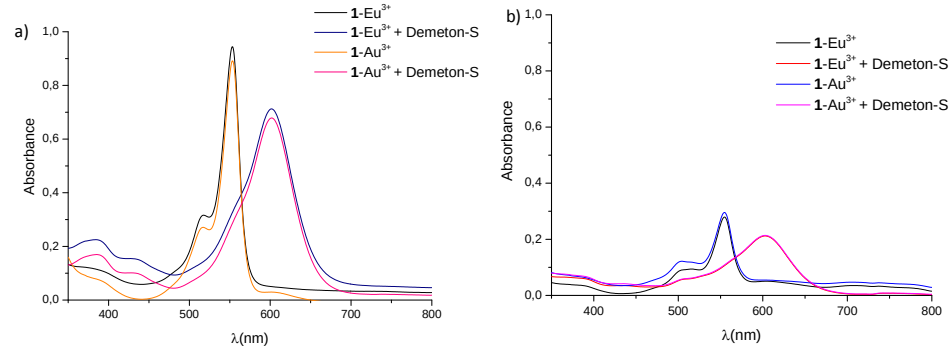

Figure SI-10: Visible spectra of **1**-Eu^{3+} and **1**-Au^{3+} (10^{-5} M) in aqueous mixtures a) H_2O:CH_3CN (10:90 v/v), b) H_2O:CH_3CN (50:50 v/v) alone and in the presence of demeton-S (100 ppm).

References

1 A. Barba-Bon, L. Calabuig, A. M. Costero, S. Gil, R. Martinez-Mañez and F. Sancenon, *RSC Adv*., 2014, **4**, 8962-8965.

2 K. G. Casey and E. L. Quitevis, *J. Phys. Chem.*, 1988, **92**, 6590-6594.

3 P. Didier, G. Ulrich, Y. Mely and R. Ziessel, *Org. Biomol. Chem*., 2009, **7**, 3639-3642.

4 M. Zhu, M. Yuan, X. Liu, J. Xu, J. Lv, C. Huang, H. Liu, Y. Li, S. Wang and D. Zhu, *Org. Lett*., 2008, **10**, 1481-1484.

Chapter 6:

Destruction of Chemical Warfare Agents

6.1 Introduction

The presence of organophosphonates in industrial and agricultural drain waters, spills, runoffs and drifts, as well as OP agent-based chemical munitions that can be released in case of warfare or terrorist attack, pose great risks to human health and environment. Detoxification and decontamination of these agents has been an ongoing priority for decades[1] in order to regain use of the affected area. Considerable work has gone[2] into developing methods to detoxify these highly toxic compounds; in some cases, mere destruction of a chemical agent is

[1] Y. C. Yang, J. A. Baker and J. R. Ward, *Chem. Rev*., **1992**, *92*, 1729-1743. b) B. M. Smith, *Chem. Soc .Rev*., **2008**, 37, 470-478.

[2] a) K. Kim, O. G. Tsay, D. A. Atwood and D. G. Churchill, *Chem. Rev*, **2011**, *111*, 5345-5403. b) D. Ajami and J. Rebek, *Org. Biomol. Chem.,* **2013**, *11,* 3936-3942.

inadequate, since the resulting products could also be highly toxic,[3] and special attention must be paid to ensure that the agent has been effectively detoxified.
Common methods employed for the neutralization/decontamination of OP-warfare agents include: incineration;[4] washes with alkaline and/or hypochlorite solutions;[5] bioremediation;[6] metal-catalyzed/assisted[7] reactions; oxidative degradation on active sorbents[8] … Even these methods destroy OP-agents they also present important shortcomings. For instance, in the case of bioremediation, free or immobilized enzymes are used; one limitation is that the hydrolysis products are acidic and the enzyme activity typically drops dramatically at pH values below about 6. Using hydrolysis catalysts to decontaminate/detoxify relatively large quantities of OP-agents therefore requires a buffer to maintain the pH of the reaction in the neutral to slightly alkaline range. Another practical limitation is the stability of these enzymes; its required cold-chain handling and the extension to pilot-scale or field-scale has scarcely been employed.
Another method for destroying the CWAs which is extremely effective for minimizing the threats inherent to hydrolysis and/or oxidation reactions are the washes with alkaline/hypochlorite solutions, however they unfortunately also promote corrosion and accelerate the degradation of metals and other materials that are commonly found on military assets. Furthermore, the continued use of large amounts of traditional decontamination solutions has the potential to negatively impact the surrounding environment.

Decontamination methods should be efficient, do not damage the surfaces they clean and must be environmental friendly. Thus, catalytic destruction is

[3] a)Y. C. Yang, F. J. Berg, L. L. Szafraniec, W.T. Beaudry, C. A. Bunton and A. Kumar, *J. Chem. Soc., Perkins Trans.2*, **1997**, 607-613. b) A. M. McAnoy, J. Williams, M. R. L. Martin, M. L. Rogers and S. J. Blanksby, *J.Org. Chem*., **2009**, *74*, 9319-9327.
[4] D .M. Laman, B. D. Weller and R. S. Skeen, *Environ. Monit. Assess.,* **2013**, *185*, 2257-2267.
[5] a) P. A. Marrone, S. D. Cantwell and D. W. Walton, *Ind. Eng. Chem. Res*., **2005**, *44*, 9030-9039. b) B. Veriansyah, J. D. Kim and J. C. Lee, *J. Hazard. Mater.,* **2007**, *147*, 8-14.
[6] a) A. J. Russell, M. Erbeldinger, J. J. DeFrank, J. Kaar and G. Drevon, *Biotechnol. Bioeng.,* **2002**, *77*, 352–357. b) B. K. Singh and A. Walker, *Microbiol. Rev*., **2006**, *30*,428–471
[7] a) L. Y. Kuo, A. P. Blum and M. Sabat*, Inorg. Chem.,* **2005***, 44*, 5537-5541. b) T. Andrea, A. A. Neverov and R. S. Brown, *Ind. Eng. Chem. Res*.,**2010,** *49*, 7027-7033.
[8] D. M. Mizrahi, S. Saphier, I. Columbus, *J. Hazard. Mat.,* **2010***, 179,* 495-499.

appropriate for hydrolysis/decomposition of OP-warfare agents. In this chapter we focused in the use of supramolecular-based organocatalysts to the hydrolysis of nerve agents. This method offer the possibility of use controlled amounts of compounds currently available that are inexpensive and friendly to the environment, that eventually could be readily dispersed in an aqueous medium.

6.2 Objectives

Because of the potential danger of chemical-warfare attacks we aim to study the use of supramolecular-based organocatalysts for the decontamination/hydrolysis of G-nerve agent mimics.

Particularly, our purposes were:

- ✓ Synthesis of a family of 1,3-Diindolylureas and thioureas able to coordinate phosphate derivatives.
- ✓ Select a family of amines and amino-containing derivatives for nerve agent remediation.
- ✓ Verify the interaction of selected organocatalysts with the G-nerve agent mimics by a usual technique (Nuclear Magnetic Resonance).
- ✓ Estimate the hydrolyzing abilities of set compounds in presence of G-nerve agent mimics at differences temperatures.
- ✓ Elucidate the catalytic cycles involved in the hydrolysis of different catalysts.
- ✓ Identify the hydrolysis products.

6.3 Neutral 1,3-Diindolylureas for Nerve Agent Remediation.

Neutral 1,3-Diindolylureas for Nerve Agent Remediation

Andrea Barba-Bon,[ab] Ana M.Costero,[a] Margarita Parra,[a] Salvador Gil,[a] Ramón Martínez-Máñez,[b] Félix Sancenón,[b] Philip A. Gale[c] and Jennifer R. Hiscock[c].

[a] Centro de Reconocimiento Molecular y Desarrollo Tecnológico (IDM), Unidad Mixta Universidad Politécnica de Valencia-Universidad de Valencia, Universidad de Valencia, Dr. Moliner, 50, 46100 Burjassot ,Valencia, (Spain).

[b] Centro de Reconocimiento Molecular y Desarrollo Tecnológico (IDM), Unidad Mixta Universidad Politécnica de Valencia-Universidad de Valencia, Departamento de Química and CIBER de Bioingeniería Biomateriales y Nanomedicina (CIBER-BBN),Universidad Politécnica de Valencia, Camino de Vera s/n, 46022 Valencia,(Spain).

[c] Chemistry, University of Southampton, Southampton SO17 1BJ (UK).

Received: *7 th June 2012*

Published online: *23 th December 2012*

Chem. Eur.J., ***2013****, 19, 1586-1590.*

Nerve gases are a class of warfare agent. Chemically, they can be described as organophosphonates that contain good leaving groups. These compounds are highly toxic to both humans and animals by inhibition of acetylcholinesterase.[1] As chemical weapons; they are classified as weapons of mass destruction by the United Nations. Even though production and stockpiling of these agents was outlawed by the Chemical Weapons Convention of 1993, their use in terrorist attacks makes the development of new sensing systems and the design of new remediation products of prime importance.[2] In relation to the latter, there has been an increased interest in the chemistry of nerve agents and in the development of methods of neutralization of these chemicals. Stockpiles of nerve agents should be destroyed and the safety as well as the environmental impact of the destruction process is of crucial concern. Remediation procedures involve the conversion of nerve agents to less toxic products. Examples under development include nerve-agent oxidation through the use of supercritical water,[3] caustic bleaching, incineration and bioremediation.[4] However these procedures show certain limitations. For instance, supercritical water has proved effective in oxidizing organophosphorous-based nerve agents. However, this procedure is associated with high energy costs. The use of bleach requires solubilization of nerve agents in large quantities of solvent, which must be dealt with later in the process. In the case of bioremediation, free or immobilized enzymes are used. But the stability of these enzymes requires a cold-chain handling and the extension of small lab-scale procedures to pilot-scale or field-scale procedures has not been widely employed. This makes high-temperature incineration the only currently approved technique for the destruction of stored nerve agents. Therefore efforts to develop new remediation methods are under investigation[5] and chemical processes that can effectively detoxify stored nerve agents are in great demand. Alternative approaches tested involve the use of catalysts able to enhance the hydrolysis of nerve agents. Even though some metal-catalyzed hydrolysis strategies have been developed[6] examples of organocatalysts in this context are very rare and include, for instance, iodosylcarboxylates promoting the hydrolysis of G-series nerve agents.[7]

Taking the above issues into account, and as a part of our interest in these chemicals, it was in our aim to test the possible use of supramolecular interactions as a route to the design of supramolecular-based organocatalysts for nerve agent remediation. In fact, host-guest chemistry has already found many applications in catalysis[8] and the construction of catalysts by supramolecular forces has recently become a powerful tool.[9] In particular, we wanted to study the use of supramolecular receptors for organophosphorus derivatives that may enhance the hydrolysis rate of these compounds through a suitable combination of coordinative forces and enhancement of the electrophilic character of the phosphorus atom. As a proof-of-concept we report herein the catalytic remediation effect of a family of 1,3-diindolylureas and thioureas (compounds **1**-**4**, see Figure 1) as potential receptors for nerve agents destruction.

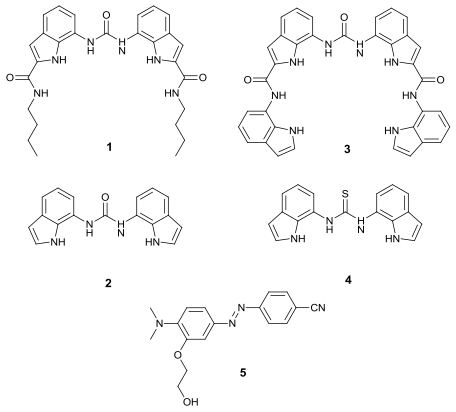

Figure 1. Catalysts **1**-**4** used for nerve-agent destruction and structure of indicator **5**.

The choice of neutral 1,3-diindolylureas and thioureas was based in their known properties to selectively coordinate phosphate anions in polar solvent mixtures and in the solid state through NH···O hydrogen-bonding interactions.[10] We expected that the corresponding formation of complexes with nerve agents might lead to an enhanced polarization of the P=O bond, which might result in an enhancement of the rate of hydrolysis. In fact, while this research was under development, the interaction between 1,3-diindolylureas and the nerve-agent Soman was demonstrated.[11] However, studies on the possible use of this

interactions in remediation has not been explored. Remediation studies have been carried out here with the safer-to-handle simulants diethylchlorophosphate (DCP) and diethylcyanophosphonate (DCNP, Figure 2). These compounds have similar reactivity, but reduced toxicity compared with the corresponding chemical warfare agents Sarin, Soman and Tabun.

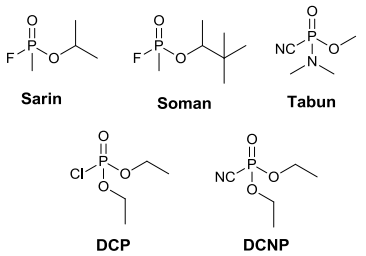

Figure 2. Chemical structures of nerve agents and the simulants DCP and DCNP.

As a first step, ^{1}H NMR experiments were carried out to verify the formation of complexes between the receptors and the simulants. Studies in [D_6]acetone with receptors **1**-**4** and DCNP clearly demonstrated the existence of interactions. This was reflected in shifts of the NH resonances of the urea and indole groups and of the CH resonance at the C6 position of the indole when **1-4** were mixed with DCNP. Figure 3 shows the aromatic region of the NMR spectra corresponding to ligands **1** and **4 (**see the Supporting Information for spectra of compounds **2** and **3**). Titration experiments demonstrated that under these conditions 1:2 and 1:1 (receptor/DCNP) complexes were formed with receptors **1** and **3** or **2** and **4**, respectively (see Figure 4). Considering these stoichiometries and by using the software package WinEQNMR[12] the corresponding association constants were determined (see Table 1).

Table 1. Stoichiometry and association constants of compounds **1**-**4** with DCNP in [D_6]acetone.

Compound	Complex stoichiometry	Association Constant
1	1:2	881±90
2	1:1	4.4±0.3
3	1:2	1743±35
4	1:1	10.1±0.9

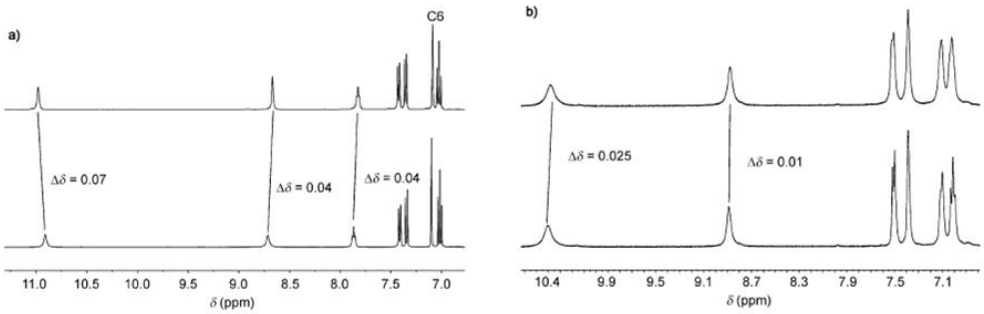

Figure 3. a) ^{1}H NMR (aromatic region) in [D_6]acetone corresponding to free compound **1**(bottom) and compound **1** in the presence of 2 equivalents of DCNP (top). b) ^{1}H NMR (aromatic region) corresponding to free compound **4** (bottom) and compound **4** in the presence of 1 equivalent of DCNP (top).

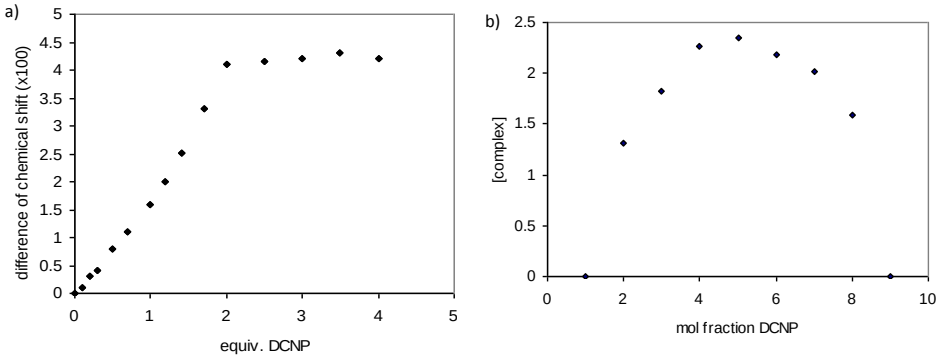

Figure 4. a) ^{1}H NMR tritiation binding curve for compound **1** plus DCNP in [D_6]acetone for which $[\mathbf{1}]_{initial}$ = 5.80 x 10^{-2}M; 293 K. b) Job plot for the DCNP-**4** system in [D_6]acetone for which [**4**]+[DCNP] = 4.23 x 10^{-2}M; 293K.

The stability constants revealed a clear relation between the number of possible interactions for each receptor, the stoichiometry of the complexes, and the strength of the interaction. For instance, for receptors **1** and **3**, which have a larger number of binding sites, the formation of 1:2 (receptor/DCNP) complexes was favoured, whereas receptors **2** and **4**, with a lower number of coordination sites, were only able to form 1:1 species. Moreover, as expected **1** and **3** showed larger association constants with DCNP than **2** and **4**. In addition when the coordination constant of DCNP with **1** was compared with that of **3**, the latter was

to a greater extent due to the presence of more NH groups. Additionally the higher value of the stability constant determined for **4** compared with **2** can be attributed to the presence of more acidic protons in the thiourea group in **4** than for the same moiety in **2**. In addition, we also tested the interaction of receptor **4** and DCNP as model simulant in [D_6]acetone/D_2O (85:15), which is similar to the medium in which the hydrolysis experiments were carried out (see below). In particular, NMR studies in this solvent mixture clearly demonstrated that formation of complexes still occurred in this competitive medium (see the Supporting Information).

After the demonstration of the formation of complexes of **1**-**4** with DCNP, remediation experiments were carried out in buffered acetone/water (80:20 v/v) solutions. A potential problem with hydrolysis of these agents is that they can form particles that might, to some extent, protect them from hydrolysis and may complicate the analysis of the results. Therefore light-scattering studies in the presence and absence of compounds **1**-**4** were performed, however no formation of such particles was observed under the conditions used in this study.

The detection of the hydrolysis of nerve-gas simulants (DCP or DCNP) in the presence of the corresponding organocatalysts (**1-4**) was based on detecting acid generated upon hydrolysis of the simulant with an appropriate indicator.[13] When the hydrolyzed simulant generates enough protons to outstrip the levelling effect of the buffer, indicator **5** (2(E)-5-(2-(4-cyanophenyl)diazenyl)2-(dimethylamino)phenoxy)ethanol), Figure 1) changes the colour of the solution from yellow to colourless. These color changes were detected with the naked-eye. Control UV and ^{1}H NMR experiments demonstrated that there was no interaction between the indicator and compounds **1**-**4**.

In a typical experiment, two series of samples (3 mL each) of indicator **5** (10^{-5} M in 1:3 v/v acetonitrile/2-morpholinoethanesulfonic acid MES (10^{-1} M) solution at pH = 5.6) were used. In addition two DCNP (or DCP) solutions were also prepared. An uncatalyzed solution contained 10% (v/v) DCNP (or 5% (v/v) DCP) in acetone/water (80:20 v/v), whereas the analogous catalysed solution, had the corresponding catalyst plus 10% (v/v) of DCNP (or 5% (v/v) DCP) in acetone/water (80:20 v/v). The time at which these solutions were prepared was noted and

considered t = 0. The temperature during these experiments was maintained at 25°C. At regular intervals (1 minute), uncatalyzed and catalyzed solutions (100 µL) were added to the corresponding indicator solutions and the color was observed. Changes in color for the different aliquots could eventually be related to the hydrolysis of the nerve-gas simulants. Although this procedure does not allow determination of the absolute hydrolysis rate, it permits calculation of the enhancement in the hydrolysis for the catalyzed reaction in relation to the uncatalyzed one. The variation of the simulant hydrolysis rate was determined as $\Delta\upsilon$=100-[(υ_{cat} x 100)/υ_{uncat}] for which υ is the time at which the color change occurred. Studies were performed with two different concentrations of catalysts (0.001 and 0.005 equiv.). The results are summarized in Table 2.

Table 2. Variation of the hydrolysis rate of the simulants DCP and DCNP in acetone/water (80:20 v/v) in the presence of organocatalysts **1-4**. Data is given as the percentage of enhancement of the hydrolysis rate compared with the hydrolysis of the simulants in the absence of catalyts.

	0.001eq[a]		0.005eq[a]	
Catalyst	**DCP**	**DCNP**	**DCP**	**DCNP**
1	44.6 ± 0.4%	17 ± 2%	30 ± 1%	6.3 ± 0.2%
2	13 ± 1%	6.4 ± 0.3%	14.8 ± 0.2%	6.3 ± 0.4%
3	27 ± 2%	19.5 ±0 .6%	29.5± 0.5%	6.4 ± 0.2%
4	9.8 ± 0.5%	6.7 ± 0.3%	12.7 ± 0.2%	11.3 ± 0.4%

[a] catalyst equivalents *vs.* simulants

The data clearly show that there is an enhancement in the hydrolysis rate of the nerve-agent simulants in the presence of the corresponding supramolecular organocatalysts. Additional conclusions can also be drawn from these data. For instance, for all four catalysts, the enhancement in the rate for DCP hydrolysis was higher than that for DCNP. These results are most likely related to the fact that Cl^- is a better leaving group than CN^-. In addition, it can be also concluded that the catalytic effect was higher when there were a larger number of hydrogen-bond donors present in the receptor. Thus, **1** and **3** catalyzed the hydrolysis more effectively than **2** and **4**. These data strongly supports the hypothesis that the

catalytic mechanism includes simulant complexation by increasing the electrophilic character of the P atom and enhancing the final nucleophilic attack of water, which results in the formation of the corresponding organo-phosphate derivative and HCl or HCN. After hydrolysis, the new generated species, which are less hydrophobic, are released from the catalyst, which is now able to start the catalytic process again. This influence of the hydrophobic effect in the binding site can be also observed if we compare the results obtained with receptors **1** and **3**. Thus, even though **3** showed higher association constants than **1,** its catalytic effect was poorer due to its lower hydrophobic character in the catalytic centre. Moreover, the presence of 1:2 complexes in **1** and **3** may also favor the existence of some autocatalytic mechanisms similar to those shown in hydrolysis studies with V-type nerve agents.[14] This suggestion is supported by the experiments carried out at different concentrations. Thus, experiments at other concentrations (from 0.0005 to 0.01 equiv of catalyst) showed that the increase in the catalyst concentration did not always lead to better results and, in some cases, lower hydrolysis rates were observed. This effect was more pronounced with **1** and **3** for which a larger amount of receptor would give rise to lower concentrations of the 1:2 complexes and as a consequence the autocatalytic effect decreases. With receptors **2** and **4,** which form 1:1 complexes this effect was not observed (see the Supporting Information).

Finally, the influence of the temperature was also considered and studies with receptor **1** and DCNP were carried out to monitor the hydrolysis enhancement from 10 to 50 ^{o}C. An increase in the hydrolysis rate was observed. However a similar increase of the hydrolysis was also found in the corresponding uncatalyzed samples (see the Supporting Information).

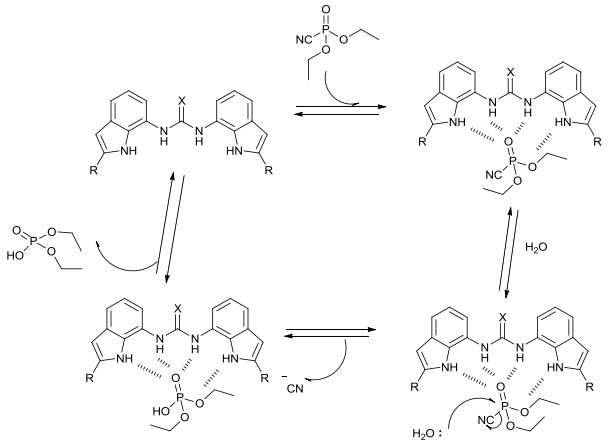

Scheme 1. The proposed catalytic cycle involving catalysts **1**-**4** and DCNP. The cycle involves 1) complexation or the nerve-gas simulants with catalysts **1**-**4,** 2) enhancement of the electrophilic character of the P atom due to coordination, 3) nucleophilic attack of water, and 4) formation of the corresponding less toxic organo-phosphate derivative.

In conclusion, we have observed that neutral 1,3-diindolylureas and thioureas (**1-4**) are useful supramolecular organo-catalysts in remediation of nerve-agent simulants. To the best of our knowledge, this is the first time that supramolecular-based organocatalysts have shown catalytic effect in remediation processes for nerve agents, such as organo-phosphorus derivatives. In addition this method shows several advantages compared with other previously described procedures for the elimination of organophosphorus hazards (see the Supporting Information). An enhancement of the hydrolysis rate up to near 45% in some cases was observed in the presence of submolar concentrations of the receptors. The formation of complexes between the receptors and DCP and DCNP suggests that the catalytic mechanism involves complexation or the nerve-gas simulants in a hydrophobic environment provided by the receptors, enhancement of the electrophilic character of the P atom, and the final nucleophilic attack of water that results in the formation of the corresponding less toxic organophosphate derivatives (see Scheme 1). Moreover our findings suggest that other hydrogen-bond-donor derivatives that are able form complexes with organophosphorus compounds can also enhance the hydrolysis rate of these hazardous compounds. By considering the large number of hydrogen-bond-donor derivatives known in

the supramolecular field, this observation opens new routes towards the possibility of designing other organocatalysts based on supramolecular coordinative concepts for new effective remediation procedures of nerve agents.

Acknowledgements

DGICYT (projects MAT2009-14564-C04-1 and MAT2009-14564-C04-3) and Generalitat Valenciana (project PROMETEO/2009/016) are gratefully acknowledged. A.B.B. thanks MICINN for a pre-doctoral FPI fellowship. SCSIE (Universidad de Valencia) is gratefully acknowledged for all the equipment employed. PAG thanks the University of Southampton for a post-doctoral fellowship (JRH).

Keywords: remediation • nerve agents • diindolylureas • catalyst • complexation

References

1 S. M. Somani, Chemical Warfare Agents, Acadenic Press, San Diego, **1992**. Nerve Agents, A FOA Briefing Book on Chemical Weapons, **1992**, (from www.fas.org/cw/cwagents).

2 (a)K. Kim, O. G. Tsay, D. A. Atwood and D. G. Churchill, *Chem*. *Rev.*, **2011**, *111*, 5345-5403;(b) B. M. Smith, *Chem. Soc. Rev*. **2008**, *37*, 470-478.

3 B. Veriansyah, J.-D. Kim and J.-C. Lee**,** *J. Hazard. Mater*. **2007**, *147*, 8-14.

4 (a)R.M. Dawsona, S. Pantelidis , H.R. Rose and S.E. Kotsonis, *J. Hazard. Mater*. **2008**, *157,* 308-314; (b) L. Briseno-Roa, J. Hill, S. Notman, D. Sellers, A.P. Smith, C.M. Timperley, J. Wetherell, N.H. Williams, G.R. Williams, A.R. Fersht and A.D. Griffiths, *J. Med. Chem*. **2006**, *49* 246-255; (c) E. Ghanem and F. M. Raushel, *Toxicol. Appl. Pharmacol*. **2005**, *207*, S459-S470.

5 (a) P. Vayron, P-Y. Renard, A. Valleix and C. Mioskowski, *Chem. Eur. J.***2000**, *6*, 1050-1063; (b) G. Saint-André, M. Kliachyna, S. Kodepelly, L. Louise-Leriche, E. Gillon, P-Y. Renard, F. Nachon, R. Baati and A. Wagner, *Tetrahedron* **2011**, *67*, 6352-;6361.; (c) Y. Zafrani, L. Yehezkel, M. Goldvaser, D. Marciano, D. Waysbort, E. Gershonov and I. Columbus, *Org. Biomol. Chem*.**2011,** *9*, 8445-8451.

6 (a) R. A. Kenley, R. H. Fleming, R. M. Laine, D. S. Tse and J. S.Winterle. *Inorg. Chem*. **1984**, *23*, 1870-1876; (b) J. R. Ward, L. L. Szafraniec, W. T. Beaudry and J. W. Hovanec, *J. Mol. Catal*. **1990**, *58,* 373-378; (c) R. S. Brown and M. Zamkanei, *Inorg. Chim. Acta***1985**, *108*, 201; P. R. Norman, A. Tate and P. Rich, *Inorg. Chim. Acta* **1988**, *145*,

211-217; (d) R. W. Hay and N. Govan, *Transition Met. Chem*. **1998**, *23*, 133-138; € Y. Xie and B. N. Popov, *Anal. Chem*. **2000**, *72*, 2075-2079.

7 H. Morales-Rojas and R. A. Moss, *Chem Rev*. **2002**, *102*, 2497-2521.

8 Supramolecular Catalysis, Ed. Piet W. N. H. van Leeuwen, Wiley-Springer Verlag GmbH &Co. **1998**.

9 P. Ballester, A. Vidal-Ferran, P. W. N. H. Van Leeuwen, *Adv. Catal*. **2011**, *54*, 63-126.

10 (a) C. Caltagirone, P. A. Gale, J. R. Hiscock, S. J. Brooks, M. B. Hursthouse and M. E. Light, *Chem. Comm*. **2008**, 3007-3009; (b) C. Caltagirone, J. R. Hiscock, M. B. Hursthouse M. E. Light and P. A. Gale, *Chem. Eur. J*. **2008**, ***14***, 10236-10243; (c) P.A. Gale, J.R. Hiscock, C. Z. Jie, M.B. Hursthouse, and M.E. Light, *Chem. Sci.,***2010**, *1*, 215-220; (d) P.A. Gale, J.R. Hiscock, S.J. Moore, C. Caltagirone, M.B. Hursthouse and M.E. Light, *Chem. Asian J.* **2010**, *5,* 555-561; (e) D. Makuc, J. R. Hiscock, P. A. Gale and J. Plavec, *BJOC*. **2011**, *7*, 1205-1214.

11 M. R. Sambrook, J. R. Hiscock, A. Cook, A. C. Green, I. Holden, J. C. Vicent and P. A. Gale, *Chem. Comm*. **2012**, *48*, 5605-5607.

12 M. J. Hynes*, J. Chem. Soc., Dalton Trans*. **1993**, *2*, 311-312.

13 (a) B. J.Jandorf, T. Wagner-Jauregg, J. J. O´Neill and M. A. Stolberg,*J.Am.Chem.Soc,* **1952**,*74*, 1521-1523; (b) R . Gustafson and A. E. Martel, *J. Am. Chem. Soc*. **1962**, *84,* 2309-2316.

14 Y-C. Yang, L. L. Szafraniec, W. T. Beaudry, D. K. Rohrbaugh, L. R. Procell and J. B. Samuel, *J. Org. Chem*.**1996**, *61*, 8407-8413.

Supporting Information

Neutral 1,3-Diindolylureas for Nerve Agent Remediation

Andrea Barba-Bon, Ana M.Costero, Margarita Parra,
Salvador Gil, Ramón Martínez-Máñez,
Félix Sancenón, Philip A. Gale and Jennifer R. Hiscock.

General remarks

CH_3CN was distilled from P_2O_5 under Ar prior to use. THF was distilled from Na/benzophenone under Ar prior to use. All other solvents and starting materials were purchased from commercial sources where available, and were used without purification. ^{1}H NMR (300 MHz) spectra were determined on a Bruker AV 300 spectrometer. Chemical shifts are reported in parts per million (ppm), calibrated to the solvent peak set. Ultraviolet (UV) spectra were recorded on a Shimadzu UV-2101P1 using a 1cm path length quartz cuvette.

^{1}H NMR spectroscopic titrations

A Bruker AV 400 NMR spectrometer was used to measure the ^{1}H NMR shifts of the NH, protons of the catalysts. NMR titrations were performed by adding aliquots of DCNP in a solution of the catalyst in d_6-acetone. The titration data were plotted as Δppm versus concentration of guest and fitted to a binding model using the WinEQNMR computer program.

Synthesis of indicator 5:

2-(N,N-dimethylamino)phenol. 2-Nitrophenol (2.68 g, 19.3 mmol), formaldehyde (3.54 mL, 42.46 mmol, 36%), and Pd/C (480 mg, 10%) were dissolved in absolute ethanol (43 mL), and placed under an H_2 atmosphere until uptake of hydrogen ceased. After filtration through celite, the solvent was evaporated, and the product was purified by sublimation at 155°C to give 2-(*N*,*N*-dimethylamino)phenol (1.81g, 69%) as a white solid. ^{1}H NMR (300 MHz, $CDCl_3$): *δ* 7.10 (dd, *J*=7.8 Hz, 1.5 Hz, 1H), 6.96 (dt, *J*=7.7 Hz, 1.5 Hz, 1 H), 6.88 (dd, *J*=8.07 Hz, 1.49 Hz, 1H), 6.76 (dt, *J*=7.55 Hz, 1.55 Hz, 1H), 6.58 (s, 1H), 2.59 ppm (s, 6H); ^{13}C NMR (75 MHz, $CDCl_3$): δ 151.46, 140.58, 125.96, 120.64, 120.02, 114.14, 45.07 ppm.

2-(2-Dimethylaminophenoxy) acetate. A mixture of 2-(*N,N*-dimethylamino) phenol (1.81 g, 13.2 mmol), ethylbromoacetate (1.50 mL, 13.2 mmol, 98%), and cesium carbonate (12.9 g, 39.6 mmol) in acetonitrile (100 mL) was refluxed overnight. The volatile materials were removed by concentration on a rotary evaporator, and the

residue was partitioned between water (100 mL) and EtOAc (100 mL). The organic layer was separated, and the aqueous layer was extracted with EtOAc (2 x 100 mL). The combined organic extracts were dried over anhydrous magnesium sulphate, filtered, and concentrated to give the title compound (2.54 g, 86%) as a brown oil. ^{1}H NMR (300 MHz, $CDCl_3$): δ 6.96–6.76 (m, 3H), 6.70–6.66 (m, 1H), 4.61 (s, 1 H), 4.17 (q, *J*=7.1 Hz, 2 H), 2.75 (s, 6H), 1.20 ppm (t, *J*=7.1 Hz, 3H); ^{13}C NMR (75 MHz, $CDCl_3$): δ 169.06, 150.37, 142.87, 122.6, 122.5, 118.49, 113.08, 65.9, 61.19, 43.19, 14.13 ppm.

Ethyl 2-[(E)-5-(2-(4-cyanophenyl) diazenyl)-2(dimethylamino) phenoxy]- acetate. 4-Aminobenzonitrile (0.230 g, 1.91 mmol, 98%), concentrated sulfuric acid (0.5 mL, 9.2 mmol), and water (10 mL) were stirred and slightly heated until the 4-aminobenzonitrile was completely dissolved. The mixture was placed in an ice bath (0–5 °C) for 10 min, and then, a solution of $NaNO_2$ (0.132 g, 1.91 mmol) in water (5 mL) was added dropwise. After stirring for an additional 10 min at 0–5 °C, a solution of ethyl 2-(2-dimethylaminophenoxy) acetate (0.425 g, 1.91 mmol) in ethanol (20 mL) was added dropwise during 30 min. The resulting red solution was stirred for 30 min in an ice bath, and another 30 min at room temperature. Then, the resulting solution was neutralized with potassium acetate. The mixture was extracted with CH_2Cl_2. The product was purified by column chromatography with silica gel using hexane/ethyl acetate (8/2, v/v) as eluent. The final pure product (0.19 g, 27%) was isolated as an orange powder. ^{1}H NMR (300 MHz, $CDCl_3$): δ 7.81 (d, *J*=8.78 Hz, 2H), 7.68 (d, *J*=8.78 Hz, 2H), 7.58 (dd, *J*=8.5 Hz, 2.1 Hz, 1 H), 7.30 (d, *J*=2.1 Hz, 1H), 6.89 (d, *J*=8.5 Hz, 1 H), 4.68 (t, *J*=6.9 Hz, 2H), 4.22 (q, *J*=7.1 Hz, 2 H), 2.96 (s, 6 H), 1.24 ppm (t, *J*=7.1 Hz, 3H); ^{13}C NMR (75 MHz, $CDCl_3$): δ 168.8, 155.3, 150.0, 147.2, 147.21, 133.5, 123.7, 123.3, 119.15, 117.2, 113.1, 104.0, 65.9, 61.8, 43.2, 14.6 ppm.

*2-[(E)-5-(2-(4-cyanophenyl)diazenyl)-2 dimethylaminophenoxy] ethanol (**6**).* To a solution of ethyl 2-[(E)-5-(2-(4-cyanophenyl) diazenyl)-2-(dimethylamino) phenoxy]-acetate (0.064 g, 0.182 mmol) in dry THF (20 mL), $LiAlH_4$ (2 M) in THF (155 mL, 0.31 mmol) was slowly added at 0 °C. The reaction was then stirred at

0°C for 1 h, warmed to room temperature, stirred for another hour, and then water (1 mL) was carefully added. The mixture was stirred for 2 h, and the precipitate was filtered off, and washed with THF (40 mL). The combined organic solutions were dried with $MgSO_4$, filtered, and evaporated. The product was purified by column chromatography with aluminium oxide using dichloromethane as solvent to give the final compound (0.044 g, 79%) as an orange powder. ^{1}H NMR (300 MHz, $CDCl_3$): δ 7.85 (d, *J*=8.7 Hz, 2H), 7.70 (d, *J*= 8.7 Hz, 2H), 7.59 (dd, *J*=8.5 Hz, 2.2 Hz, 1H), 7.44 (d, *J*=2.2 Hz, 1H), 6.95 (d, *J*=8.5 Hz, 1 H), 4.20 (t, *J*=4.42 Hz, 2 H), 3.92 (t, *J*=4.42 Hz, 2H), 2.89 (s, 6H) ppm; ^{13}C NMR (75 MHz, $CDCl_3$): δ 155.3, 151.6, 148.0, 147.6, 133.5, 123.4, 123.1, 119.1, 117.7, 113.4, 106.1, 72.0, 61.5, 43.5 ppm; HRMS (EI): m/z (%) calc for $C_{17}H_{19}N_4O_2$: 311.1508 $[M+1]^+$; found: 311.1511.

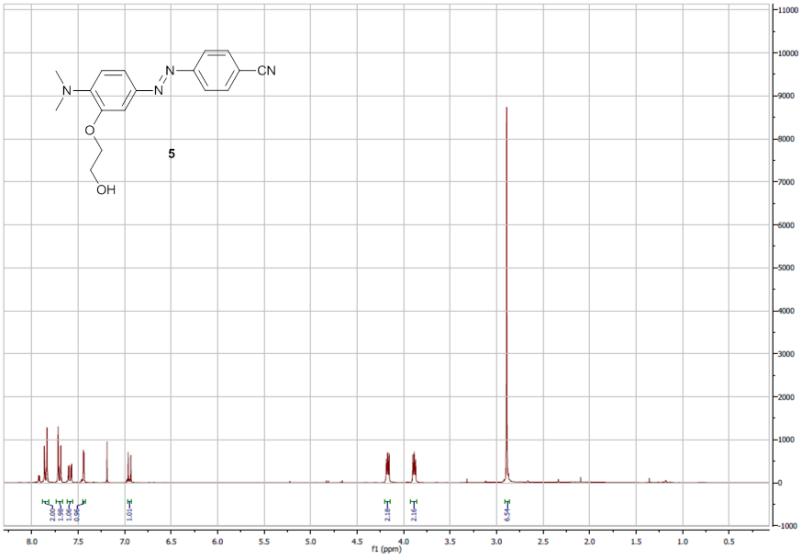

Figure SI-1. ^{1}H NMR spectrum of compound **5** in $CDCl_3$.

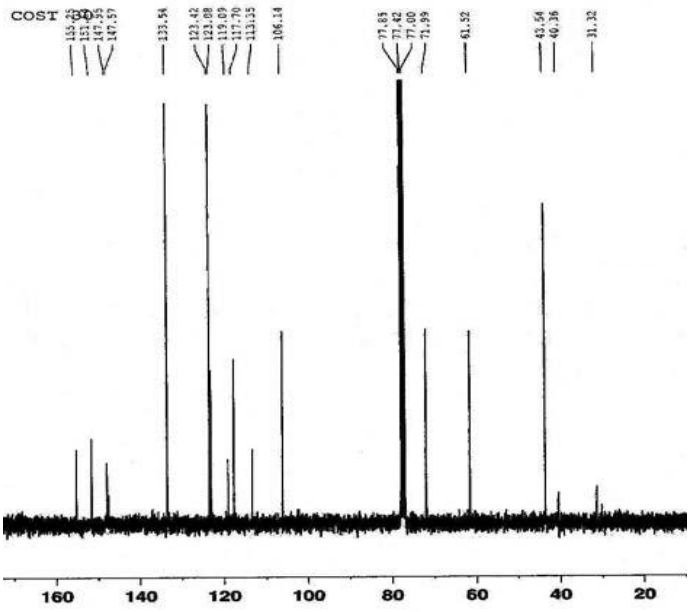

Figure SI-2. ^{13}C NMR spectrum of compound **6** in $CDCl_3$.

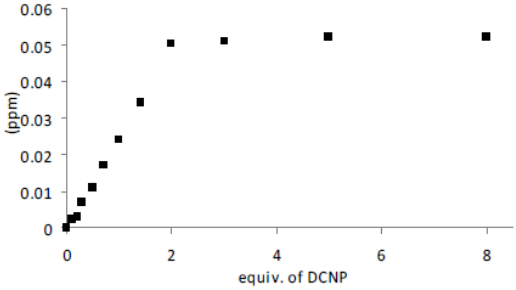

Figure SI-3. ^{1}H NMR titration binding curve for compound **3** plus DCNP in d_6-acetone where y=Δδ for proton at 8.6 ppm at 293 K.

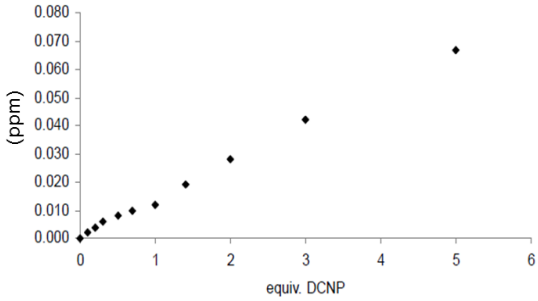

Figure SI-4.^{1}H NMR titration binding curve for compound **2** plus DCNP in d_6-acetone where y= Δδ for proton at 10.5 ppm at 293 K.

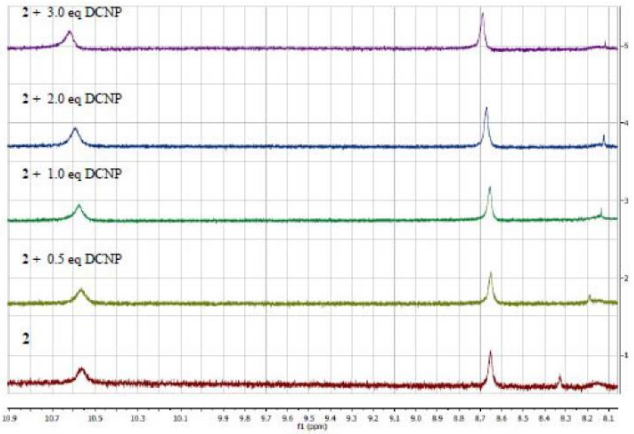

Figure SI-5. ^{1}H NMR titration of compound **2** with DCNP in d_6-acetone.

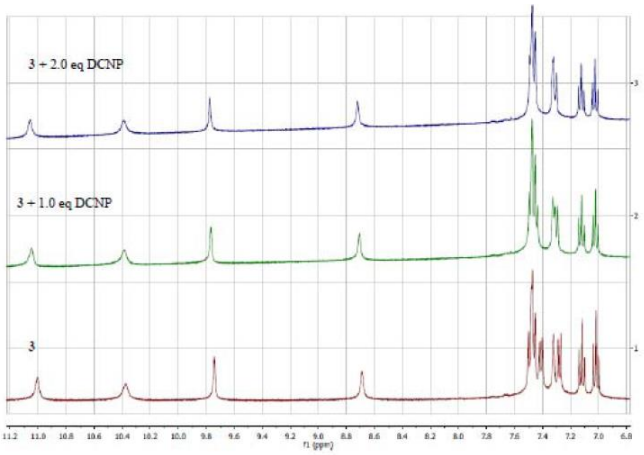

Figure SI-6. ^{1}H NMR titration of compound **3** with DCNP in d_6-acetone.

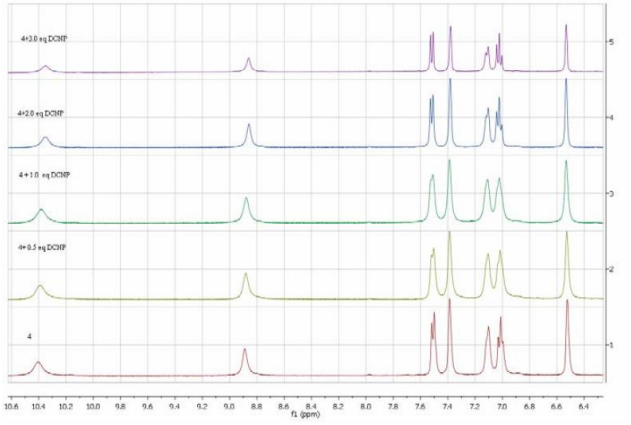

Figure SI-7.^{1}H NMR titration of compound **4** with DCNP in d_6-acetone.

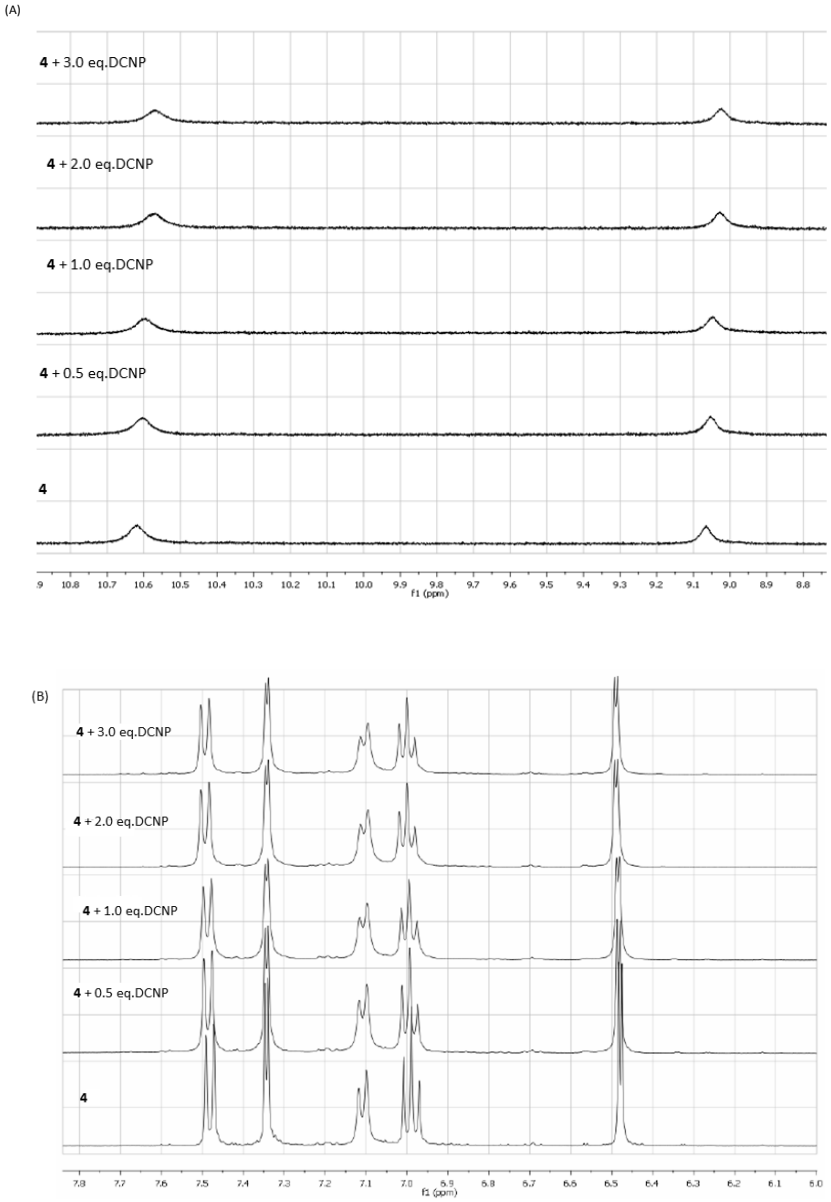

Figure SI-8. ^{1}H NMR titration of compound **4** with DCNP in d_6-acetone/D_2O (85/15). (A) N-H zone and (B) aromatic zone.

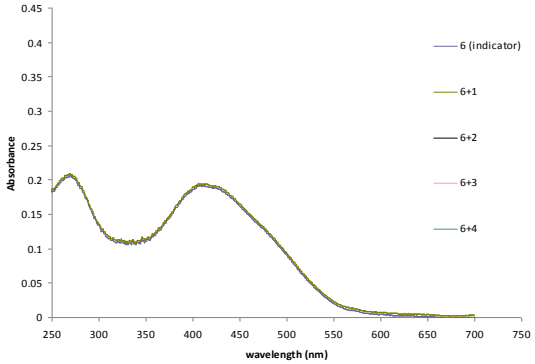

Figure SI-9. UV spectrum of indicator **5** with catalyst **1**-**4**. (10^{-5} M CH_3CN:MES 1:3 pH= 5.60).

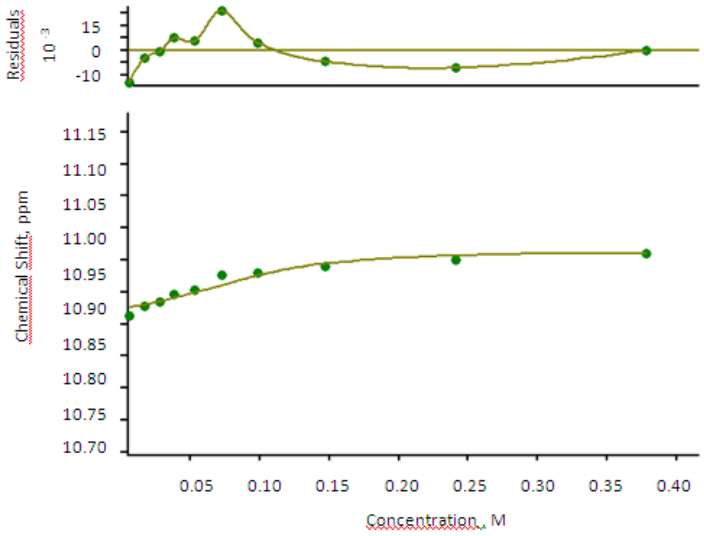

Calculations by WinEQNMR2 Version 2.00 by Michael J. Hynes

Program run at 16:28:27 on 05/17/2012

DCNP-G-1

Reaction of DCNP con G-1

NO.	A	PARAMETER	DELTA	ERROR	CONDITION	DESCRIPTION
1	1		8.81239E+02	1.000E-02	9.061E+01	1.341E+00 K
2	1	1.09252E+01		1.000E-02	5.302E-03	1.518E+00 Shift G-1
3	1	1.10101E+01		1.000E-02	5.387E-03	1.173E+00 Shift G-1DCNP

0RMS ERROR = 8.90E-03 MAX ERROR = 1.60E-02 AT OBS.NO. 6

RESIDUALS SQUARED = 5.54E-04

RFACTOR = 0.0679 PERCENT

Figure SI-10. Calculation by winEQNMR2 of the association constant of ligand **1** with DCNP (1:2 stoichiometry).

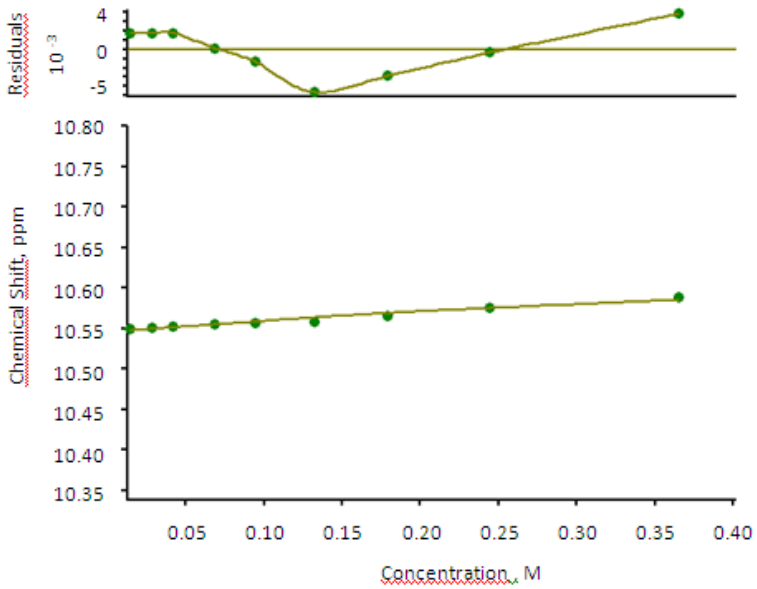

Calculations by WinEQNMR2 Version 2.00 by Michael J. Hynes

Program run at 17:47:18 on 05/17/2012

DCNP-G-2

Reaction of DCNP con G-2

NO.	A	PARAMETER	DELTA	ERROR	CONDITION	DESCRIPTION
1	1	4.41734E+00	1.000E-02	3.125E-01	1.148E+00	K
2	1	1.05453E+01	1.000E-02		1.728E-03	2.159E+00 Shift G-2
3	1	1.06530E+01	1.000E-02		8.061E-03	2.154E+00 Shift g-2DCNP

0RMS ERROR = 3.03E-03 MAX ERROR = 4.64E-03 AT OBS.NO. 6

RESIDUALS SQUARED = 5.51E-05

RFACTOR = 0.0234 PERCENT

Figure SI-11. Calculation by winEQNMR2 of the association constant of ligand **2** with DCNP (1:1 stoichiometry).

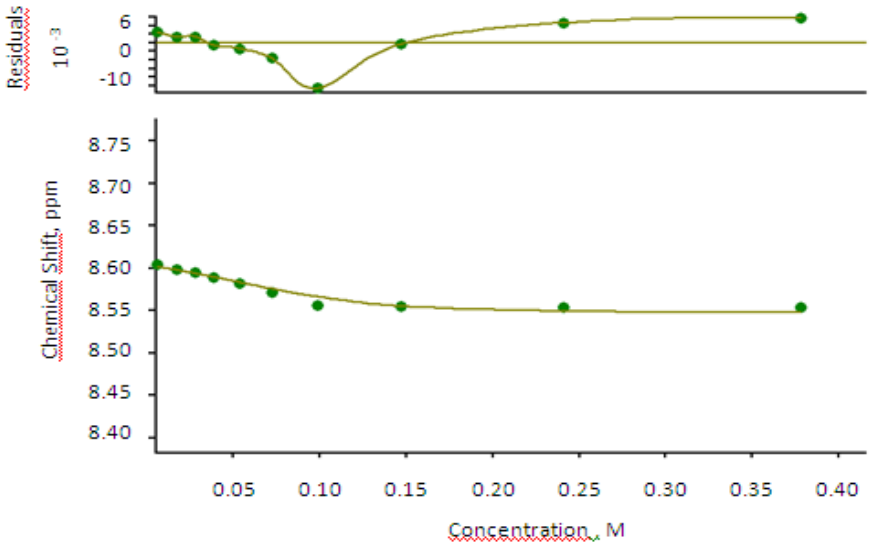

Calculations by WinEQNMR2 Version 2.00 by Michael J. Hynes

Program run at 12:51:13 on 05/18/2012

DCNP-G-3

Reaction of DCNP con G-3

NO.	A	PARAMETER	DELTA	ERROR	CONDITION	DESCRIPTION
1	1	1.74338E+03	1.000E-02	3.528E+01	1.539E+00	K
2	1	8.60323E+00	1.000E-02	3.407E-03	1.672E+00	Shift G-3
3	1	8.54705E+00	1.000E-02	3.239E-03	1.355E+00	Shift G-3DCNP

0RMS ERROR = 5.24E-03 MAX ERROR = 1.06E-02 AT OBS.NO. 7

RESIDUALS SQUARED = 1.92E-04

RFACTOR = 0.0511 PERCENT

Figure SI-12. Calculation by winEQNMR2 of the association constant of ligand **3** with DCNP (1:2 stoichiometry).

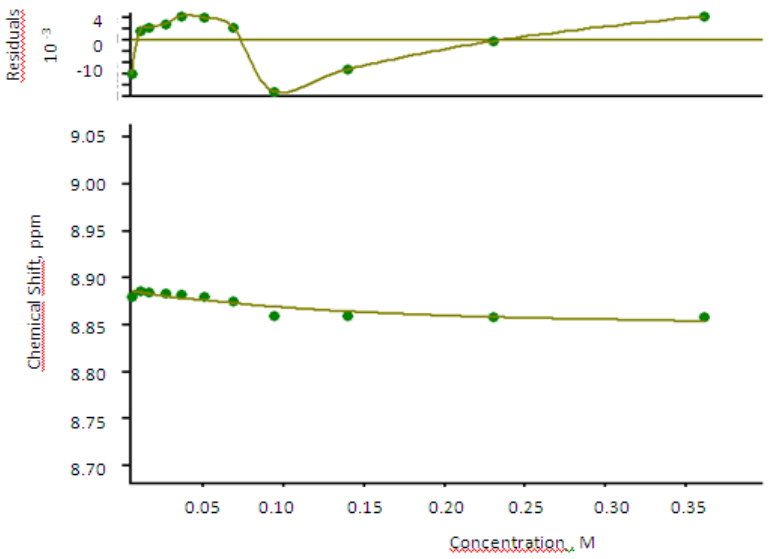

Calculations by WinEQNMR2 Version 2.00 by Michael J. Hynes
Program run at 17:59:18 on 05/17/2012

DCNP-G-4
Reaction of DCNP con G-4

NO.	A	PARAMETER	DELTA	ERROR	CONDITION	DESCRIPTION
1	1	1.01552E+01	1.000E-02	9.473E-01	1.482E+01	K
2	1	8.88769E+00	1.000E-02	4.344E-03	3.974E+00	Shift G-4
3	1	8.84252E+00	1.000E-02	1.109E-02	8.161E+00	Shift G-1DCNP

0RMS ERROR = 5.17E-03 MAX ERROR = 9.11E-03 AT OBS.NO. 8
RESIDUALS SQUARED = 2.14E-04
RFACTOR = 0.0497 PERCENT

Figure SI-13. Calculation by winEQNMR2 of the association constant of ligand **4** with DCNP (1:1 stoichiometry).

Table SI-1. Variation of the hydrolysis rate of the nerve agent analogues (NAAs) at different concentrations of catalysts in acetone/ water (80:20) at 25.

	0.01eq	0.002eq
Receptor	**DCP**	**DCNP**
1	14 ±1 %	10.3 ± 1.7%
2	23.4 ±1.4 %	6.7 ± 0.2%
3	7.2 ± 0.6%	6.4 ± 0.1%
4	13.9 ±0,7%	11.2 ±0,4%

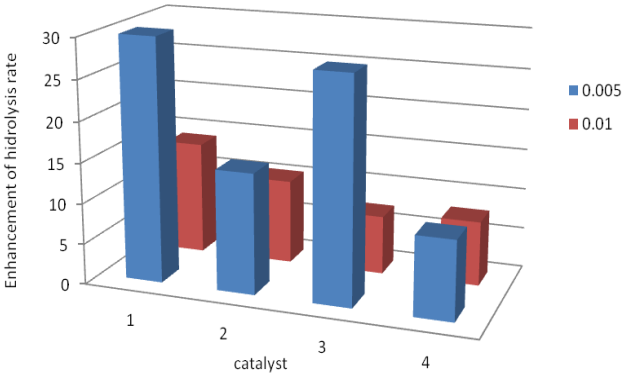

DCP

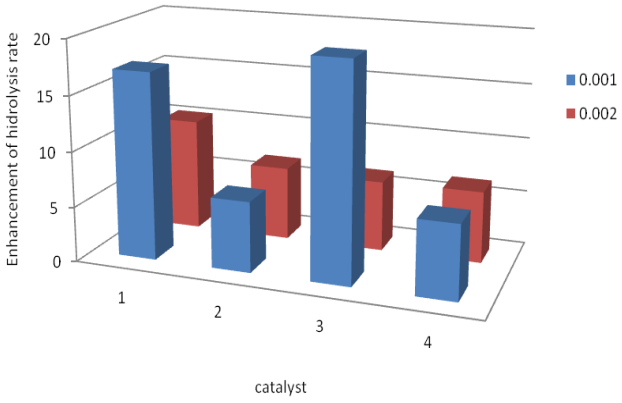

DCNP

Figure SI-14. Variation of the hydrolysis rate of the nerve agent analogues (NAAs) at different concentrations of catalysts in acetone/ water (80:20) at 25 °C.

Table SI-2. Variation of the hydrolysis rate of the DCNP in acetone/water (80:20) at different temperatures (all measurements were carried out with 0.001 equiv. vs. of receptor **1**).

Temperature	Hydrolysis rate
10 °C	8.3 ± 1.2 %
25 °C	17.7 ± 2.3 %
30 °C	18.4 ± 2.3 %
35 °C	30 ± 1 %
50 °C	32.6 ± 1.5 %

Dynamic Light scattering measurements. A Malvern Zetasizer NanoZS was used to perform light scattering studies. Dispersant RI, Material RI and Count rate(kcps) were consider 1.3556, 1.45 and 17.9 respectively. The Temperature was maintained at 25.1°C. Experiments were carried out in acetone/water (80/20) solutions in the presence and in the absence of putative catalyst. An uncatalyzed solution was prepared containing 10 %(v/v) DCNP (or 5% (v/v) DCP) and a catalyzed solution containing 0.001 eq. of catalyst **4** plus 10% of DCNP (or 5% (v/v) DCP). The measures were taken 5 minutes later the sample preparation.

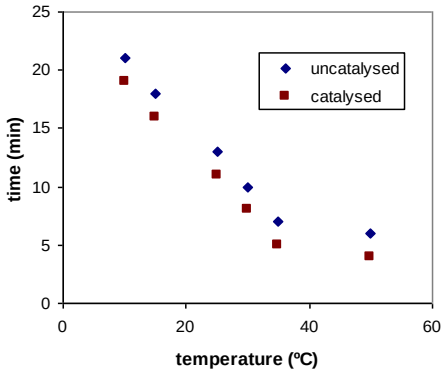

Figure SI-15. Influence of the temperature on the hydrolysis time for catalyst **1** (7.5×10^{-4} M) and DCNP (0.7 M).

Table SI-3. Comparison between 1,3-diindolylureas and thioureas (receptors **1**-**4**) as supramolecular organo-catalysts and previously described procedures for the elimination of organophosphorus hazards.

Method	Steps	T (ºC)	Compound	Advantages	Disadvantages
Incineration	3 stages i)separation of chemical agents ii)incineration of agents iii) treatment of gaseous effluents	1480-1090 ºC	---	It is a full-scale prototype	Danger from the emissions of incineration. Large energetic cost
Base hydrolysis	2stages i) water hydrolysis ii) supercritical water oxidation	600-650 ºC	NaOH	Within ≈ 30 s the agents are largely oxidized	Corrosion of heating and cooling elements in reactor. Large amount of water that has to be evaporated
Use of peroxides	one step	r.t.	R-O-O-R`	Peroxides are nontoxic and noncorrosive	Perhydrolysis could avoid formation of toxics compounds.
Biotechnological degradation	several steps	37 ºC	Enzymes, antibodies	Very selective	It is necessary to work at physiological conditions and to keep a temperature control
Metal transition ion catalysed hydrolysis	one step	25ºC	Cu^{2+}, Ag^{+}, Hg^{2+}	Good accelerations and catalytic	Environmental contamination
Nanosize CaO or MgO	one step	r.t.	Supported CaO or MgO	Small contamination	No catalytic and spectroscopic scale
Organic catalysed hydrolysis with Neutral 1,3-Diindolylureas	one step	r.t.	Neutral 1,3-Diindolylureas	Good acceleration and catalytic. Low energetic cost for recovering organic solvent. Small contamination. No corrosion	It uses acetone

6.4 Towards the design of organocatalysts for nerve agents remediation: the case of the active hydrolysis of DCNP (a Tabun mimic) catalyzed by simple amine-containing derivatives.

Towards the design of organocatalysts for nerve agents remediation: the case of the active hydrolysis of DCNP (a Tabun mimic) catalyzed by simple amine-containing derivatives.

Andrea Barba-Bon, [acb] Ramón Martínez-Máñez,[abc] *Felix Sancenón* [abc]*,Ana M.Costero,*[ad] *Salvador Gil,*[ad] Francisco Pérez-Pla,[e] *and Elisa Llopis* [e]

[a] *Centro de Reconocimiento Molecular y Desarrollo Tecnológico (IDM). Unidad Mixta Universidad de Valencia-Universidad Politécnica de Valencia, Spain.*
[b] *Departamento de Química Orgánica, Universidad de Valencia, Dr. Moliner 50, 46100 Burjassot, Valencia, Spain*
[c] *CIBER de Bioingeniería Biomateriales y Nanomedicina (CIBER-BBN).*
[d] *Departamento de Química. Universidad Politécnica de Valencia, Camino de Vera s/n, 46022, Valencia, Spain.*
[e] *Institut de Cíencia dels Materials (ICMUV) c/Catedratico Beltrán 2, 46980 Paterna, Valencia, Spain.*

Submitted

Abstract

We report herein a study of the hydrolysis of the Tabun mimic DCNP in the presence of different amines, aminoalcohols and glycols as potential suitable organocatalysts for DCNP degradation. Hydrolysis studies were also performed for DCNP alone and with a base (TBAOH). Experiments were performed in CD_3CN in the presence of 5% D_2O, which proved to be a suitable solvent mixture to follow the DCNP hydrolysis. These studies allowed the definition of different DCNP depletion paths, resulting in the formation of diethylphosphoric acid, tetraethylpyrophosphate and phosphoramide species as the main final products. In the absence of organocatalysts, DCNP hydrolysis occurred mainly via an autocatalysis path, on which acceleration of the reaction rate was promoted by own reaction products. Addition of tertiary amines in sub-stoichiometric amounts largely enhanced DCNP depletion whereas non tertiary polyamines reacted even faster. Glycols induced a very slight increment in the DCNP hydrolysis, whereas DCNP hydrolysis increased sharply in the presence of certain aminoalcohols. This was so for diethanolmethylamine and, especially, for 2-(2-aminoethylamino)ethanol. For the latter compound, DCNP depletion occurred ca. 80-fold faster than in the absence of organocatalysts. The kinetic studies revealed that, apart from non-catalytic reactions, DCNP hydrolysis in the presence of 2-(2-aminoethylamino)ethanol occurred via a catalytic process, in which the aminoalcohol was involved. This catalytic path was also found for other tested compounds. DCNP hydrolysis generally depended strongly on the structure of the amine, aminoalcohol and glycol used and it was found that the presence of the $OH\text{-}CH_2\text{-}CH_2\text{-}N$- moiety in the organocatalyst structure seems important to induce a fast degradation of Tabun simulant DCNP.

Keywords: Diethylcyanophosphonate • Nerve agent simulant • Tabun • Hydrolysis • Organocatalysts • Reaction mechanism • Kinetics.

Introduction

Currently growing international concern about criminal terrorist attacks using chemical warfare agents (CWAs) has meant that not only the reliable detection of toxic gases, but also suitable, simple and affordable destruction and decontamination processes, are required. Although a number of international treaties have banned the development, production and storage of chemical weapons, these agents are still being produced or stockpiled in some countries.[1]

CWAs are classified into several groups according to their toxic mechanism of action; i.e., nerve agents, asphyxiant/blood agents, vesicant agents, choking/pulmonary agents, lachrymatory agents, incapacitating agents and cytotoxic proteins.[2,3] Of all these, nerve agents are among the most dangerous chemical warfare species.[4] Nerve agents are highly toxic phosphoric acid esters that are structurally related to the larger family of organophosphonate derivatives. Given their toxicity, nerve gases agents have been used since they were discovered as chemical weapons and in terrorist acts; for instance, in the subway attack in Tokyo in 1995; in the Iraq repression against Kurdish communities in 1988; and very recently, in the Syrian civil war. Deadly nerve agents have severe effects on humans and animals as a gas, aerosol or liquid. They enter the body through inhalation or through the skin. Poisoning may also occur through the intake of liquids or foods contaminated with these agents. Toxicity of nerve agents is due mainly to their ability to inhibit the action of acetylcholinesterase,[5–7] that results in the excessive concentration and accumulation of acetylcholine, which triggers a crisis of the nerve system which may even lead to death.[8–12]

The fact that nerve gases are easy to produce, and given their indiscriminate use by certain nations and terrorist groups, have meant that the scientific community has made more efforts towards the design of new procedures for detection and remediation of these deadly chemicals.[13–16] In such studies, nerve gas simulants such as diethylcyanophosphate (DCNP), diisopropylfluorophosphate (DFP) and diethylchlorophosphate (DCP), are habitually employed. These compounds show similar reactivity to real nerve agents Sarin, Soman and Tabun, but lack their

severe toxicity (see Figure 1). Remediation of nerve gases is still a matter of concern, and active research to find safe, effective methods that do not endanger human life or the natural environment is currently underway.[17–19,20,21]

There are several remediation examples currently being developed, which include nerve agent oxidation through the use of supercritical water,[22–24] caustic bleaching,[25,26] incineration,[27] and bioremediation.[28–30] electrolytic methods,[31,32] oxidative degradation on active sorbents,[33] catalytic degradation methods,[22,34] atmospheric pressure plasma[35] and photolytic procedures.[36–39] Recently, highly porous multifunctional metal oxide/hydroxide micro- and nanoparticles,[40–47] clays,[48] metal-organic frameworks (MOFs),[49–51] porous organic polymers (POPs),[52] mesoporous silica materials[53,54] and zeolites[55,56] have also been used for nerve gas remediation purposes.

Even though these methods offer some advantages, they also entail important shortcomings. For instance, supercritical water has proven effective to oxidize organophosphorous-based nerve agents. However, the energy costs associated with this procedure are high. With bioremediation, the stability of the used immobilized enzymes requires a cold chain and the extension of a small lab-scale to the pilot-scale or field-scale is not widely employed. The use of bleach requires the solubilization of nerve agents in large quantities of solvent, which must be dealt with later. In this context, sodium hydroxide-containing mixtures have also been developed. For instance, decontaminant DS2[57,58] is a polar, non-aqueous liquid composed, by weight, of 70% diethylenetriamine, 28% ethylene glycol monomethylether and 2% sodium hydroxide. While DS2 is a highly effective decontaminant for CW agents, ethylene glycol monomethyl ether has shown teratogenicity in mice, and replacement with propylene glycol monomethyl ether has been proposed (DS2P).[59]

In addition, DS2 attacks paints, plastics and leather materials. To minimize these problems, the contact time with DS2 is limited to 30 minutes, followed by rinsing with vast amounts of water. The personnel who handle DS2 have to wear respirators with eye shields and chemically protective gloves.[60] To overcome these limitations, the GD-5 mixture was developed for the decontamination of sensitive

equipment, vehicles, airplanes, etc. This decontaminant contains potassium hydroxide (KOH) in combination with organic solvents (aminoethanol, benzylalcohol and propanol). More recently, GD-5 has been substituted for GD-6, of similar composition, but is more effective in decontaminating. Besides for large quantities, high-temperature incineration is currently the most approved technique to destroy stored nerve agents.

In line with new remediation methods for nerve agents, alternative suggestive approaches, which involve the use of catalysts able to enhance the hydrolysis of nerve agents, have been proposed. Some metal-catalyzed hydrolysis procedures have been developed;[61,62] however, examples of organocatalysts are rarer. In this sense, we and others have recently reported that 1,3-diindolylureas and thioureas are useful supramolecular systems in the remediation of nerve agent simulants.[63] These recent findings strongly suggest that other hydrogen-bond donor derivatives, also capable of reacting or forming complexes with organo-phosphorus nerve agents, can enhance the degradation of these deadly hazards. Inspired by these previous studies,[64] we decided to test the possible use of amines and amine-containing derivatives as simple low-cost compounds for nerve agents remediation.

Accordingly, we report herein a study of the hydrolysis of the Tabun mimic DCNP in the presence of different amines, aminoalcohols and glycols as potential and suitable organocatalysts (see Figure 1). A clearly structure-dependent response was observed for different derivatives and, in some cases, remarkably enhanced DCNP hydrolysis was noted, especially when 2-(2-aminoethylamino)ethanol was used. A complete kinetic study was also performed to understand the mechanism involved in the catalytic hydrolysis of this Tabun simulant.

Experimental

NMR experiments

^{31}P NMR was used to monitor DCNP hydrolysis at 25°C. This technique, in addition to ^{1}H NMR and GC/MS, allowed the identification of reaction products. All the hydrolyses were carried out in CD_3CN in the presence of 5% D_2O. Reaction

mixtures were prepared by introducing 475 mL of CD_3CN, 25 mL of D_2O and 0.1 (or 0.01) equivalents of the corresponding compound (see figures 1) into an NMR tube. Immediately before measurements were taken, 50 mL of DCNP were added, and NMR signals were recorded every 10 min for 120 min. ^{31}P NMR spectra were recorded in a Bruker DRX-500 provided with a BBOF probe (^{31}P (202.5 MHz)).

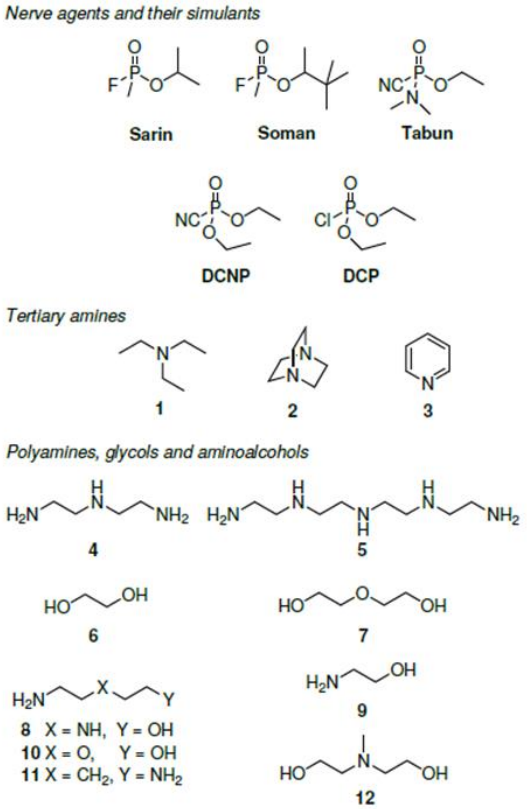

Figure 1. Chemical structure of nerve agents and their simulants and the potential organocatalysts used in this study (**1**: triethylamine; **2**: 1,4-diazabicyclo[2.2.2]octane; **3**: pyridine; **4**:diethylenetriamine; **5**: tetraethylenepentamine; **6**: ethylene glycol; **7**: diethylene glycol; **8**:2-(2-aminoethylamino)ethanol; **9**: ethanolamine; **10**: 2-(2-aminoethoxy)-ethanol; **11**: 1,5-diaminopentane; **12**: diethanolmethylamine).

GC measurements

CG-FID was used to monitor some kinetic runs to corroborate the NMR results. Chromatograms were recorded using an HP-6890+ GC (from Agilent) equipped with an HP-5 (30 m-0.32 mm, ID 0.25 mm) column. The chromatographic

conditions were as follows: initial oven temperature was set at 60 °C and this temperature was maintained for 1 minute. Then the temperature was raised by 50ºC/min to 180°C, and this temperature was maintained for 3 min. Finally, the oven temperature was raised by 50°C /min to 250°C and was maintained for 3 minutes. The injector and FID-detector temperatures were set at 250°C and 270°C, respectively. The carrier gas (He) flow was set at 1 mL/min. The DCNP and $PO(OH)(EtO)_2$ peaks were assigned by comparing their retention times with standards. Diethylpyrophosphate was also identified from its mass spectrum (M^+=291 m/z). Kinetics was followed for at least 350 min by analyzing the 0.5 mL aliquots taken from the reactor every 15-20 minutes, using toluene as an internal standard.

Results and discussion

Hydrolysis studies

As stated above, DCNP was selected as the model for nerve agent Tabun. Typical experiments were performed in CD_3CN in the presence of 5% D_2O, which was found to be a suitable solvent mixture and allowed us to follow the DCNP hydrolysis extent using ^{31}P NMR. Moreover, ^{1}H RMN and GC/MS were employed to identify the reaction products. DCNP hydrolysis was studied alone, in the presence of a base, and also in the presence of amines, aminoalcohols and glycols (see Figure1).

The DCNP reaction in the presence of the derivatives shown in Figure 1 resulted in final spectra, which usually showed up to three different phosphorus signals attributed to diethylphosphoric acid (+0.18 ppm), tetraethylpyrophosphate (-14.12 ppm) and unreacted DCNP (-21.22ppm). The spectra of the reaction mixtures carried out in the presence of certain compounds (e.g., **4**, **5**, **8**-**11**) showed an additional signal, which was attributed to the formation of diethylphosphoramide species (ca. +10 - +13 ppm depending on the phosphoramide formed). As representative examples, figure (ESI 1) into the supplementary material show the ^{31}P NMR spectra after 15 minutes for DCNP

alone and in the presence of derivatives **2**, **5** or **10** in acetonitrile: water 95:5 v/v mixtures.

Figure 2 shows the variation over time of the DCNP hydrolysis extent alone in acetonitrile: water 95:5 v/v mixtures, with a base (TBAOH) or in the presence of the amino derivatives and glycols shown in Figure 1. In all cases, the compounds depicted in Figure 1 were added in sub-stoichiometric amounts (0.1 equiv. in relation to DCNP). Figure 2(a) shows that when DCNP was alone, the extension of hydrolysis was less than a 5% after 15 minutes, yet the degree of hydrolysis increased to ca. 80% after 120 min. Figure 2 also shows that the presence of different derivatives in sub-stoichiometric amounts led to a higher hydrolysis rate. This increment approximately followed the sequence **7** < **6** < **3** ≈ TBAOH < **11** < **1** ≈ **9** ≈ **2** ≈ **10** < **5** ≈ **4** << **12** << **8**. It is apparent from Figure 2(a) that glycols (**6** and **7**) induced a very slight increment in DCNP hydrolysis, whereas a major DCNP depletion was noted in the presence of polyamines **4** and **5**. In some cases, the increased DCNP hydrolysis was quite remarkable as, for instance, observed in the presence of aminoalcohols **8** and **12**, which induced almost complete DCNP hydrolysis under 15 min.

Similar DCNP hydrolysis experiments were carried out using 0.01 and 0.001 equiv. of the corresponding catalytic derivative. These studies demonstrated that a threshold of 0.1 equiv. of the corresponding compound was required to induce an appreciable increment in the hydrolysis rate of the simulant. By way of example, Figure 2b shows the variation versus time of the DCNP hydrolysis extent in the presence of different concentrations of polyamine **5**. As seen, a concentration below 0.06 mol dm^{-3} (0.1 equiv) of the catalyst resulted in poor DCNP hydrolysis.

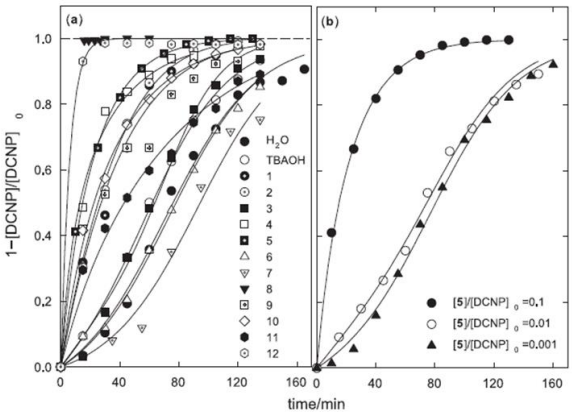

Figure 2. Experimental (symbols) and calculated (solid lines) variation over time of the DCNP hydrolysis extent (0.6 M) in acetonitrile: water (95:5 v/v): (a) in the presence of TBAOH (0.006 M), and the compounds in Figure 1 in sub-stoichiometric amounts (0.06 M) (b) in the presence of **5** at variable amine concentrations.

DCNP hydrolysis in acetonitrile: water 95:5 v/v. Autocatalysis

In a first step, the hydrolytic behavior of DCNP in the solvent used in all the experiments (i.e., acetonitrile: water 95:5 v:v) was considered. This allowed us to evaluate the DCNP hydrolysis due only to presence of water. Figure 3(a) displays the results obtained. Studies on this simple system revealed that the concentration of the unique product $PO(OH)(EtO)_2$ increases as that of DCNP lowers. Under these conditions, the DCNP hydrolysis also resulted in a negligible amount of tetraethylpyrophosphate ($(EtO)_2OP\text{-}O\text{-}PO(EtO)_2$). However, despite the simplicity of the system, the reaction exhibited a complicated kinetics. The sigmoid shape of DCNP and the $PO(OH)(EtO)_2$ concentration curves cannot be explained by the simple rate laws of type $r = k[DCNP]^a[X]^b$ (X = water), which should lead to profiles without inflexion points. Nevertheless, sigmoid behavior can be easily explained by autocatalysis; that is, an acceleration of the reaction rate promoted by own reaction products.[65]

Additional kinetic runs followed by CG-MS and ^1H NMR, in which $PO(OH)(EtO)_2$ or HCN was added to the DCNP/water mixtures, were carried out to check this hypothesis. Only the addition $PO(OH)(EtO)_2$ clearly resulted in higher reaction rates (see Figure 3(c)), which allowed us to identify this compound as the autocatalyst. Moreover, it is worth noting that both the ^1H NMR and GC studies

consistently indicated that ethanol was absent as a reaction product. For this reason, the EtO– groups were not considered to be leaving groups in the reaction schemes considered below.

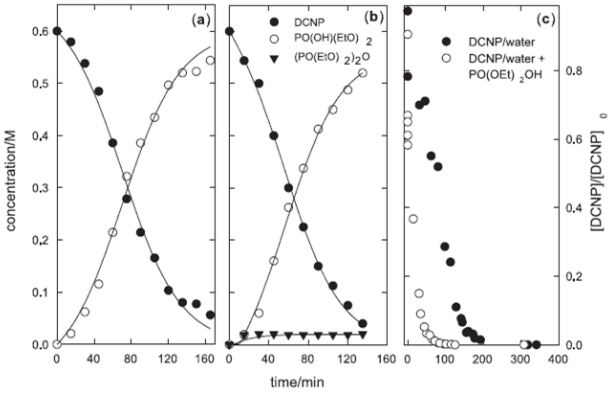

Figure 3. Experimental (symbols) and calculated (solid lines) concentration curves in acetonitrile: water 95:5 v/v for (a) DCNP and (b) DCNP/ TBAOH. [DCNP] = 0.6 M, [TBAOH] = 0.006 M. (c) Relative variation of the DCNP concentration over time obtained from GC/MS in acetonitrile: water 95:5 v/v. (•) [DCNP] = 0.12 M, [$PO(OH)(EtO)_2$] = 0.0 M; (o) [DCNP] = 0.12 M, [$PO(OH)(EtO)_2$] = 0.12 M.

Experimental data were analyzed according to the mechanism which consisted in Equations (1) and (2) involving autocatalysis (see the Supporting Information).

$$\mathrm{DCNP} + \mathrm{H_2O} \xrightarrow{k_1} \mathrm{PO(OH)(OEt)_2} + \mathrm{HCN} \quad (1)$$

$$\mathrm{DCNP} + \mathrm{PO(OH)(OEt)_2} + \mathrm{H_2O} \xrightarrow{k_2} 2\mathrm{PO(OH)(OEt)_2} + \mathrm{HCN} \quad (2)$$

The calculation results are presented in Figure 3(a) and Table 1, which shows the kinetic constants, along with some statistical indices that witness the quality of the least-squares fits. It is worth mentioning that the ratio between the rate constants associated with the autocatalytic and non-catalytic pathways was approximately $k_2/k_1 \approx 40$, suggesting that autocatalysis is the most relevant pathway for DCNP hydrolysis in the presence of water. This agrees with some reported results, which have also proposed the existence of an autocatalytic process in the hydrolysis of V agents.[66]

Hydrolysis in the presence of tetrabutylammonium hydroxide

In a second step, the effect of small amounts of hydroxide on the DCNP hydrolysis rate was analyzed. This was evaluated bearing in mind that studies with amines (vide infra) in the presence of water can result in both the formation of protonated amines and the generation of hydroxide anions, which could eventually lead to basic catalysis. Therefore this section attempts to evaluate the DCNP hydrolysis extent due to the presence of OH^- groups. These studies were performed in acetonitrile: water 95:5 v/v in the presence of 0.006 M in tetrabutylammonium hydroxide (TBAOH), which was used at the resulting concentration produced by the generation of hydroxide anions in case of amine protonation. Figure 3(b) shows the variation of the DCNP concentration for this system with time. The sigmoid shape of DCNP and the $PO(OH)(EtO)_2$ curves was similar to that found in the absence of TBAOH (see Figure 3(a)). Conversely, however, in this case small amounts of tetraethylpyrophosphate formed from the very beginning of the reaction. Presence of tetraethylpyrophosphate was clearly confirmed by ^{31}P NMR studies. $(EtO)_2OP\text{-}O\text{-}PO(EtO)_2$ formation can be explained by reactions (1) and (2) assuming that the $PO(OH)(EtO)_2$ species deprotonated in the presence of hydroxide to yield phosphate according to equation (3). The $PO2(OEt)_2^-$ species reacted with DCNP or $PO(OH)(EtO)_2$ to yield tetraethylpyrophosphate thereafter, as shown in equations (4) and (5). In particular, reaction (4) would be responsible for early $(EtO)_2OP\text{-}O\text{-}PO(EtO)_2$ formation.

$$PO(OH)(OEt)_2 + OH^- \overset{K_1}{\leftrightarrow} PO_2(OEt)_2^- + H_2O \quad (3)$$

$$PO_2(OEt)_2^- + DCNP \overset{k_3}{\rightarrow} (EtO)_2OP - O - PO(EtO)_2 + CN^- \quad (4)$$

$$PO_2(OEt)_2^- + PO(OH)(OEt)_2 \overset{k_4}{\rightarrow} (EtO)_2OP - O - PO(EtO)_2 + OH^- \quad (5)$$

Other possible reactions in which hydroxide anions can be involved are the substitution of cyanide on DCNP to form $PO(OH)(EtO)_2$,

$$DCNP + OH^- \overset{k_5}{\rightarrow} PO(OH)(OEt)_2 + CN^- \quad (6)$$

and the acid-base equilibrium in equation (7), as released cyanhydric acid neutralizes hydroxides to diminish their activity:

$$CN^- + H_2O \overset{K_2}{\leftrightarrow} HCN + OH^- \quad (7)$$

Data from the DCNP/TBAOH system were analyzed according to the mechanism formed by equations (1)-(7) (see the Supporting Information). Relevant statistical and kinetic information is presented in Table 1.

Table 1. Rate constants for the DCNP systems alone in acetonitrile: water 95:5 v:v uncatalyzed and in the presence of TBAOH.

Medium	k_i		R^a	*SSR*	*LOF*	*AIC*
Uncatalized	k_1	1.20×10^{-3}	0.996	7.65×10^{-3}	4.938	−113.0
	k_2	4.97×10^{-2}				
TBAOH	k_1	1.70×10^{-3}	0.999	2.20×10^{-3}	3.040	−233.4
	k_2	6.05×10^{-2}				
	k_3	9.43×10^{-2}				
	k_4	1.80×10^{-4}				
	k_5	1.40×10^{-5}				
	K_1	7.28×10^{-9}				
	K_2	1.79×10^{2}				

[a] *R*: Correlation coefficient; *SSR*: Sum of squares of residuals; *LOF*: Lack of fit; *AIC*: Akaike's information criterium.

The rate constant for direct DCNP hydrolysis by hydroxide, equation (6), was quite low if compared to those of autocatalysis (equation (2)) or hydrolysis by water (equation (1)), suggesting that autocatalysis is still the main route for DCNP hydrolysis under these experimental conditions.

The results also suggest that the $PO_2(OEt)_2^-$ species preferentially reacts with DCNP ($k_3/k_4 \approx 5x10^2$), so the path that involves $PO(OH)(EtO)_2$ in equation (5) is neglected. From the data, value of *p*K*a* ≈15.9 was calculated for cyanhydric acid in acetonitrile: water 95:5 v/v, which concurs with that estimated by Roses (*p*K*w* = 18.18) in the same media.[67]

Hydrolysis catalyzed by amines, aminoalcohols and glycols

From the data provided in Figure 2, it is apparent that the presence of certain amines and aminoalcohols in sub-stoichiometric amounts enhanced the DCNP hydrolysis rate if compared to that found in the presence of only water or TBAOH (vide ante). On the contrary, the presence of glycols had no major effect on the hydrolysis DCNP rate. When only amines were taken into account, it was also apparent from the kinetic studies that the catalysis observed in the presence of tertiary amines (**1**, **2** and **3**) followed a different path to that followed by polyamines **4**, **5** and **11**.

Tertiary amines

Figure 4 shows the concentration profiles for DCNP hydrolysis in the presence of tertiary amines **1**-**3**. Some remarkable features of these profiles, when compared to DCNP hydrolysis by water or TBAOH (vide ante), are the rapid depletion of DCNP, whose concentration curve is no longer sigmoidal for **1** and **2**, the marked sigmoid shape observed for $PO(OH)(EtO)_2$ formation, and the good yield in tetraethylpyrophosphate. Special emphasis must be placed on the generation of tetraethylpyrophosphate from the very beginning of the reaction, which is indicative of an early phosphate reaction with DCNP. These changes in the hydrolysis profile are tentatively assigned to the formation of intermediate phosphoramide species via equation (8):

$$\mathrm{DCNP} + \mathrm{NR_3} \rightarrow (\mathrm{EtO})_2\mathrm{OPNR_3^+} + \mathrm{CN^-}\ (\mathrm{slow}) \qquad (8)$$

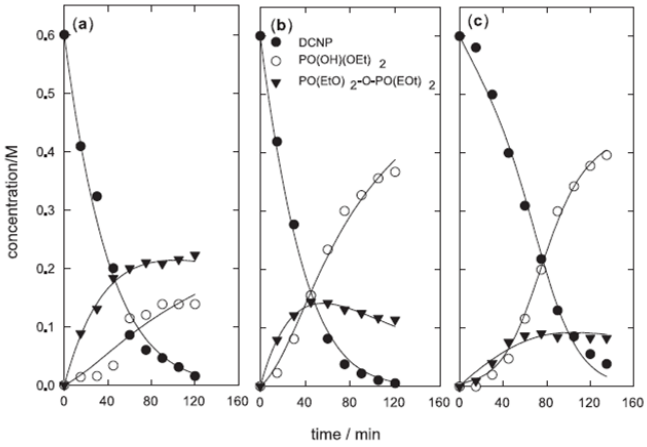

Figure 4. Experimental (symbols) and calculated (solid lines) concentration curves for the DCNP hydrolysis in acetonitrile: water 95:5 v/v in the presence of (a) **1**, (b) **2**, and (c) **3**; [DCNP] = 0.6 M, [amine] = 0.06 M. Solid lines were calculated from the chemical model described in the text.

Despite the $(EtO)_2OPNR_3^+$ intermediate being clearly observed in the ^{31}P NMR spectra in the presence of other amines (vide infra), it was not seen when DCNP hydrolysis was studied with tertiary amines. This indicates that these $(EtO)_2OPNR_3^+$ intermediates are short-living species and quite reactive to water and $PO_2(OEt)_2^-$ following equations (9) and (10):

$$(EtO)_2OPNR_3^+ + H_2O \rightarrow PO(OH)(OEt)_2 + HNR_3^+ \text{ (fast)} \quad (9)$$

$$(EtO)_2OPNR_3^+ + PO_2(OEt)_2^- \rightarrow (EtO)_2OP-O-PO(EtO)_2 + NR_3 \text{ (fast)} \quad (10)$$

For tertiary amines, the sum of processes (8) and (9) is the equivalent to the amine-catalyzed hydrolysis shown in equation (11), which is responsible for the loss of the sigmoid shape for DCNP:

$$DCNP + H_2O + NR_3 \xrightarrow{k_6} PO(OH)(OEt)_2 + HCN + NR_3 \quad (11)$$

This process competes with the non-catalyzed (1) and autocatalyzed (2) hydrolysis pathways. The sum of processes (8) and (10) leads to the formal process shown in

equation (12), which is responsible for the increased tetraethylpyrophosphate concentration in early DCNP hydrolysis stages:

$$\mathrm{DCNP} + \mathrm{PO_2(OEt)_2}^- + \mathrm{NR_3} \overset{k_7}{\rightarrow} \mathrm{(EtO)_2OP-O-PO(EtO)_2} + \mathrm{CN^-} + \mathrm{NR_3} \quad (12)$$

Moreover, equation (13) should also be taken into account in the chemical hydrolysis model as a stop, or a slight reduction in the tetraethylpyrophosphate concentration was observed after ca. 50 min after the reaction started.

$$\mathrm{(EtO)_2OP-O-PO(EtO)_2} + \mathrm{H_2O} \overset{k_8}{\rightarrow} 2\mathrm{PO(OH)(OEt)_2} \quad (13)$$

Finally, the equilibria established by amines **1**, **2** or **3** with cyanhydric acid, $PO(OH)(EtO)_2$, and water must also be contemplated to complete the hydrolysis model. The full mechanism is illustrated in Scheme 1.

$$\mathrm{NR_3} + \mathrm{H_2O} \overset{K_3}{\leftrightarrow} \mathrm{HNR_3^+} + \mathrm{OH^-} \quad (14)$$

$$\mathrm{NR_3} + \mathrm{PO(OH)(OEt)_2} \overset{K_4}{\leftrightarrow} \mathrm{HNR_3^+} + \mathrm{PO_2(OEt)_2}^- \quad (15)$$

$$\mathrm{NR_3} + \mathrm{HCN} \overset{K_5}{\leftrightarrow} \mathrm{HNR_3^+} + \mathrm{CN^-} \quad (16)$$

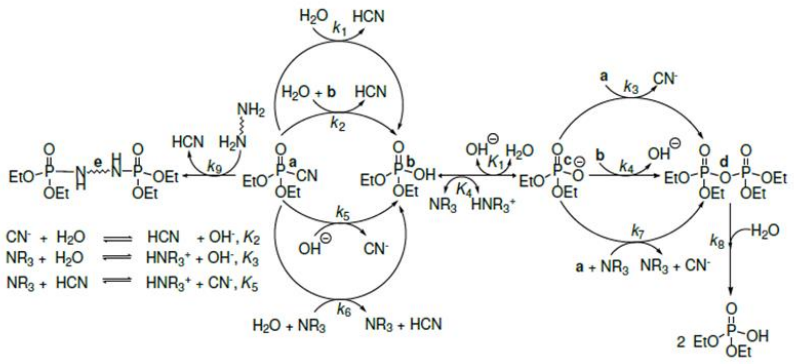

Scheme 1. Reaction mechanism.

The data for DCNP hydrolysis in the presence of tertiary amines **1**-**3** were analyzed in accordance with the chemical model formed by equations (1) to (4), and by equations (6) to (16).

Relevant kinetic and statistical information is provided in Table 2.

Figure 4 shows that the tetraethylpyrophosphate conversion increased as the basicity of the amines did. According to the model, tetraethylpyrophosphate formation was governed by the competing processes shown in (4) and (12). A comparison of k_3 to k_7 revealed that the amine catalyzed reaction (12) proceeded faster in all cases, except when pyridine (3) was used, which accounts for the larger tetraethylpyrophosphate formation when compared with the data observed in the presence of TBAOH. Nevertheless, the rate constants associated with catalytic condensation to obtain tetraethylpyrophosphate (k_7) were similar for **1** and **2**, with the tetraethylpyrophosphate yield being, however, clearly greater for **1**. Therefore, it is obvious that the k_7 values alone do not explain the observed tetraethylpyrophosphate formation, the other factor being amine basicity.

Thus, reaction (4) depends on the $PO_2(OEt)_2^-$ concentration which, in turn, is driven mainly by hydrolysis equilibrium (14) and the deprotonation process shown in (15). A clear correlation between tetraethylpyrophosphate yield and amine basicity was observed as the K_3 and K_4 values decreased from **1** to **3** following the observed tetraethylpyrophosphate formation extent.

As observed above, Figure 4 shows that the DCNP hydrolysis rate is faster in the presence of amines when compared with that of water or TBAOH, and that the sigmoid shape for the DCNP concentration vs. time is lost for **1** and **2**. The DCNP hydrolysis rate was determined mainly by equations (1) (k_1), (2) (k_2), and (11) (k_6), where the latter two processes represented the auto-catalyzed and amine-catalyzed hydrolyses. The rate constants associated with the amine-catalyzed process, k_6, were similar for **1** and **2**, but smaller for pyridine (**3**). In fact in the latter case, the autocatalytic constant from equation (2) (k_2) was even greater than the constant relating with reaction (11) (k_6). The rapid drop in the DCNP concentration for **1** and **2**, and the loss of the sigmoid shape, were due chiefly to

the presence of the amine-catalyzed pathway. In **3**, autocatalysis competed with the amine-catalyzed pathway, with hydrolysis proceeding more slowly, and the sigmoid shape of the DCNP concentration was not completely lost.

Polyamines, aminoalcohols and glycols

In this section, the catalytic behavior of polyamines diethylenetriamine (**4**) and tetraethylenepentamine (**5**) was first studied. Figure 5 shows the concentration curves for the DCNP hydrolysis in acetonitrile: water 95:5 v/v and that for the different products obtained in the presence of **4** and **5**. The distinctive features of these systems include loss of sigmoid shape for DCNP and $PO(OH)(EtO)_2$, early tetraethylpyrophosphate formation and the formation of phosphoramide derivatives. The time scale of the figure indicates that the DCNP hydrolysis with **4** and **5** proceeded at a similar rate. It is also apparent from Figure 5 that DCNP hydrolysis behaved somehow differently in the presence of **4** and **5** when compared with the results obtained with tertiary amines, with the main difference lying in the presence for the formers of phosphoramide species. However, additional studies demonstrated that at a low amine concentration, phosphoramide was not observed, and the concentration curves of $PO(OH)(EtO)_2$ and tetraethylpyrophosphate become similar to those found in the TBAOH/DCNP system (see the Supporting Information).

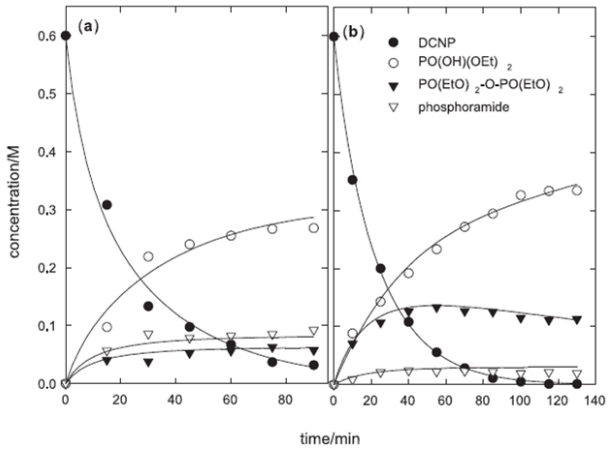

Figure 5. Experimental (symbols) and calculated (solid lines) concentration curves for the DCNP (0,6M) hydrolysis in acetonitrile: water 95:5 v/v in the presence of (a) **4** 0.09 M, and (b) **5** 0.06 M; Solid lines were calculated from the chemical model described in the text.

As **4** and **5** contain primary amines, phosphoramide can be formed by the displacement of cyanide, coupled to a proton transfer from the amino group assisted by water. Several structures for the phosphoramide species (shown in Scheme 2 for amine **4**) are feasible given the bi-functional nature of amines **4** and **5**. Structure I can be safely discarded as an inspection of the ^{1}H NMR spectra and GCFID/MS chromatograms undoubtedly confirms the absence of ethanol as a product, and suggests that a second amino group in **4** and **5** did not undergo cyclization.

Moreover, structure II is unlikely bearing in mind that an estimation of the phosphoramide concentration from the ^{31}P NMR peak areas can lead to inconsistent results when a 1:1 stoichiometry for reaction (17) is considered.

$$2\mathrm{DCNP} + \mathbf{4} \overset{k_9}{\rightarrow} (\mathrm{EtO})_2\mathrm{OPNR}_3^+ + 2\mathrm{HCN} \qquad (17)$$

In contrast, the kinetics and spectral features are adequately explained when stoichiometry 2:1 is assumed (see equation 17). Furthermore, the ^{1}H NMR of the phosphoramide obtained when **4** or **5** was used is highly symmetric, which was also coherent with structure III.

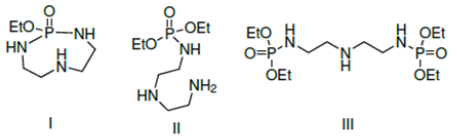

Scheme 2. Phosphoramide structures.

The kinetic data for **4** and **5** were analyzed with the chemical model, which comprised the reactions used for tertiary amines, but now includes new reaction (17), which accounts for the formation of the phosphoramide species. Figure 5 provides evidence that an increased phosphoramide yield correlated with a drop in the tetraethylpyrophosphate concentration. An inspection of Table 2 reveals that the most significant difference between the two polyamines **4** and **5** was related to the phosphoramide formation rate values, k_9 ($k_9^{\mathbf{4}}$=1.6x10^{-1},$k_9^{\mathbf{5}}$=4.3x10^{-2}).

Differences in reactivity should be attributed to the structure adopted in solution by the long chain of **5**, which probably makes the amino groups less accessible.

Unlike the enhanced DCNP hydrolysis observed in the presence of polyamines **4** and **5**, glycols **6** and **7** induced poor DCNP hydrolysis. In fact after 15 minutes, they only gave rise to 15.4% and 14.0% of the DCNP decomposition, respectively. Interestingly, glycols **6** and **7** mainly catalyzed DCNP condensation to tetraethylpyrophosphate according to reaction (18). The rate constants obtained for these systems are also provided in Table 2.

$$2\mathrm{DCNP} + \mathrm{H_2O} \xrightarrow[\mathbf{6,7}]{k_{10}} (\mathrm{EtO})_2\mathrm{OP} - \mathrm{O} - \mathrm{PO}(\mathrm{EtO})_2 + 2\mathrm{HCN} \qquad (18)$$

When the remaining compounds are taken into account, the most interesting feature is the very fast DCNP hydrolysis observed in the presence of compound **8** when compared with that observed in the presence of tertiary amines (**1**, **2**, **3**), polyamines **4** and **5**, water and a basic medium. From the reactions that involve the presence of compounds in Figure 1, we can differentiate between paths that are not catalytic and those in which the corresponding compound acts as a catalyst.

From a practical viewpoint, and in relation to the potential use of these compounds in remediation applications, it is important to achieve a quick and catalytic hydrolysis to decompose the nerve gas in a short time and with a minimum amount of catalysts. In this context, a closer look at the DCNP hydrolysis in the presence of **8** shows that the reaction yielded negligible amounts of tetraethylpyrophosphate, and that phosphate and phosphoramide were the products mainly detectable by the end of the reaction (data not shown). These facts suggest that catalyzed hydrolysis (12) and phosphoramide formation (17) constitute the predominant processes in the reaction pathway.

Table 2. Rate Constants for the DCPN hydrolysis

Catalyst	**1**	**2**	**3**	**4**	**5**	**6**	**7**	**8**	**9**	**10**	**11**	**12**
k_6	1.8×10^{-1}	1.6×10^{-1}	2.1×10^{-2}	3.5×10^{-1}	4.3×10^{-1}			5.0×10^{4}	1.7×10^{-1}	1.8×10^{-1}	7.0×10^{-2}	2.2
k_7	2.1×10^{-1}	2.0×10^{-1}	4.8×10^{-2}	1.2×10^{-1}	2.8×10^{-1}			1.8×10^{1}	2.7×10^{-1}	2.1×10^{-1}	1.5×10^{-1}	4.2×10^{-1}
k_8	6.7×10^{-4}	4.6×10^{-3}	1.1×10^{-3}	1.8×10^{-7}	2.0×10^{-3}			3.1×10^{-2}	8.3×10^{-4}	6.7×10^{-4}	8.2×10^{-4}	7.0×10^{-4}
k_9				1.6×10^{-1}	4.3×10^{-2}			1.8×10^{1}	2.5×10^{-2}	2.0×10^{-2}	1.2×10^{-2}	
k_{10}						4.6×10^{-3}	2.2×10^{-3}					
[c] k_h	0.5	0.5	0.3	0.8	0.9	0.2	0.2	86.8	0.6	0.4	0.4	2.7
K_3	2.0×10^{-4}	1.1×10^{-6}	2.0×10^{-9}	2.1×10^{-5}	2.0×10^{-5}			1.5×10^{-8}	6.3×10^{-6}	9.1×10^{-6}	2.5×10^{-6}	4.9×10^{-7}
K_4	7.9×10^{-6}	1.6×10^{-8}	7.8×10^{-6}	5.5×10^{-7}	1.3×10^{-5}			8.4×10^{-6}	7.9×10^{-7}	7.9×10^{-6}	7.1×10^{-7}	6.8×10^{-5}
K_5	2.7×10^{-5}	8.3×10^{-9}	1.8×10^{-7}	1.2×10^{-7}	3.2×10^{-4}			1.3×10^{-6}	2.1×10^{-3}	2.7×10^{-5}	3.2×10^{-3}	1.1×10^{-7}
R	0.996	0.999	0.998	0.995	0.999	0.998	0.994	0.996	0.994	0.998	0.997	0.999
SSR	4.1×10^{-3}	1.7×10^{-3}	4.4×10^{-3}	5.0×10^{-3}	1.9×10^{-3}	4.4×10^{-3}	1.3×10^{-2}	7.9×10^{-3}	9.0×10^{-3}	2.4×10^{-3}	5.1×10^{-3}	2.7×10^{-3}
LOF	6.6	3.8	4.8	7.6	3.8	4.5	8.7	7.7	9.2	4.8	6.6	3.5
AIC	−154.3	−183.1	−195.4	−161.4	−289.8	−204.8	−110.7	−169.5	−211.8	−278.6	−239.8	−215.3
SD	1.4×10^{-2}	8.9×10^{-3}	1.2×10^{-2}	1.5×10^{-2}	7.0×10^{-3}	1.1×10^{-2}	2.4×10^{-2}	1.7×10^{-2}	1.5×10^{-2}	7.9×10^{-3}	1.2×10^{-2}	9.6×10^{-3}
F	200.2	606.4	447.5	135.6	893.6	863.3	134.4	140.2	136.6	568.9	204.0	531.7

[a] Least-squares fits were carried out fixing the values of k_1, k_2, k_3, pK_1, and pK_2 to those of the TBAOH/DCPN system collected in Table 1.

[b] Second order rate constants, k_i, in $s^{-1}M^{-1}$.

[c] k_h. Global hydrolysis rate $k_h = \Sigma_i k_i$

Submitted

More interestingly, it is noteworthy that compound **8** is extremely similar to **4**, with the only difference being the change from a terminal amino group in **4** to an alcohol moiety in **8**. This result also motivates the idea that very minor changes in the catalyst may have a major effect on the hydrolysis of the Tabun simulant DCNP. Accordingly, and in order to understand this remarkable effect, additionally hydrolysis studied were performed with other aminoalcohols (**9**, **10** and **12**) and diamine **11**. For these compounds, DCNP hydrolysis followed the general path shown in Scheme 1. Moreover, the rate constants obtained are listed in Table 2.

In order to compare the kinetic results simply, the global hydrolysis rate (k_h), defined as $k_h = \sum_i k_i$, was calculated. This value is plotted in Figure ESI 6 for all the studied compounds (see also Table 2). From this figure, it is apparent that the highest global hydrolysis rate is observed for **8** and **12**. A closer look at the structure of these compounds shows that they both contained an R-N(R)-CH_2-CH_2-OH moiety. As we saw before, the compounds that only had O heteroatoms generally induced poorer DCNP hydrolysis than the corresponding derivatives with N atoms. Moreover a comparison made of compounds **4**, **5** and **11**, containing only nitrogen atoms, indicates that the presence of ethylenediamine units made the compound more efficient to hydrolyze DCNP (**11** displays a lower overall decomposition rate than **4** and **5**). When the compounds whose structure contained both N and O atoms were compared (i.e., **8**, **9**, **10**, and **12**), we can see that their ability to hydrolyze DCNP depended on several factors: i.e., the chain length and the relative position of the heteroatoms. The effect of the chain length is observed by comparing **9** and **12**; a remarkable higher hydrolysis rate was observed for **12**. Moreover when compounds of similar length bearing the N,O heteroatoms (**8**, **10** and **12**) were compared, the global hydrolysis rate followed this sequence: **8** >> **12** > **10**. Besides if the compounds displaying a higher k_h value were selected (**8** and **12**), it is noteworthy that the OH-CH_2-CH_2-N- moiety was present in both compounds. Moreover, the difference between **12** and **8** was the presence of other -CH_2-CH_2-NH_2 group in **8**, whereas **12** contained a -CH_2-CH_2-OH moiety.

In order to explain the very good results obtained in the DCNP catalysis with compound **8** (via the catalytic hydrolysis shown in equation 12), and bearing in

mind the particular structure of 8 in terms of heteroatoms and their position when compared with other studied compounds, the catalytic mechanism shown in Scheme 3 is proposed.

It is well-known that phosphate compounds react more easily with hydroxyl groups than with amino groups to give rise to the corresponding phosphate ester compounds.[68–71] Based on this concept, intermediate derivative **IV** was formed, in which the amino group close to the hydroxyl group stabilized the intermediate. In a second step, the additional amine at the end of the chain placed a water molecule in the appropriate position (see structure **V** in Scheme 3) to carry out the hydrolysis process, which regenerated the catalyst to allow the process to continue. It is not possible to observe this latter process in shorter amines and it appears to be less effective for the compounds bearing an OH group at the end of the molecule.

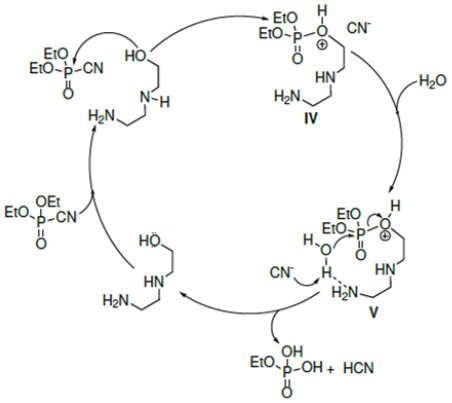

Scheme 3. Proposed catalytic DCNP hydrolysis in the presence of **8**.

In summary we have shown that DCNP hydrolysis is effectively catalyzed by amines and aminoalcohols. Tertiary amines (**1**-**3**) enhance the reaction rate by displacing cyanide from DCNP to form a labile intermediate, which undergoes fast hydrolysis to yield $PO(OH)(EtO)_2$. The Bronsted base nature of amines promotes deprotonation of diethylphosphoric acid to provide a route to phosphate condensation. The efficiency of these amines as hydrolysis catalysts is directly related to their basicity. Polyamines, such as diethylenetriamine (**4**) or tetraethylenepentamine (**5**), exhibit an additional reaction pathway via the

formation of stable P-N bonds after cyanide displacement and form symmetric diphosphoramides. The reactivity of polyamines is governed by their basicity, and also by the structure and size of the polyamine chain, and they produce faster DCNP depletion than tertiary amines. Glycols (**6** and **7**) induce a poor increment in the DCNP hydrolysis. In contrast, amino alcohols (**8**-**12**) generally induce faster DCNP hydrolysis. This is especially so for compound **8**. For instance, DCNP depletion took place ca. 80 times faster in the presence of **8** than when DCNP was alone, and a remarkable complete DCNP hydrolysis was observed under 15 min. The kinetic studies indicate that, apart from non-catalytic reactions, DCNP hydrolysis in the presence of certain amines and aminoalcohols occurs via a catalytic process. This allows us to explain, at least in part, the complete DCNP depletion observed; even when sub-stoichiometric amounts of amines and aminoalcohols are used. In general, DCNP hydrolysis is highly dependent on the structure of the amine, aminoalcohol and glycol used. In this context, the presence of the OH-CH_2-CH_2-N- moiety in the organocatalyst seems crucial to promote the fast hydrolytic reaction of Tabun simulant DCNP. We believe that these findings may help in the design of new and effective organocatalysts for nerve agent remediation.

Acknowledgement

This research has been supported by the Ministerio de Educacin y Ciencia (MAT2012-38429-C04). A.B.B. acknowledges being awarded a pre-doctoral FPI fellowship. SCSIE (Universidad de Valencia) is gratefully acknowledged for all the equipment employed shown in this document.

References

1 Organization for the prohibition of Chemical Weapons. Convention on the prohibition of the development, production, stockpiling and use of chemical weapons and on their destruction: See: www.opcw.nl.

2 Walt, D. R.; Franz, D. R. Biological Warfare Detection. *Anal. Chem*. **2000**, 72, 738A.

3 Angerson, W. S. *Chemical and Biological Warfare Agents. RAND Reports*; 2000.

4 Sadik, O. A.; Jr., W. H. L.; Wang, J. Targeting Chemical and Biological Warfare Agents at the Molecular Level. *Electroanalysis* **2003**, 15, 1149–1159.

5 Gunderson, C. H.; Lehmann, C. R.; Sidell, F. R.; Jabbari, B. Nerve agents: A review. *Neurology,***1992**, 42, 946–950.

6 J. A. Vale, P. R.; Marrs, *T. C. In Chemical Warfare Agents: Toxicology and Treatment*; T. C. Marrs, R. L. M., Sidell, F. R., Eds.; John Wiley & Sons: Chichester, 2007.

7 Taylor, P. In *The Pharmacological Basis of Therapeutics*, 10th ed.; Hardman, J. G., Limbird, L. E., Gilman, A. G., Eds.; McGraw-Hill: New York, 2001; pp 175–191.

8 Pohanka, M. Cholinesterases, a target of pharmacology and toxicology. *Biomed. Papers* **2011**, 155, 219–223.

9 Rao, G. R.; Battacharya, B. K. Multiple signal transduction pathways alterations during nerve agent toxicity. *Toxicol. Letters* **2012**, 208, 16–22.

10 Spradling, K. D.; Dillman, J. F. The Molecular Toxicology of Chemical Warfare Nerve Agents. *Adv. Mol. Toxicol*. **2011**, 5, 111–144.

11 Collombet, J. M. Nerve agent intoxication: Recent neuropathophysiological findings and subsequent impact on medical management prospects. *Toxicol. Appl. Pharmacol*. **2011**, 255, 229–241.

12 Colovic, M. B.; Krstic, D. Z.; Lazarevic-Pasti, T. D.; Bondzic, A. M.; Vasic, V. M. Acetylcholinesterase inhibitors: Pharmacology and toxicology. *Curr. Neuropharm*. **2013**, 11, 315-335.

13 Ajami, D.; Rebek, J. Chemical approaches for detection and destruction of nerve agents. *Org. Biomol. Chem.* **2013**, 11, 3936–3942.

14 Royo, S.;Martínez-Máñez, R.; Sancenón,F.; Costero, A. M.; Parra, M.; Gil, S. Chromogenic and fluorogenic reagents for chemical warfare nerve agents' detection. *Chem. Commun*. **2007,** 4839–4847.

15 Eubanks, L. M.; Dickerson, T. J.; Janda, K. D. Technological advancements for the detection of and protection against biological and chemical warfare agents. *Chem. Soc. Rev* **2007**, 36, 458–470.

16 Smith, B. M. Catalytic methods for the destruction of chemical warfare agents under ambient conditions. *Chem. Soc. Rev.* **2008**, 37, 470–478.

17 Mercey, G.; Verdelet, T.; Renou, J.; Kliachyna, M.; Baati, R.; Nachon, F.; Jean, L.; Renard, P. Y. Reactivators of acetylcholinesterase inhibited by organophosphorus nerve agents. *Acc. Chem. Res*. **2012,** 45, 756–766.

18 Weissman, B. A.; Raveh, L. Multifunctional drugs as novel antidotes for organophosphates poisoning. *Toxicology* **2011**, 290, 149–155.

19 Bajgar, J.; Kuca, K.; Fusek, J.; Jun, D.; Bartosova, L. Cholinesterase reactivators as prophylactics against nerve agents. *Curr. Bioact. Comp*. **2010**, 6, 2–8.

20 Veriansyah, B.; Kim, J. D.; Lee, J. C. Destruction of chemical agent simulants in a supercritical water oxidation bench-scale reactor. *J. Hazard. Mater* **2007**, 147, 8 14.

21 *Nerve Agents, A FOA Briefing Book on Chemical Weapons*; (from www.fas.org/cw/cwagents), 1992.

22 Dawson, R. M.; Pantelidis, S.; Rose, H. R.; Kotsonis, S. E. Degradation of nerve agents by an organophosphate-degrading agent (OpdA). *J. Hazard. Mater*. **2008**, 157, 308–314.

23 Briseno-Roa, L.; Hill, J.; Notman, S.; Sellers, D.; Smith, A. P.; Timperley, C. M.; Wetherell, J.; Williams, N. H.; Williams, G. R.; Fersht, A. R.; Griffiths, A. D. Analogues with fluorescent leaving groups for screening and selection of enzymes that efficiently hydrolyze organophosphorus nerve agents*. J. Med. Chem*. **2006**, 49, 246–255.

24 E., G.; Raushel, F. M. Detoxification of organophosphate nerve agents by bacterial phosphotriesterase. *Toxicol. Appl. Pharmacol*. **2005**, 207, S459–470, Suplement 1.

25 Talmage, S. S.; Watson, A. P.; Hauschild, V.; Munro, N. B.; King, J. Chemical warfare agent degradation and decontamination. *Curr. Org. Chem*. **2007**, 11, 285–298.

26 Walters, F.; Taylor, E. R. Chemical agent decontamination chemical terrorism attack decontamination-household oxidizers: what works. *J. Undergrad. Chem. Res.* **2003**, 2, 107–112.

27 Laman, D. M.;Weller, B. D.; Skeen, R. S. Reducing health risk assigned to organic emissions from a chemical weapons incinerator. *Environ. Monit. Assess*. **2013**, 185, 2257–2267.

28 Vayron, P.; Renard, P.; Valleix, A.; Mioskowski, C. Design and synthesis of an a;a-difluorophosphinate hapten for antibody-Catalyzed-hydrolysis of organophosphorus nerve agents. *Chem. Eur. J*. **2000**, 6, 1050–1063.

29 Saint-André, G.; Kliachyna, M.; Kodepelly, S.; Louise-Leriche, L.; E. Gillon, P. Y. R.; Nachon, F.; Baati, R.; Wagne, A. Design, synthesis and evaluation of new -nucleophiles for the hydrolysis of organophosphorus nerve agents: application to the reactivation of phosphorylated acetylcholinesterase. *Tetrahedron* **2011**, 67, 6352–6361.

30 Zafrani, Y.; Yehezkel, L.; Goldvaser, M.; Marciano, D.;Waysbort, D.; Gershonov, E.; Columbus,I. The reactivity of quaternary ammonium- versus potassium- fluorides supported onmetal oxides: paving the way to an instantaneous detoxification of chemical warfare agents. *Org. Biomol. Chem*. **2011**, 9, 8445–8451.

31 Lee, T. J.; Chun, B. C.; Chung, Y. C. Detoxification of reactive compounds by a cyclic electrolytic system with surface-modified ion-exchange resin. *React. Func. Polym*. **2003**, 56, 37–44.

32 Nassar, A. E. F.; Lucas, S. V.; Jones, W. R.; Hoffland, L. D. Separation of chemical warfare agent degradation products by the reversal of electroosmotic flow in capillary electrophoresis. *Anal. Chem*. **1998**, 70, 1085–1091.

33 Mizrahi, D. M.; Saphier, S.; Columbus, I. Efficient heterogeneous and environmentally friendly degradation of nerve agents on a tungsten-based POM. *J. Hazard. Mater*. **2010**, 179, 495–499.

34 Bailey, M. M.; Heddelstone, J. M.; Davis, J.; Staymates, J. L.; Walker, A. R. H. Functionalized, carbon nanotube material for the catalytic degradation of organophosphate nerve agents. *Nano Res*. **2014**, 7, 390–398.

35 Wille, T.; Thiermann, H.; Worek, F. In vitro kinetics of nerve agent degradation by fresh frozen plasma (FFP). *Arch. Toxicol.* **2014**, 88, 301–307.

36 Petrick, L. M.; Sabach, S.; Dubowski, Y. Degradation of VX surrogate profenofos on surfaces via in situ photo-oxidation. *Environ. Sci. Technol.* **2013,** 47, 8751–8758.

37 Komano, A.; Hirakawa, T.; Sato, K.; Kishi, S.; Nishimoto, C. K.; Mera, N.; Kugishima, M.; Sano, T.; Negishi, N.; Ichinose, H.; Hiromichi, S.; Y. Seto, K. T. Titanium dioxide photocatalytic decomposition of ethyl-S-dimethylaminoethyl methylphosphonothiolate (VX) in aqueous phase. *Appl. Catal. B* **2013**, 134-135, 19–25.

38 Grandcolas, M.; Sinault, L.; Mosset, F.; Louvet, A.; Keller, N.; Keller, V. Selfdecontaminating layer-by-layer functionalized textiles based on WO3-modified titanate nan-otubes. Application to the solar photocatalytic removal of chemical warfare agents. *Appl.Catal. A* **2011**, 391, 455–467.

39 Letant, S. E.; Kane, S. R.; Hart, B. R.; Hadi, M. Z.; Cheng, T. C.; Rastogi, V. K.;Reynolds, J. G. Hydrolysis of acetylcholinesterase inhibitors organophosphorus acid anhydrolase enzyme immobilization on photoluminescent porous silicon platforms. *Chem. Commun.* **2005,** 7, 851–853.

40 Dai, K.; Peng, T. Y.; Chen, H.; Liu, J.; Zan, L. Photocatalytic degradation of dommercial phoxim over la-doped TiO2 nanoparticles in aqueous suspension. *Environ. Sci. Technol.* **2009**,43, 1540–1545.

41 Wagner, G. W.; Bartram, P. W.; Koper, O.; Klabunde, K. J. Reactions of VX, GD, and HD with nanosize MgO. *J. Phys. Chem. B*, **1999**, 103, 3225–3228.

42 Wagner, G. W.; Procell, L. R.; OConnor, R. J.; Munavalli, S.; Carnes, C. L.; Kapoor, P. N.; Klabunde, K. J. Reactions of VX, GB, GD, and HD with nanosize Al_2O_3. Formation of aluminophosphonates. *J. Am. Chem. Soc*. **200**1, 123, 1636–1644.

43 Wagner, G. W.; Procell, L. R.; Munavalli, S. ^{27}Al, $^{47,49}Ti$, ^{31}P, and ^{13}C MAS NMR Study of VX, GD, and HD reactions with nanosize Al_2O_3, conventional Al_2O_3 and TiO_2, and Aluminum and Titanium Metal. *J. Phys. Chem. C* **2007**, 111, 17564–17569.

44 Mahato, T. H.; Prasad, G. K.; Singh, B.; Acharya, J.; Srivastava, A. R.; Vijayaraghavan, R. Nanocrystalline zinc oxide for the decontamination of sarin. *J. Hazard. Mater*. **2009**, 165,928–932.

45 Panayotov, D. A.; Morris, J. R. Catalytic degradation of a chemical warfare agent simulant: Reaction mechanisms on TiO_2-Supported Au nanoparticles. *J. Phys. Chem. C* **2008**, 112, 7496–7502.

46 Wagner, W.; Koper, O. B.; Lukas, E.; Decker, S.; Klabunde, K. J. Reactions of VX, GD, and HD with nanosize CaO: Autocatalytic dehydrohalogenation of HD. *J. Phys. Chem. B* **2000**, 104, 5118–5123.

47 Narske, R. M.; Klabunde, K. J.; Fultz, S. Solvent effects on the heterogeneous adsorption reactions of (2-chloroethyl)ethyl sulfide on nanocrystalline magnesium oxide. *Langmuir*,**2002**, 18, 4819–4825.

48 Seger, M. R.; Maciel, G. E. NMR investigation of the behavior of an organothiophosphate pesticide, Chlorpyrifos, sorbed on montmorillonite clays. *Eviron. Sci. Technol*. **2006**, 40,797–802.

49 Schultz, A. M.; Farha, O. K.; Hupp, J. T.; Nguyen, S. T. A catalytically active, permanently microporous MOF with metalloporphyrin struts. *J. Am. Chem. Soc*. **2009**, 131, 4204–4205.

50 Ma, L.; Abney, C.; Lin, W. Enantioselective catalysis with homochiral metalorganic frameworks. *Chem. Soc. Rev*. **2009**, 38, 1248–1256.

51 Katz, M. J.; Mondloch, J. E.; Totten, R. K.; Park, J. K.; Nguyen, S. B. T.; Farha, O. K.;Hupp, J. T. Simple and compelling biomimetic metalorganic framework catalyst for the degradation of nerve agent simulants. *Angew. Chem. Int. Ed.* **2014**, 53, 497–501.

52 Totten, R. K.; Kim, Y. S.; Weston, M. H.; Farha, O. K.; Hupp, J. T.; Nguyen, S. T. Enhanced catalytic activity through the tuning of micropore environment and supercritical CO_2 processing: Al(porphyrin)-based porous organic polymers for the degradation of a nerve Aagent simulant. *J. Am. Chem. Soc*. **2013**, 135, 11720–11723.

53 El-Boubbou, K.; Schofield, D. A.; Landry, C. C. Enhanced enzymatic activity of OPH in ammonium-functionalized mesoporous silica: Surface modification and pore effects. *J. Phys. Chem. C* **2012**, 116, 17501–17506.

54 Saxena, A.; Srivastava, A. K.; Singh, B.; Goyal, A. Removal of sulphur mustard, sarin and simulants on impregnated silica nanoparticles. *J. Hazard. Mater*. **2012**, 211-212, 226–232.

55 Knagge, K.; Johnson, M.; Grassian, V. H.; Larsen, S. C. Adsorption and thermal reaction of DMMP in nanocrystalline NaY. *Langmuir* **2006**, 22, 11077–11084.

56 Meng, Q.; Doetschman, D. C.; Rizos, A. K.; Lee, M.-H.; Schulte, J. T.; A.Spyros,; Kanyi, C. W. Adsorption of organophosphates into microporous and mesoporous NaX zeolites and subsequent chemistry. *Environ. Sci. Technol*. **2011**, 45, 3000–3005.

57 Jackson, J. B. *Development of decontamination solution DS2. Technical report*; 1960.

58 Richardson, G. A. *Development of a package decontamination system. Final report*; Contract DAAA15-71-C-0508, 1972.

59 Singh, B.; Prasad, G. K.; Pandey, K. S.; Danikhel, R. K.; Vijayaraghavan, R. Decontamination of chemical warfare agents. *Defense Sci. J*. **2010**, 60, 428–441.

60 Yang, Y. C.; Baker, J. A.; Ward, J. R. Decontamination of chemical warfare agents. *Chem.Rev*. **1992**, 92, 1729–1743.

61 Gahan, L. R.; Smith, S. J.; Neves, A.; Schenk, G. Phosphate ester hydrolysis: Metal complexes as purple acid phosphatase and phosphotriesterase analogues. *Eur. J. Inorg. Chem.* **2009**, 2745–2758.

62 Xie, Y.; Popov, B. N. Catalyzed hydrolysis of nerve gases by metal chelate compounds and potentiometric detection of the byproducts. *Anal. Chem*. **2000**, 72, 2075–2079.

63 Barba-Bon, A.; Costero, A. M.; Parra, M.; Gil, S.; Martínez-Máñez, R.; Sancenón, F.; Gale, P. A.; Hiscock, J. R. Neutral 1,3-diindolylureas for nerve agent remediation. *Chem. Eur. J.* **2013**, 19, 1586–1590.

64 Sambrook, M. R.; Hiscock, J. R.; Cook, A.; Green, A. C.; Holden, I.; Vicent, J. C.; Gale, P. A. Hydrogen bond-mediated recognition of the chemical warfare agent soman (GD). *Chem.Commun* **2012**, 48, 5605–5607.

65 Gray, P.; Scott, S. *Chemical oscillations and inestabilities. Non linear Chemical Kinetics,* 1st ed.; Oxford University Press, 1994; Chapter 1, pp 5–13.

66 Yang, Y.; Szafraciec, L. L.; Beauddy, W. T.; Rohrbaugh, D. K.; Procelland, L. R.; Samuel, J. B. Autocatalytic hydrolysis of V-Type nerve agents. *J. Org. Chem.* **1996**, 61, 8407–8413.

67 Roses, M.; Bosch, E. Influence of mobile phase acid-base equilibria on the chromatographic behaviour of protolytic compounds. *J. Chromatograph. A* **2002**, 982, 1–30.

68 Barba-Bon, A.; Costero, A. M.; Gil, S.; Harriman, A.; Sancenón, F. Highly selective detection of nerve-agent simulants with BODIPY dyes. *Chem. Eur. J.* **2014**, 20, 6339–6347.

69 Gotor, R.; Costero, A. M.; S.Gil,; Parra, M.; Mart´ınez-M´a˜nez, R.; Sancen´on, F. A Molecular Probe for the Highly Selective Chromogenic Detection of DFP, a Mimic of Sarin and Soman Nerve Agents. *Chem. Eur. J.* **2011**, 17, 11994–11997.

70 Costero, A. M.; Gil, S.; Parra, M.; Mancini, P. M. E.; Martínez-Máñez, R.; Sancenón, F.;Royo, S. Chromogenic detection of nerve agent mimics. *Chem. Commun*. **2008**, 6002–6004.

71 Royo, S.; Costero, A. M.; Parra, M.; Gil, S.; Martínez-Máñez, R.; Sancenón F. Chromogenic, specific detection of the nerve-agent Mimic DCNP (a Tabun mimic). *Chem. Eur. J.* **2011**, 17, 6931–6934.

Supporting Information

Towards the design of organocatalysts for nerve agents remediation: the case of the active hydrolysis of DCNP (a Tabun mimic) catalyzed by simple amine-containing derivatives.

Andrea Barba-Bon, Ramón Martínez-Máñez*,*
Felix Sancenón, Ana M.Costero, Salvador Gil,
Francisco Pérez-Pla, *and Elisa Llopis*

Table of Contents

1 ^{31}P NMR spectra of selected systems

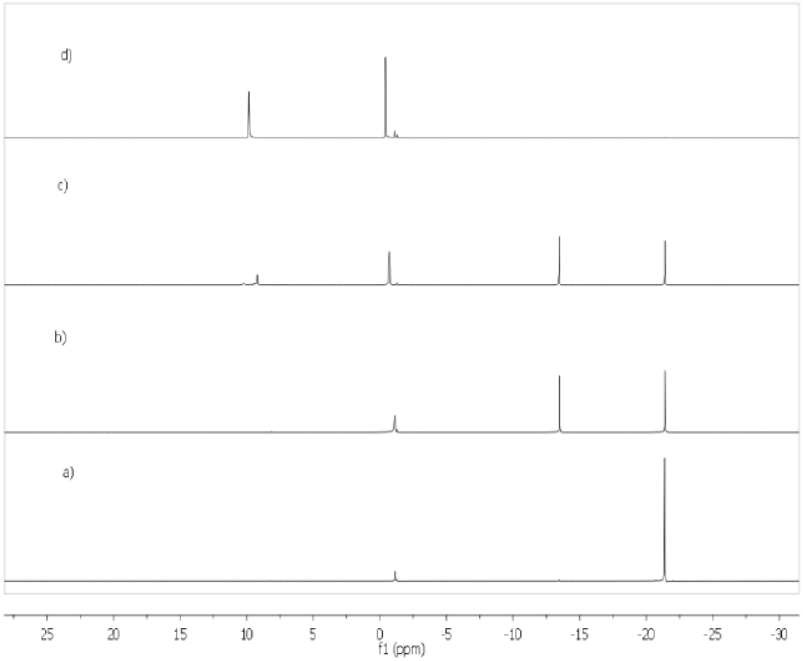

Figure SI- 1. ^{31}P NMR of DCNP (a) alone and in the presence of 0.1 eq. of (b) **2**, (c) **5** and (d) **10** after 15 minutes in acetonitrile: water 95:5 v/v.

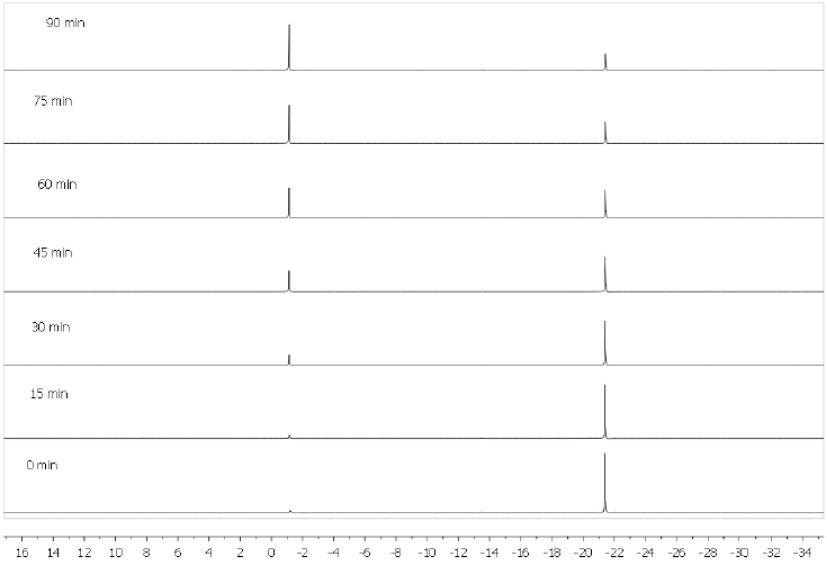

Figure SI-2. ^{31}PNMR stacked plot of DCNP hydrolysis (0.6 M in acetonitrile: water 95:5 v/v).

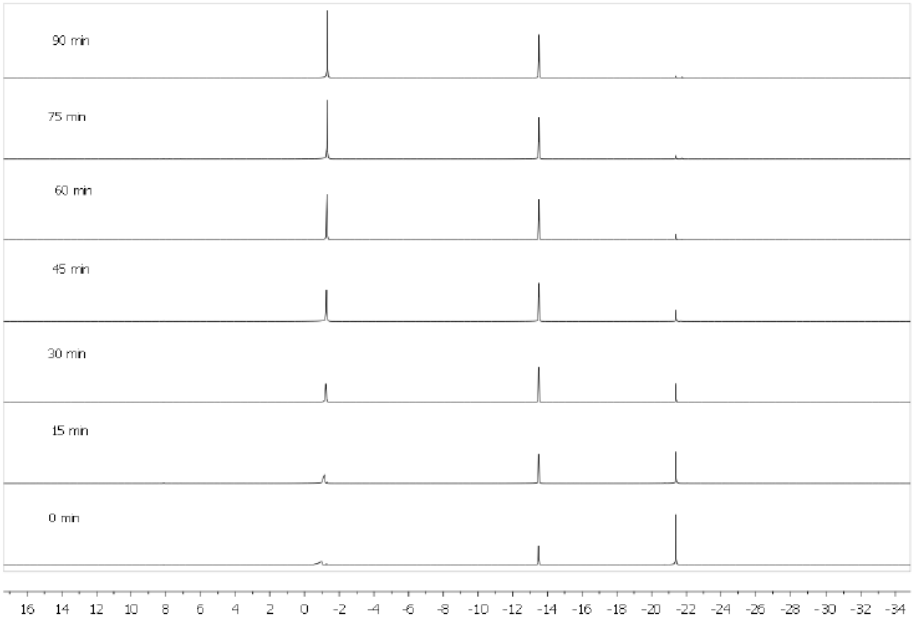

Figure SI-3. ^{31}PNMR stacked plot of DCNP (0.6 M) hydrolysis by **2** (0.06 M) (acetonitrile: water 95:5 v/v).

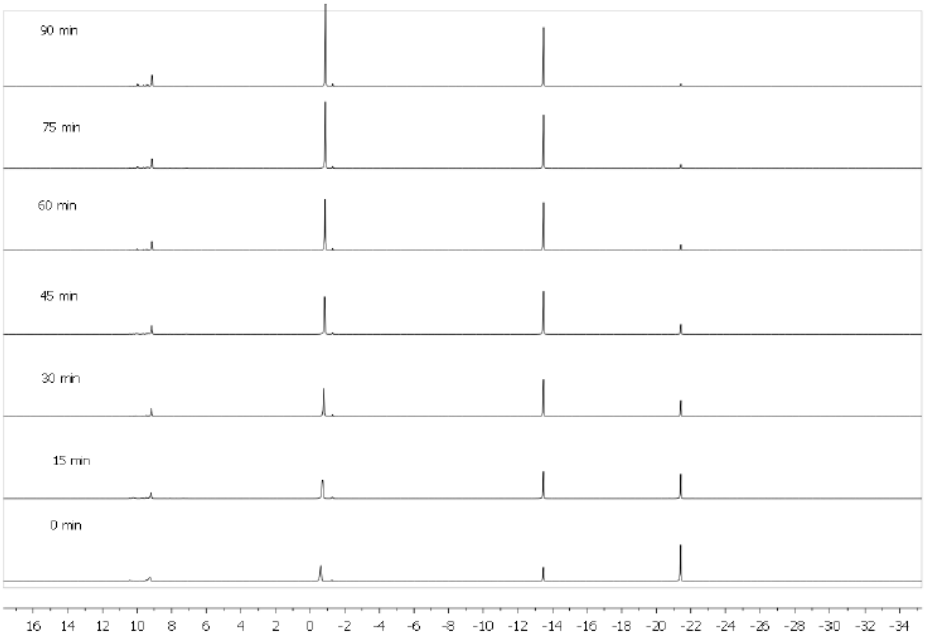

Figure SI-4. ^{31}PNMR stacked plot of DCNP (0.6 M) hydrolysis by **10** (0.06 M) (acetonitrile: water 95:5 v/v).

2 Relative efficiency of catalysts

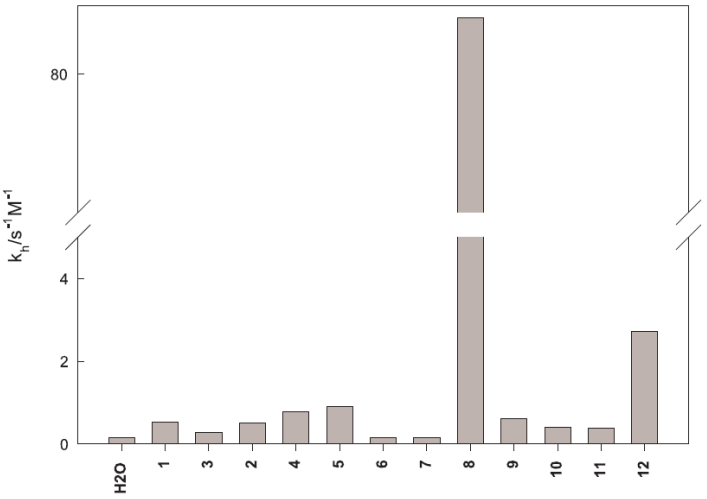

Figure SI-5. Bar diagram of the efficiency of the different compounds in the decomposition of DCNP.

3 Calculation procedures

3.1 Data treatment

The concentration of the phosphorous-containing species (**C**) was calculated from the area of the peaks in the corresponding ^{31}P NMR spectra. Experimental curves were compared to those calculated from the chemical model, ($\hat{\mathbf{C}}$) by the standard least-squares method; that is, by minimizing function $\phi(k) = \sum_{ij} R_{ij}^2$ in relation to rate constants, **k**. In the previous function, residuals were defined as **R** = **C**-$\hat{\mathbf{C}}$. Minimization of the least-squares function was achieved by the Nelder-Mead method,[1] and by refining stationary points using gradient methods and, in particular, using the BFGS algorithm.[2,3,4,5] Stationary points were characterized by analyzing the eigenvalues of the Hessian matrix. Theoretical concentration curves were calculated by integrating the ODE system associated with each model. Stiff-adapted methods were used for integration.[6] Calculations were made by OPKMCR, a software designed to process multi-response kinetic data based on previous versions of the OPKINE algorithm.[7].

3.2 General features of calculation procedure

The calculation procedure described below has been carried out by means of OPKMCR software[1], a new version of the old OPKINE program,[7] specialized in the analysis of multi-response kinetic data.[2] For the sake of simplicity, the following nomenclature is used for concentrations of chemical species, **c**(*t*). Molar units are assumed along this work.

c_1 = [DCNP]
c_2 = [$OP(OEt)_2(OH)$]
c_3 = [$OP(OEt)_2O^-$]
c_4 = [tetraethylpyrophosphate]
c_5 = [H_2O]
c_6 = [OH^-]
c_7 = [H_3O^+]
c_8 = [HCN]
c_9 = [CN^-]
c_{10} = [NR_3]
c_{11} = [HNR_3^+]
C_{12} = [phosphoramide]
C_{13} = [EG or DEG]

Concentrations were calculated integrating the ordinary differential equation system (ODE) (1), under initial conditions **c**(0).

$$\frac{d_c}{d_t} = \mathbf{Mr} \tag{1}$$

Matrix **M** in Equation (1) designates the stoichiometric coefficients arranged in columns, and vector **r** the reaction rates. Integration was carried out by using the lsode [8] stiff-adapted routines interfaced by OPKMCR. Concentrations were worked out at time **t** = {t_1; t_2,…, t_{nt} }, and stored in a two-dimensional array $\hat{\mathbf{C}}(n_t x n_s)$.[3] Parameters n_s and n_t are equal to the number of chemical species of the model and the number of times at which recording of spectra was carried out.

Concentration of phosphorus containing species, was calculated by integration of peak areas of ^{31}PNMR spectra at the times indicated above, and stored in a two-

[1] Unpublished results.
[2] OPKMCR is free distributable software encoded in the *octave* programing environment. It is available under request.
[3] The symbol ^ stands for “calculated from the model”

dimensional array **X** (n_t x n_r). Model responses, **ˆX** (n_t x n_r), were calculated from equation (2), where **F** is a (n_s x n_s) array containing the response factors, and matrix **S** is included to remove the columns of **ˆX** associated to ^{31}PNMR silent species,

$$\mathbf{\hat{X}} = \mathbf{\hat{C}} \times \mathbf{F} \times \mathbf{S} \quad (2)$$

For ^{31}PNMR data, **F** is a diagonal matrix whose elements are '1' or '0' depending whether the species contain phosphorus or not. Experimental responses, **X**, were compared to those of the model, **ˆX**, by means of the least-squares criteria (Equation (3)), that is, by minimizing the sum of the squares of the residuals, **R** = **X**-**ˆX**. Objective function ϕ is solely dependent on **k**, an array containing the rate constants of reactions involved in the mechanism.

$$\phi(\mathbf{k}) = \sum_{i,j}^{n_t n_r} R_{i,j}^2 \quad (3)$$

Rate constants were calculated minimizing function (3) with regard **k**. The minimum was localized by means of the Nelder-Mead [1] method, and it was further refined employing gradient methods, specifically the BFGS method.[2,3,4,5] After completing the calculation, the stationary point was characterized analyzing the eigenvalues of the Hessian matrix (**H**), λ_H.

$$\mathbf{H}/H_{ij} = \frac{d^2\phi}{dk_i\, dk_j} \quad (4)$$

3.3 Calculations for DCNP hydrolysis in pure water

Concentration data for DCNP hydrolysis in water were calculated by integrating the ordinary differential equation system (ODE) (5) involving reactions R1 and R2 and equilibria EQ1,EQ2 and EQ6, under the initial conditions **c**(0) = {c_1(0)=0.6; c_2(0)= 0.0; c_5(0)=2.53; c_6(0)=0; c_7(0)=0; c_8(0)=0; c_9(0)=0} (the matrix collects the stoichiometric coefficients of reactions listed in Table (1)). Columns refer to reactions whereas rows refer to compounds).

$$\frac{d}{dt}\begin{pmatrix} c_1(t) \\ c_2(t) \\ c_3(t) \\ c_5(t) \\ c_6(t) \\ c_7(t) \\ c_8(t) \\ c_9(t) \end{pmatrix} = \begin{pmatrix} -1 & -1 & 0 & 0 & 0 & 0 & 0 & 0 \\ 1 & 1 & 0 & 0 & 0 & 0 & 0 & 0 \\ 0 & 0 & -1 & 1 & 0 & 0 & 0 & 0 \\ -1 & -1 & -1 & 1 & -1 & 1 & -2 & 2 \\ 0 & 0 & 1 & -1 & 1 & -1 & 1 & -1 \\ 0 & 0 & 0 & 0 & 0 & 0 & 1 & -1 \\ 1 & 1 & 1 & -1 & 1 & -1 & 0 & 0 \\ 0 & 0 & 0 & 0 & -1 & 1 & 0 & 0 \end{pmatrix} \times \begin{pmatrix} r_1(\mathbf{c}) \\ r_2(\mathbf{c}) \\ r_1^{(eq)} \\ r_{-1}^{(eq)} \\ r_2^{(eq)} \\ r_{-2}^{(eq)} \\ r_6^{(eq)} \\ r_{-6}^{(eq)} \end{pmatrix} \tag{5}$$

Equilibria E1, E2 and E6 were introduced as couples of opposite reactions see Equations (10)-(12),

$$\left.\begin{aligned} r_1^{(eq)} &= k_1^{(eq)} c_3 c_5 \\ r_{-1}^{(eq)} &= k_{-1}^{(eq)} c_2 c_6 \end{aligned}\right\} \; K_1 = \frac{k_1^{(eq)}}{k_{-1}^{(eq)}} \tag{6}$$

$$\left.\begin{aligned} r_2^{(eq)} &= k_2^{(eq)} c_5 c_9 \\ r_{-2}^{(eq)} &= k_{-2}^{(eq)} c_6 c_8 \end{aligned}\right\} \; K_2 = \frac{k_2^{(eq)}}{k_{-2}^{(eq)}} \tag{7}$$

$$\left.\begin{aligned} r_6^{(eq)} &= k_6^{(eq)} c_5 c_5 \\ r_{-6}^{(eq)} &= k_{-2}^{(eq)} c_6 c_7 \end{aligned}\right\} \; K_w = \frac{k_6^{(eq)}}{k_{-6}^{(eq)}} \tag{8}$$

where $\{k_1^{(eq)} k_{-1}^{(eq)} k_2^{(eq)} k_{-2}^{(eq)} k_6^{(eq)} k_{-6}^{(eq)}\}$ were dummy parameters. The following values near the diffusion limit were set up fixed during calculations:

$k_{-1}^{(eq)} = k_{-2}^{(eq)} = k_{-6}^{(eq)} = 10^{10}$, and the objective function was minimized with regard to K_1 and K_2. K_w was set constant and equal to the values found in the literature (pK_w = 18:18).

The ODE describes the kinetics of the formal processes R1 and R2 shown in Table (1).Equation R1 stands for the non-catalyzed hydrolysis induced by water, whereas R2 describes the $OP(OEt)_2(OH)$ autocatalytic process. Table (1) also collects the expressions employed for reaction rates, r_1 and r_2. The objective function was minimized respect to **k** = {k_1; k_2}. Diagonalization of the Hessian at the minimum resulted in positive eigenvalues, so that the stationary point found was a minimum. Calculation results are given in the manuscript.

Table 1. Reaction mechanism. Associated reaction rates and equilibrium constants

	Reaction	Expression for rate
R1	$DCNP + H_2O \xrightarrow{k_1} OP(OEt)_2(OH) + HCN$	$r_1 = k_1[DCNP][H_2O]$
R2	$DCNP + OP(OEt)_2(OH) + H_2O \xrightarrow{k_2} 2OP(OEt)_2(OH) + HCN$	$r_2 = k_2[DCNP][OP(OEt)_2(OH)]$
R3	$DCNP + OP(OEt)_2O^- \xrightarrow{k_3} TEPP + CN^-$	$r_3 = k_3[DCNP][OP(OEt)_2O-]$
R4	$OP(OEt)_2O^- + OP(OEt)_2(OH) \xrightarrow{k_4} TEPP + OH^-$	$r_4 = k_4[OP(OEt)_2O-][OP(OEt)_2(OH)]$
R5	$DCNP + OH^- \xrightarrow{k_5} OP(OEt)_2(OH) + CN^-$	$r_5 = k_5[DCNP][OH-]$
R6	$DCNP + H_2O + NR_3 \xrightarrow{k_6} OP(OEt)_2(OH) + HCN + NR_3$	$r_6 = k_6[DCNP][NR_3]$
R7	$DCNP + OP(OEt)_2O^- + NR_3 \xrightarrow{k_7} TEPP + CN^- + NR_3$	$r_7 = k_7[DCNP][NR_3]$
R8	$TEPP + H_2O \xrightarrow{k_8} 2OP(OEt)_2(OH)$	$r_8 = [TEPP][H_2O]$
R9	$DCNP + H_2NRNH_2 \xrightarrow{k_9} phosphoramide + HCN$	$r_9 = [DCNP][H_2NRNH_2]$
R10	$2DCNP + H_2O + ethyleneglycol \xrightarrow{k_{10}} TEPP + 2HCN + ethyleneglycol$	$r_{10} = [DCNP]^2[ethyleneglycol]$
	Equilibrium	**Equilibrium constant**
E1	$OP(OEt)_2O^- + H_2O \overset{K_1}{\rightleftharpoons} OP(OEt)_2(OH) + OH^-$	$K_1 = \frac{[OP(OEt)_2(OH)][OH-]}{[OP(OEt)_2O-][H_2O]}$
E2	$CN^- + H_2O \overset{K_2}{\rightleftharpoons} HCN + OH^-$	$K_2 = \frac{[HCN][OH-]}{[CN-][H_2O]}$
E3	$NR_3 + H_2O \overset{K_3}{\rightleftharpoons} HNR_3^+ + OH^-$	$K_3 = \frac{[HNR_3^+][OH-]}{[NR_3][H_2O]}$
E4	$NR_3 + OP(OEt)_2(OH) \overset{K_4}{\rightleftharpoons} HNR_3^+ + OP(OEt)_2O^-$	$K_4 = \frac{[HNR_3^+][OP(OEt)_2O-]}{[NR_3][OP(OEt)_2(OH)]}$
E5	$NR_3 + HCN \overset{K_5}{\rightleftharpoons} HNR_3^+ + CN^-$	$K_5 = \frac{[HNR_3^+][CN-]}{[NR_3][HCN]}$
E6	$2H_2O \overset{K_6}{\rightleftharpoons} H_3O^+ + OH^-$	$K_w = \frac{[H_3O^+][OH-]}{[H_2O]^2}$

3.4 Calculations for DCNP hydrolysis in presence of tetrabutyl hydroxide (TBAOH)

Reactions R1, R2, R3, R4, E1, E2, and E6 in Table (1) describe the hydrolysis mechanism in presence of TBAOH. A previous calculation indicated that the objective function was quite insensitive to parameter k_5 related to DCNP hydrolysis by OH^-. A close inspection of the concentration array at the minimum revealed that hydroxide was consumed from the very beginning, its concentration being quite small throughout the entire reaction. This was an expected result, as hydrolysis yielded acidic media due to the forming species $OP(OEt)_2(OH)$ and HCN. For this reason, the rate of reaction R5 did not contribute significatively under these experimental conditions, and it was, therefore, excluded from further calculations. Concentration array was calculated integrating Equation (9), under

initial conditions **c**(0) = {c_1(0)=0.6; c_2(0)= 0.0; c_3(0)=0.0; c_4(0)=0.0; c_5(0)= 2.53; c_6(0)= 0.006; c_7(0)=0.0; c_8(0)=0.0; c_9(0)=0.0}

$$\frac{d}{dt}\begin{pmatrix} c_1(t) \\ c_2(t) \\ c_3(t) \\ c_4(t) \\ c_5(t) \\ c_6(t) \\ c_7(t) \\ c_8(t) \\ c_9(t) \end{pmatrix} = \begin{pmatrix} -1 & -1 & 0 & -1 & 0 & 0 & 0 & 0 & 0 & 0 \\ 1 & 1 & -1 & 0 & 1 & -1 & 0 & 0 & 0 & 0 \\ 0 & 0 & -1 & -1 & -1 & 1 & 0 & 0 & 0 & 0 \\ 0 & 0 & 1 & 1 & 0 & 0 & 0 & 0 & 0 & 0 \\ -1 & -1 & 0 & 0 & -1 & 1 & -1 & 1 & -2 & 2 \\ 0 & 0 & 1 & 0 & 1 & -1 & 1 & -1 & 1 & -1 \\ 0 & 0 & 0 & 0 & 0 & 0 & 0 & 0 & 1 & -1 \\ 1 & 1 & 0 & 0 & 0 & 0 & 1 & -1 & 0 & 0 \\ 0 & 0 & 0 & 1 & 0 & 0 & -1 & 1 & 0 & 0 \end{pmatrix} \times \begin{pmatrix} r_1 \\ r_2 \\ r_3 \\ r_4 \\ r_1^{(eq)} \\ r_{-1}^{(eq)} \\ r_2^{(eq)} \\ r_{-2}^{(eq)} \\ r_6^{(eq)} \\ r_{-6}^{(eq)} \end{pmatrix} \tag{9}$$

Equilibria E1, E2 and E6 were introduced as couples of opposite reactions, see Equations (10)-(12),

$$\left.\begin{aligned} r_1^{(eq)} &= k_1^{(eq)} c_3 c_5 \\ r_{-1}^{(eq)} &= k_{-1}^{(eq)} c_2 c_6 \end{aligned}\right\} \; K_1 = \frac{k_1^{(eq)}}{k_{-1}^{(eq)}} \tag{10}$$

$$\left.\begin{aligned} r_2^{(eq)} &= k_2^{(eq)} c_5 c_9 \\ r_{-2}^{(eq)} &= k_{-2}^{(eq)} c_6 c_8 \end{aligned}\right\} \; K_2 = \frac{k_2^{(eq)}}{k_{-2}^{(eq)}} \tag{11}$$

$$\left.\begin{aligned} r_6^{(eq)} &= k_6^{(eq)} c_5 c_5 \\ r_{-6}^{(eq)} &= k_{-2}^{(eq)} c_6 c_7 \end{aligned}\right\} \; K_w = \frac{k_6^{(eq)}}{k_{-6}^{(eq)}} \tag{12}$$

where $\{k_1^{(eq)} k_{-1}^{(eq)} k_2^{(eq)} k_{-2}^{(eq)} k_6^{(eq)} k_{-6}^{(eq)}\}$ were dummy parameters. The following values near the diffusion limit were set up fixed during calculations: $k_{-1}^{(eq)} = k_{-2}^{(eq)} = k_{-6}^{(eq)} = 10^{10}$, and the objective function was minimized with regard to K_1 and K_2. Diagonalization of the Hessian at the minimum resulted in positive eigenvalues (λ_H = {2.2245x10^{-6}; 4.8452 x10^{-4}; 5.2219 x10^{-2}; 2.4603 x10^{-1}; 7.9703}), so that the stationary point found was a minimum. Calculation results are given in the manuscript.

3.5 Calculations for DCNP hydrolysis in presence of tertiary amines

Hydrolysis of DCNP in presence of tertiary amines was analyzed using the reaction set R1, R2, R3, R6, R7, R8, E1, E2, E3, E4,E5, and E6, see table (1). This is basically the reaction scheme described in (§3.4), but adding processes related to amine-

catalysis (R6, R7), and amine acid-base equilibria (E3, E4, E5). Calculation of concentration of species was achieved integrating Equation (13), under initial conditions **c**(0) = {c_1(0)=0.6; c_2(0)= 0.0; c_3(0)=0.0; c_4(0)=0.0; c_5(0)= 2.53; c_6(0)= 0.0; c_7(0)=0.0; c_8(0)=0.0; c_9(0)=0.0; c_{10}(0)=0.06; c_{11}(0)=0.0},

$$\frac{d}{dt}\begin{pmatrix} c_1(t) \\ c_2(t) \\ c_3(t) \\ c_4(t) \\ c_5(t) \\ c_6(t) \\ c_7(t) \\ c_8(t) \\ c_9(t) \\ c_{10}(t) \\ c_{11}(t) \end{pmatrix} = \mathbf{M}_{TEA} \times \begin{pmatrix} r_1 \\ r_2 \\ r_6 \\ r_3 \\ r_7 \\ r_8 \\ r_1^{(eq)} \\ r_{-1}^{(eq)} \\ r_2^{(eq)} \\ r_{-2}^{(eq)} \\ r_3^{(eq)} \\ r_{-3}^{(eq)} \\ r_4^{(eq)} \\ r_{-4}^{(eq)} \\ r_5^{(eq)} \\ r_{-5}^{(eq)} \\ r_6^{(eq)} \\ r_{-6}^{(eq)} \end{pmatrix} \tag{13}$$

where the value of MTEA is given by expression (14),

$$\mathbf{M}_{TEA} = \begin{pmatrix} -1 & -1 & -1 & -1 & -1 & 0 & 0 & 0 & 0 & 0 & 0 & 0 & 0 & 0 & 0 & 0 & 0 \\ 1 & 1 & 1 & 0 & 0 & 2 & 1 & -1 & 0 & 0 & 0 & 0 & -1 & 1 & 0 & 0 & 0 & 0 \\ 0 & 0 & 0 & -1 & -1 & 0 & -1 & 1 & 0 & 0 & 0 & 0 & 1 & -1 & 0 & 0 & 0 & 0 \\ 0 & 0 & 0 & 1 & 1 & -1 & 0 & 0 & 0 & 0 & 0 & 0 & 0 & 0 & 0 & 0 & 0 & 0 \\ -1 & -1 & -1 & 0 & 0 & -1 & -1 & 1 & -1 & 1 & -1 & 1 & 0 & 0 & 0 & 0 & -2 & 2 \\ 0 & 0 & 0 & 0 & 0 & 0 & 1 & -1 & 1 & -1 & 1 & -1 & 0 & 0 & 0 & 0 & 1 & -1 \\ 0 & 0 & 0 & 0 & 0 & 0 & 0 & 0 & 0 & 0 & 0 & 0 & 0 & 0 & 0 & 0 & 1 & -1 \\ 1 & 1 & 1 & 0 & 0 & 0 & 0 & 0 & 1 & -1 & 0 & 0 & 0 & 0 & -1 & 1 & 0 & 0 \\ 0 & 0 & 0 & 1 & 1 & 0 & 0 & 0 & -1 & 1 & 0 & 0 & 0 & 0 & 1 & -1 & 0 & 0 \\ 0 & 0 & 0 & 0 & 0 & 0 & 0 & 0 & 0 & 0 & -1 & 1 & -1 & 1 & -1 & 1 & 0 & 0 \\ 0 & 0 & 0 & 0 & 0 & 0 & 0 & 0 & 0 & 0 & 1 & -1 & 1 & -1 & 1 & -1 & 0 & 0 \end{pmatrix} \tag{14}$$

Equilibria E3, E4 and E5 were introduced as described below, through couples of opposite reactions. The following equations were used,

$$\left.\begin{aligned} r_3^{(eq)} &= k_3^{(eq)} c_5 c_{10} \\ r_{-3}^{(eq)} &= k_{-3}^{(eq)} c_6 c_{11} \end{aligned}\right\} \; K_3 = \frac{k_3^{(eq)}}{k_{-3}^{(eq)}} \tag{15}$$

$$\left.\begin{aligned} r_4^{(eq)} &= k_4^{(eq)} c_2 c_{10} \\ r_{-4}^{(eq)} &= k_{-4}^{(eq)} c_3 c_{11} \end{aligned}\right\} \; K_4 = \frac{k_4^{(eq)}}{k_{-4}^{(eq)}} \tag{16}$$

$$\left.\begin{aligned} r_5^{(eq)} &= k_5^{(eq)} c_{10} c_8 \\ r_{-5}^{(eq)} &= k_{-5}^{(eq)} c_9 c_{11} \end{aligned}\right\} \; K_5 = \frac{k_5^{(eq)}}{k_{-5}^{(eq)}} \tag{17}$$

As described previously, the dummy parameters $k_{-1}^{(eq)} = k_{-2}^{(eq)} = k_{-3}^{(eq)} = k_{-4}^{(eq)} = k_{-5}^{(eq)} = k_{-6}^{(eq)} = 10^{10}$ were set up fixed near the diffusion limit, and the objective function was minimized with regard to the equilibrium constants.

The resulting objective function depends on {k_1; k_2; k_3; k_6; k_7; k_8;K_1; K_2; K_3; K_4; K_5}. It is not possible to determine unambiguously all these parameters due to the multi-minima nature of the least-squares surface, originated by the lack of information on the evolution of concentration of silent ^{31}PNMR species. In order to get reliable rate constants, some restrictions were imposed to the minimization procedure. Thus, the values of {k_1; k_2 ; k_3; K_1; K_2}. were set up fixed and equal to those calculated previously from the DCNP/TBAOH system. Moreover, the hydrolysis constant of amines (K_3) in acetonitrile: water 95:5 v/v was estimated applying the Rosés equation, see (§3.8), and set up fixed during calculations. A good match between calculated and experimental responses was observed in spite of application of these restrictions. Diagonalization of the Hessian the minimum resulted in positive eigenvalues for all tertiary amines, so that stationary points found were minimal. Calculation results are given in the manuscript.

3.6 Calculations for DCNP hydrolysis in presence of polyamines

In order to describe the kinetics in the presence of polyamines, reaction R9 was added to the set describing the mechanism of hydrolysis in presence of tertiary amines. Process R9 takes into account phosphoramide formation. Concentrations were calculated integrating Equation (18), where MPOLY is given by Equation (19).

The same procedure used for tertiary amines described in (§3.5) was employed to analyze data from hydrolysis catalyzed by polyamines.

$$\frac{d}{dt}\begin{pmatrix} c_1(t) \\ c_2(t) \\ c_3(t) \\ c_4(t) \\ c_5(t) \\ c_6(t) \\ c_7(t) \\ c_8(t) \\ c_9(t) \\ c_{13}(t) \\ c_{11}(t) \\ c_{12}(t) \end{pmatrix} = \mathbf{M}_{POLY} \times \begin{pmatrix} r_1 \\ r_2 \\ r_6 \\ r_3 \\ r_7 \\ r_8 \\ r_9 \\ r_1^{(eq)} \\ r_{-1}^{(eq)} \\ r_2^{(eq)} \\ r_{-2}^{(eq)} \\ r_3^{(eq)} \\ r_{-3}^{(eq)} \\ r_4^{(eq)} \\ r_{-4}^{(eq)} \\ r_5^{(eq)} \\ r_{-5}^{(eq)} \\ r_6^{(eq)} \\ r_{-6}^{(eq)} \end{pmatrix} \tag{18}$$

$$\mathbf{M}_{POLY} = \begin{pmatrix} -1 & -1 & -1 & 0 & -1 & 0 & -2 & 0 & 0 & 0 & 0 & 0 & 0 & 0 & 0 & 0 & 0 & 0 & 0 \\ 1 & 1 & 1 & -1 & 0 & 2 & 0 & 1 & -1 & 0 & 0 & 0 & 0 & -1 & 1 & 0 & 0 & 0 & 0 \\ 0 & 0 & 0 & -1 & -1 & 0 & 0 & -1 & 1 & 0 & 0 & 0 & 0 & 1 & -1 & 0 & 0 & 0 & 0 \\ 0 & 0 & 0 & 1 & 1 & -1 & 0 & 0 & 0 & 0 & 0 & 0 & 0 & 0 & 0 & 0 & 0 & 0 & 0 \\ -1 & -1 & -1 & 0 & 0 & -1 & 0 & -1 & 1 & -1 & 1 & -1 & 1 & 0 & 0 & 0 & 0 & -2 & 2 \\ 0 & 0 & 0 & 1 & 0 & 0 & 0 & 1 & -1 & 1 & -1 & 1 & -1 & 0 & 0 & 0 & 0 & 1 & -1 \\ 0 & 0 & 0 & 0 & 0 & 0 & 0 & 0 & 0 & 0 & 0 & 0 & 0 & 0 & 0 & 0 & 0 & 1 & -1 \\ 1 & 1 & 1 & 0 & 0 & 0 & 2 & 0 & 0 & 1 & -1 & 0 & 0 & 0 & 0 & -1 & 1 & 0 & 0 \\ 0 & 0 & 0 & 0 & 1 & 0 & 0 & 0 & 0 & -1 & 1 & 0 & 0 & 0 & 0 & 1 & -1 & 0 & 0 \\ 0 & 0 & 0 & 0 & 0 & 0 & -1 & 0 & 0 & 0 & 0 & -1 & 1 & -1 & 1 & -1 & 1 & 0 & 0 \\ 0 & 0 & 0 & 0 & 0 & 0 & 0 & 0 & 0 & 0 & 0 & 1 & -1 & 1 & -1 & 1 & -1 & 0 & 0 \\ 0 & 0 & 0 & 0 & 0 & 0 & 1 & 0 & 0 & 0 & 0 & 0 & 0 & 0 & 0 & 0 & 0 & 0 & 0 \end{pmatrix} \tag{19}$$

3.7 Calculations for DCNP hydrolysis in presence of ethylene glycol and diethylene glycol

In order to describe the kinetics in the presence of ethylene glycol and diethylene glycol, reactions R1, R2, R3, and R10 were used together equilibria E1, E2 and E6. Process R10 takes into account DCNP hydrolysis catalyzed by diols. Concentrations were calculated integrating Equation (20), where $\mathbf{M}_{DIOL}$ is given by Equation (21).

$$\frac{d}{dt}\begin{pmatrix} c_1(t) \\ c_2(t) \\ c_3(t) \\ c_4(t) \\ c_5(t) \\ c_6(t) \\ c_7(t) \\ c_8(t) \\ c_9(t) \\ c_{13}(t) \end{pmatrix} = \mathbf{M}_{DIOL} \times \begin{pmatrix} r_1 \\ r_2 \\ r_3 \\ r_{10} \\ r_1^{(eq)} \\ r_{-1}^{(eq)} \\ r_2^{(eq)} \\ r_{-2}^{(eq)} \\ r_6^{(eq)} \\ r_{-6}^{(eq)} \end{pmatrix} \tag{20}$$

$$\mathbf{M}_{DIOL} = \begin{pmatrix} -1 & -1 & -1 & -2 & 0 & 0 & 0 & 0 & 0 & 0 \\ 1 & 1 & 0 & 0 & 1 & -1 & 0 & 0 & 0 & 0 \\ 0 & 0 & -1 & 0 & -1 & 1 & 0 & 0 & 0 & 0 \\ 0 & 0 & 1 & 1 & 0 & 0 & 0 & 0 & 0 & 0 \\ -1 & -1 & 0 & -1 & -1 & 1 & -1 & 1 & -2 & 2 \\ 0 & 0 & 0 & 0 & 1 & -1 & 1 & -1 & 1 & -1 \\ 0 & 0 & 0 & 0 & 0 & 0 & 0 & 0 & 1 & -1 \\ 1 & 1 & 0 & 0 & 0 & 0 & 1 & -1 & 0 & 0 \\ 0 & 0 & 1 & 2 & 0 & 0 & -1 & 1 & 0 & 0 \\ 0 & 0 & 0 & 0 & 0 & 0 & 0 & 0 & 0 & 0 \end{pmatrix} \tag{21}$$

3.8 Estimation of hydrolysis equilibrium constants of amines in acetonitrile: water

Hydrolysis equilibrium constant values in acetonitrile/water were calculated from the corresponding $pK_{a,0}$'s of the protonated amines in pure water through Equation (22), where ϕ is the volumetric fraction of the acetonitrile-water mixture (ϕ = 0.95), $pK_{a,\phi}$ is the desired equilibrium constant, and a_s and b_s are two parameters depending on solvent composition and amine nature.

$$pK_{a,\phi} = a_s(\phi) \text{ x } pK_a(0) \text{x } b_s(\phi) \quad (22)$$

Values of as and bs were calculated by using equations (23) and (24),

$$a_s(\phi) = \frac{1+ a_1\phi+ a_2\phi^2}{1+ a_3\phi+ a_4\phi^2} \quad (23)$$

$$b_s(\phi) = \frac{b_1\phi+ b_2\phi^2}{1+ b_3\phi+ b_4\phi^2} \quad (24)$$

Parameters $\{a_i\}$ and $\{b_i\}$ were calculated for tertiary amines, polyamines, and pyridine by fitting the Rosés's data[9] to the above equations. Parameters are collected in in Table (2). Once a_s and b_s parameters were calculated, equilibrium constants were estimated by using Equation (22). Results are collected in Table (3). Finally, hydrolysis constants (K_b) were calculated from pK_a's as usual ($pK_{b,\phi} = pK_{w,\phi} - pK_{a,\phi}$).The ionic product of water in acetonitrile/water, $pK_{w,\phi}$, was obtained fitting Rosés's data[10] to Equation (25),

$$pK_w(\phi) = \frac{c_1\phi+ c_2\phi^2}{1+ c_3\phi+ c_4\phi^2} \quad (25)$$

Least-squares fit yields the **c** coefficients {c_1=-6.99098; c_2=-6.78757; c_3=-0.747467; c_4 =-0.246096}, from which a value of $pK_{w,0.95}$=18.18 was estimated in the reaction media.

Table 2. Least-squares calculated parameters for equations (23) and (24).

	a_i		b_i	
i	amine/polyamine	pyridine	amine/polyamine	pyridine
1	−0.7269340	−1.669670	−1.816255	−1.780396
2	−0.2624561	0.672855	2.250987	1.889665
3	−0.8695120	−1.668669	−1.745831	−0.581156
4	−0.1233137	0.671113	0.898798	−0.401035

Table 3. Parameters used to calculate amine hydrolysis equilibrium constants, K_b.

Amine	$a_s(0.95)$	$b_s(0.95)$	$pK_a(0)$	$pK_a(0.95)$	$pK_b(0.95)$
NEt_3	1.1575	2.0054	10.78	14.48	3.70
DABCO			8.82	12.21	5.97
DETA			9.94	13.51	4.67
TEPA			9.92	13.49	4.69
PDA			9.13	12.57	5.61
EA			9.48	12.98	5.20
DEA			8.52	11.86	6.32
AEE			9.62	13.14	5.04
AEAE			7.21	10.35	7.83
pyridine	1.0303	0.1634	5.17	5.59	12.69

[a] $pK_b = pK_w(0.95) - pK_a(0.95)$ ($pK_w(0.95) = 18.18$)

References

[1] J.A. Nelder and R. Mead. A simple method for function minimization. *Computer Journal*, 7:308–313, 1965.

[2] C.G. Broyden. The convergence of a class of double-rank minimization algorithms. i: General considerations. *J. Inst. Math. Appl*., 6:76–90, 1970.

[3] D. Goldfarb. A family of variable metric updates derived by variational means. *Mathematics of Computation*, 24(109):23–26, 1970.

[4] R. Fletcher. A new approach to variable metric algorithms. *The Computer Journal*, 13(3):317–322, 1970.

[5] D.F. Shanno. Conditioning of quasi-newton methods for function minimization. *Math. Comp*, 24(111):647–656, 1970.

[6] C. Gear and L. Petzold. Ode methods for the solution of differential/algebraic systems. *SIAM Journal on Numerical Analysis*, 21(4):716–728, 1984.

[7] F.F. Perez Pla, J.F. Bea Redon, and R. Valero. A new algorithm for the kinetic data analysis. *Chemom. Intell. Lab. Syst*., 53:1–19, 2000.

[8] K. Radhakrishnan and A.C. Hindmarsh. Description and use of lsode, the livermore solver for ordinary differential equations. Technical report, NASA Reference Publication 1327, 1993.

Chapter 7:

Conclusions

Conclusions

In particular we wanted to develop new optical sensors for the selective and sensitive detection of contaminating species; and obtain a reliable method for their destruction to avoid the dangerous effects they produce.

In the general introduction the main aspects of molecular recognition and optical sensors were reported. In particular the chemistry and properties of BODIPY-dyes were emphasized, in order to understand the basis for the new prepared sensors.

In the third chapter, new sensors for the selective detection of trivalent cations were described. The design, synthesis and characterization of the recognition system were reported. Subsequently the chromo-fluorogenic response to different cations was evaluated and we were able to state that our sensors displayed a great selectivity towards Al^{3+}, Fe^{3+} and Cr^{3+}, with remarkable low limits of detection in the μM range and the chromo-fluorogenic sensing ability could be simply observed by the naked eye. In the case of BODIPY-probes, the sensing behavior was observed in mixed aqueous solutions (even with 80 % H_2O) and selective sensing of Al^{3+} and Cr^{3+} versus Fe^{3+} was observed with ligand **2**.

The remaining chapters of the thesis have focused in the detection and removal of nerve agents. The design, synthesis, characterization and application of new BODIPY-probes for detection of nerve agent surrogates were reported. In particular the driving force of this part of the thesis was the achievement of a system as selective as possible in the presence of other interfering species. The first part of the study was focused on the design and synthesis of compounds based on the BODIPY-core containing two reactive sites: (i) a nucleophilic hydroxyl group that provides a suitable reactive site for electrophilic phosphorus atoms and (ii) a basic pyridine moiety that is known to react with acid. The reaction of such compounds with nerve agent mimics results in phosphorylation of a hydroxyl group, following by an intramolecular *N*-alkylation. These transformations are

evidenced by a significant blueshift for the lowest-energy absorption transition, and an escalation in the fluorescence yield. These changes were easily detected by the naked-eye. Thanks to the presence of a basic pyridine the sensing mechanism is still working in the presence of acids, thus avoiding a false negative response.

In order to obtain more selectivity a chemosensor based on a BODIPY derivative containing three reactive sites; (i) a nucleophilic phenol group, (ii) a carbonyl group; and (iii) a triisopropylsilyl (TIPS) protecting group, was synthesized and studied. In a first step the reaction with DCNP or DFP resulted in the phosphorylation of the phenoxy group, with the subsequent release of a fluoride (for DFP) or cyanide (for DCNP) anion. Further cyanide nucleophilic addition of the probe to the carbonyl group resulted in a hypsochromic shift of the absorption band. In contrast, the released fluoride anion was able to hydrolyze the TIPS group of the probe to yield a highly coloured phenoxide anion with a charge transfer band located in the NIR region. Allowing the discernment between DFP and DCNP. In order to achieve practical application, hydrophobic polyethylene oxide films and silica gel plates containing the new synthesized chemosensors were prepared and evaluated. The signaling abilities are retained in the solid state, allowing the development of simple colorimetric tests for the detection of nerve-agent simulants in gaseous and liquid phases in real-time monitoring.

Finally two new Eu^{3+} and Au^{3+} BODIPY-complexes capable of chromo-fluorogenically detecting V-type nerve agent surrogates by a simple displacement assay were described. The mechanism of detection occurs *via* the displacement of the BODIPY ligand by coordination of target surrogate with the metallic centre, resulting in a colour modulation and a fluorescence quenching which were observed easily to the naked eye. Moreover the new probes were able to selectively detect V-type versus G-type nerve agent.

In the last chapter of this thesis, supramolecular-based organocatalysts were used for the decontamination/hydrolysis of G-nerve agent mimics. Neutral 1,3-diindolylureas and thioureas were found to be useful for the nerve agent hydrolysis by the complexation of the mimics in a hydrophobic environment. The electrophilic character of the P atom was enlarged and the final nucleophilic attack of water results in the formation of the corresponding less toxic organophosphate derivatives. In some cases an enhancement of the hydrolysis rate up to 45% was observed in the presence of submolar concentrations of the receptors. Evaluation of ability of amines, aminoalcohols and glycols to promote the hydrolysis of DCNP (tabun mimic) were carried out. Kinetics studies allowed the definition of different DCNP depletion paths, resulting in the formation of diethylphosphoric acid, tetraethylpyrophosphate and phosphoramide species as the main final products. DCNP hydrolysis generally depended strongly on the structure of the amine, aminoalcohol and glycol used and it was found that the presence of the OH-CH_2-CH_2-N- moiety in the organocatalyst structure seems important to induce a fast degradation (DCNP depletion took place ca. 80 times faster) of Tabun simulant DCNP.

Gracias al Ministerio de Economía y Competitividad (Secretaría de estado de Investigación, Desarrollo e Innovación) por concederme una beca de Formación de Personal Investigador (FPI).